THE UNIVERSITY OF CHICAGO

THE DEVELOPMENT OF ACRYLAMIDE-BASED INHIBITORS OF DHHC FAMILY PROTEINS TO REGULATE ERK ACYLATION AND ACTIVITY

A DISSERTATION SUBMITTED TO

THE FACULTY OF THE DIVISION OF BIOLOGICAL SCIENCES

AND THE PRITZKER SCHOOL OF MEDICINE

IN CANDIDACY FOR THE DEGREE OF

DOCTOR OF PHILOSOPHY

INTERDISCIPLINARY SCIENTIST TRAINING PROGRAM:

CHEMISTRY

BY

SAARA-ANNE AZIZI

CHICAGO, ILLINOIS

DECEMBER 2021

What you leave behind is not what is engraved in stone monuments, but what is woven into the lives of others.
(Pericles, apocryphal)

For all my family and friends, with especial thanks to

Drs. Rahul Kathayat and Clémence Delalande, for kindness and mentorship even from afar.
Noah Brookes, for unflagging equanimity, humor, and determination.
&
Tian Qiu, for steadfast patience, constant collaboration, and true friendship.

TABLE OF CONTENTS

List of figures v

List of tables vii

List of publications viii

Abstract ix

1. Introduction 1
   1.1 Lipids as protein post-translational modifications 1
   1.2 Overview of *S*-acylation 3
   1.3 Substrates, writers, and erasers of *S*-acylation in pathophysiology 5
   1.4 Chemical tools to study *S*-acylation 9
   1.5 Scope of this thesis 10

2. CMA: An acrylamide-based inhibitor of DHHC family proteins 12
   2.1 Introduction 12
   2.2 Results 14
   2.3 Discussion 24
   2.4 Supplementary Figures and Tables 26

3. A structure-activity study of CMA 40
   3.1 Introduction 40
   3.2 Results 41
   3.3 Discussion 44

4. A high-throughput assay for the discovery of DHHC inhibitors 46
   4.1 Introduction 46
   4.2 Results and discussion 48
   4.3 Conclusion 52
   4.4 Supplementary Figures 53

5. Acylation as a novel PTM for ERK1/2 54
   5.1 Introduction 54
   5.2 Results 56
   5.3 Discussion 70

6. Development of fluorescent probes for the SARS-CoV-2 proteases 78
   6.1 Introduction 78
   6.2 Results and discussion 79

7. Methods 82
   7.1 Biochemical 82
   7.2 Synthetic 89

References 140

LIST OF FIGURES

1.1 Overview of S-acylation and its relevance in cell biology and organismal physiology ___3
1.2 Activation of the EGFR pathway induces a decrease in global APT activity _____4
1.3 Palmitate stress results in global activation of the APTs _____8
1.4 Chronological progression of chemical and biochemical methods to assess and probe protein lipidation in the decades since its initial observation _____9
2.1 *In vitro* discovery of CMA as an inhibitor of human zDHHC20 _____14
2.2 Characterization of CMA _____16
2.3 Validation of CMA *in cellulo* _____18
2.4 Engagement of CMA with DHHC family proteins _____22
2.5 Confirmation of CMA functional activity *in cellulo* _____23
2.S1 Docking of 1 (cyan) within the 2BP-binding pocket of human zDHHC20 _____26
2.S2 Validation of zDHHC20 biochemical assay _____27
2.S3 Inhibition of zDHHC20 *in vitro* _____28
2.S4 IC_{50} of CMA and 2BP with different preincubation times (7, 10, 15, 20, and 25 min.) __28
2.S5 CMA and 2BP cell viability assays _____29
2.S6 CMA and 2BP global acylation changes _____30
2.S7 Global ABE of HEK293T cells treated with CMA or 2BP (20 μM, 6 hours) in serum-free media _____30
2.S8 Timecourse of changes in the *S*-acylation of exogenous GobX and endogenous Ras in HEK293T cells upon 20 μM CMA treatment in serum-free media as measured by ABE _____31
2.S9 Serum affects global acylation changes with inhibitor treatment _____31
2.S10 The *in cellulo* time-course labeling of 8 (20 μM) in media _____32
2.S11 In-gel fluorescence analysis of 16C-BYA (1) and 8 (2) labeling _____33
2.S12 8 labeling (3 hours) of endogenous DHHC proteins zDHHC5, 7, 13, and 18 in HEK293T cells in serum-free media _____33
2.S13 In-gel fluorescence analysis of 8 and 16C-BYA labeling of a selection of human DHHC proteins and their DHHS mutants in serum-free media _____34
2.S14 The raw fluorescence image for the data shown in Figure 3A _____34
2.S15 Proteomic profiling and analysis of 20 μM 8 labeling in HEK293T cells _____35
2.S16 EGFR acylation and CMA treatment _____36
2.S17 Treatment with CMA and control molecules yields different downstream effects _____37
2.S18 In-gel fluorescence (FL) analysis of target engagement of CMA with mouse zDHHC4 _37
2.S19 Representative fluorescence microscopy images of the effect of CMA on lipid droplet formation and lipid uptake in 3T3-L1 preadipocytes _____38
3.1 Aliphatic chain substitutions of lipid acrylamides CMA and 1 _____42
3.2 Screening of acrylamide library against human zDHHC20 using a fluorescence polarization (FP) assay _____42
3.3 Plots of IC_{50} curves for SA20, SA75, and CD_17A _____43
3.4 Partial library of CMA derivatives to be screened DHHC family proteins _____45
4.1 Designing a fluorogenic probe for DHHCs _____48
4.2 DPP5 is a DHHC substrate _____49
4.3 Panel of pro-fluorescent probes for DHHC family proteins _____50
4.4 Plot of concentration (μM) against velocity (RFU per minute) for zDHHC20 _____50
4.5 Validation with known chemical inhibitors _____51

4.6 Plot of HTS Enamine library screen against zDHHC20 _____52
4.S1 Screen of a panel of fluorescent probes against zDHHCs 2, 3, and 20 to identify the best substrate for each protein _____53
4.S2 The activity of zDHHC20 and zDHHS20 against the probe C63 _____53
4.S3 GobX as a substrate to improve DHHC/probe turnover _____53
5.1 ERK1/2 are *S*-acylated _____57
5.2 ERK1/2 *S*-acylation responds to EGF stimulation _____58
5.3 Mapping crosstalk between ERK2 *S*-acylation and phosphorylation _____60
5.4 Chemical perturbation of ERK1/2 *S*-acylation affects its transcriptional program _____63
5.5 C254 of ERK2 is critical for its protein-protein interactions _____66
5.6 Identification of ERK1/2 writer and eraser proteins _____67
5.7 ERK1/2 *S*-acylation is responsive to metabolic stress *in cellulo* and *in vivo* _____70
5.S1 The extracellular signaling regulated kinases (ERK1/2) are dynamically palmitoylated _73
5.S2 Understanding the molecular determinants of ERK1/2 dynamic *S*-acylation _____74
5.S3 Mapping crosstalk between ERK2 *S*-acylation and TEY phosphorylation _____74
5.S4 Chemical inhibition of ERK1/2 *S*-acylation _____75
5.S5 Identification of the writer and eraser enzymes mediating ERK2 *S*-acylation _____76
5.S6 ERK1/2 *S*-acylation in a model of metabolic syndrome _____77
6.1 Schematic of assay design _____79
6.2 Screening and validation of CV6 as a fluorogenic probe for 3CL _____80
6.3 Screening and validation of CV2 as a fluorogenic probe for PLpro_____80
6.4 Application of assay to identify a PLpro inhibitor _____81

LIST OF TABLES

2.S1 Antibodies used in this work _____ 39

LIST OF PUBLICATIONS

Azizi, S-A., Qiu, T., Brookes, N., Lan, T., Dickinson, B.C. *A high-throughout fluorescence-based assay for the identification of DHHC family inhibitors. In preparation.*

Azizi, S-A., Qiu, T., Brookes, N., Dickinson, B.C. *Regulation of ERK2 activity by S-acylation. In preparation.*

Gupta, Y., Kumar, S., Zak, S., Jones, K., Upadhyay, C., Sharma, N., Azizi, S-A., Kathayat, R., Poonam, Herbert, A.S., Durvasula, R., Dickinson, B.C., Dye, J., Rathi, B., Kempaiah, P. *Antiviral Evaluation of Hydroxyethylamine Analogs: Inhibitors of SARS-CoV-2 Main Protease (3CLpro), A Virtual Screening and Simulation Approach. Bioorganic & Medicinal Chemistry.* 2021, https://doi.org/10.1016/j.bmc.2021.116393.

Drayman, N., Demarco, J., Jones, K.J., Azizi, S-A., Froggat, H., Tan, K., Malsteva, N., Chen, S., et al. *Masitinib is a broad coronavirus 3CL inhibitor that blocks replication of SARS-CoV-2. Science,* 2021, 373, 6557, 931-936.

Dewey, J.A., Azizi, S-A., Lu, V., Dickinson, B.C. *A system for the evolution of protein-protein interaction inducers. ACS Syn. Biol.,* 2021, 10, 2096-2110.

Azizi, S-A.,* Lan, T.,* Delalande, C., Kathayat, R., Banales-Mejor, F., Qin, A., Brookes, N., Sandoval, P.J., Dickinson, B.C. *Development of an acrylamide-based inhibitor of protein S-acylation. ACS Chem. Biol.* 2021, 16, 8, 1546–1556.

Osipiuk, J.; Azizi, S.-A.; Dvorkin, S.; Endres, M.; Jedrzejczak, R.; Jones, K.; Kathayat, R.S.; Lisnyak, V.G.; Maki, S.; Kang, S.; Kim, Y.; Nicolaescu, V.; Taylor, C.A.; Tesar, C.; Zhang, Y,; Zhou, Z.; Randall, G.; Michalska, K.; Snyder, S.A.*; Dickinson, B.C.*; Joachimiak, A.* *Structure of papain-like protease from SARS-CoV-2 and its complexes with non-covalent inhibitors. Nat. Commun.*, 2021, 12, 743.

Gupta, Y., Maciorowskib, D., Zak, S.E., Jones, K., Kathayat, R., Azizi, S-A., Mathurb, R., Pearce, C., Ilc, D., Husein, H., Herbert, A., Bartif, A., Rathi, B., Durvasulaa, R., Becker, D., Dickinson, B.C., Dye, J., Kempaiaha, P. *Bisindolylmaleimide IX: A novel anti-SARS-CoV2 agent targeting viral main protease 3CLpro demonstrated by virtual screening pipeline and in-vitro validation assays. Methods,* 2020.

Azizi, S.A. and Azizi, S-A., *Neurological injuries in COVID-19 patients: direct viral invasion or a bystander injury after infection of epithelial/endothelial cells. Journal of NeuroVirology,* 2020, 26, 631-641.

Azizi, S-A.,* Kathayat, R. S.,* Dickinson, B.C. *Activity-based sensing of S-depalmitoylases: Chemical Technologies and Biological Discovery. Acct. Chem Research.* 2019, 52, 11, 3029–3038.

Cao Y.,* Qiu, T.*, Kathayat,* R. S., Azizi, S-A., Thorne, A.K., Ahn, D., Fukata, Y., Fukata, M., Rice, P. A., Dickinson, B.C. *ABHD10 regulates mitochondrial redox homeostasis through S-depalmitoylation of PRDX5. Nat Chem Biol.* 2019, 15, 1232-1240.

ABSTRACT

Protein *S*-acylation, an enzymatically modulated lipid post-translational modification, is frequent and consequential; at the cellular level, it regulates protein subcellular trafficking and signaling activity, and at the organismal level, has been implicated in cancer and neurologic and inflammatory disease. However, the impact of dynamic *S*-acylation for many proteins remains unknown, in part due to lack of inhibitors for the enzymes that catalyze lipid addition, the DHHC family proteins. Not only is the most commonly used pan-DHHC inhibitor, 2-bromopalmitate (2BP), toxic and poorly potent, it also concurrently inhibits the *S*-acylation eraser proteins, the acyl protein thioesterases (APTs). Here, we report the synthesis and characterization of CMA a DHHC inhibitor with improved potency and selectivity. We then use it to establish the dynamics and functional consequences of *S*-acylation for a previously undescribed acylated protein, the extracellular signal-regulated kinase (ERK1/2), whose *S*-acylation is resistant to current DHHC inhibitors.

As an α-halo fatty acid, 2BP reacts with a range of nucleophilic amino acids and forms reactive acyl CoA intermediates *in cellulo*. We therefore proposed to exchange the α-halo with an acrylamide, a warhead known to react with cysteine over serine residues that will not undergo metabolic conversion. Synthesis and screening of a panel of acrylamide-containing lipids revealed CMA as a potent DHHC20 inhibitor *in vitro,* with the ability to significantly decease both substrate and global protein *S*-acylation *in cellulo*. Competitive activity-based protein profiling (ABPP) demonstrated that SA8 engages directly with a panel of DHHCs in cells. Moreover, CMA is less toxic than 2BP, does not inhibit eraser APT activity, and is able to effect cellular responses previously reported to result from loss of *S*-acylation. These results position the acrylamide as an inhibitory scaffold for DHHC family proteins.

We next CMA to probe the effects of perturbing palmitoylation on epidermal growth factor (EGF)-triggered signal transduction. Characterization of disruptions along this signaling cascade enabled the identification of a previously undescribed acylated protein, the extracellular signal-regulated kinase (ERK1/2), whose S-acylation is resistant to 2BP but responsive to CMA. We describe the molecular determinants of ERK1/2 acylation and cross-talk between ERK1/2 phosphorylation and palmitoylation, suggesting the criticality of S-acylation in regulating the activation and downstream behavior of this key effector protein.

We then conduct a structure-activity study of CMA, which demonstrates the criticality of the lipid tail and the potential of scaffold extension, but also underscores the need for novel inhibitors. To meet this need, we design and validate a fluorescence-based high-throughput assay for DHHC activity *in vitro* using a panel of fluorogenic probes. These palmitoyl-CoA mimetic probes are recognized and cleaved by the DHHC family proteins, providing a direct, sensitive, and simple readout of zDHHC2, 3, and 20 activities. After establishing its suitability for a high throughput screen, we screen a library of ~1,000 molecules against zDHHC20, identifying new acrylamide-based inhibitory scaffolds for zDHHC20.

In sum, this work reveals the potential of acrylamide-based DHHC family inhibitors, introduces a novel platform for the identification of new inhibitors, and emphasizes that much remains unknown about the significance of dynamic S-acylation in regulating protein activity and cellular events.

Chapter 1: Introduction

1.1 Lipids as protein post-translation modifications

The post-translational modification of proteins is critical in expanding the coding capacity of the genome and facilitating the flow of cellular information. Broadly described as chemical alterations to a polypeptide substrate following biosynthesis, post-translational modifications (PTMs) are ubiquitous across time and lifeforms, with some PTMs even posited to date back to the universal last common ancestor.[1] By modifying the properties of amino acids that harbor them, PTMs fulfill a multitude of functions, influencing enzyme activity, protein conformation, (sub)cellular localization, and protein-protein/biomolecule interactions. Besides increasing the function and diversity of the proteome, such modifications are also notable for their kinetics; PTMs can be installed or removed rapidly, on a timescale relevant to developmental or physiological stimuli.[2] This allows the cell to swiftly regulate protein activity in response to changes in external conditions or internal states – thereby exerting dynamic control in diverse contexts.[3, 4] Although sometimes non-enzymatic, this process can be orchestrated by the activation of enzymes that function as 'writers' and 'erasers,' which add and remove PTMs to control the location and duration of the response.[5]

PTMs come in all shapes and sizes and include chemical modifications (phosphorylation, acetylation, methylation), redox-based modifications (thiolation, nitrosylation, sulfenation), polypeptide modifications (ubiquitination, SUMOylation), and complex molecule modifications (glycosylation, ADP-ribosylation, AMPylation).[6] Contained in the latter category is the attachment of cellular metabolites, including lipids. Although united by a hydrophobic nature and an indispensability across biological systems, lipids are remarkably diverse in form and versatile in function. Enclosing both cells and their internal organelles, lipids – phospholipids, interspersed

with cholesterol and glycolipids – compartmentalize cellular operations and provide a fluid organizational interface, while also enabling the regulation and maintenance of a homeostatic environment. Intracellularly, lipids – mainly triglycerides and steryl esters – exist in lipid droplets and provide pools of mobilizable energy, as epitomized macroscopically by the energy reservoirs distinct in humped ungulates.[7] In addition, lipids are also substrates for dynamic and potent secondary signaling messengers; prostaglandins, endocannabinoids, leukotrienes, phosphatidylinositol-phosphates, and diacylglycerol are all lipid-derived, transient signaling molecules.[8] In all these roles, lipids frequently interact with proteins, assisting in structure maintenance, organelle targeting, and signaling complex assembly. However, it is as PTMs that lipids most directly modulate protein function.

Not surprisingly, the addition of a lipid PTM increases target hydrophobicity, with functional consequences, including, but not limited to, changes in membrane association, protein-protein interactions, subcellular localization, protein stability, and enzyme activity.[9] At least six types of lipids are covalently tethered to proteins *via* nucleophilic moieties of at least five amino acids. [10] Such modifications commonly utilize thioether (cysteine *S*-prenylation), amide (glycine *N*-myristoylation), and ester (serine *O*-octanoylation) linkages; generally, the resultant bond stability renders them irreversible. It was only recently discovered that the ester-linked Wnt serine *O*-palmitoleoylation is enzymatically reversible [11]. Similarly, a growing body of evidence suggests that certain HDAC and Sirtuin family members possess N^{ε}-lysine deacylase activity.[9]

Within the family of protein lipid modifications, *S*-acylation – most commonly, the incorporation of the C16:0 fatty acid palmitate on a cysteine residue via a thioester bond – is conspicuous for the enzymatic regulation of both addition and removal. Protein acyltransferases (PATs) catalyze acyl-CoA addition, while acyl protein thioesterases (APTs) cleave the resultant

thioester bond. In mammalian systems, there are 23 known DHHC-domain containing PATs, typically localized to the endomembrane system. While thus far members of metabolic serine hydrolase (mSH) superfamily, the number of known APTs is still growing and includes APT1/2, PPT1, and ABHD17A/B/C, which can be found in the cytosol, mitochondria, and lysosomes.[12-16] The interplay of writer and eraser activity subcellular trafficking, localization, and stability of numerous soluble and integral membrane proteins.

1.2 Overview of S-acylation

Recent reviews present comprehensive lists of palmitoylated proteins, from scaffolding and signaling proteins to ion channels and receptors, highlighting the broad physiological consequences of *S*-acylation in areas including synaptic transmission, the innate immune response, GPCR and tyrosine kinase signaling, and transcription factor function (Figure 1.1).[9, 10] Particularly striking in these enumerations is how crucial regulated cycles of acylation and deacylation are for target function and the maintenance of cellular homeostasis. For example, the immuno-metabolic glycoprotein CD36, a scavenger receptor and fatty acid translocase, requires acylation by DHHC4 and DHHC5 for its transport to

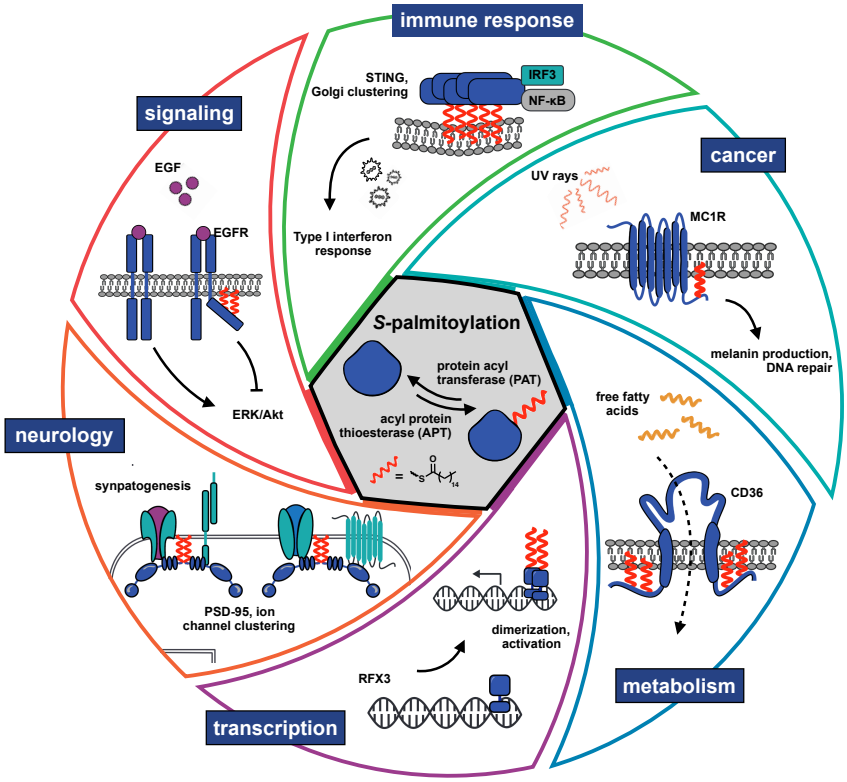

Figure 1.1. Overview of *S*-acylation and its broad relevance in cell biology and organismal physiology.

and continued presence at the plasma membrane, respectively.[17] Disruption of CD36 palmitoylation alters fatty acid uptake, JNK/NF-κB signaling, and even AMPK-activated fatty acid β-oxidation, with implications for non-alcoholic steatohepatitis.[17, 18] Treatment with palmostatin B (PalmB), a deacylase inhibitor, can mitigate the loss of membrane-localized CD36 observed in DHHC5 knockdown cells, underscoring the importance of both writer and eraser activity in modulating *S*-acylation-dependent protein function.[17]

The importance of DHHC and APT activity highlights another feature that renders *S*-acylation a critical regulator of protein function and the cellular response: its rapid temporal regulation. In fact, it is well-established that a host of proteins involved in cell signaling events are *S*-acylated, with dynamic *S*-acylation resulting from stimulation and occurring with the kinetics required for signal transduction. For example, stimulation of the β-adrenergic receptor results in an increase of $G\alpha_s$ and $G\alpha_i$ palmitoylation – mediated by zDHHC5 – on a timescale congruent with cAMP production, while the activation of the Fas receptor sparks a rapid, transient increase in the zDHHC2-regulated acylation of the Src family kinase, Lck, that parallels the activation timing of downstream effectors Zap70 and PLC-γ1.[19, 20] The small GTPase Ras that has one of the best-characterized dynamic palmitoylation cycles, with changes in its acylation status correlated to altered signaling and proliferation in cells. Moreover, stimulation with epidermal growth factor (EGF) results in a diminishment of fluorescently measured APT activity and therefore an inhibition or relocalization of *S*-deacylase activity (Figure 1.2).[21] *S*-deacylase dynamics have been discovered along other signaling pathways

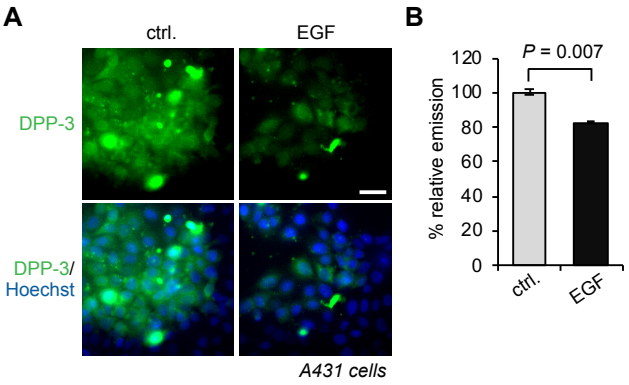

Figure 1.2. Activation of the EGFR pathway induces a decrease in global APT activity.

as well; in Wnt5a-stimulated cells, the activity of APT1 is increased, reducing the palmitoylation of the downstream effector and cell adhesion protein MCAM.[22] Thus, it is clear that *S*-acylation is responsive to internal and external cellular events, with its regulation arising from modulation of writer and eraser activity in a manner parallel to other established regulatory PTMs.

1.3 Substrates, writers, and erasers of *S*-acylation in pathophysiology

As our knowledge of *S*-acylation as a key regulator of protein and cellular function has increased, so too has our knowledge of how its regulation and dysregulation affect human pathophysiology.[23-25] Given the diverse array of acylated substrates, it is no surprise that this modification is consequential and relevant to a wide range of disease states, from cancer and metabolic disease to autoimmunity and microbial infection.

Cancer

Acylated proteins include enzymes involved in proliferation, apoptosis, angiogenesis, and invasiveness, and it is estimated that at least 26% of cancer driver genes are acylated, underscoring the relevance of this modification in the development of malignant cell growth.[26] Besides the aforementioned RAS family proteins, the scaffolding protein Scribble (SCRIB) presents a key example of acylation in the regulation of a cancer-associated protein.[27] An effector component of the Hippo pathway, whose activation is important for tumor growth, SCRIB relies on acylation to localize to cell junctions in healthy cells but is found in the cytoplasm of cancer cells due to the overexpression of APT2.[27] Inhibition of APT2 results in relocalization of SCRIB and growth attenuation. On the writer level, changes in DHHC expression are associated with a range of cancers, and DHHC family proteins have been found to acylate and thus regulate the function of several oncogenes.[28-34] For example, zDHHC20, which is overexpressed in ovarian, breast, and prostate tumors, is known to acylate the epidermal growth factor receptor (EGFR), which requires

acylation for its basal activation and regulation of its signal transduction via MAPK/PI3K pathway "switching." [29, 35] It has been recently found that in both cell culture and mouse models of KRAS-mutant lung cancer, blocking EGFR acylation via zDHHC20 knockdown can lead to reduced tumor growth and increased sensitivity to a PI3K inhibitor – suggesting that DHHC inhibition could be beneficial to patients with KRAS-mutant tumors.[36]

Neurological disorders

S-acylation is the most abundant lipid modification in the brain, and DHHC family proteins have been implicated in the modification and functional regulation of a numerous neuronal proteins. Although the role of this PTM in neurological pathogenesis is not yet fully described, its importance in this context is clear. At the broadly correlative level, zDHHCs 5 and 8 have been shown to be associated with schizophrenia in a genome-wide association study.[37] At the substrate level, zDHHC4 acylation of the long dopamine receptor (D2L) – a protein whose dysregulated signaling is connected to Parkinson's and Alzheimer's diseases – regulates D2L stability and trafficking.[38] Furthermore, deficient palmitoylation of the AMPA receptor, which is mediated by zDHHC3, leads to higher seizure susceptibility *in vivo*.[39] Both zDHHC13 and zDHHC17 palmitoylate huntingtin (HTT), a protein known to be involved in the fatal protein aggregation of Huntington's Disease. Mutant HTT is less palmitoylated than wild type HTT, and acylation has been established to contribute to its cytotoxic accumulation.[28, 33, 40]

Immunity and autoimmune disease

S-palmitoylation is a key regulator of immune signaling pathways, especially in T cells, and has been shown to directly influence inflammatory signaling and tune the immune response.[41-43] One example is lymphocyte-specific protein tyrosine kinase (Lck), a critical T cell kinase palmitoylated by DHHC21.[20] Similar to phosphorylation dynamics, its palmitoylation is driven by

Fas receptor signaling and is rapid and transient. Knockdown of DHHC21 significantly suppresses Fas receptor signaling, suggesting that inhibition of DHHC21 as a therapeutic strategy for diseases associated with altered T-cell homeostasis.[20] Most recently, a cycle of palmitoylation–depalmitoylation cycle by zDHHC7 and APT2 has been shown to regulate STAT3 activation and promote T_H17 cell differentiation. Perturbation of either writer or eraser attenuates T_H17 overaction and mitigates symptoms associated with inflammatory bowel disease (IBD).[44]

Infectious disease

It has been found that many pathogens, including viruses, can hijack S-acylation machinery of host cells, promoting viral internalization, survival, and replication inside the host cells.[45] The most studied viral acylated proteins are those of enveloped viruses. The *S*-acylation of the Chikungunya virus (CHIKV) nsP1 protein by zDHHCs 2 and 19 is critical for its plasma membrane localization and subsequent viral replication.[46] Three key membrane proteins found in the SARS-CoV-2 virion – Spike, envelope protein E, and the accessory protein Orf3a – are acylated by zDHHC20. This acylation, in particular for Spike, which possesses ten lipidated cysteine residues, is critical for the formation of viruses with fusion capacity and infectivity. There are currently no drugs available for the treatment of SARS-CoV-2 instigated disease and the efficacy of vaccines is dwindling in the face of viral evolution; thus, the targeting DHHC-mediated acylation represents both a novel and critical node for therapeutic development.

Metabolic disease

As the cycle of palmitoylation/depalmitoylation relies on palmitic acid, a lipid metabolite whose circulating and intracellular levels are aberrant in obesity and metabolic disease, potential connections between palmitoylation status, cell signaling, and metabolic health are both particularly intriguing and likely. Indeed, proteomic profiling of palmitoylation in adipose tissue,

an energy reservoir and an integral endocrine signaling site, revealed a host of palmitoylated proteins associated with metabolism and energy production, including JAK-STAT pathway signaling proteins, the aminopeptidase IRAP, and the glucose transporter Glut4.[47-49] The *S*-palmitoylation of Glut4 is required for its insulin-dependent membrane translocation, and in obesity models, its palmitoylation levels are increased. Acylation of the fatty acid translocase CD36, which regulates both its localization and FA uptake, is increased in livers of patients with non-alcoholic steatohepatitis (NASH).[18] In the context of signal events, long-term treatment of endothelial cells with insulin affected the palmitoylation status of ~10% of proteins, while a high-fat diet (HFD) and resulting palmitic acid deposition induced hippocampal insulin resistance and impaired synaptic plasticity via zDHHC3-mediated hyperpalmitoylation of an AMPA glutamate receptor subunit in mice.[50, 51] In cell culture, palmitate treatment is known to induce ER stress, which in turn has been correlated with overall increases in the level of *S*-acylation.[52] APT activity is enhanced in response to the increase in extra- and intracellular lipid levels (Figure 1.3).[53] In addition to bolus treatment of palmitate, alterations in APT activity upon perturbation of local lipid pools mediated by various acyl-CoA thioesterase (ACOT) proteins further underscore the connection between metabolic stress and *S*-acylation.[54]

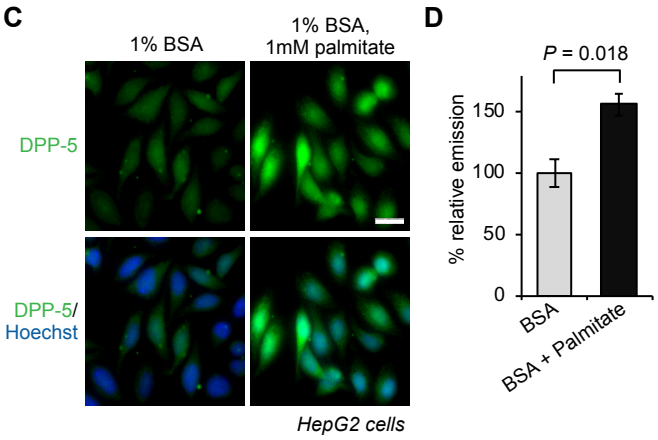

Figure 1.3. Palmitate stress results in global activation of the APTs.

Articulating the global and specific mechanisms connecting disrupted *S*-deacylase activity, altered substrate lipidation, and aberrant downstream signaling could help define a new lipidation-centric paradigm connecting metabolism and cell signaling.

1.4 Chemical tools to study *S*-acylation

Our understanding of the function and regulation of protein *S*-palmitoylation has progressed in-step with the development of chemical and biochemical methods to assay and perturb protein lipidation (Figure 1.4). Although posited in 1979 and validated in cell culture in 1980, it was in the twenty-first century, with the advent of chemical and biochemical methods to assess protein *S*-palmitoylation, that knowledge acquisition in the field accelerated [55,56]. With acyl-biotin exchange (ABE), which exploits the lability of the thioester bond to substitute an enrichment handle for the acyl group, substrate palmitoylation can be observed in a cysteine-specific manner, while the stoichiometry of acylation can be assessed with a homologous method, acyl-PEG exchange (APE) [57,58]. Metabolic labeling, once requiring radiolabeled fatty acids and immunoprecipitation, now utilizes fatty acid analogues chemically functionalized with ω-alkynes or azides suitable for biorthogonal Cu(I)-catalyzed "click" chemistry [59-61]. This offers a more sensitive, fatty acid-specific method for detecting acylated proteins [62]. In addition, activity-based protein profiling (ABPP), in which target enzymes are labeled in an active-site directed manner, has been applied

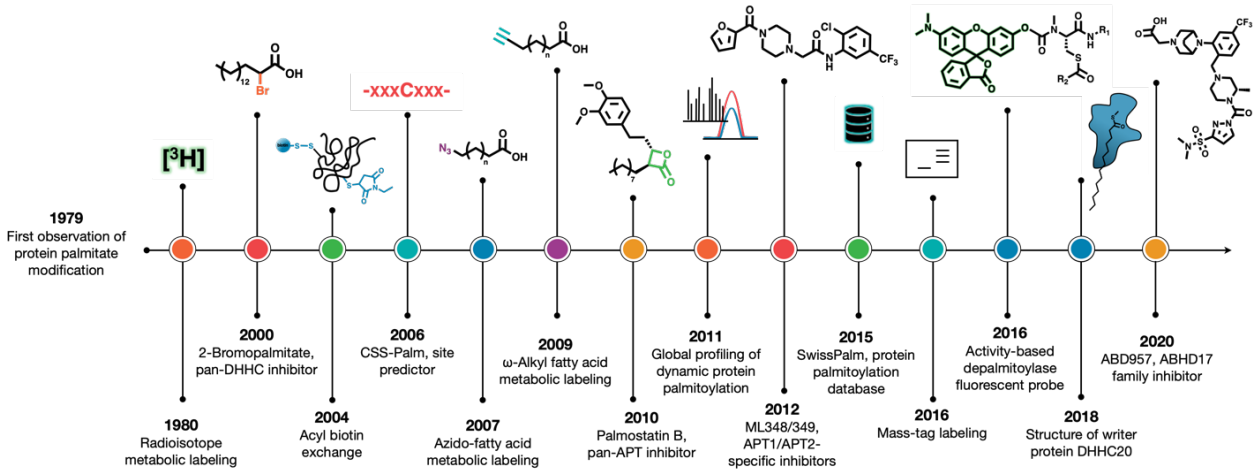

Figure 1.4. Chronological progression of chemical and biochemical methods to assess and probe protein lipidation in the decades since its initial observation.

to the mSH family (which encompasses APTs) and to the DHHCs, in order to broadly profile the enzymes and their functions across cell states. [63-65]

Mainstays in the *S*-acylation toolbox are small molecule inhibitors. These molecules – generally 2-bromopalmitate (2BP) for writer DHHCs and palmostatin B/M for eraser APTs – disrupt the steady-state acylation/deacylation cycle, allowing assessment of target phenotypes.[66-68] The development of inhibitors specific for two principle *S*-depalmitoylases, APT1 and APT2, as well as one for ABHD17 family proteins, enables greater precision in such assays.[69, 70] However, such precision is significantly lacking on the writer front. The aforementioned 2BP is widely employed as a pan-inhibitor of DHHC family proteins and thus substrate acylation, but it is poorly potent (IC_{50} ~10 μM) and highly non-selective. Due to its structural similarity with the natural lipid ligand, 2BP covalently modifies upwards of 450 proteins – meaning that more than 99% of its targets are not DHHC family proteins. In fact, as 2BP perturbs lipid synthesis, transport, and metabolism, it is hypothesized that its effects on substrate *S*-acylation are not in fact DHHC-mediated, but rather through the disruption of cellular lipid homeostasis. Other drugs, including tunicamycin and cerulenin, have been repurposed as DHHCs inhibitors, but these still possess inadequate potency and selectivity.[28, 71-73] While 2-(2-hydroxy-5-nitro-benzylidene)-benzo[b]thiophen-3-one, or compound V, was identified more recently as a possible, it was less potent than 2BP and its mechanism of action is completely undescribed.[71] Therefore, developing more potent, selective, and drug-like inhibitors for the DHHC proteins would be of significant benefit to research efforts at both the basic and translational levels.

1.5 Scope of this thesis

In the past two decades, there has been rapid progress in deciphering the consequences of *S*-palmitoylation at the molecular and cellular level in variety of eukaryotes, including microbes,

plants, and animals [24]. This expansion of knowledge has been propelled by the development of methods to observe changes in substrate *S*-palmitoylation levels and visualize steady-state enzyme activity. However, our understanding of the regulation of *S*-acylation and its biological consequences remains incomplete. New approaches are required to directly assay writer protein activity, while further studies of acylated substrates are needed to deepen our understanding of the implications of *S*-acylation at the organismal level.

In Chapter 2, we present the design and validation of a broad-spectrum inhibitor of DHHC family proteins, CMA, an acrylamide-lipid molecule that improves upon the potency, toxicity profile, and off-target APT interactions of 2BP.

In Chapter 3, we undertake a structure-activity study of CMA, with the aims of limiting its acyl-chain driven off-target interactions, improving its potency, and identifying isoform-specific inhibitors of DHHC family proteins.

In Chapter 4, we adapt a panel of pro-fluorescent probes for a high throughput screen for DHHC inhibitors, not only developing an assay with an excellent Z'-factor and applicability to multiple DHHCs, but also using it to screen a 1,000-member library and identify novel inhibitory scaffolds.

In Chapter 5, we identify *S*-acylation as a novel post-translational modification of the kinases ERK1/2 and ascertain its significance and dynamics in the context of EGF-mediated cell signaling events. Characterization of the molecular determinants of ERK acylation and an observation of its sensitivity to metabolic stress introduce this PTM as a therapeutic node for signaling-driven pathologies.

Finally, *in Chapter 6,* we pivot and apply the toolbox of chemical biology to toward the development of chemical probes to visualize the activity of the SARS-CoV-2 viral proteases, establishing an *in vitro* node in the Covid-19 drug development pipeline.

Chapter 2: CMA: An acrylamide-based inhibitor of DHHC family proteins

2.1 Introduction

Protein *S*-acylation is the post-translational addition of a long chain fatty acid to cysteine thiols via a thioester bond and is often referred to as *S*-palmitoylation due to the prevalence of C16:0 modification.[24, 25] *S*-acylation has complex and wide-ranging effects on target proteins; not only can it alter membrane association and subcellular trafficking, as for the well-studied oncogene Ras[3], but it also regulates protein oligomerization, activity, and stability.[23, 74-77] *S*-acylation is enzymatically reversible, with lipid addition catalyzed by the protein acyl transferases (PATs), which possess an active site Asp-His-His-Cys domain (earning them the moniker "DHHC") and lipid removal, by a suite of serine hydrolase family acyl-protein thioesterases (APTs), including APT1[14], APT2[78], ABHD10[76], and ABHD17A/B/C.[15] The activity of both these DHHC "writer" and APT "eraser" proteins is tightly regulated, and together, they in turn dynamically regulate protein *S*-acylation. Disruption of this cycle is consequential at the cellular and organismal levels.[9, 43, 79]

In particular, dysregulation of DHHC family proteins is associated with human pathology, including cancer progression, inflammation, and neurological dysfunction.[80-82] For example, zDHHC9 is upregulated in colorectal cancer and has been implicated in the pathogenesis of leukemia,[83, 84] while its loss-of-function mutations are associated with X-linked intellectual disability (XLID).[85, 86] ZDHHC20 regulates the signaling of the receptor tyrosine kinase EGFR, and its activity has been implicated in cellular transformation and lung tumorigenesis.[35, 36] Finally, knockdown of zDHHC7 has been shown to mitigate symptoms of inflammatory bowel disease, possibly via loss of STAT3 palmitoylation and activation.[87]

Despite the annotation of the first palmitoyl transferase in yeast two decades ago, a paucity of tools to perturb the function of the DHHC family has hindered progress in our understanding of their mechanism, regulatory roles, and connections to disease states. [88, 89] Functional redundancy between many DHHCs, as well as inter-family regulation, limit the use of classic genetic tools and highlight the necessity of small molecule inhibitors. [17, 90, 91] While the α-brominated fatty acid 2-bromopalmitate (2BP) is the most commonly used small molecule tool to study DHHC functions in live cells, its frequent use obscures its promiscuity, poor utility, and cellular toxicity. 2BP is hypothesized to act as a pan-DHHC inhibitor by covalently modifying the active cysteine residues of DHHC proteins, either as 2BP or the 2BP-CoA adduct, with the latter metabolic product displaying enhanced reactivity with proteome.[72] In fact, 2BP inhibits at least two of the *S*-acylation erasers, APT1 and APT2, in cells.[90] Moreover, 2BP is often used at micromolar concentrations (10-100 μM), concentrations that are at or above its toxicity threshold.[17, 72, 91] Other reported *S*-acylation inhibitors, such as cerulenin, tunicamycin, and compound V, suffer from significant toxicity, poor selectively, and/or a lack of characterization in cells.[64, 71, 92] Thus, there is a critical need for new chemical probes to study DHHC-mediated *S*-acylation in endogenous contexts.

Here, we report the development of CMA, a covalent broad-spectrum DHHC inhibitor with an acrylamide warhead and improved properties relative to 2BP. Not only is CMA more potent than 2BP *in vitro*, it is also less toxic and does not inhibit APT1 or APT2, thereby addressing two key limitations of 2BP. We demonstrate that CMA inhibits *S*-acylation and engages directly with DHHC family proteins *in cellulo*. Finally, we show that CMA can modulate DHHC-dependent cellular effects, including EGFR-mediated cell signaling and CD36-mediated lipid uptake and droplet formation. Overall, this work introduces CMA as a chemical tool that inhibits a broad range

of DHHCs and complements current methods to study the biological implications of disrupting DHHC-mediated *S*-acylation.

2.2 Results

Acrylamide-based molecules inhibit zDHHC20

The DHHC family proteins are thought to employ a two-step mechanism, in which the cysteine thiolate of the active site attacks the fatty acyl-CoA thioester, resulting in an autoacylated

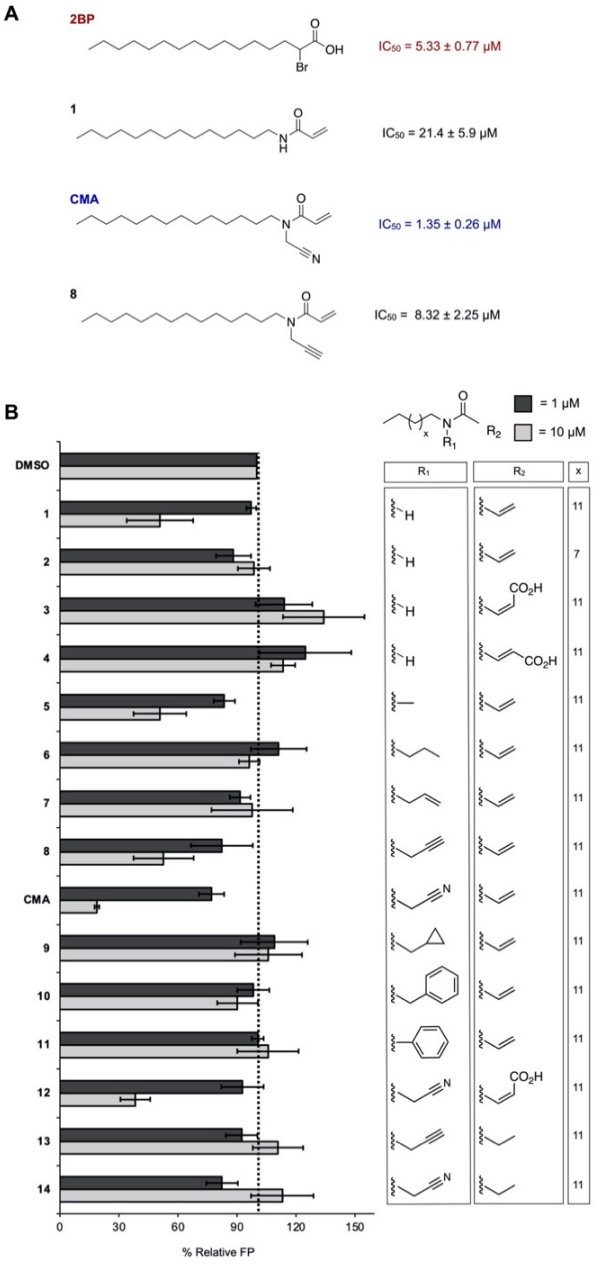

Figure 2.1. *In vitro* discovery of CMA as an inhibitor of human zDHHC20. (A) Structure and IC_{50} against human zDHHC20 of key molecules used in this work. (B) Fluorescence polarization (FP) screening of a panel of acrylamide-based molecules against zDHHC20, with activity normalized to DMSO. Data are presented as the mean ± standard deviation (*n=3*).

DHHC with the acyl chain bound in the hydrophobic groove. The fatty acyl chain is then transferred from the cysteine to a protein substrate. This nucleophilic cysteine can be targeted by electrophiles – like 2BP – to hamper DHHC activity. In pursuit of a still potent but less reactive inhibitor *in cellulo*, we proposed to exchange the α-halo carbonyl of 2BP with an acrylamide warhead. Acrylamides are known to react faster with cysteine thiols than serine alcohols, and, unlike the 2BP fatty acid, will likely not undergo metabolic conversion to

reactive and nonspecific acyl CoA intermediates.[72,93] Moreover, the acrylamide scaffold is achiral and readily synthetically accessible. Therefore, we designed and synthesized 1 (Figure 2.1), which features a 14 carbon-long lipid tail appended to the acrylamide warhead. Docking of 1 on the only published crystal structure of a human DHHC (zDHHC20) showed that the warhead is proximal (3.5 Å) to the active site Cys (Figure 2.S1). We therefore tested 1 against purified zDHHC20 using a fluorescence polarization (FP) assay adapted from Acyl-cLIP and using a fluorophore-tagged peptide that we identified as a substrate of zDHHC20, 5-FAM-NRas (Figure 2.S2).[94] 1 (IC_{50} = 21.4 ± 5.9 μM) successfully inhibited zDHHC20, although with decreased activity as compared to 2BP (IC_{50} = 5.33 ± 0.77 μM), confirming that an acrylamide-based lipid inhibitor can inhibit zDHHC20. Thus, we decided to explore the structure-activity relationship of 1 in an effort to enhance its potency.

CMA is a potent zDHHC20 inhibitor

To optimize 1, we designed and synthesized a panel of compounds, all with an acrylamide appended to a lipid tail. First, we targeted the lipid tail, shortening it by four carbons (2). This change abrogated the zDHHC20 inhibitory properties entirely, demonstrating the criticality of extensive contacts with the hydrophobic channel and inspiring us to instead focus on modifying the acrylamide moiety. We next tested compounds with either a substituted acrylamide amine and/or a butenoic acid-modified amide (Figure 2.1). While most performed worse than the parent molecule, one molecule functionalized with a cyanomethyl group, CMA, showed significantly improved activity against zDHHC20, with approximately 80% inhibition at 10 μM. CMA was found to have an IC_{50} of 1.35 ± 0.26 μM against zDHHC20 with 1 hour of preincubation, a 5-fold improvement over 2BP (Figure 2.S3). We further characterized the kinetic parameters of covalent modification, k_{inact} and K_I for both CMA and 2BP, observing that CMA had both a faster reaction

rate (2.08 vs. 1.35 min^{-1}) and a stronger affinity towards zDHHC20 (5.8 vs. 6.4 μM) than 2BP (Figure S4). Moreover, addition of the cyanomethyl group to the *cis* butenoic acid derivative (3) improved its activity (12), highlighting the criticality of this moiety. A second molecule, 8, which possesses a terminal alkyne in lieu of the cyanomethyl, was similar in potency to 2BP, with an IC_{50} of 8.32 ± 2.25 μM (Figure 2.S3). To confirm that the reactivity of CMA and 8 stemmed from the acrylamide warhead and not reversible thioimidate complex formation, we synthesized and tested 13 and 14, the alkyl amide analogues of 8 and CMA, respectively (Figure 2.1). Both molecules were inactive, verifying the acrylamide as the DHHC-reactive moiety. In sum, CMA is a potent zDHHC20 inhibitor *in vitro* and requires both the cyanomethyl group and acrylamide warhead for activity. Therefore, to assess its utility in live cells, we next assessed its inhibition of APTs and toxicity.

CMA does not inhibit APTs and is less toxic than 2BP

To determine if CMA inhibits eraser APTs, as observed with 2BP, we evaluated the effects of CMA relative to 2BP on APT1 and APT2 activity *in vitro* using a fluorogenic probe for APT activity, DPP5.[53] CMA showed little inhibition of APT1 and APT2, while 2BP, in agreement with previous reports, significantly inhibited both APT1 and APT2 (Figure 2.2).[90] At 25 μM, a

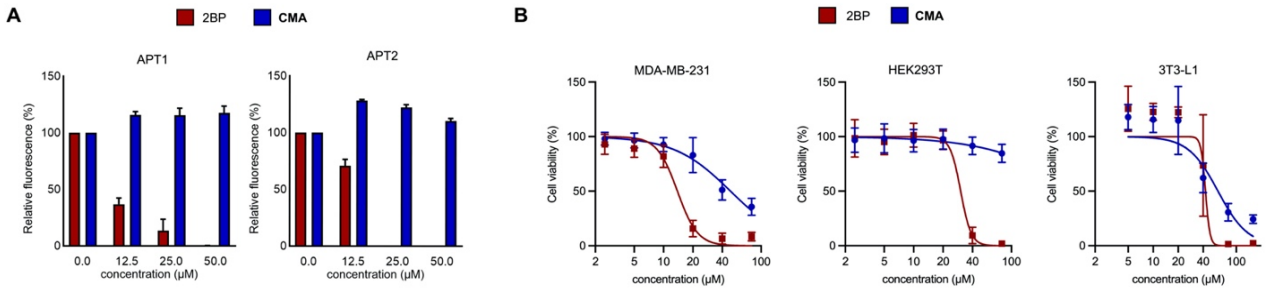

Figure 2.2. Characterization of CMA. (A) Incubation of purified APT1 or APT2 (50 nM) with either 2BP or CMA, followed by measurement of APT activity using the fluorogenic probe DPP-5. Data are presented as the mean ± standard deviation (*n=3*). (B) Viability of HEK293T, MDA-MB-231, and 3T3-L1 cells treated with varied concentrations of either 2BP or CMA (24 hours), as measured by MTS assay. Data are presented as the mean ± standard deviation (*n≥3*).

concentration at or below which 2BP is often used, 2BP abolished most activity of APT1 and all activity of APT2. In striking contrast, CMA showed no inhibition of APT1 or APT2 even at 50 μM, the highest concentration assayed. This data suggests that CMA, unlike 2BP, can be used to monitor the dynamics and the kinetics of acylation without perturbing APT-mediated deacylation.

We also compared the toxicity of CMA to that of 2BP across a panel of commonly used mammalian cell lines, including MDA-MB-231, HEK293T, and 3T3-L1. After 24 hours of treatment, CMA's toxicity was limited up to 40 μM, while 2BP significantly reduced cell viability at much lower concentrations (Figure 2.2, 2.S5). For example, in MDA-MB-231 cells, treatment with 2BP resulted in ~90% cell death at 20 μM, whereas at the same concentration of CMA, no toxicity was observed. However, as the toxicity of both compounds was cell-line dependent, CMA treatment time and concentration will need to be optimized for a particular experimental system. As CMA was non-toxic at 20 μM across all cell lines we tested, we designated this as our maximum concentration of CMA to use for assessment in these cell lines. Overall, these results – the lack of APT inhibition and decreased toxicity – paired with the robust inhibition of zDHHC20 *in vitro*, suggested that CMA might be an inhibitor of zDHHC-mediated acylation in cells.

CMA inhibits protein S-acylation in live cells

To validate the use of CMA as an inhibitor of *S*-acylation, we next sought to assess its efficacy and potency in live cells. Using 17-octadecynoic acid (17-ODYA) metabolic labeling, wherein a clickable fatty acid is used to monitor lipid incorporation, we observed a dose-dependent decrease in global *S*-acylation when cells were treated with CMA (Figure 2.3, 2.S6).[60] We further confirmed the global inhibition of protein *S*-acylation by CMA using acyl-biotin exchange (ABE), a method for the enrichment and visualization of acylated cysteine residues (Figure 2.3, 2.S7). [57]

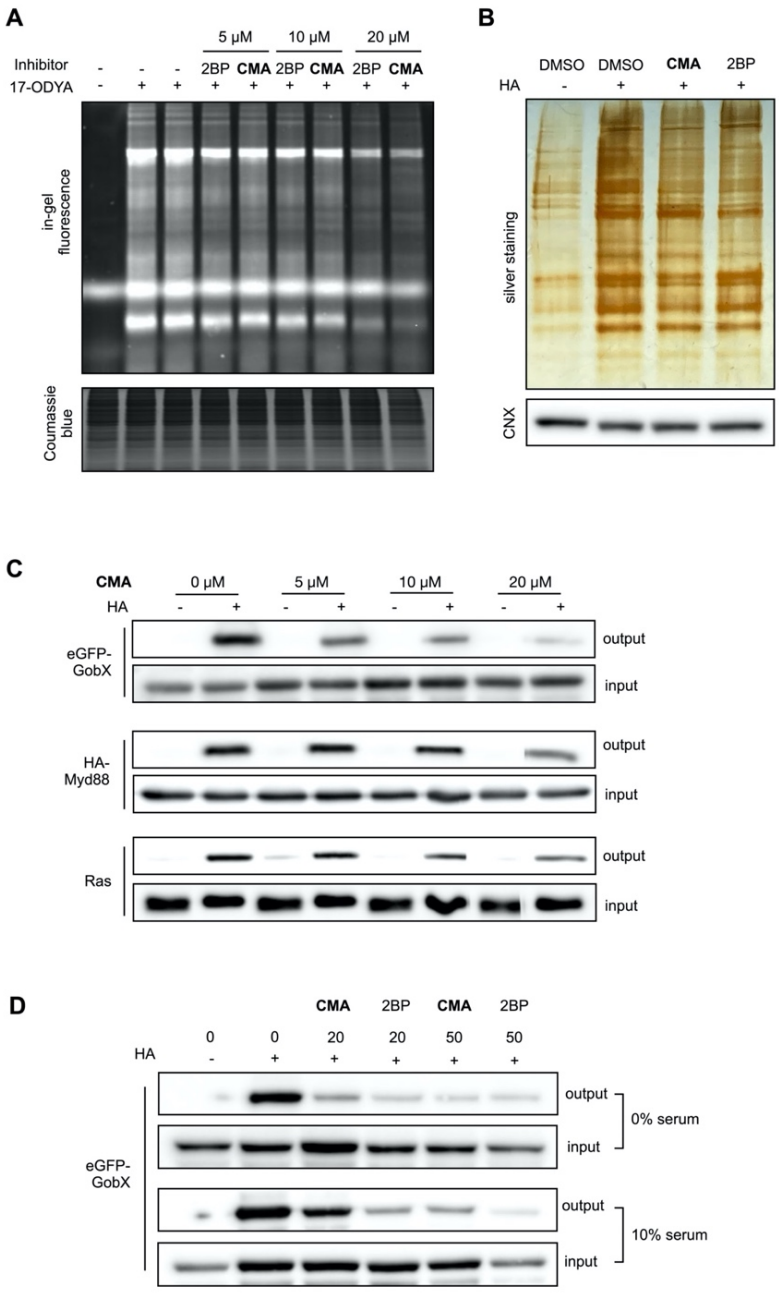

Figure 2.3. Validation of CMA *in cellulo*. (A) HEK293T cells pretreated with DMSO, 2BP or CMA (0, 5, 10, and 20 μM, 3 hours) before treatment with 17-ODYA (6 hours) to label palmitoylated proteins. Isolated proteomes were then subject to click chemistry to conjugate TAMRA-azide to proteins modified by 17-ODYA, followed by SDS-PAGE. In-gel fluorescence revealed a proteome-wide decrease in protein palmitoylation with CMA treatment. (B) Acyl-biotin exchange (ABE) of HEK293T cells treated with 2BP or CMA (20 μM, 6 hours). Global *S*-acylation visualized using silver staining, with CNX as a loading control ($n \geq 2$). (C) Dose-response change in the *S*-acylation of exogenous eGFP-tagged GobX or HA-tagged Myd88 and endogenous Ras in HEK293T cells upon CMA treatment in serum-free media (6 hours) as measured by ABE. CNX serves as an assay and loading control ($n \geq 2$). (D) ABE of HEK293T cells expressing eGFP-tagged GobX and treated with 2BP or CMA (0, 20, 50 μM) carried out in serum-free or serum-full media.

To corroborate these proteome-wide observations and also to evaluate the conditions of CMA inhibition, we next tested whether and when CMA could inhibit the *S*-acylation of several well-studied DHHC substrate proteins. We first assessed its effect on the *S*-acylation status of overexpressed Legionella E3 ligase GobX, the overexpressed human immune adaptor protein Myd88, and the endogenous GTPase Ras, which are regulated by zDHHC20, zDHHC9, and

zDHHC6, respectively.[41, 95] After treating HEK293T cells with a range of concentrations of CMA under serum-free conditions, we observed a dose-dependent decrease in the *S*-acylation of overexpressed GobX and Myd88 and endogenous Ras, with a significant loss of acylation at 20 μM after 6 hours of treatment for all three substrates (Figure 2.3). We then assessed the time course of CMA inhibition of these two targets at 0, 1, 3, and 6 hours, observing significant inhibition for these particular substrates only after 6 hours of treatment (Figure 2.S8). However, as the turnover of acylation is substrate-dependent, the time component of CMA inhibition will need to be optimized for individual substrates.[96, 97] Additionally, as the non-specific binding with serum proteins in culture media is a known challenge for small molecule inhibitors, we also assayed the effect of serum concentration on CMA alongside 2BP, probing both global and GobX *S*-acylation. Using ABE, we observe that in up to 1% FBS, both CMA and 2BP inhibit global and GobX *S*-acylation, but with 10% FBS, the activity of both molecules appears extremely limited (Figure 2.3, 2.S9). Overall, all targets displayed reduced acylation at a concentration of 20 μM CMA with 6 hours of treatment, establishing this as our working concentration. Collectively, these data confirm that CMA inhibits protein *S*-acylation in live cells.

CMA engages DHHCs in live cells

Having verified that CMA inhibits zDHHC20 *in vitro* and blocks protein *S*-acylation in live cells, we next sought to confirm direct engagement of DHHC family proteins by CMA in live cells. We postulated that 8, an analogue of CMA possessing a terminal alkyne instead of the cyanomethyl group, could be used to visualize CMA engagement across the DHHC family by reporter conjugation via copper-catalyzed azide-alkyne "click" cycloaddition (Figure 2.1). Therefore, we first visualized 8 labeling across the proteome, subjecting 8-treated HEK293T cell lysates (10 μM, 2 hours) to the click reaction with TAMRA-azide. In-gel fluorescence indicated

labeling in both serum-free and 10% FBS-complemented media, although labeling rate and intensity were decreased under the latter conditions (Figure 2.S10). We next determined which DHHCs could be labeled by 8. HEK293T cells overexpressing individual DHHCs were treated with 8 (10 μM, 2 hours), and, as above, following cell lysis, subjected to a click reaction with TAMRA-azide in order to label 8-modified proteins. Analysis of in-gel fluorescence showed that 8 labels zDHHC2, 4, 6, 9, 11, 13, 14, 15, 16, 18, 20, 23, and 24, all of the DHHCs in our human and murine libraries with strong expression (Figure 2.S10A-C, 11). Furthermore, 8 was also found to label endogenous DHHC proteins, including zDHHC5 and 7, which was not labeled in the fluorescence screen, likely due to poor expression (Figure 2.S12). Notably, the labeling intensity and range of 8 differed from 16C-BYA, possibly suggesting different selectivity profiles for CMA and 2BP.

We next examined the residues of DHHC proteins labelled by 8. As the cysteine residue within the DHHC motif is critical for the *S*-acyltransferase activity for DHHC proteins, we performed 8 labeling on a subset of exogenous catalytically dead (DHHS) mutants.[88, 89, 98, 99] While some DHHCs, such as zDHHC9 and 24, evinced decreased labeling of the active site mutant, other DHHCs, including zDHHC20, did not, suggesting that the DHHC motif Cys is not the only residue modified by 8, as is also observed with 16C-BYA, an alkyne-containing analogue of 2BP (Figure 2.S13).[63] While the functional consequences of the 2BP and CMA reactivity with peripheral cysteines remain unknown, this result could suggest a possible role for these residues in the mechanism of inhibition.

The background fluorescence observed during in-gel labeling with 8 suggested that CMA has off-targets in cells. Thus, we decided to use mass spectrometry (MS) to profile the proteome-wide reactivity of 8 and therefore CMA. To this end, following treatment of HEK293T cells with 20

μM 8 or DMSO, click reaction with biotin-azide, enrichment, and on-bead trypsin digestion, digested peptides were identified and quantified by dimethyl labeling. Consistent with the gel-based results, we found that 8 had a wide range of off-targets in cells (Figure 2.S15, Table 2.S1). When filtered with ≥2 unique peptides and ≥5-fold enrichment in at least 2 of 3 replicates, 271 targets can be identified. Top enriched proteins include chitobiosyldiphosphodolichol beta-mannosyltransferase (ALG1), threonylcarbamoyl adenosine tRNA methylthiotransferase (CDKAL1), and neutral cholesterol ester hydrolase 1 (NCEH1), while off-targets (targets other than DHHC family members) more broadly included transferases, translocases, and channel proteins. Unsurprisingly, due to the low abundance and have high hydrophobicity of DHHC family proteins, LC-MS/MS analysis only identified one DHHC protein (zDHHC6), which did not even pass the threshold when the enrichment cutoff was set to 5 (Figure 2.S15, Table 2.S1).[63, 72, 100, 101] Overall, we hope that this proteomics data can provide a guide for optimizing future derivatives of CMA against off-targets.

Having profiled the reactivity of 8 and validated its ability to label DHHC family proteins, we next performed competitive labeling with CMA for exogenous (zDHHC2, zDHHC9, zDHHC14, zDHHC15, and zDHHC24) and endogenous (zDHHC5, 13, and 18) DHHC proteins labeled by 8 in order to confirm CMA target engagement in live cells. For the exogenous DHHCs, cells overexpressing each targeted protein were treated with CMA (0, 10, and 20 μM, 2 hours) in either serum-free or 10% FBS media, chased with 8 (1 μM, 2 hours), and then lysed. After TAMRA-azide ligation, in-gel fluorescence indicated that CMA blocked 8 labeling, confirming that CMA engages each of these DHHC targets (Figure 2.4, 2.S10D, 2.S14). To probe the endogenous DHHCs, we again performed competitive labeling, this time on non-transfected HEK293T cells and using 8 at 20 μM for 3 hours for the chase. Here, after conjugation with biotin-azide, pulldown,

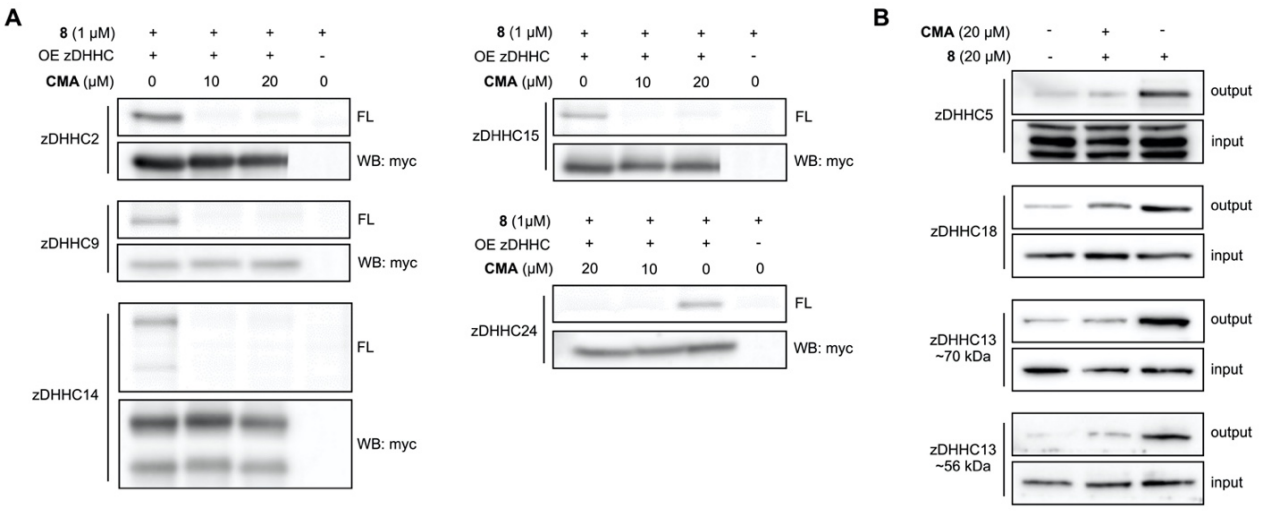

Figure 2.4. Engagement of CMA with DHHC family proteins. (A) In-gel fluorescence analysis of myc-tagged DHHC proteins overexpressed in HEK293T cells treated with CMA or DMSO (2 hours), followed by labeling with 8 (1 μM, 2 hours). Cell lysates subject to click chemistry to conjugate TAMRA-azide to proteins modified by 8, followed by protein separation via SDS-PAGE. Expression levels visualized via anti-myc tag Western blot ($n \geq 2$). (B) Western blot analysis of endogenous DHHC proteins in HEK293T cells treated with CMA or DMSO (3 hours), followed by labeling with 8 (20 μM, 3 hours). Cell lysates were subject to click chemistry to conjugate biotin-azide to proteins modified by 8, followed by streptavidin enrichment, protein separation via SDS-PAGE, and Western blotting for indicated targets ($n \geq 2$).

and Western blotting, we observed that CMA impeded the 8 labeling of zDHHC5, zDHHC18, and two isoforms of zDHHC13 (Figure 2.4) – confirming CMA directly engages with these DHHCs as well. The ability of CMA to outcompete 8 labeling of both exogenous and endogenous DHHCs suggests that CMA inhibition of *S*-acylation in live cells likely stems from inhibition of DHHC family proteins.

CMA inhibits the S-acylation of EGFR and CD36

Finally, we sought to test whether CMA could recapitulate observations reported to stem from DHHC disruption and establish that, along with on-target binding, CMA can be used to discern cellular outcomes from loss of *S*-acylation. A critical *S*-acylated protein and substrate of zDHHC20 is the epidermal growth factor receptor (EGFR), a receptor tyrosine kinase whose activity is widely dysregulated in cancer.[35] There are several mechanisms by which its C-terminal acylation regulates

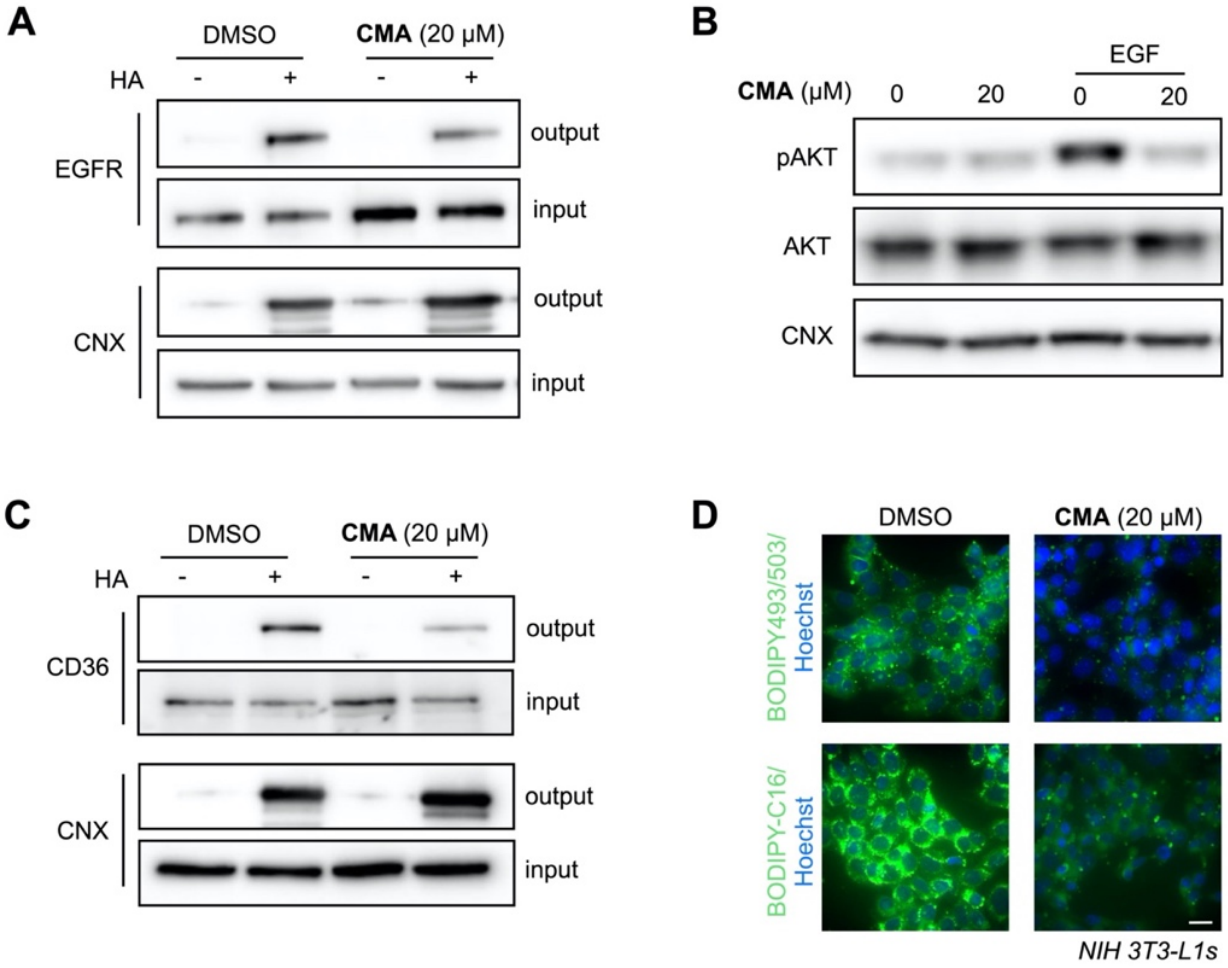

Figure 2.5. Confirmation of CMA functional activity *in cellulo.* (A) Analysis of EGFR *S*-acylation via ABE upon CMA treatment (20 μM, 3 hours) in MDA-MB-231 cells, with CNX as an assay and loading control ($n \geq 2$). (B) EGF (100 ng/mL, 15 minutes)-induced phosphorylation of AKT with and without CMA treatment (20 μM, 3 hours) ($n \geq 2$). (C) Analysis of CD36 *S*-acylation via ABE upon CMA treatment (20 μM, 6 hours) in 3T3-L1 cells, with CNX as an assay and loading control ($n \geq 2$). (D) Representative images of fluorescence imaging of 3T3-L1 preadipocytes starved (12 hours) and treated with DMSO or CMA (20 μM, 3 hours), followed by 10 μM BSA-bound oleate and BODIPY493/503 or BODIPY-palmitate (2 μM, 3 hours) *(n=5).* Scale bar = 20 μM.

its activity; in a KRAS-mutant context, loss of its palmitoylation is reported to disrupt signaling along the phosphatidylinositol 3-kinase (PI3K) pathway.[36] Thus, we first confirmed that CMA diminished EGFR *S*-acylation in MDA-MB-231 cancer cells at its working concentration, but that 14, the non-covalent analogue of CMA did not (Figure 2.5, 2.S16). We then assessed whether

CMA-mediated interruption of EGFR acylation impacted downstream PI3K pathway signaling. We observed that treatment with CMA, but not with 14, moderated the phosphorylation of protein kinase B (Akt) and the abundance of the transcription factor MYC, two markers of EGFR-P13K pathway activity (Figure 2.5, 2.S17). Interestingly, treatment with 10, a molecule inactive against zDHHC20 *in vitro*, inhibited EGFR acylation and PI3K pathway activation *in cellulo*, possibly implicating another zDHHC in the regulation of the EGFR pathway (Figure 2.S16, 2.17C). Overall, these results paralleled those seen with genetic knockdown of zDHHC20 and established CMA's ability to validate results downstream of acylation disruption.[36]

To further substantiate CMA's ability to modulate DHHC-dependent cellular functions, we next evaluated whether CMA could inhibit the *S*-acylation and subsequently the activity of CD36. CD36 is an immuno-metabolic glycoprotein and a substrate of zDHHC4 and zDHHC5, two DHHCs we confirmed were targeted by CMA (Figure 2.4, 2.S11). The *S*-acylation of CD36 mediates its localization and in turn its fatty acid translocase activity.[102] We found that treatment of 3T3-L1 pre-adipocytes with CMA not only reduced CD36 acylation levels (Figure 5C), but also decreased the uptake of fatty acids and formation of lipid droplets, results previously observed with knockdown of zDHHC4/5 (Figure 2.5, 2.S19). Together, these results indicate that not only does CMA perturb the acylation of significant endogenous targets, it also modulates their known acylation-dependent activity and functionality.

2.3 Discussion

As our understanding of the role of protein *S*-acylation in regulating cell and organismal biology grows, the toxicity and limited potency of current inhibitors demand improved chemical tools. In this Article, we introduced CMA, a broad-spectrum inhibitor of DHHC family proteins, to complement current methods to probe *S*-acylation and its consequences in cells. Featuring an

acrylamide warhead functionalized with a cyanomethyl group, CMA's potency is on par with 2BP – the leading inhibitor in the field – and, more importantly, has a significantly improved toxicity profile across multiple mammalian cells lines. We also show that CMA does not inhibit eraser APTs, a critical limitation of 2BP. These improvements were achieved without a loss of in-cell efficacy; for example, CMA inhibited the acylation of CD36 at 20 μM under our conditions, while 2BP was used at 100 μM[102]. Furthermore, we used 8, an alkyne-containing derivative of CMA, to show that CMA engages with DHHC family proteins across clades, validating CMA as a broad-spectrum DHHC inhibitor and confirming its role in perturbing DHHC-dependent acylation. Finally, we applied CMA to assess cellular responses previously reported to result from loss of *S*-acylation. We demonstrated that decreases in the acylation of EGFR and CD36 caused by CMA treatment were paired with changes in signaling activity and lipid uptake, respectively – changes aligned with results reported using both genetic manipulation and 2BP treatment.[17, 35] These results not only emphasize the importance of *S*-acylation in biological processes, but also highlight the potential of CMA in elucidating the regulatory roles of DHHC family proteins.

While this work reveals the promise of acrylamide based DHHC family inhibitors, it also underscores the need for additional improvements in selectivity and potency. MS analysis suggests that 8 can label 271 proteins with high confidence in cells, over 75% of which are annotated as acylated proteins (Table 2.S1). These results suggest that 8, and in turn CMA, interact with acylated targets and emphasize the disadvantage of their lipid "tails." As mimetics of fatty acids and their derivatives, aliphatic chains are thought to lead to numerous off-targets in cells.[103] Therefore, modification or replacement of the lipid will be critical in the next generation of molecules. As comparison of 1 with 2 indicates, though, the loss of hydrophobic contacts would need to be compensated for by expansion of the scaffold and increased contacts with the protein

elsewhere. Interestingly, we observed that the cyanomethyl group was crucial for CMA potency; however, the reasons for its criticality are unclear. We envision that a crystal structure of a CMA-bound DHHC would both aid in deciphering the mechanism of the cyanomethyl-mediated increase in potency and highlight opportunities for structure-based design. The ability of 10 to inhibit *S*-acylation *in cellulo*, but not zDHHC20 *in vitro,* was also intriguing and suggests that some members of our acrylamide panel might serve as a starting point for a DHHC inhibitor with intra-family specificity. In addition, the capability of zDHHC20 to acylate NRas peptide, as well as recent reports of DHHC-targeted peptide inhibitors, hint at the potential of peptide scaffolds as DHHC inhibitors.[104, 105] Our future work will focus on developing new small molecule and peptide scaffolds to achieve improvements in selectivity and potency.

2.4 Supplementary Figures and Tables

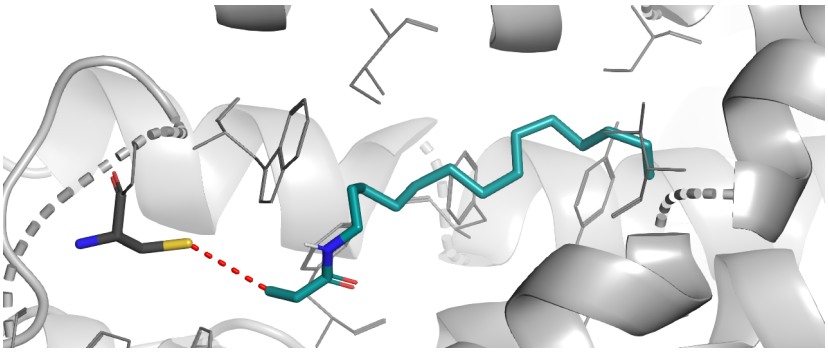

Figure 2.S1. Docking of 1 (cyan) within the 2BP-binding pocket of human zDHHC20 (PDB: 6BMN). The acrylamide moiety of 1 is 3.5 Å from C156 (dark grey), as indicated by the red dashed line in the figure. Key interacting residues in the hydrophobic pocket are highlighted in grey.

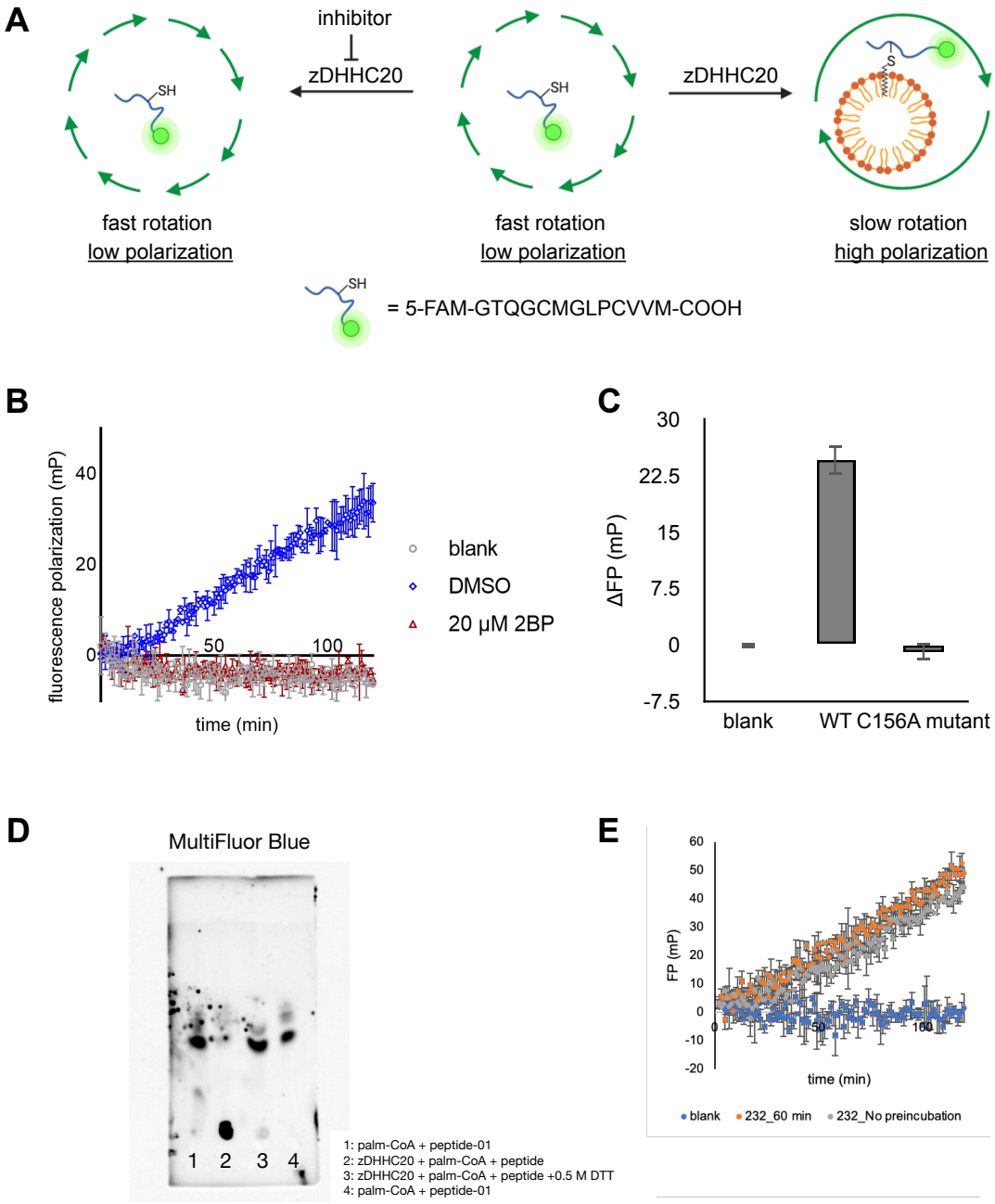

Figure 2.S2. Validation of zDHHC20 biochemical assay. (A) Schematic representation of the fluorescence polarization (FP) assay for zDHHC20. (B) Real-time FP of FAM-NRas peptide (peptide-01) with buffer only (grey), wild-type (WT) zDHHC20 treated with DMSO (blue), or WT zDHHC20 treated with 20 μM 2BP (red). (C) Endpoint FP of peptide-01 at t=60 min with buffer only (grey), WT zDHHC20, or zDHHA20. (D) Peptide-01 was incubated with or without zDHHC20 for 2 hours, and the final products were resolved on reverse-phase TLC plate. (E) Real-time fluorescence polarization curves and slopes of the curves of blank (without zDHHC20), zDHHC20 with or without 1-hour preincubation at 37 ˚C in reaction buffer. Data represent the mean ± standard deviation (*n=2*).

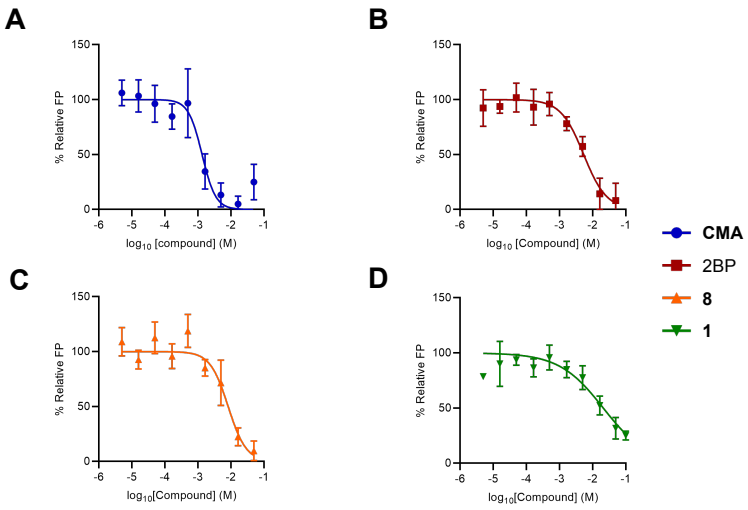

E

Compound	IC_{50} (μM)
CMA	1.35 ± 0.26
2BP	5.33 ± 0.77
8	8.32 ± 2.25
1	21.4 ± 5.9

Figure 2.S3. Inhibition of zDHHC20 *in vitro*. Dose-response curves of (A) CMA (blue), (B) 2BP (red), (C) 8 (orange), and (D) 1 (green) on zDHHC20 measured by the FP assay. Data represent mean ± standard deviation (*n=3*). (E) The IC_{50} values were calculated from a four-parameter dose-response curve.

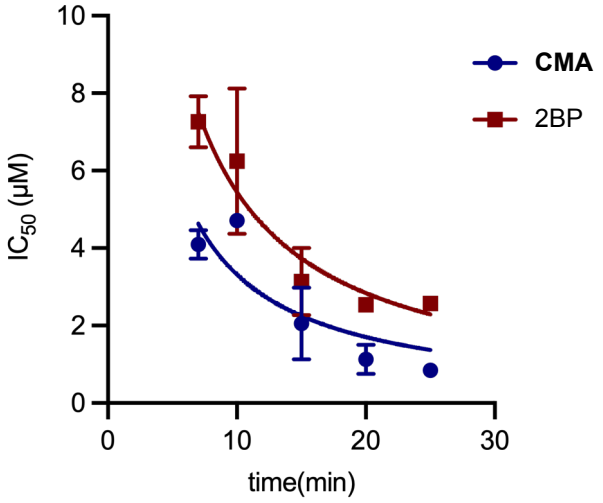

	k_{inact} (min^{-1})	K_I (μM)
CMA	2.08	5.8
2BP	1.35	6.4

Figure 2.S4. IC_{50} of CMA and 2BP with different preincubation times (7, 10, 15, 20, and 25 min.). ZDHHC20's K_M for palmitoyl-CoA is reported to be 0.58 μM[106] and thus is used here for curve fitting. The final concentrations of the FAM-NRas peptide and palmitoyl-CoA are 4 μM and 1.25 μM, respectively. A detailed protocol for curve fitting can be found in the Methods. Data represent mean ± standard deviation (*n=2*).

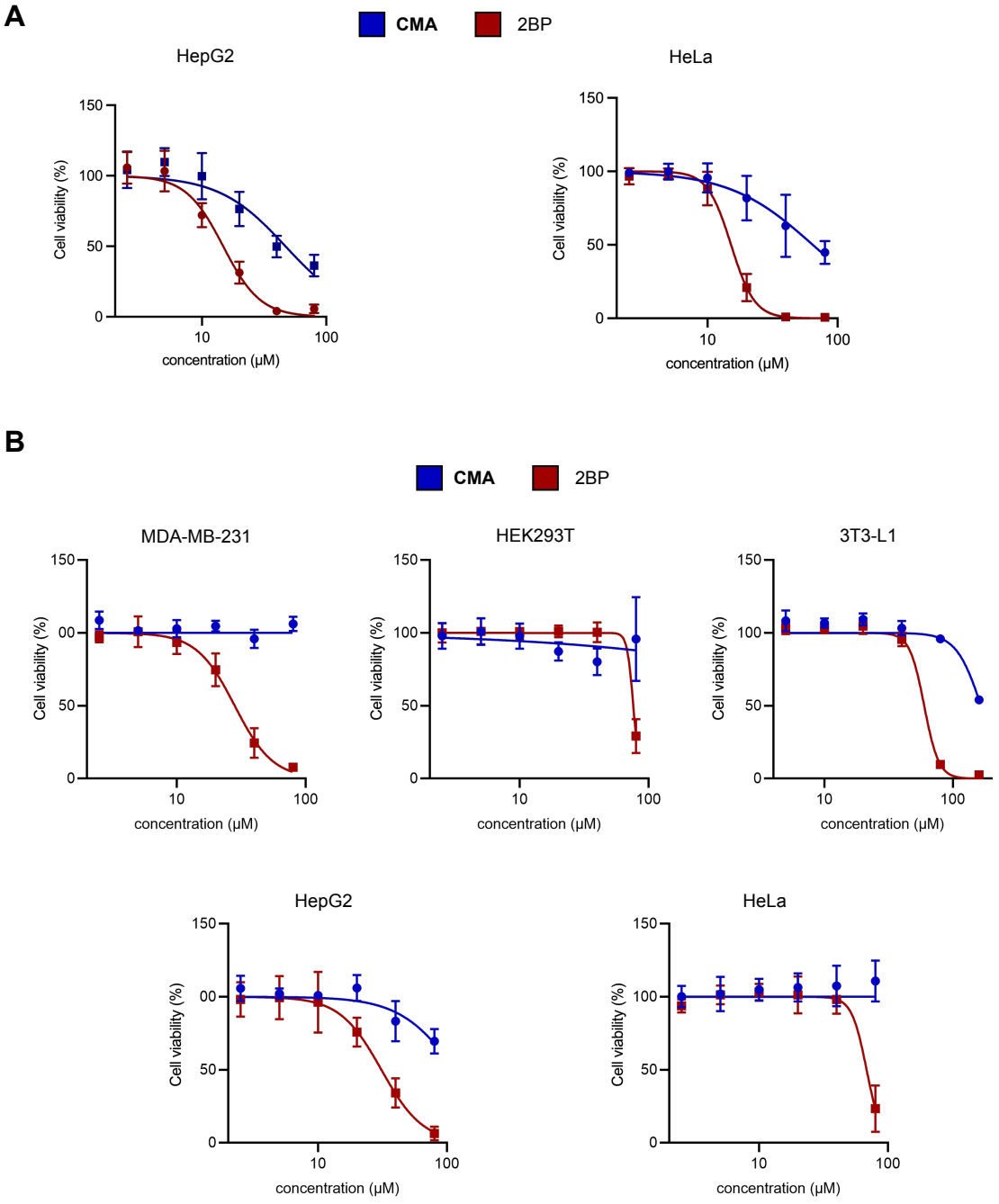

Figure 2.S5. CMA and 2BP cell viability assays. (A) Dose-response curves for MTS cell viability assay after 24 hours of treatment in serum-free media with CMA (blue) or 2BP (red) treatment in HepG2 cells and HeLa cells. (B) Dose-response curves for MTS cell viability assay after 6 hours of treatment in serum-free media with CMA (blue) or 2BP (red) treatment in HEK293T, MDA-MB-231, 3T3-L1, HepG2, and HeLa cells. Data represent mean ± standard deviation (*n=2 for 24 hours treatment; n=3 for 6 hours treatment*)

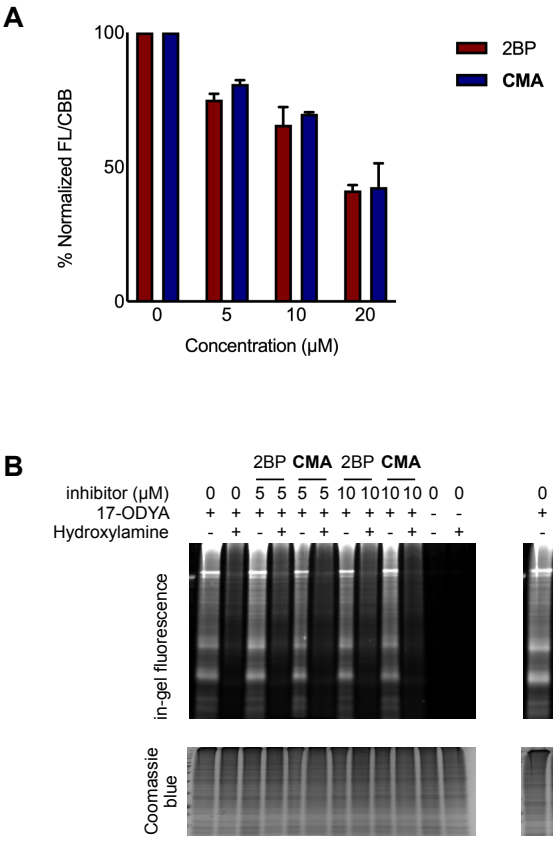

Figure 2.S6. CMA and 2BP global acylation changes. (A) Quantification of the effect of CMA (blue) or 2BP (red) with 3 hours pretreatment on global *S*-acylation levels with 6 hours of 17-ODYA metabolic labeling in serum-free media. Data represent mean ± standard deviation (*n=2*). (B) The effect of CMA or 2BP (1 hour pretreatment) on global *S*-acylation levels using 6 hours 17-ODYA metabolic labeling in serum-free media. HA was used to cleave thioester bond. TAMRA-azide was conjugated to 17-ODYA-labeled species via Cu-AAC click reaction. Quantification was done using ImageJ. (FL)/Coumassie Blue (CBB) staining ratios normalized to DMSO.

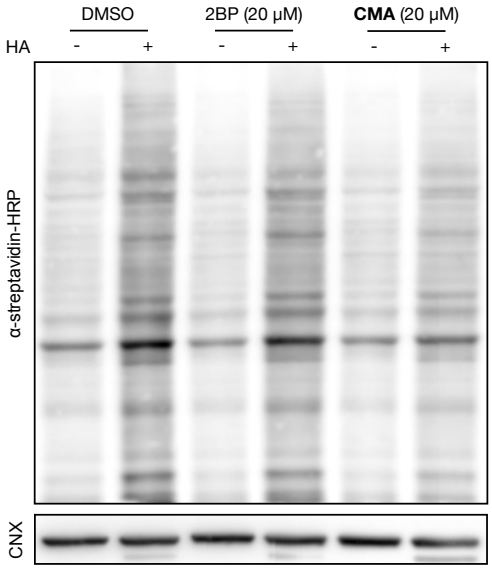

Figure 2.S7. Global ABE of HEK293T cells treated with CMA or 2BP (20 μM, 6 hours) in serum-free media. Global *S*-acylation was visualized using streptavidin-HRP without enrichment (*n=2*).

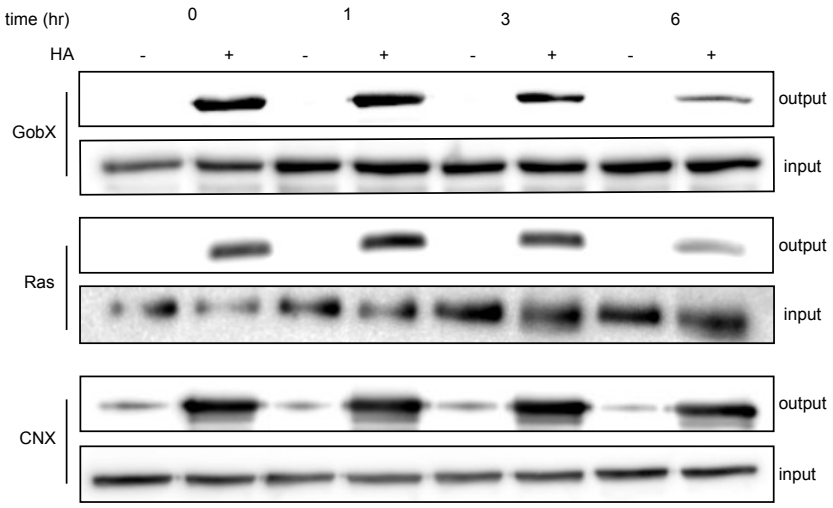

Figure 2.S8. Timecourse of changes in the *S*-acylation of exogenous GobX and endogenous Ras in HEK293T cells upon 20 μM CMA treatment in serum-free media as measured by ABE. α-CANX Western blotting was used as an assay and loading control (*n=2*).

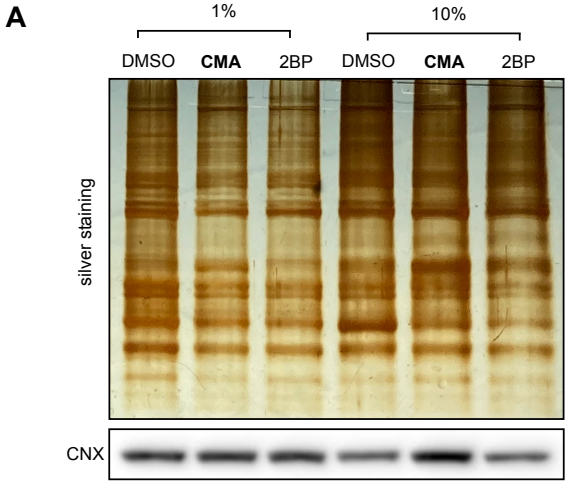

Figure 2.S9. Serum affects global acylation changes with inhibitor treatment. (A) Global change in *S*-acylation upon CMA and 2BP treatment in media with 1 and 10% FBS (20 μM, 6 hours) visualized by silver staining after streptavidin agarose enrichment. (B) The effect of serum (0%, 0.1%, 1%, and 10% FBS) on CMA and 2BP inhibition of exogenous GobX *S*-acylation in HEK293T cells after 6 hours of treatment. α-CANX Western blotting was used as

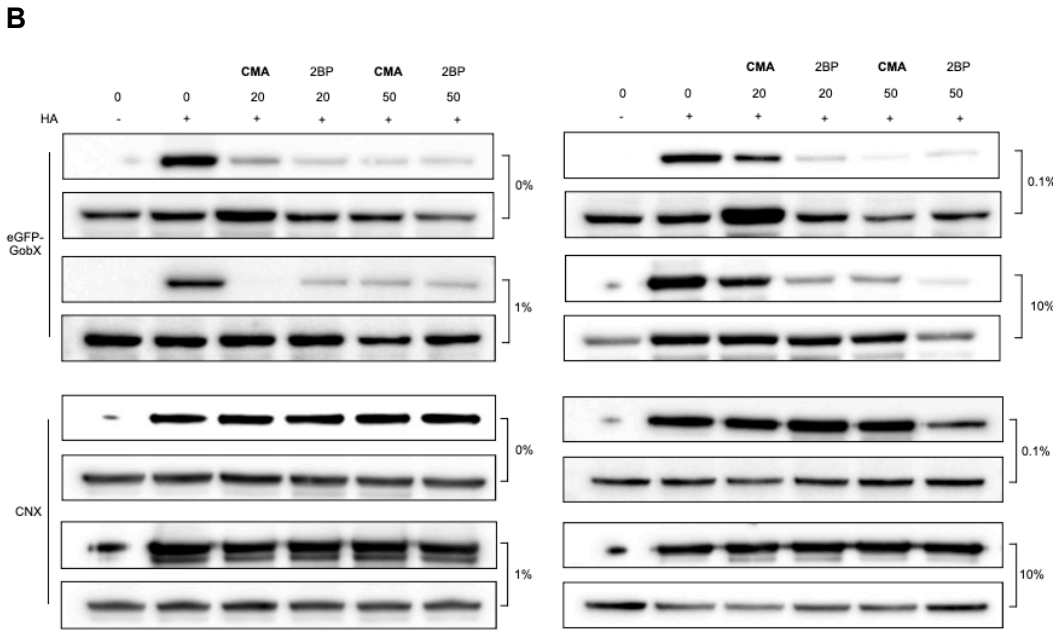

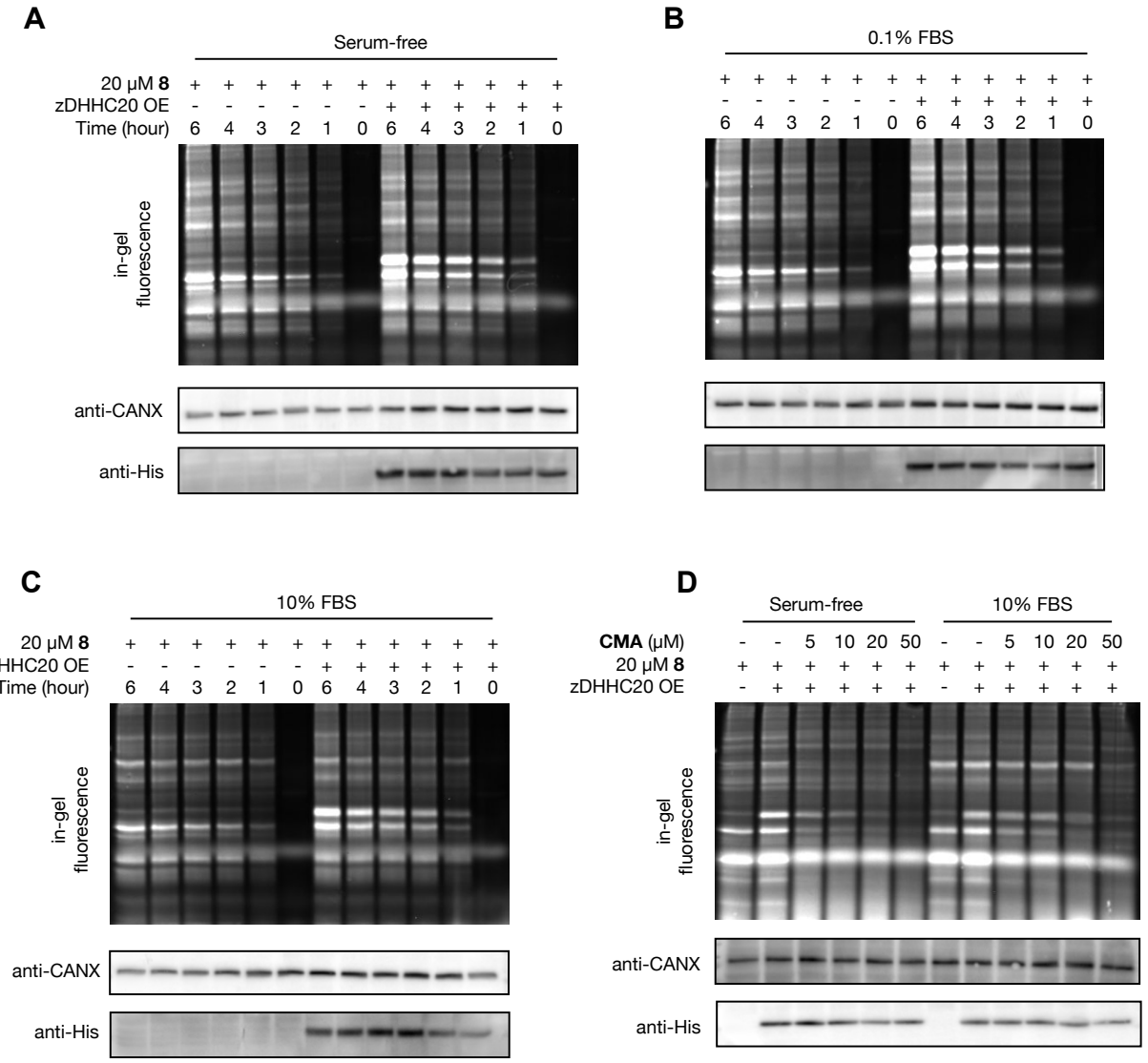

Figure 2.S10. The *in cellulo* time-course labeling of 8 (20 μM) in media with (A) serum-free, (B) 1% FBS, or (C) 10% FBS in non-transfected or overexpressing zDHHC20 HEK293T. (D) The *in cellulo* target engagement of CMA in media with or without serum in non-transfected or overexpressing zDHHC20 HEK293T. TAMRA-azide was conjugated to 8-labeled species via Cu-AAC click reaction, thus 8's labeling intensity was visualized by in-gel fluorescence. α-His Western blotting (WB) was used to verify zDHHC20 expression levels and α-CANX Western blotting was used as loading control (*n=2*).

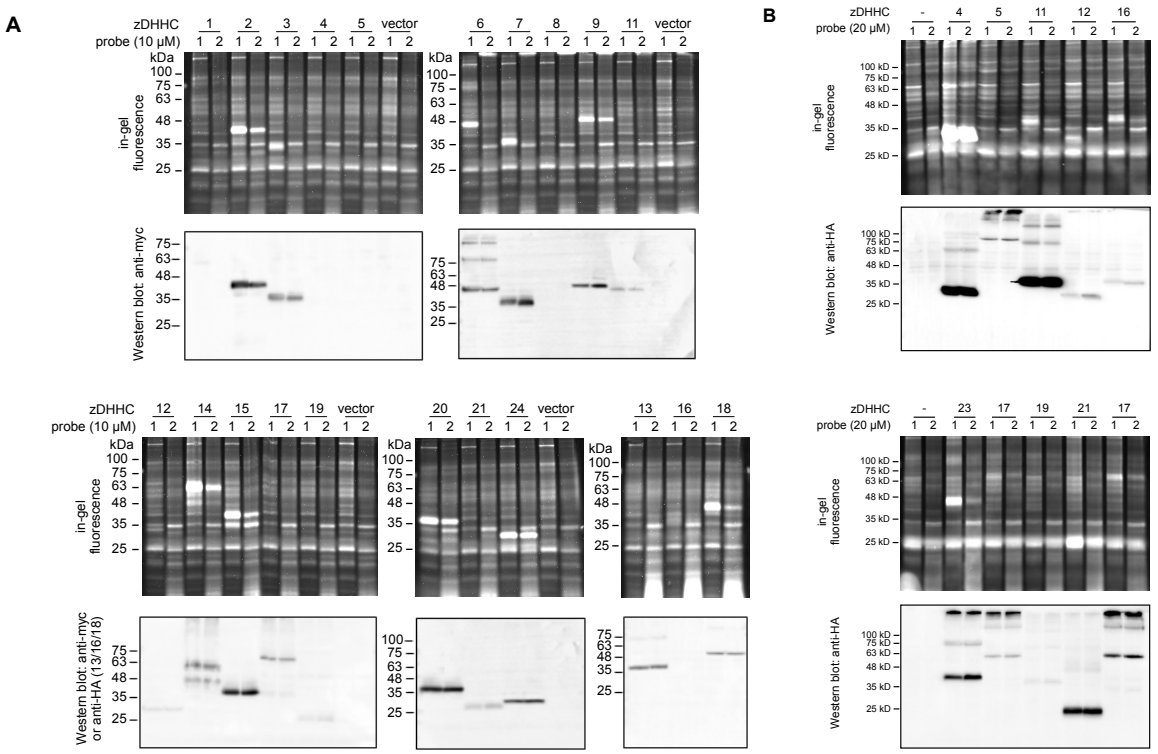

Figure 2.S11. In-gel fluorescence analysis of 16C-BYA (1) and 8 (2) labeling of (A) human and (B) mouse DHHC family proteins in serum-free media, following TAMRA-azide conjugation to 8 and 16C-BYA labeled species via Cu-AAC click reaction HEK293T cells overexpressing a DHHC protein were treated with either 16C-BYA or 8 (10 μM, 2 hours in (A), 20 μM, 2 hours in (B)). α-Myc (human zDHHCs) or α-HA (mouse zDHHCs) Western blotting was used to verify the expression and size of DHHC proteins (*n=1*).

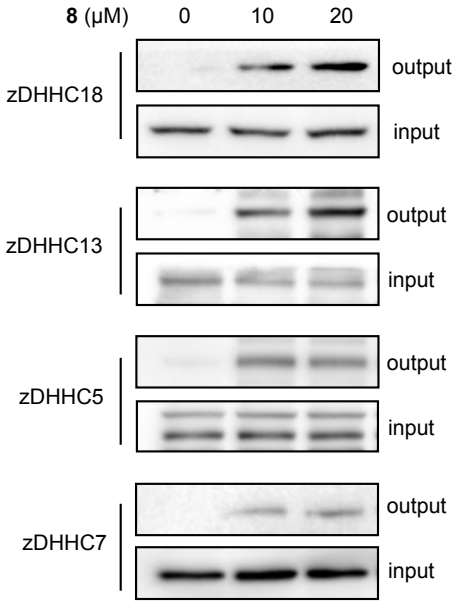

Figure 2.S12. 8 labeling (3 hours) of endogenous DHHC proteins zDHHC5, 7, 13, and 18 in HEK293T cells in serum-free media. The labelled proteins were conjugated with biotin-azide followed by enrichment using streptavidin agarose. The zDHHC proteins before enrichment ('input') and enriched zDHHC proteins ('output') were visualized via Western blot (*n=2*).

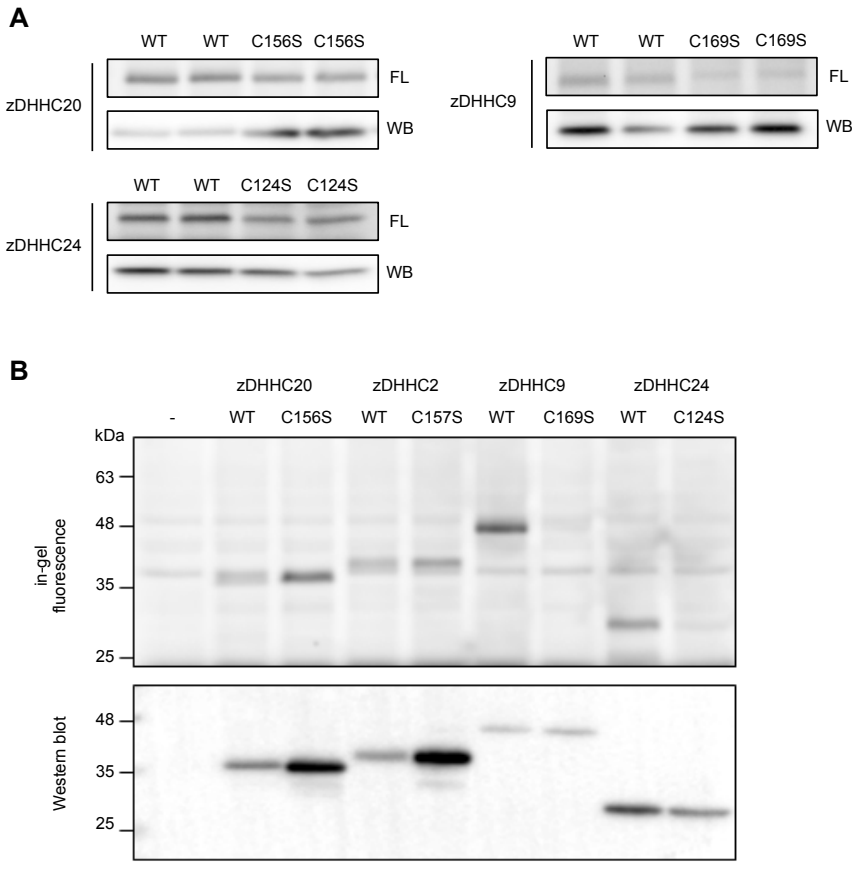

Figure 2.S13. In-gel fluorescence analysis of 8 and 16C-BYA labeling of a selection of human DHHC proteins and their DHHS mutants in serum-free media. (A) 8 (1 μM, 2 hours) labeling in HEK293T cells overexpressing either WT or DHHS zDHHC20, 9, or 24; (B) 16C-BYA (1 μM, 2 hours) labeling on HEK293T cells overexpressing either WT or DHHS zDHHC20, 2, 9 or 24. TAMRA-azide was conjugated to 8/16C-BYA-labeled species via Cu-AAC click reaction. α-Myc Western blotting was used to verify expression and size. (FL, in-gel fluorescence; WB, Western blot, *n=2*)

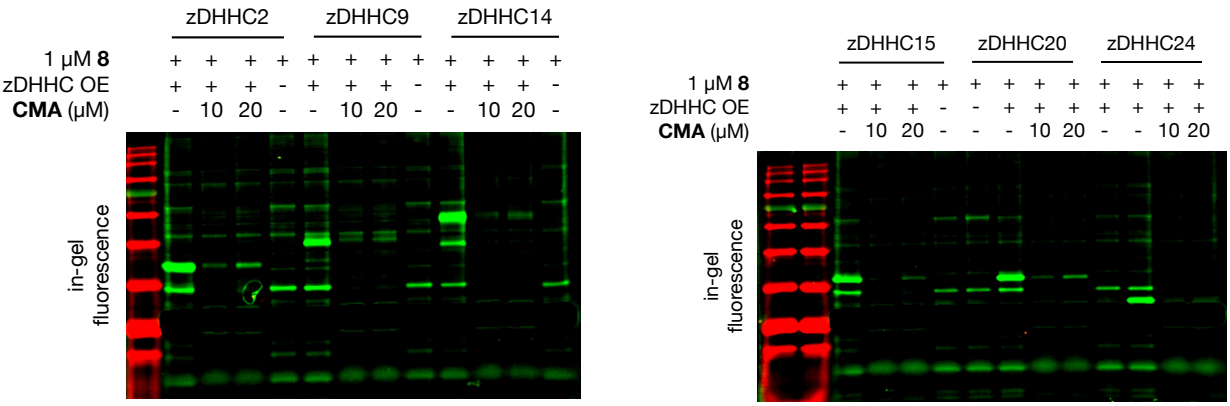

Figure 2.S14. The raw fluorescence image for the data shown in Figure 3A

A

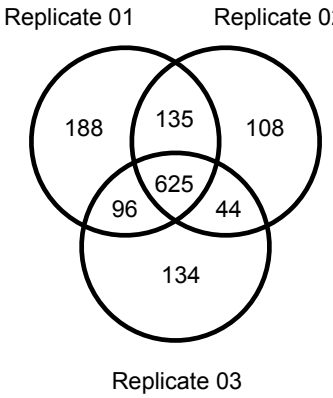

B

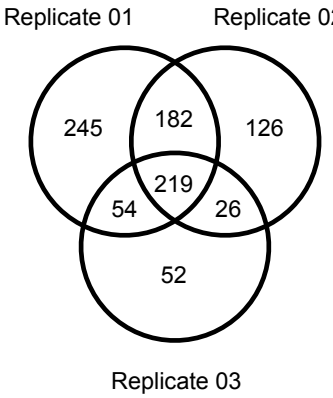

C

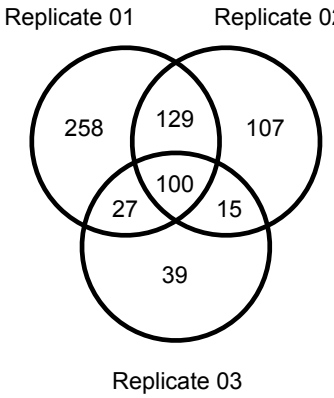

D

Protein names	Gene name	1_8/DMSO	2_8/DMSO	3_8/DMSO
Chitobiosyldiphosphodolichol beta-mannosyltransferase	ALG1	71.075	13.6308493	12.694
Threonylcarbamoyladenosine tRNA methylthiotransferase	CDKAL1	58.412	11.3351696	7.3053
Neutral cholesterol ester hydrolase 1	NCEH1	38.093	7.51992781	11.292
Rab GDP dissociation inhibitor beta	GDI2	39.077	5.4312405	4.3189
Redox-regulatory protein FAM213A	FAM213A	22.452	12.7985256	13.026
Reticulon-4	RTN4	20.146	18.030038	10.058
Receptor expression-enhancing protein 5	REEP5	20.266	16.5081881	11.419
Reticulon-3	RTN3	22.226	13.0601157	12.72
PRA1 family protein 2	PRAF2	25.018	10.7743527	11.15
Up-regulated during skeletal muscle growth protein 5	USMG5	21.551	15.1446312	8.6309

Figure 2.S15. Proteomic profiling and analysis of 20 μM **8** labeling in HEK293T cells. (A) Venn diagram of the overlaps between proteins whose **8**/DMSO ratio is above (A) 2, (B) 4, or (C) 5 that quantified in three independent experiments. (B) The list of top 10 most enriched proteins by **8**.

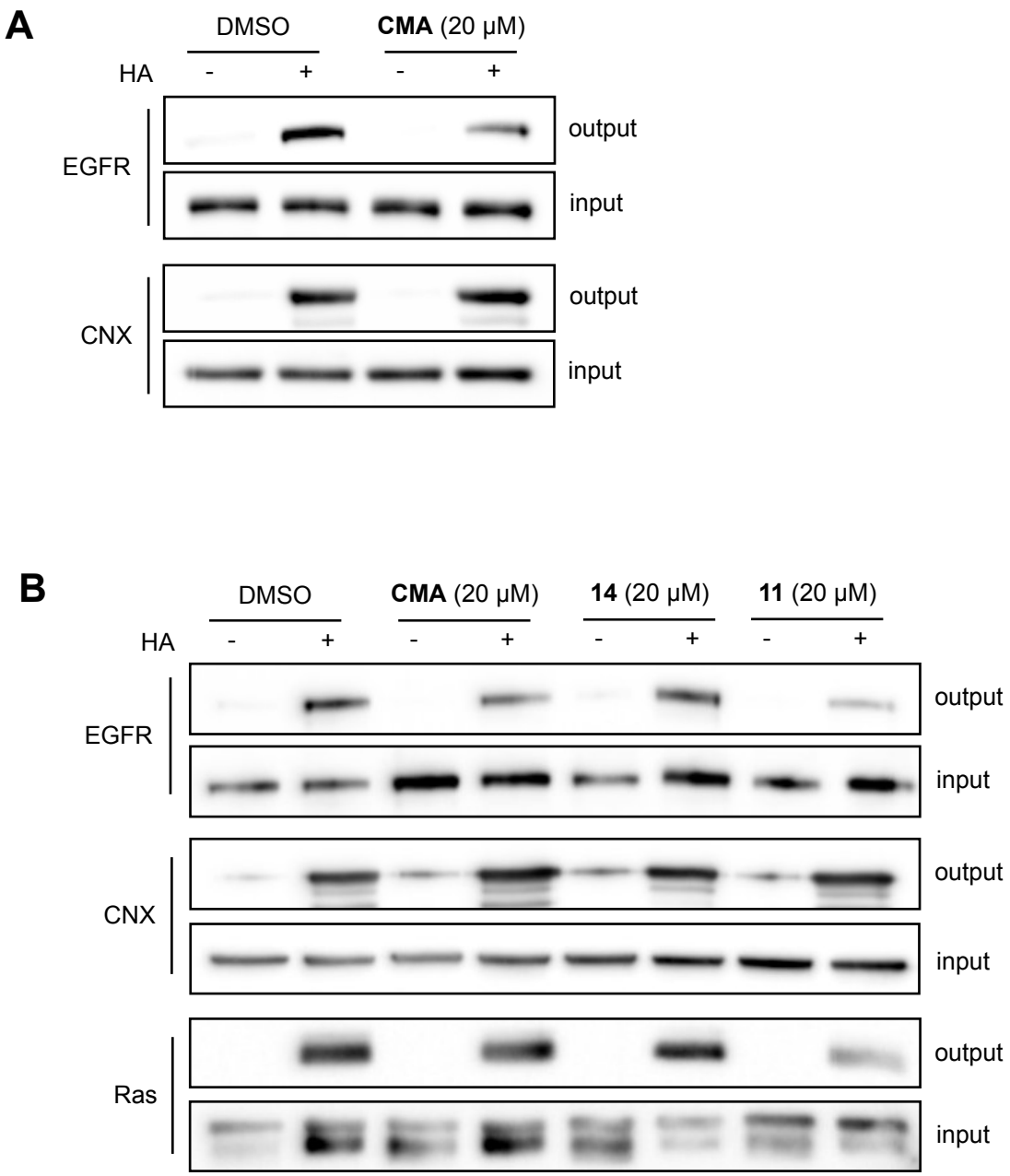

Figure 2.S16. EGFR acylation and CMA treatment. (A) Analysis of EGFR *S*-acylation via ABE upon CMA treatment (20 μM, 6 hours) in MDA-MB-231 cells (*n=3*). (B) Analysis of EGFR *S*-acylation via ABE after treatment with **CMA**, **11** or **14** (20 μM, 3 hours) in MDA-MB-231 cells (*n=1*).

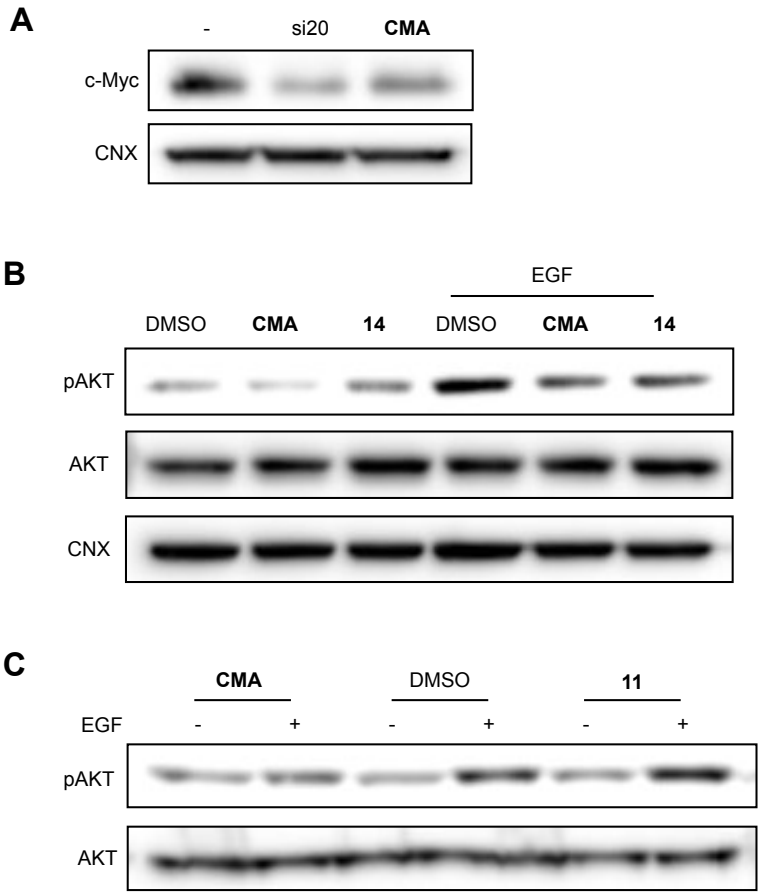

Figure 2.S17. Treatment with CMA and control molecules yields different downstream effects. (A) Expression of c-Myc upon treatment with DMSO, siRNA-mediated zDHHC20 knockdown, or treatment with CMA (20 μM, 6 hours) in serum-free media in MDA-MB-231 cells. (B) (C) Changes in AKT phosphorylation with (B) 14 or (C) 11 treatment in serum-free media in MDA-MB-231 cells. Calnexin (CNX) and AKT Western blotting were used as loading controls for total protein and AKT, respectively (*n=2*).

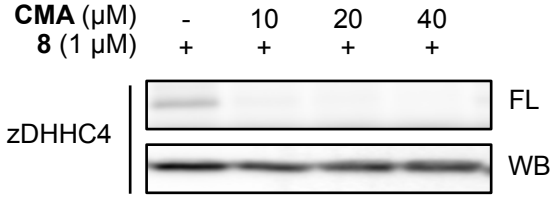

Figure S18. In-gel fluorescence (FL) analysis of target engagement of CMA with mouse zDHHC4. HEK293T cells expressing HA-tagged mouse zDHHC4 were treated with 0, 10, 20, or 40 μM of CMA (2 hours) and chased with 8 (1 μM, 2 hours) in serum-free media. TAMRA-azide was conjugated to 8-labeled species via Cu-AAC click reaction, thus 8's labeling intensity on overexpressed zDHHC4 was visualized by in-gel fluorescence. α-HA Western blotting (WB) was used to verify zDHHC4 expression levels (*n=2*).

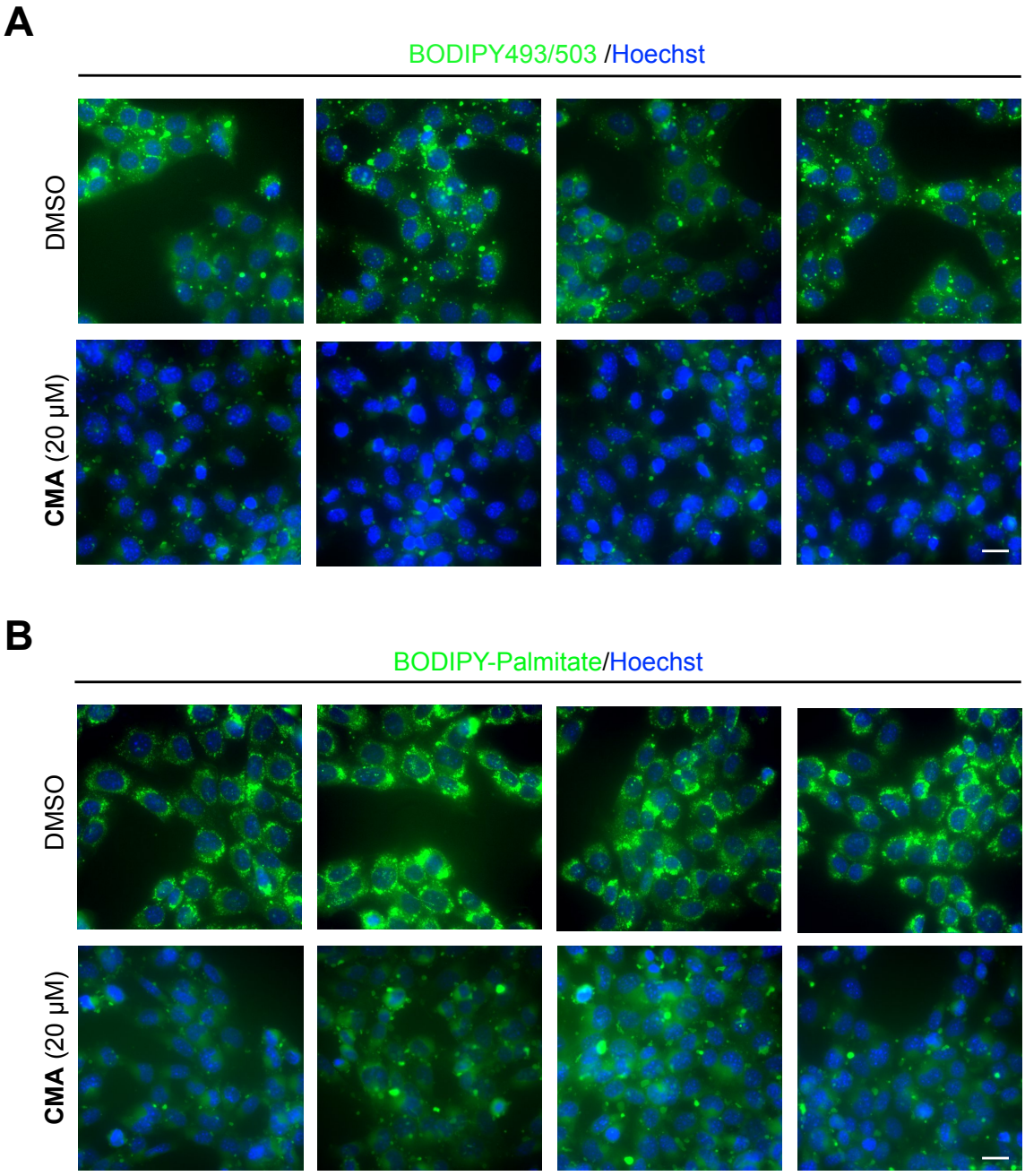

Figure 2.S19. Representative fluorescence microscopy images of the effect of CMA on lipid droplet formation and lipid uptake in 3T3-L1 preadipocytes. Cells were starved (12 hours) and treated with DMSO or CMA (20 μM, 3 hours) and then with 10 μM BSA-bound oleate and 2 μM (A) BODIPY493/503 or (B) BODIPY-palmitate (6 hours). Images represent replicates of the data shown in Figure 4D. Scale bar = 20 μM.

Table 2.S1. Antibodies used in this work

Protein	Species	Cat. No. (company)
HA-tag (F-7)	Mouse	SC-7392 (Santa Cruz)
EGFP	Mouse	MA1-952 (Invitrogen)
RAS	Mouse	05-516 (EMD Millipore)
Calnexin	Rabbit	AB22595 (Abcam)
C-Myc (9E10)	Mouse	Sc40 (Santa Cruz)
C-Myc	Rabbit	D84C12 (Cell Signaling Technology)
ZDHHC5	Rabbit	HPA014670 (Sigma)
ZDHHC18	Rabbit	AB154790 (Abcam)
ZDHHC13	Goat	AB28759 (Abcam)
ZDHHC7	Rabbit	AB138210 (Abcam)
CD36	Rabbit	AB133625 (Abcam)
EGF Receptor	Rabbit	2232S (Cell Signaling Technology)
AKT	Mouse	SC82434 (Santa Cruz)
p-AKT (S473)	Rabbit	9271S (Cell Signaling Technology)
m-IgGkappaBP-HRP	-	SC516102 (Santa Cruz)
Anti-rabbit lgG-HRP	-	7074S (Cell Signaling Technology)
Anti-goat lgG-HRP	-	AB205723 (Abcam)
Streptavidin-HRP	-	3999S (Cell Signaling Technology)
His-HRP	-	SC-8036 (Santa Cruz)

Chapter 3: A structure-activity study of CMA

3.1. Introduction

Termed *S*-acylation, the addition of a fatty acid to cysteine thiols is a post translational modification (PTM) noteworthy for its ability to regulate protein activity and function. The increase in hydrophobic character conferred by the lipid, often the 16C palmitate, is known to have diverse effects on target proteins, affecting the subcellular trafficking of the small GTPase Ras, the dimerization of the transcription factor RFX3, and the stability of neurotransmitter pump dopamine transporter DAT. Central to its regulatory ability is its enzymatic reversibility, with the addition of palmitate catalyzed by the palmitoyl acyl transferases (PATs). Conserved from yeast to humans, this family of proteins possesses an aspartate–histidine–histidine–cysteine "DHHC" motif and has been associated with or directly linked to a variety of pathological conditions, including cancers, autoimmune disease, and neurodegenerative disease.

While our understanding of DHHCs and the significance of their role in regulating substrate *S*-acylation has increased in recent years, our ability to probe the functional roles of the 23 individual mammalian family members remains limited. While classic genetic tools can be employed, functional redundancy between DHHCs and inter-family regulation often results in compensatory effects that obscure both molecular mechanisms and cellular phenotypes. Chemical inhibitors, which can rapidly impede protein activity, represent a promising approach for the study of this family. However, to-date, only pan-inhibitors with limited potency and selectivity have been identified. The lack of isoform specificity not only precludes the study of individual DHHC proteins, it also limits the utility of these molecules as potential therapeutics, given that individual DHHC family members can modulate diverse and sometimes opposing cellular pathways. For

example, DHHC-mediated acylation can regulate both important oncogenes (e.g., NRAS, EGFR) and tumor suppressors (e.g., SCRIB, MC1R).

We recently reported the discovery of cyano-myracrylamide (CMA) as a broad-spectrum inhibitor of DHHC family proteins. While offering several improvements over 2BP, the standard inhibitor in the field, this molecule is still limited by off-target interactions. Here, we report the synthesis of an extended panel of CMA-based molecules. While our studies indicate that substitution of the acyl chain remains a challenge, we show that modification of warhead terminus has the potential to increase interactions with the DHHC protein without loss of potency.

3.2. Results

DHHC-catalyzed *S*-acylation is thought to proceed via two steps: reaction with an acyl coenzyme A (CoA) donor and formation of an acyl:DHHC intermediate, followed by transfer of the lipid from the DHHC cysteine to a protein substrate. Central to this mechanism are the lipid-binding and reactivity of the active site thiol, both of which were targeted by our previously reported lipid-acrylamide inhibitor, CMA. Despite some improvements in potency and selectivity, proteomic analysis of the interactions of 8, an alkyne derivative, revealed that CMA interacted with ~200 proteins - over 75% of which are annotated as acylated proteins. These results underscore the disadvantage of aliphatic chains, which are thought to lead to numerous off-targets in cells. Therefore, we first targeted the acyl chain in hopes of creating a compound with improved lipophilicity, as measured by the partition coefficient (logP), and increased potency.

As initial studies with 2 indicated that shortening of the acyl chain would dramatically decrease a molecule's efficacy against DHHC20, we first aimed to substitute the acyl chain with pseudo-bioisosteres. We hoped that exchange of the aliphatic chemical motif with another uncharged chain possessing broadly similar properties would maintain its inhibitory capability.

Therefore, we appended a series of biphenyl and methylated biphenyl groups to both the acrylamide warhead of 1 and the cyano-methyl substituted warhead of CMA (Figure 3.1). Screening of these molecules against DHHC20 revealed that loss of the acyl chain abrogated the activity of all molecules (Figure 3.2). Positing that the rigidity of these structures impeded their reactivity, we next synthesized bibenzyl (SA45) and phenethylpiperidine (SA79) derivatives; again, screening indicated little to no inhibitory activity. To further probe the sensitivity of the lipid tail, we next exchanged a methylene group of the aliphatic chain with an oxygen (SA20). Happily, this heteroatom substitution resulted in a molecule with both a potency on par with CMA (IC_{50} = 1.97 ± 0.67 μM) and an improved logP of 4.10, relative to CMA at 5.48. However, this molecule was also resistant to acyl chain shortening, as seen with SA23 (Figure 3.2). Thus, it appears that sterics, conformational flexibility, loss of lipophilicity, or a combination thereof preclude the binding of this acrylamide-based scaffold to DHHC family proteins.

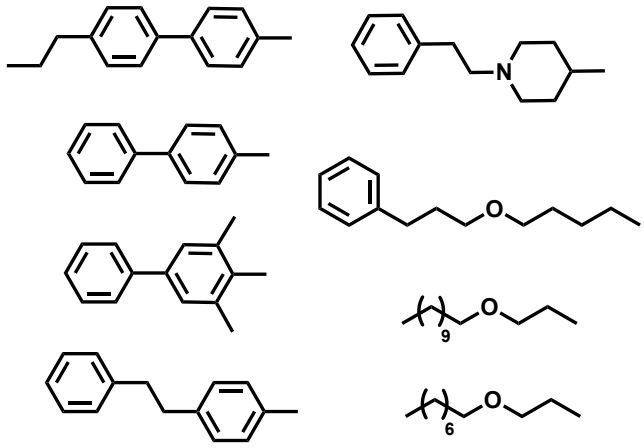

Figure 3.1. Aliphatic chain substitutions of lipid acrylamides CMA and 1.

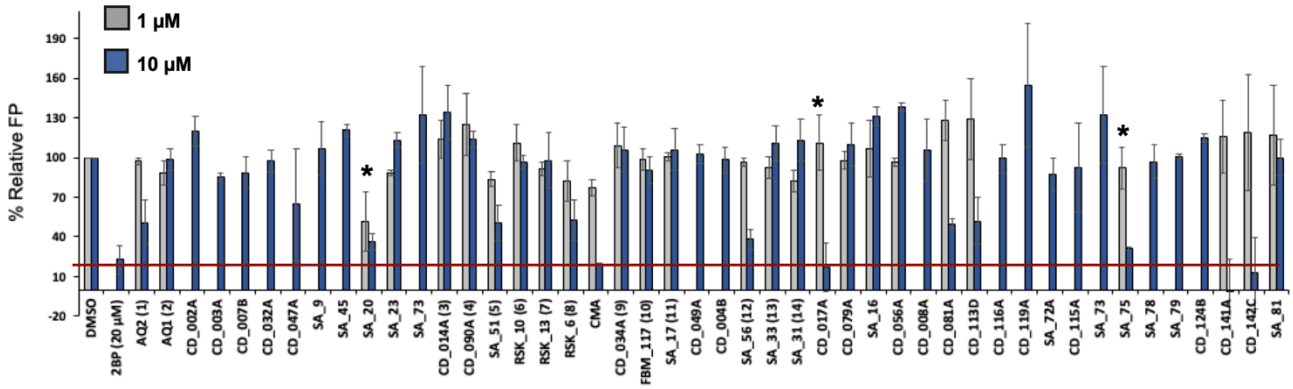

Figure 3.2. Screening of acrylamide library against human zDHHC20 using a fluorescence polarization (FP) assay.

As no improvement in activity or logP could be achieved via modification of the lipid tail, we next turned to modification of the warhead. Notably, the native substrate of DHHC proteins is an acyl-CoA, and so these enzymes feature not only a lipid-binding domain, but also a charged ADP-binding pocket. We hypothesized that extension of this warhead could increase protein contacts and perhaps even interaction with the ADP-binding site, thereby increasing the potency of this scaffold while also diminishing off-target interactions. To explore this potential, we used the previously described butenoic acid derivative of 1, which possesses a more reactive acrylamide and an acid for suitable for modification, as a starting point. Here, while we observed a slight improvement in the potency of the methyl ester derivative, it was CD_017 and SA75 that were significantly active. Further analysis demonstrated that these two molecules, which possess either an alkyne (CD_017) and methyl cyano ester (SA75), had IC_{50} values against DHHC20 on par with CMA (Figure 3.3). Given the potential of the alkyne for both utilization as an activity-based profiling probe and extension of the inhibitor scaffold, we decided to explore derivatives of this scaffold further. Strikingly, the *E* isomer of CD_017 displayed no activity against DHHC20 (Figure 3.2). In addition, exchange of the ester for an amide – an attempt to improve *in cellulo* stability – also resulted in a loss of activity against zDHHC20. Thus, CD_17 itself emerged as our new synthetic focal point.

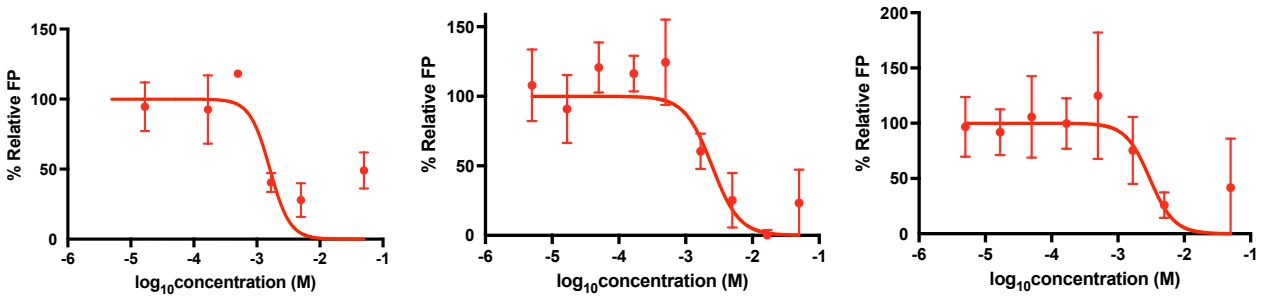

Figure 3.3. Plots of IC_{50} curves for SA20, SA75, and CD_17A, giving values of 1.97 ± 0.67 μM, 3.43 ± 0.15 μM, and 2.87 ± 0.57 μM, respectively.

As mentioned, the native substrate of DHHC family proteins is an acyl-CoA. The CoA moiety can be divided into three parts: a cysteamine linkage, pantothenic acid, and a 3'phosphoadenosine diphosphate group. As our acrylamide warhead mimicked the cysteamine linkage, we next aimed to add an additional CoA element, the pantothenic acid. Here, we exploited the presence of the alkyne, using click chemistry to attach pantothenic acid via a tetrazole linker. The resulting molecule, CD_142, retained inhibitory activity against DHHC20. When the pantothenic acid linker was exchanged for a PEG-4 linker (CD_141), activity was also retained, validating the further extension of this scaffold with the readily synthesizable and solubilizing PEG linker. Notably, click analogues with smaller linkers possessing either an H-bond donors or acceptors are inactive against DHHC20, suggesting that close substrate mimetics are needed (Figure 3.2). Overall, these results validate the extended scaffolds of CD_142 and CD_141 and suggest that coupling to the 3'phosphoadenosine diphosphate group could yield a more potent and more selective molecules.

3.3. Discussion

Overall, these results reveal both the challenges of exchanging the acyl chain and the potential of extending the warhead. The structure-activity relationship study on both CMA and 1 led to the identification of SA20, which offers a slight improvement of the lipophilicity of the molecule, and CD_017 and SA75, which offer possibilities for further derivatization (Figure 3.4). In particular, the derivative of CD_017, CD_141, which mimics the native palmitoyl CoA ligand via addition of the pantothenic acid, opens the door to possibility of accessing the ADP-binding pocket of DHHCs. Furthermore, this compound can be further modified 3'phosphoadenosine diphosphate to give a stronger substrate mimetic, while a heteroatom could be inserted into its acyl chain a la SA20 to improve its lipophilicity. Finally, while much of this acrylamide library displayed limited inhibition of DHHC20, it is possible that these molecules will possess greater reactivity against

other DHHCs. Besides the conserved cysteine-rich domain (CRD), DHHC family proteins display little sequence homology, possessing different protein-binding domains (eg, PDZ) and variable numbers of transmembrane domains. These structural differences could lead to differences in the potency of inhibitors. Thus, we aim to screen this library of inhibitors against zDHHC proteins with little sequence homology to 20, such as zDHHC3. The identification of an isoform specific inhibitor, especially for zDHHC3 with its numerous roles in neurobiology, represents an exciting possibility

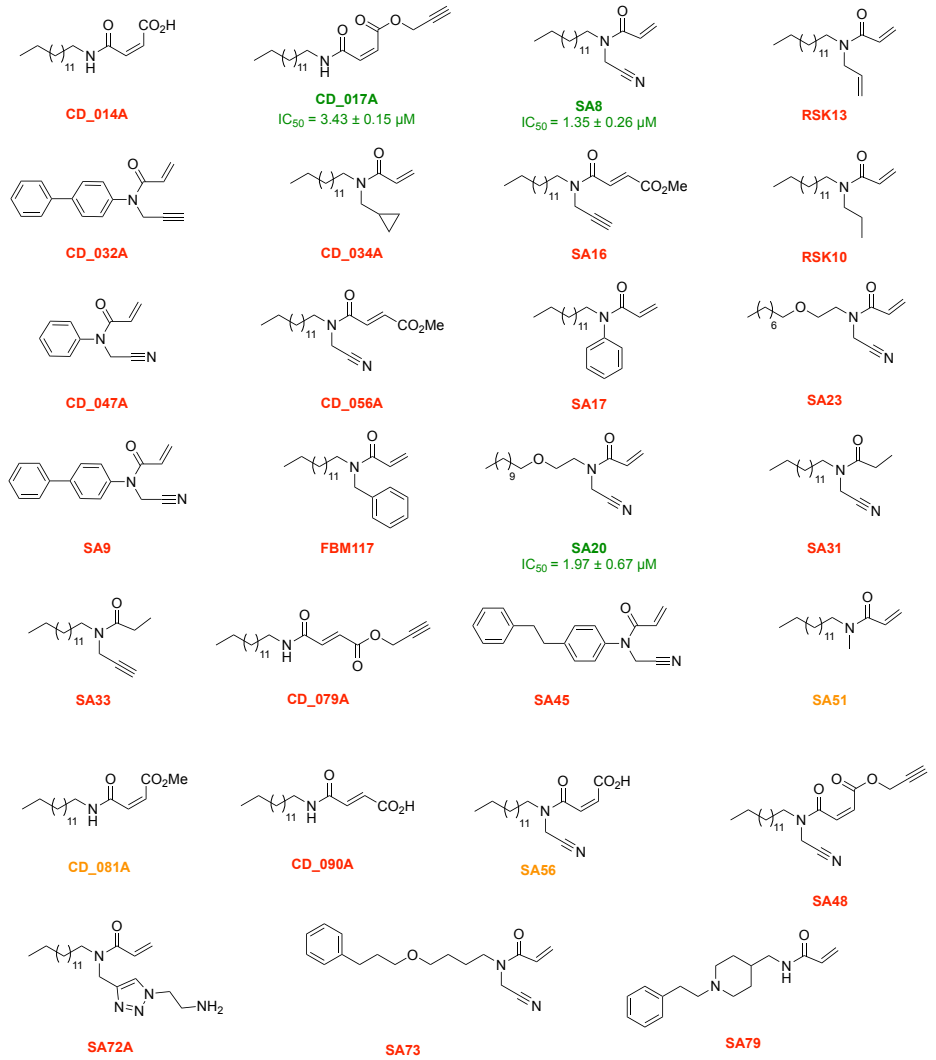

Figure 3.4. Partial library of CMA derivatives to be screened DHHC family proteins.

Chapter 4: A high-throughput fluorescent assay for the identification of DHHC family inhibitors

4.1. Introduction

The addition of a long chain fatty acid to a protein, termed *S*-acylation or *S*-palmitoylation given the frequent occurrence of the C16:0 lipid, is an abundant and important post-translational modification (PTM).[25] Modifying substrates from scaffolding and signaling proteins to ion channels and receptors, *S*-acylation can influence protein activity, stability, interactions, and subcellular trafficking.[106, 107] Critically, it is dynamic and enzymatically regulated, mediated by 23 zDHHC (zinc finger Asp-His-His-Cys) domain-containing "writer" protein acyltransferases (PATs) and serine hydrolase family "eraser" acyl protein thioesterases (APTs), including APT1/2, PPT1/2, ABHD17A/B/C, and ABHD10.[12, 14-16, 70, 76]

In recent years, an appreciation of DHHCs and APTs not only as regulators of the cycle of acylation/deacylation and subsequent protein behaviors, but also as targets for the mitigation of human pathologies, has emerged. For example, the palmitoylation and depalmitoylation of N-Ras by zDHHC9 and ABHD17, respectively, drive its activation and signal propagation in growth factor signaling and therefore could be targeted in N-Ras-dependent cancers.[70, 108] Perturbing the palmitoylation cycle of STAT3 by inhibiting either zDHHC7 or APT2 activity can preclude T_H17 cell differentiation and reduce symptoms of inflammatory bowel disease.[109] Additionally, zDHHC20 activity has been implicated in cellular transformation and lung tumorigenesis via regulation of epidermal growth factor receptor (EGFR) signaling, while zDHHC9 is upregulated in colorectal cancer.[35, 36] Thus, disruption of acylation regulation represents an emerging strategy for the treatment of disease.

However, while potent pan and isoform-specific *S*-deacylase inhibitors exist, parallel tools – much less ones with clinical potential – for the DHHC-PATs remain scant. 2-Bromopalmitate (2BP) is the most commonly used DHHC inhibitor, but low potency, high cytotoxicity, and poor selectivity significantly curtail its applications.[72] Our lab has recently developed an acrylamide-based zDHHC inhibitor, CMA, which has decreased cytotoxicity and an altered reactivity profile as compared to 2BP. However, CMA targets a broad spectrum of zDHHC family proteins, making it unsuitable for probing the biology of individual zDHHCs.[110] In order to disentangle the functions of DHHC proteins, new zDHHC-isoform specific inhibitors are needed.

A central challenge in the identification and development of new zDHHC inhibitors is the lack of a truly robust high-throughput screening (HTS) assay. Alkyne or isotope labeled palmitoyl-CoA can be used to assess DHHC transferase activity *in vitro*, but such assays require multiple processing steps and can be difficult to apply in a high-throughput manner.[111] While the coupled enzyme assay, which detects the release of CoA during the palmitoyl transfer process, is fluorescence-based and therefore suitable for a HTS, the indirect readout renders it prone to false positives.[112] Most recently, our lab has successfully adapted the acylation-coupled lipophilic induction of polarization (Acyl-cLIP) assay for zDHHC20.[94] Here, a fluorophore-labeled peptide is palmitoylated by a zDHHC enzyme and inserted into detergent micelles, resulting in a change in fluorescence polarization (FP). However, the dynamic range of this assay is limited, and it also requires a specific peptide for each DHHC isoform.

Here, we report the development of a fluorescence-based high-throughput assay for DHHC activity *in vitro* using a panel of fluorogenic probes. These palmitoyl-CoA mimetic probes are recognized and cleaved by the DHHC family proteins, with palmitoyl thioester bond hydrolysis triggering the release of fluorophore. The resulting fluorescence provides a direct, sensitive, and

simple readout of enzyme activity. We validate the assay with three zDHHCs (2, 3, and 20) and establish its suitability for a high throughput screen. We then screen a library of ~1,000 molecules against zDHHC20, identifying certain compounds as inhibitory scaffolds for zDHHC20 *in vitro* to be corroborated *in cellulo*.

4.2. Results and discussion

DHHC catalysis of protein S-acylation is thought to occur via a two-step mechanism.[113] First, the active site cysteine of the signature DHHC motif is auto-acylated by an acyl CoA donor, resulting in an acyl:DHHC intermediate. Then, the acyl moiety is transferred from the DHHC cysteine to a protein substrate. In designing a probe for DHHC activity, we sought to exploit the DHHC recognition of the acyl (frequently palmitoyl) CoA donor (Figure 4.1). Our lab has previously reported depalmitoylation probes (DPPs), whose deacylation results in thiol-initiated cleavage of the carbamate linker and release of the fluorescent product.[21, 114] Intriguingly, we observed that the structure of DPP5 shares some similarities with palmitoyl CoA, namely a palmitoyl chain, a cysteamine, and a negatively charged terminal group – leading us to posit that this probe could be recognized by DHHC family proteins and serve as a starting scaffold for a

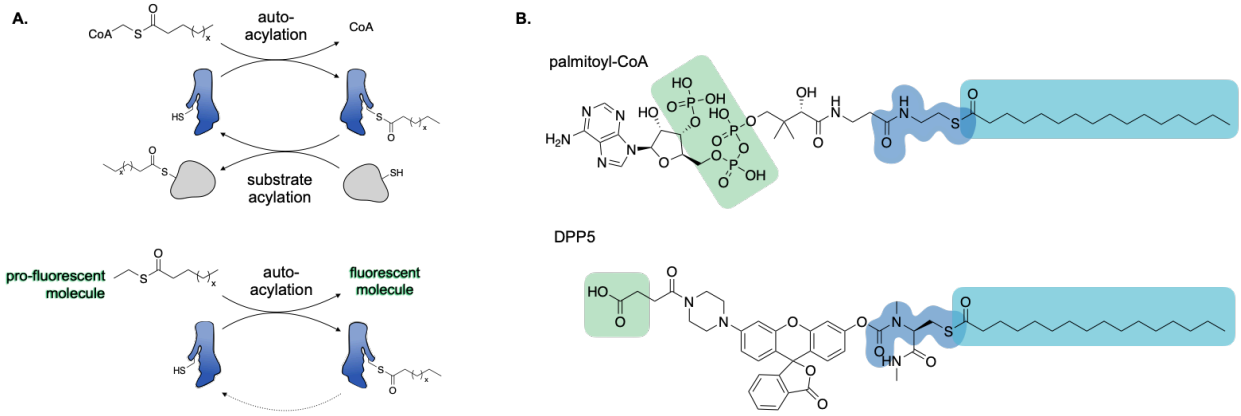

Figure 4.1. Designing a fluorogenic probe for DHHCs. (A) Mechanism of DHHC catalysis of acylation and proposed model for a fluorescent probe. (B) Structure of the DHHC substrate palmitoyl CoA and depalmitoylation probe 5 (DPP5). Highlighted are structural similarities, including the negatively charged group (green), cysteamine (blue), and lipid chain (turquoise).

fluorescence-based DHHC probe (Figure 4.1).[53] To substantiate this hypothesis, we performed flexible ligand–rigid receptor docking in Autodock Vina with the previously reported crystal structures of zDHHC20.[106, 115] Analysis of the few lowest-energy conformations revealed that the lipid portion of DPP5 could be docked into hydrophobic groove and that the carboxylate could engage with the highly positive CoA binding pocket.

To validate these in silico observations, we then tested the ability of zDHHC20 to uncage DPP5 in vitro. Excitingly, incubation of purified human zDHHC2, 3, and 20 with DPP5 resulted in a significant increase in fluorescent signal, confirming that the DPP5 scaffold could be adapted to visualize DHHC activity (Figure 4.2). Therefore, we next aimed to optimize this fluorogenic scaffold for interactions with DHHC family proteins. As an APT substrate, DPP5 contains a palmitoylated cysteine, which is absent in the palmitoyl CoA substrate (Figure 4.1). We therefore reasoned that removal of the methyl amide from the DPP5 scaffold (C61) would both minimize steric clashes and result in a better acyl-CoA mimic (Figure 4.3). Indeed, C61 docking against zDHHC20 revealed a tightly bound ligand-receptor complex, with the carboxylate interacting with a distal lysine residue in the ADP-binding pocket (Figure .S1). After several series of dockings to maximize the carboxylate interaction with lysine residue, we found that the addition of one extra carbon to the carboxylate (C63) resulted in the best hit. We also reasoned that different DHHC isoforms may have individuated interactions in the CoA binding region. Thus, we also synthesized two additional probes, one with a terminal morpholino group (C68) and one with a terminal amino acid group (C70). (Figure 4.3). Notably, each of these probes

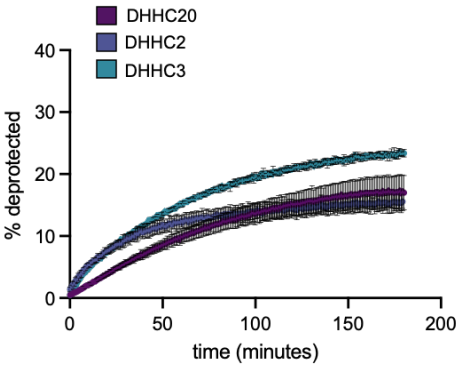

Figure 4.2. DPP5 is a DHHC substrate. Incubation of DPP5 with zDHHCs 2, 3, and 20 results in fluorescent signal.

shares a native substrate mimetic, a masked fluorophore, and a negatively charged group to facilitate binding.

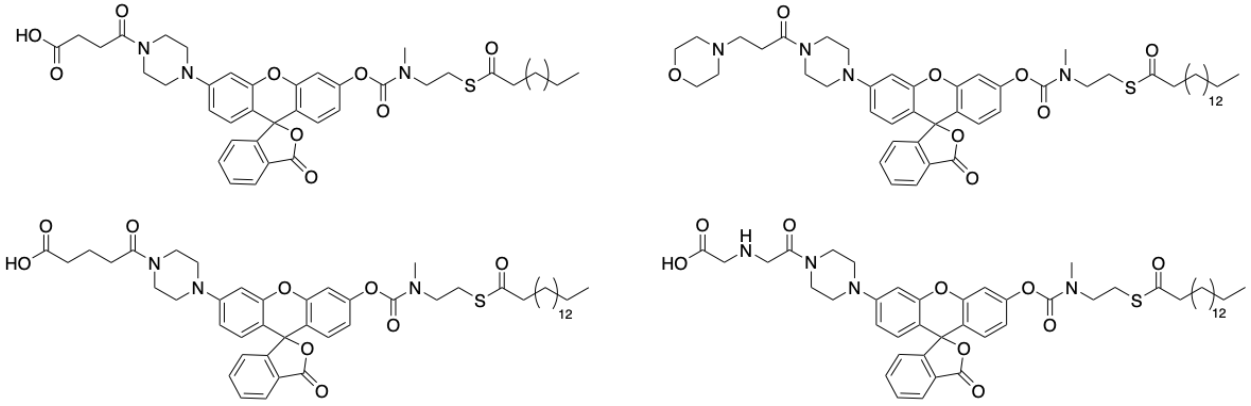

Figure 4.3. Panel of pro-fluorescent probes for DHHC family proteins.

With this small panel of probes in hand, we next screened them against zDHHC20 to identify the best substrate, i.e., the most uncaged molecule, for this protein. While all probes gave significant fluorescent signal, C63 emerged as the probe most deprotected by zDHHC20 (Figure 4.S1). This result paralleled the docking experiments and confirmed the utility of engaging with the ADP-binding pocket. Moreover, incubation with a catalytically inactive mutant (DHHA) resulted in an 80% decrease in fluorescent signal (Figure 4.S2). We next measured the enzyme kinetics to elucidate the affinity of the zDHHC20-C63 interaction. We determined the K_m and k_{cat} to be 24.3 μM and 0.160 s^{-1}, respectively, while the calculated k_{cat}/K_m value was 2.08 x 10^7 $M^{-1}s^{-1}$ (Figure 4.4). Finally, to establish the adaptability of this assay for other DHHC family proteins, we also screened the

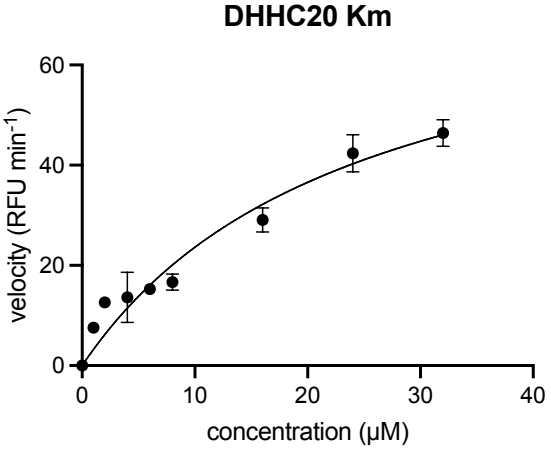

Figure 4.4. Plot of concentration (μM) against velocity (RFU per minute) for zDHHC20.

probes against zDHHC2 and 3. Interestingly, we observed here that C68, the morpholino compound, was the best substrate for these two zDHHCs (Figure 4.S1). Together, these data confirm the ability of these fluorogenic probes to report on the activity of DHHC family proteins.

We next sought to establish the suitability of this assay for a high-throughput screen. The Z'-factor is a statistical characteristic used to evaluate the quality of an assay, with a Z'-factor > 0.5 indicating congruence with an HTS. Here, evaluation of the Z'-factor during the linear reaction rate time (t = 60 min) afforded a value of 0.84 for zDHHC20. This Z'-factor compares favorably with other published assays, including the DHHC-acyl-cLIP (Z' = 0.553). We next confirmed its ability to detect zDHHC inhibition using known inhibitors. ZDHHC2, 3, and 20 were incubated with 20 μM of both 2BP and CMA and the fluorescent readout recorded. Here, we observed that both CMA and 2BP were able to inhibit zDHHC2, 3, and 20 (Figure 4.5). These results establish the utility of this assay for a HTS.

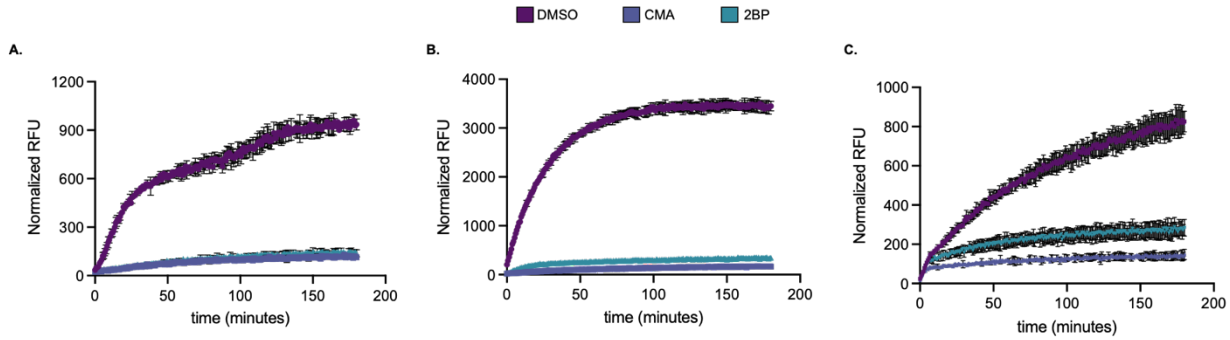

Figure 4.5. Validation with known chemical inhibitors. Inhibition of zDHHC2 (A), zDHHC3 (B), and zDHHC20 (C) with known DHHC family inhibitors CMA and 2BP.

Having validated the compatibility of this assay for HTS, we next conducted a pilot screen. Our previous work has verified the ability of acrylamide-containing molecules to inhibit DHHC family proteins, and so we have begun to screen a library of acrylamide-containing compounds from Enamine, ~2,000 in number (Figure 4.6). With a threshold set for at least 30% inhibition at 25 μM, we have thus far found that 43 molecules successfully inhibited zDHHC20.

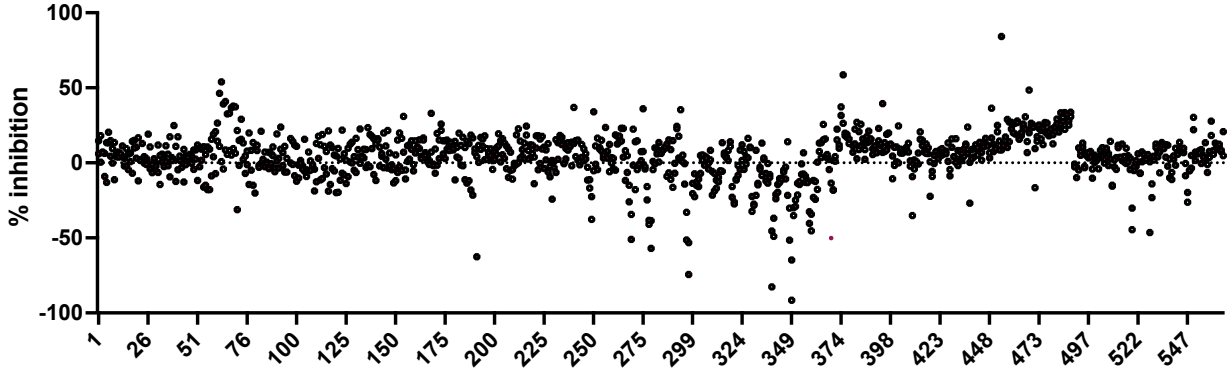

Figure 4.6. Plot of HTS Enamine library screen against zDHHC20. Graph represents the results of the first 500 compounds *(n = 2)*.

4.3 Conclusion

The increasing awareness of the importance of DHHC activity in both health and disease states underscores the need for chemical inhibitors to probe the biology and therapeutic potential of these targets. However, the development of inhibitors is hindered by the limitations of current biochemical assays for DHHC activity. In this Article, we introduce a fluorescence-based assay for DHHC activity. Using molecular docking as a guide, we rationally designed a panel of pro-fluorescent probes that capitalize on DHHC recognition of palmitoyl CoA during the autoacylation step of its catalytic cycle. Then, the active site cysteine initiates cleavage of the carbamate linker, uncaging the probe and providing a fluorescent readout of DHHC activity.

Not only does this assay possess an excellent Z'-factor (0.84), we show that it can be applied to multiple members of the DHHC family of proteins. Interestingly, probe C63 was observed to be the best substrate for zDHHC20, while zDHHCs2 and 3 engaged the most with probe C68. This suggests that individual DHHCs bind their acyl CoA substrates differently and could provide biochemical insights into the mechanism of DHHC selectivity for certain acyl groups. In addition, during the reaction, the active site of DHHC protein is acylated by the probe, decreasing its

turnover rate over time. We explored the ability GobX, a known zDHHC20 substrate, to facilitate acyl transfer, regenerate the active site, and increase fluorescence signal. Inclusion of GobX improved the fluorescence increase 1.5-fold, confirming that inclusion of a substrate has the potential to improve the signal-to-noise ratio of this assay (Figure 4.S3).

Finally, we employed this assay to identify novel scaffolds for DHHC inhibitors. While screening of the library (~2,000 in total) remains in progress, we have identified several novel scaffolds. After cross-validating the activity of this compounds, we will assess their efficacy *in cellulo* and apply medicinal chemistry approaches to improve their potency. We will also screen against zDHHCs2 and 3, potentially identifying orthogonal hits for the development of isoform-specific inhibitors.

4.4 Supplementary Figures

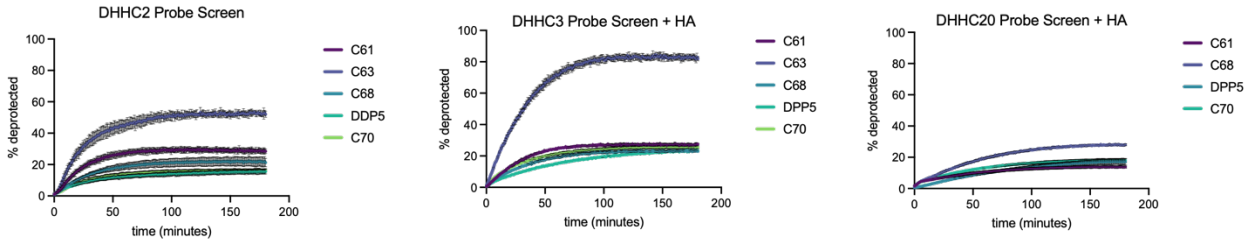

Figure 4.S1. Screen of a panel of fluorescent probes against zDHHCs 2, 3, and 20 to identify the best substrate for each protein.

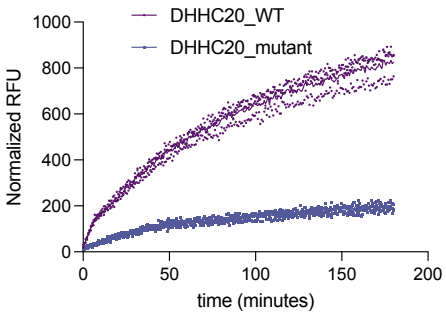

Figure 4.S2. The activity of zDHHC20 and zDHHS20 against the probe C63.

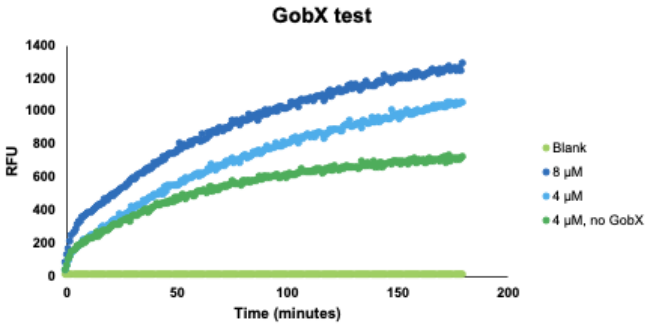

Figure 4.S3. GobX as a substrate to improve DHHC/probe turnover.

Chapter 5: Acylation as a novel PTM for ERK1/2

5.1. Introduction

Protein *S*-acylation, the addition of a long-chain fatty acid to a cysteine residue, is a lipid post-translation modification (PTM) known to affect substrate activity and function. Its dynamics are enzymatically mediated, with DHHC domain-containing protein acyl transferases (PATs) acting as "writers" and acyl protein thioesterases (APTs) as "erasers" [9] At the cellular level, these cycles of *S*-acylation and deacylation regulate protein subcellular tracking and activity, and at the organismal level, have been implicated in cancer and neurological and inflammatory disease. [116] One area in which the role of *S*-acylation has been increasingly recognized is signal transduction, with both receptors (MC1R, EGFR) and effectors (AKT, JNK, STAT3) requiring *S*-acylation for activity and downstream functionality. [35, 109, 117-119] However, while the advent of chemical and biochemical techniques to study protein lipidation has precipitously increased our knowledge of the frequency and significance of *S*-acylation, the consequences of dynamic *S*-acylation for many proteins remains unknown.

The mitogen-activated kinases (MAPKs) are an evolutionarily conserved family of proteins that are critical in transducing extracellular signals to the interior of the cell and in regulating a diverse array of cellular programs. [120, 121] Particularly well-studied within this venerable family are the extracellular signal regulated kinases (ERK1/2). As the primary mediators of the Ras cascade, ERK1/2 phosphorylate hundreds of cytoplasmic and nuclear substrates, regulating processes such as embryogenesis, cell motility, proliferation, differentiation, and apoptosis. [122-124] ERK1/2-dependent signal transduction is also critical in cellular and organismal metabolism, contributing to glycolytic pathway reprogramming (Warburg effect) in normal and cancer cells and to the development of metabolic syndrome. [125]

The simple architecture of the central three-tiered cascade belies its complexity and finely tuned ability to determine specific cell responses. In fact, the master regulators ERK1/2 are themselves intricately regulated. Subcellular localization, docking motif-mediated interactions with substrates and regulatory elements, scaffolding proteins, phosphatases, and cross-talk with other signaling pathways – all modulate ERK specificity and activity. [126-128] Central to the ERK1/2 regulatory scheme are PTMs, in particular phosphorylation. MEK1/2-mediated dual phosphorylation of a threonine-glutamic acid-tyrosine (TEY) motif is critical in regulating ERK1/2 activity following upstream signaling events. The magnitude and duration of phosphorylation at this motif determines the specific ERK1/2 transcriptional program. Other serine and threonine residues in ERK1/2, including a three-amino acid SPS motif posited to be of import in nuclear translocation, are also phosphorylated and regulate ERK1/2 activity. [129] More recently, other PTMs have emerged as negative regulators of ERK1/2 activity, including *S*-nitrosylation of Cys183 and the acetylation of Lys72 of ERK1. [130, 131]

However, even when taken as a whole, this network of regulatory mechanisms does not fully explain how the activation of ERK1/2 by multiple extracellular stimuli results in distinct cellular outcomes, suggesting there is still more to be discovered about the regulation of ERK1/2 activity and function. [132-134] Intriguingly, proteomic studies suggest that ERK1/2 might be subject to *S*-acylation. [49] Here, we show that ERK1/2 is *S*-acylated, in particular *S*-palmitoylated, *in cellulo* and *in vivo*. Moreover, we establish that its *S*-acylation is dynamic in the context of epidermal growth factor (EGF) stimulation and that *S*-acylation regulates the pattern of its TEY and SPS phosphorylation and subsequent activation. We then show that in the context of EGF signaling, ERK1/2 *S*-acylation is mediated by dynamic associations with writers zDHHCs7 and 14 and the eraser APT2. Finally, we use a mouse model of metabolic syndrome to profile changes in *S*-

acylation correlated to aberrant activity and changes in writer protein expression. This work introduces *S*-acylation as a novel regulatory module of ERK1/2 activity and potential therapeutic node for targeting ERK1/2 activity, not only in metabolic syndrome but in cancer and other MAPK signaling-driven pathologies.

5.2 Results

ERK1/2 S-acylation are dynamically regulated by EGF

ERK1/2 *S*-acylation has been hinted at by acyl exchange methods carried out in adipocytes. [49] Therefore, we sought to confirm that *S*-acylation, and more specifically, *S*-palmitoylation, is an a PTM of ERK1/2. To visualize cysteine acylation, we first used acyl biotin exchange (ABE), in which the labile thioester bond of acylated cysteine is cleaved by hydroxylamine (HA) and substituted with an enrichment handle. [57] This assay, carried out in HEK293T, A431, and HepG2, cells clearly demonstrated that ERK1/2 are *S*-acylated (Figure 5.1). Next, to further corroborate these results and confirm palmitate incorporation, we used metabolic labeling with 17-octadecynoic acid (17-ODYA), the ω-alkyne analogue of the 16C palmitic acid. Here, we observed incorporation of the tagged palmitic acid, therefore affirming ERK1/2 *S*-palmitoylated (Figure 5.1). [135] Importantly, hydroxylamine (HA) treatment diminished the signal in this experiment, confirming thioester bond formation and thus cysteine modification (Figure 5.1). We also probed in ERK *S*-acylation by ABE in mouse tissues, observing significant *S*-acylation across all tissues profiled, especially in the brain, liver, and pancreas, confirming ERK *S*-acylation *in vivo* (Figure 5.1). Together, these results establish that ERK1/2 are *S*-acylated across systems.

Central to ERK1/2's mediation of cellular events is their ligand-induced activation, which stimulates a rapid increase in their phosphorylation and then downstream kinase activity. Therefore, we next sought to determine whether the levels of ERK1/2 *S*-acylation are sensitive to

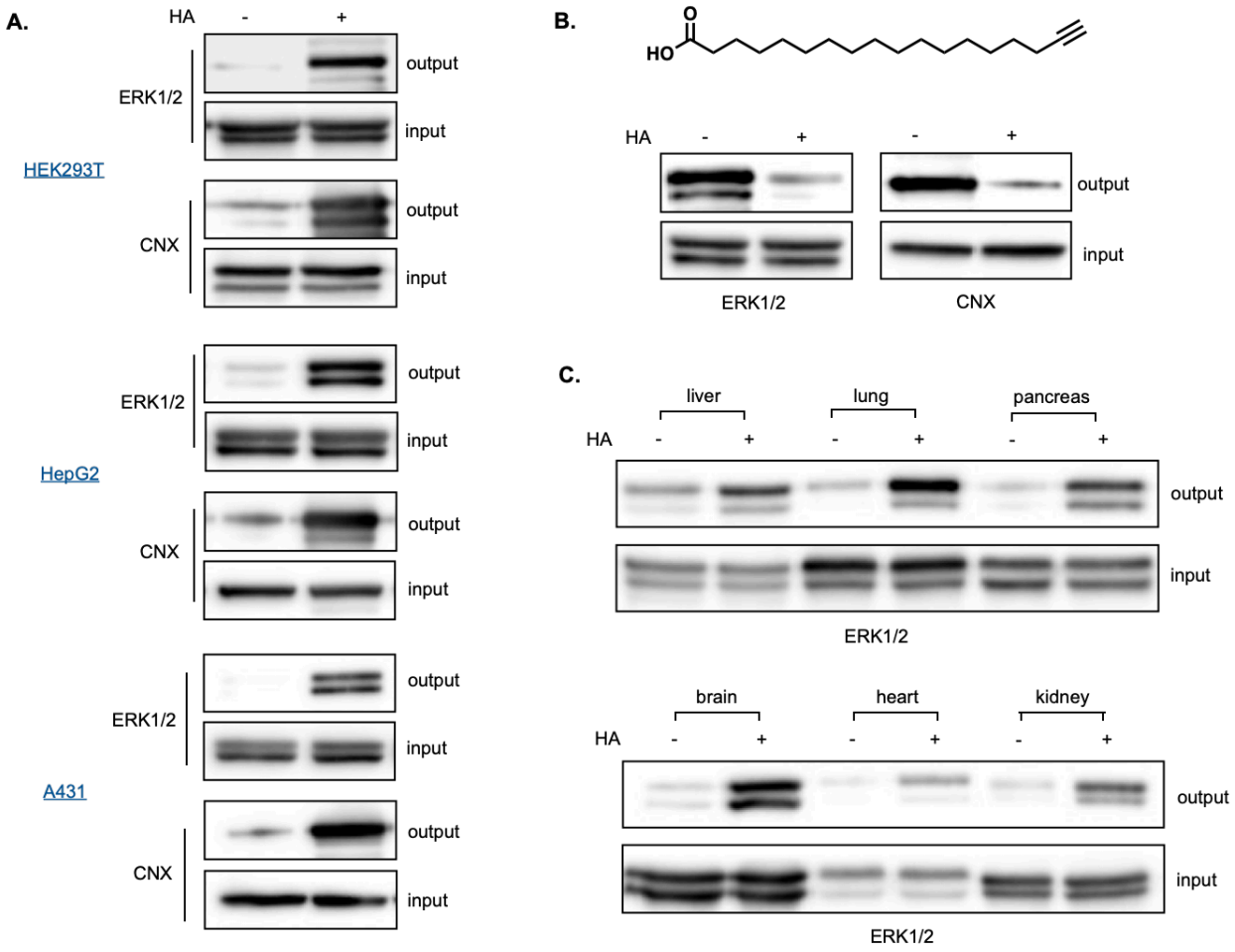

Figure 5.1. ERK1/2 are *S*-acylated. (A) Acyl biotin exchange (ABE) assay carried out in HEK293T, A431, and HepG2 cells, wherein signal in the hydroxylamine (HA) treated samples indicates *S*-acylation. Calnexin (CNX) is used as loading and assay control. (B) Metabolic labeling with 17-octadecanoic (17-ODYA) in HEK293T cells. Signal in -HA lanes indicates the incorporation of the 16C fatty acid, while loss of signal in the +HA samples indicates cysteine bond formation. (C) ABE carried on a panel of tissues harvested from C57BL/6 to visualize *S*-acylation *in vivo*.

stimulation, as changes in ERK1/2 S-palmitoylation concurrent with activity changes could hint at a regulatory role for *S*-palmitoylation in ERK1/2 activation. We therefore monitored ERK1/2 *S*-acylation levels upon stimulation with the epidermal growth factor (EGF), a secreted peptide which activates a signal transduction network that includes the RAS/ERK pathway.[134] Upon treatment of serum-starved cells with EGF, the basal *S*-acylation of ERK1/2 increases within 5 minutes and stays elevated through 15 minutes of stimulation, with a return to baseline acylation

levels occurring by 30 minutes in HepG2 and A431 cells (Figure 5.2, 5.S1). Significantly, this pattern mirrors that of ERK phosphorylation, which also remains elevated through 15 minutes and decreases by 30 minutes.[136] Since much remains unknown about how the extracellular concentration of ligand (signal strength) is relayed intracellularly, we next assessed the dose-dependence of ERK1/2's *S*-acylation increase. As EGF concentration increased from 0 to 1 to 10 ng mL^{-1}, ERK1/2 *S*-acylation increased in-step, with a lessening increase at 100 ng mL^{-1} in HepG2 and A431 cells. This suggests that *S*-acylation is responsive to the flow of quantitative information through the pathway (Figure 5.2, 5.S1). These results established our activating concentration of EGF at 1 ng mL^{-1}, a concentration congruent with physiologic levels of the growth factor.[137] Finally, to assess the generality of the ERK *S*-acylation dynamics, we probed for ERK1/2 *S*-acylation changes upon treatment with insulin-like growth factor (IGF), another signaling ligand also established to activate the ERK MAPK pathway. To our surprise, IGF treatment did not trigger an increase in ERK1/2 *S*-acylation in either HepG2 or A431 cells, although a decrease in *S*-

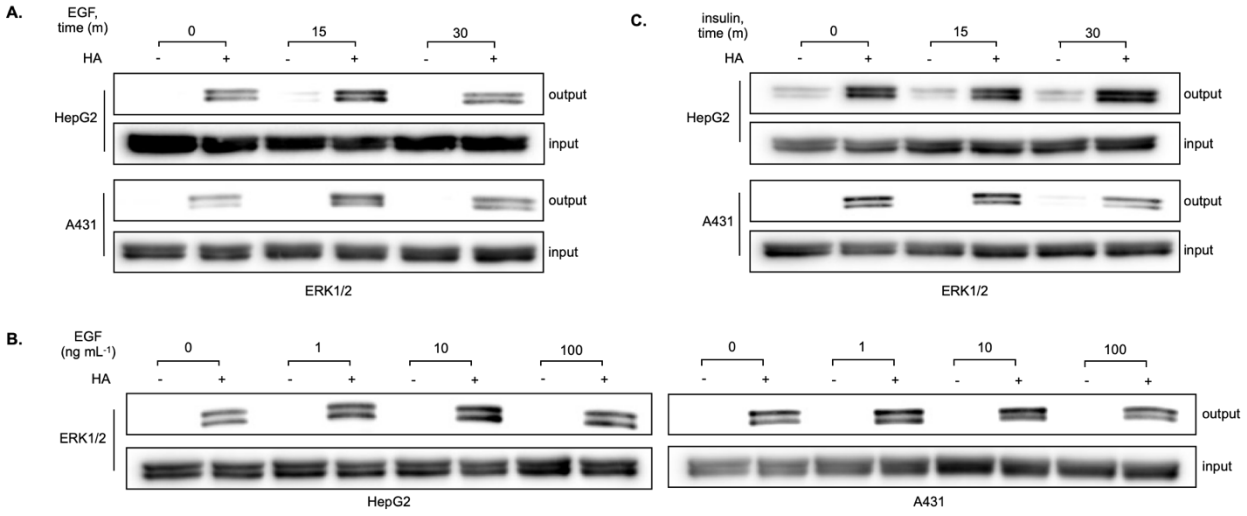

Figure 5.2. ERK1/2 *S*-acylation responds to EGF stimulation. (A) ABE assay carried out in HepG2 and A431 cells following stimulation with EGF (1 ng mL^{-1}) for 0, 15, and 30 minutes. (B) ABE assay carried out in HepG2 and A431 cells following stimulation with 0, 1, 10, and 100 ng mL^{-1} EGF for 15 minutes. (C) ABE assay carried out in HepG2 and A431 cells following stimulation with insulin for 0, 15, and 30 minutes.

acylation was observed in A431 cells at 30 minutes (Figure 5.2C, 5.S1). Thus, it is clear that the *S*-acylation of ERK1/2 is not only dynamic, but also sensitive to signal strength and signal identity, emphasizing its potential as a regulator of ERK1/2 activity.

Dynamic ERK S-acylation does not depend on TEY motif phosphorylation

Given that the timing of ERK1/2's dynamic *S*-acylation corresponds to that of its dynamic TEY phosphorylation, we next attempted to parse the connection between the two modifications. First, we used ABE to determine the *S*-acylation status of active ERK1/2, i.e., ERK1/2 that have been phosphorylated at the TEY motif of their activation loops. Here, we observed palmitoylated ERK1/2 increasing concomitantly with ERK1/2 phosphorylation (Figure 5.3). This result confirms that the two PTMs can co-occur on ERK1/2. We next used established MAPK pathway inhibitors to investigate whether the signaling elements that regulate phosphorylation also regulate ERK1/2's dynamic palmitoylation. Pre-treatment with upstream inhibitors for MEK (AZD6244, CI-1040) and RAF (PLX-4720), as well as with okadaic acid, an inhibitor of ERK1/2-directed phosphatase activity, inhibited the EGF-induced increase in ERK1/2 *S*-acylation (Figure 5.S2).[138-141] These results suggest that intact regulatory infrastructure is necessary for the dynamic S-acylation of ERK1/2. This observation is further supported by treatment with wortmannin, a PI3K pathway inhibitor, which decreases ERK1/2 *S*-acylation – implicating pathway crosstalk in the regulation of ERK *S*-palmitoylation (Figure 5.S2). However, while these data establish that the dynamic *S*-acylation of ERK1/2 is connected to pathway activation, they do not reveal whether ERK1/2 phosphorylation itself is necessary for *S*-acylation.

In order to gain insight into the sequentiality and interdependence of the two modifications, we created variants of ERK2 – the more widely and abundantly expressed of these ERKs – in which the three sites of the phospho-acceptor motif were mutated to either alanine (AAA) or

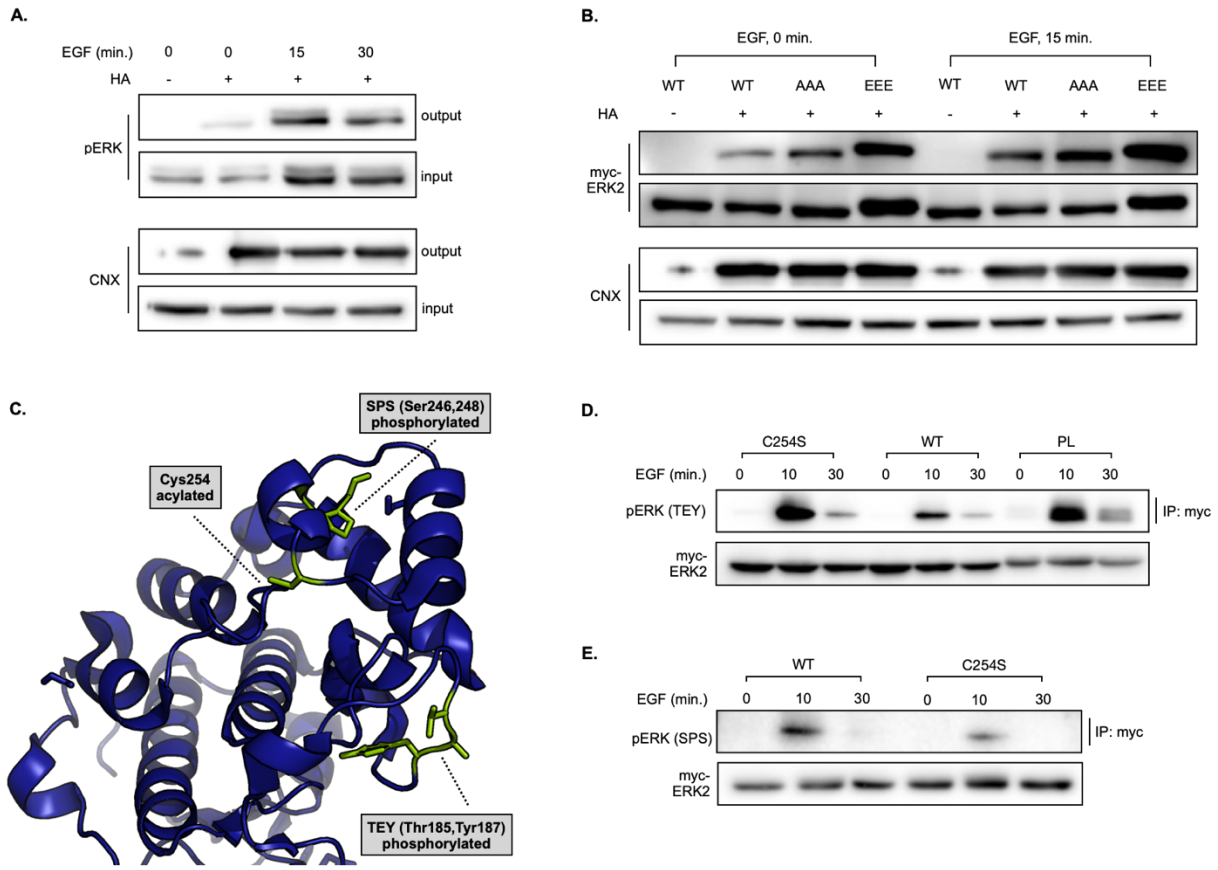

Figure 5.3. Mapping crosstalk between ERK2 *S*-acylation and phosphorylation. (A) ABE assay carried out in HepG2 cells and analyzed for phospho ERK1/2 (Thr185/202,Tyr187/204) via Western blotting. (B) ABE assay carried out in HEK293T cells overexpressing WT, TEY(AAA), or TEY (EEE) ERK2 and stimulated with EGF (1 ng mL^{-1}) for 15 minutes. (C) Crystal structure of the C-terminal lobe of ERK2 indicating phosphorylation and acylation sites. (D) Immunoprecipitation of myc-ERK2 (WT, C254S, and PL-tagged) in HEK293T cells, with or without EGF stimulation (10 minutes, 1 ng mL^{-1}). Analyzed via Western blotting for phospho-ERK (Thr185/Tyr187). (E) Immunoprecipitation of myc-ERK2 (WT, C254S), with or without EGF stimulation (10 minutes, 1 ng mL^{-1}), analyzed via Western blotting for phosphoserine.

glutamic acid (EEE). These mutations respectively confer resistance to or mimic constitutive phos phorylation, enabling us to probe the result of perturbing ERK1/2 phosphorylation on its palmitoylation. Overexpression of these constructs in HEK293T cells, followed by EGF stimulation and visualization of acylated proteins, indicated that ERK2's dynamic *S*-acylation was not disrupted in either the constitutively inactive or active constructs (Figure 5.3). This suggests that the EGF-mediated increase in ERK1/2's *S*-acylation is not dependent on its phosphorylation

status. Interestingly, the levels of basal *S*-acylation in serum-starved cells increased for both constructs relative to the wild type (WT), again hinting at a more complicated regulatory network (Figure 5.3). Collectively, these results demonstrate that dynamic ERK1/2 *S*-palmitoylation is dependent on pathway activation but likely precedes active site phosphorylation.

Palmitoylation-deficient ERK2 displays altered phosphorylation patterns

To determine the consequences of *S*-acylation for the regulation and activation of ERK1/2, we next sought to generate palmitoylation-resistant variants of each ERK. This required mapping of the *S*-acylation site(s), wherein we individually mutated each of the six cysteines of ERK1 and the seven cysteines of ERK2 to alanine, and then used ABE to visualize the *S*-acylation status of each CΔA mutant. For ERK1, we observed a decrease in ABE signal for both C239A and C77A, while for ERK2, a decrease was seen for both C216A and C254A – signifying that these cysteines are sites of *S*-acylation (Figure 5.S2). As the loss of signal for C239 in ERK1 and C216 in ERK2 were accompanied by a significant loss of expression of these mutants, implicating these residues (and possibly their *S*-acylation) in the stability or proteasome degradation of ERK1/2, we chose to focus on the *S*-acylation of C254. Importantly, these residues are located in the C-terminal lobe of ERK1/2, which contains their activation and catalytic loops and is also subject to other regulatory PTMs.[142]

With these biochemical tools in hand, we first assessed the impact of ERK1/2 *S*-acylation on their activation, as measured by TEY phosphorylation. Here, given its generally wider and higher expression levels, we used ERK2 as a sentinel. Overexpression of myc-ERK2/ERK2(C254A), followed by EGF stimulation and immunoprecipitation of the epitope tagged-constructs, allowed for visualization and comparison of TEY phosphorylation of the WT vs. *S*-acylation-resistant ERK, while eliminating background signal from endogenous ERK2. Strikingly, myc-

ERK2(C254A) was dramatically more phosphorylated at the TEY motif than its WT counterpart (Figure 5.3, 5.S2). This TEY hyperphosphorylation upon EGF stimulation was also seen when we fused the prenylated and dual palmitoylated motif of paralemmin to the C-terminus of ERK2 to simulate constitutive *S*-acylation (Figure 5.3C).[143] Together, these results demonstrate that dynamic ERK2 *S*-acylation is critical for the regulation of its active site phosphorylation.

Examination of the structure of ERK2 indicates that the site of *S*-acylation, C254, is most proximal not to the Thr185/Tyr187 phosphorylation sites, but rather to the Ser246/248 of the SPS motif, is part of a purported 19-amino acid long nuclear translocation motif (NTS) (Figure 5.3B). [129] Therefore, we next determined the influence of *S*-acylation on this PTM used overexpression of both myc-tagged WT and C254A ERK2, followed by EGF stimulation, myc-tag immunoprecipitation, and visualization of serine phosphorylation. Here, we observed that the serine residue phosphorylation of myc-ERK2(C254A) was considerably diminished relative to that of WT ERK2, a marked difference from the increase seen in TEY phosphorylation (Figure 5.3D). This suggests that the *S*-acylation of C254 for its activation and confirms that dynamic *S*-acylation has a substantial role in regulating the phosphorylation of ERK2 at both its active site TEY and NTS SPS motifs.

Chemical inhibition of ERK1/2 S-acylation disrupts its transcriptional program

Upon EGF stimulation and translocation to the nucleus, ERK signaling elicits a gene expression program linked to diverse cellular events, such as proliferation and differentiation. Given the significant but opposing changes in TEY and SPS phosphorylation, we next aimed to determine how loss of dynamic ERK1/2 *S*-acylation affects this transcriptional program. To do this, we first identified chemical tools to disrupt the cycle ERK1/2 *S*-acylation and deacylation, as overexpressed proteins have the potential to overload biological pathways. [144] First, we targeted

the installation of the lipid by the DHHC-PATs using both 2-bromopalmitate (2-BP), a widely used albeit promiscuous inhibitor, and cyano-myracrylamide (CMA), another small inhibitor with a different reactivity profile recently developed by our group. [66,110] ABE revealed that treatment with 2-BP (20 μM, 6 hours) failed to decrease the *S*-acylation of ERK, possibly due the poor potency and/or poor targeting of ERK-specific writers (Figure 5.4A). However, ABE analysis showed that

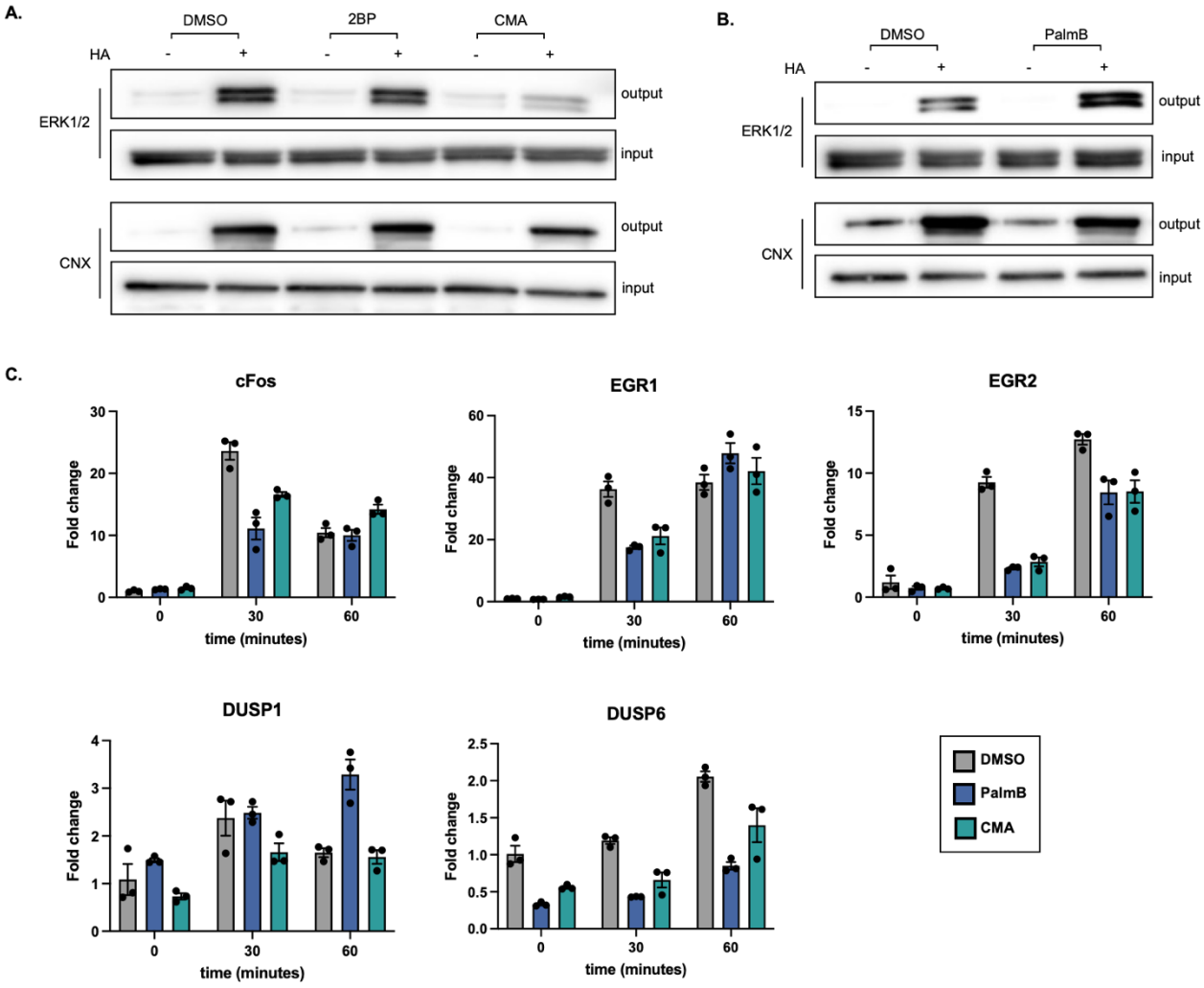

Figure 5.4. Chemical perturbation of ERK1/2 *S*-acylation affects its transcriptional program. (A) ABE assay carried out in HepG2 cells treated with DMSO, 2BP (20 μM), or CMA (20 μM) for 6 hours. Calnexin (CNX) is used as loading and assay control. (B) ABE assay carried out in HepG2 cells treated with DMSO or PalmB (20 μM) for 6 hours. Calnexin (CNX) is used as loading and assay control. (C) RT-qPCR of key transcripts in the EGF-stimulated transcriptional program in HepG2 cells treated with DMSO, CMA (20 μM), or PalmB (20 μM) for three hours, followed by stimulation with EGF (1 ng mL^{-1}) for 30 and 60 minutes.

treatment with CMA, but not its inactive analogue, under parallel conditions (20 μM, 6 hours) resulted in a significant decrease of the *S*-acylation of ERK1/2, with maximum inhibition of *S*-acylation reached after three hours of treatment in HepG2 cells (Figure 5.4A, 5.S3A,B). These results validate CMA as a tool to analyze the downstream consequences of inhibiting ERK1/2 *S*-acylation.

Next, we used palmostatin B (PalmB), a pan inhibitor of the eraser APTs, to interrupt lipid removal and therefore increase the *S*-acylation of ERK1/2. [68] Treatment of HepG2 cells with PalmB (20 μM, 6 hours) and visualization of acylated proteins via ABE showed increased ERK1/2 *S*-acylation, confirming the utility of this inhibitor in probing the effects of perturbing ERK1/2 *S*-acylation (Figure 4B). In addition, while the β-lactone PalmB acts on globally on APTs, ML-348 and ML-349 are inhibitors specific for two of the principal *S*-deacylases, APT1 and APT2, respectively. [145, 146] Therefore, we employed these inhibitors to determine if one could increase the *S*-acylation of ERK1/2 more significantly and more selectively; here, we observed via ABE an increase in *S*-acylation upon ML-34 treatment only (Figure 4.S3C). This result suggests that APT2, but not APT1, regulates the deacylation of ERK1/2. However, as the increase was less than that observed with PalmB, it also introduces the possibility that additional APTs have a role in the regulation of ERK1/2 and establishes PalmB as a key tool to disrupt ERK1/2's deacylation.

With these chemical tools in hand, we next aimed to use them to assess the consequences of disrupted acylation for ERK1/2 transcriptional regulation. As the key activator of MAPK pathway, ERK1/2 is connected to the induction of hundreds of gene targets, including cFos, early growth response proteins 1/2 (EGR1/2), and the dual specificity phosphatases 1/6 (DUSP1/6).[147] RT-qPCR analysis, following pretreatment of HepG2 cells with DMSO, CMA, or PalmB and stimulation with EGF (0, 30, and 60 minutes), revealed inhibitor-dependent changes in the induction pattern

of these transcripts (Figure 5.4C). In the case of the immediate early response genes cFos and EGR1/2, treatment with both CMA and PalmB limited the rapid RNA amplification typically observed after 30 minutes of EGF treatment, as compared to the DMSO control. However, after 60 minutes, cFos and EGR1 transcript levels matched the control sample, while EGR2 transcript levels continued to rise. This suggests that disruption of ERK1/2 *S*-acylation delays rather than inhibits its EGF-stimulated transcriptional program. For the immediate late gene DUSP1, PalmB resulted in increased activation at 60 minutes, while DUSP6 expression was dampened at all time points. Together, these alterations suggest that *S*-acylation is significant in regulating both the timing and amplitude of ERK-mediated gene expression changes.

C254 is critical for ERK2 protein-protein interactions

Given the disrupted transcription of canonical ERK targets, we next considered whether this effect was due to altered upstream interactions of ERK2. Following stimulation and activating TEY phosphorylation, ERK2 undergoes a conformational change that releases it from cytoplasmic anchors and exposes the SPS motif for phosphorylation by, among others, casein kinase II (CKII). Its phosphorylation is thought to establish a negatively charged interface for the binding of importin7, which then escorts ERK2 through the nuclear pores and into the nucleus. [129, 148] In order to identify changes in association with these two transient interacting partners, we generated both WT and C254A myc-ERK2 tagged with TurboID, a biotin ligase that generates biotin–AMP to rapidly label proximal proteins and enable the mapping of the protein-protein interactions (Figure 5.S4A). [149] After validating the expression and ligase activity of the constructs, we assayed for CKII and importin7 labeling by WT and acylation-deficient ERK2. Here, we observed a dramatic decrease in labeling of CKII by ERK2(C254A) relative to the WT (Figure 5.5A). In addition, robust labeling of importin7 above background biotinylation with WT ERK2, no signal was seen

for ERK2(C254A) – indicating that C254 is necessary for ERK2's interaction with both CKII and importin7 (Figure 5.5A,B).

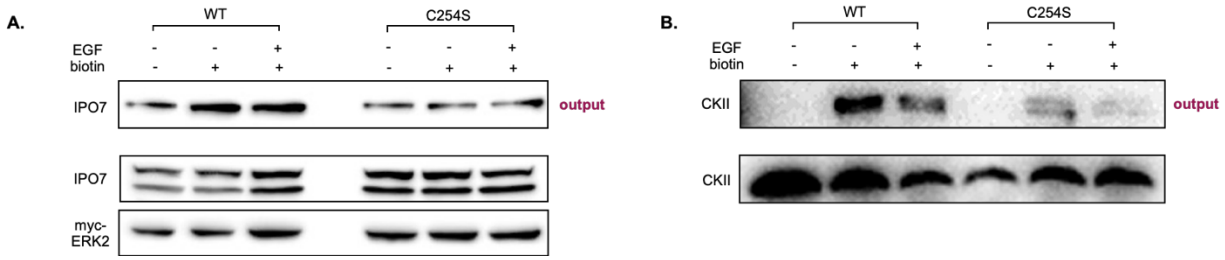

Figure 5.5. C254 of ERK2 is critical for its protein-protein interactions. Overexpression of myc-ERK2 (WT or C254A) tagged with TurboID in HEK293T cells, followed by visualization of its interactions with importin 7 (A) or CKII (B).

Dynamic ERK2 S-acylation is mediated by associations with DHHCs and APTs

Having determined that dynamic *S*-acylation is significant for ERK2 activity, we next sought to identify the molecular determinants of *S*-acylation. Identification of these regulatory elements, i.e., the writers and erasers, could enable more controlled modulation ERK *S*-acylation and therefore represents a novel way to manipulate ERK1/2 activity. Typically, the "Fukata assay" – overexpression of 23 mammalian zDHHCs, followed by visualization of *S*-acylation via ABE – is used to ascertain the DHHC-PAT writers of a particular substrate. However, in this screen, while slight increases in ERK1/2 *S*-acylation were observed with overexpression of some zDHHCs, no definitive writers for ERK1/2 were identified (Figure 5.S5A). This could suggest that ERK1/2 *S*-acylation is regulated by multiple PATs, with compensatory down-regulation complicating observation of increases in *S*-acylation. In addition, the levels of ERK1/2 *S*-acylation are likely tightly regulated, and the ABE assay reveals the steady-state levels of *S*-acylation for a target, not the cycling of *S*-acylation mediated in part by the PATs. Therefore, we next used metabolic labeling to visualize a change in the rate of *S*-acylation via increased incorporation of a tagged fatty acid. Here, we observed that a panel of PATs – zDHHC2, 3, 7, 9, 10, 11, 12, 14, 17, 20, and 21 – all

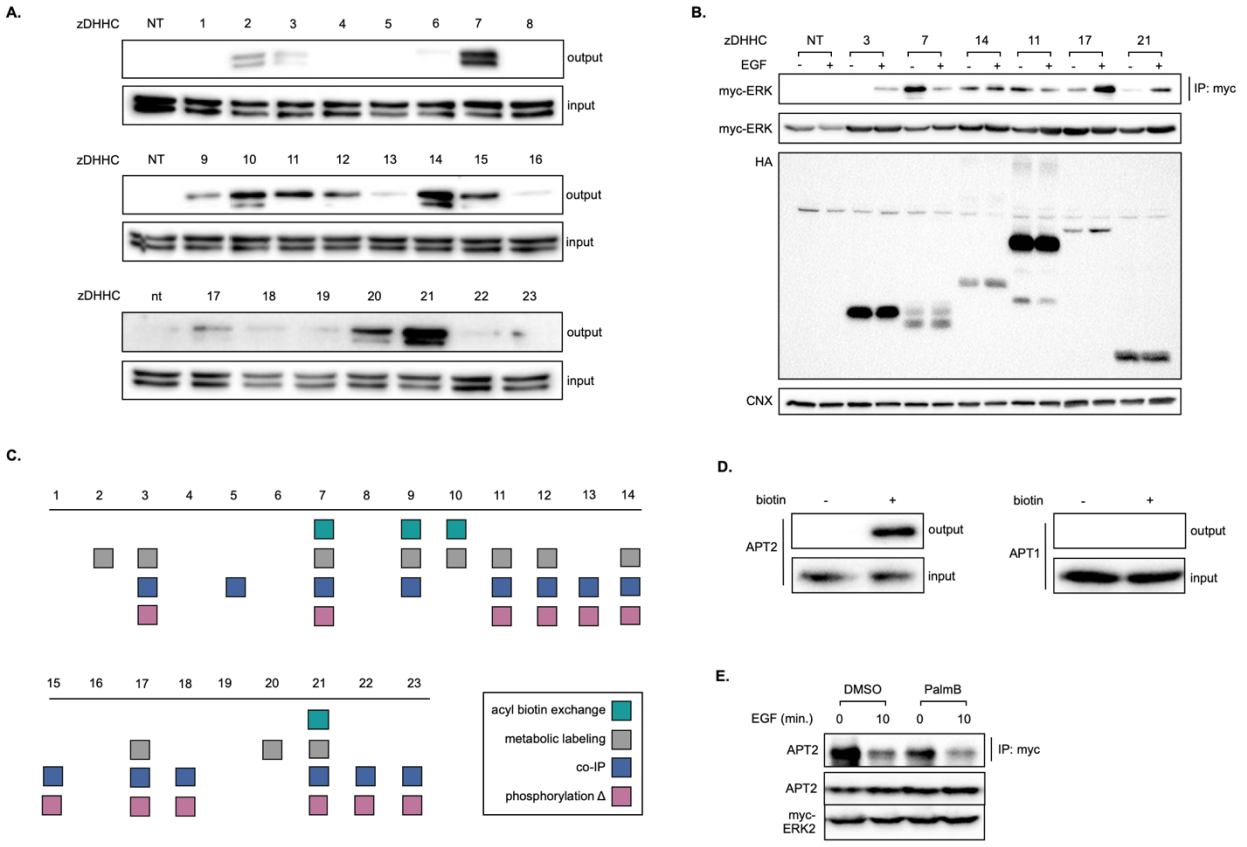

Figure 5.6. Identification of ERK1/2 writer and eraser proteins. (A) ERK1/2 metabolic labeling with 17-ODYA in HEK293T cells overexpressing murine DHHC family proteins. (B) Co-immunoprecipitation of myc-ERK2 with HA-tagged DHHC proteins in HEK293T cells with or without EGF stimulation (10 minutes, 1 ng mL^{-1}). Co-immunoprecipitated proteins were visualized via Western blotting for myc-ERK2. (C) Table of ERK1/2 writer hits, as assessed by four assays. (D) Co-immunoprecipitation of APT2 with myc-tagged ERK in HEK293T cells with or without EGF stimulation (10 minutes, 1 ng mL^{-1}), pretreated with DMSO or PalmB. (E) TurboID validation of APT2's association with ERK2.

increased ERK1/2 palmitoylation, with zDHHCs 7, 10, 14, 17, 20, 21 being the strongest hits (Figure 5.6A).

To further validate these potential writers and determine which were significant in ERK2's EGF-promoted dynamic *S*-acylation, we next used both TEY phosphorylation changes and co-immunoprecipitation to assess the interaction between each zDHHC and ERK2 under with and without conditions. In the first screen, a panel of PATS – zDHHC 3, 7, 11, 12, 13, 14, 17, 18, 21, 22, and 23 – increased ERK2 TEY phosphorylation, while an orthogonal panel– zDHHC3, 5, 7, 9,

11, 14, 17, 18, 20, 21, 22, and 23 – were all shown to interact with ERK2, with zDHHC7, 14, 17, and 21 emerging as the most likely writers, given the results of the metabolic labeling screen (Figure 5.A-C, 5.S5C). Significantly, ERK2 association with certain PATs was dynamic, with ERK2 dissociating from zDHHCs 7, 11, and 21 upon stimulation with EGF and associating more zDHHCs 3 and 17 (Figure 5.6B, 5.S5C). These results demonstrate that the DHHCs are not only writers of ERK2 *S*-acylation, they are also central to its dynamic *S*-acylation during EGF signaling.

The eraser APTs are the other vital element in a cycle of *S*-acylation/deacylation. To identify candidate erasers, we first overexpressed the serine hydrolases APT1, APT2, and ABHD17A/B/C and assayed for changes in ERK1/2 *S*-acylation. Here, no discernible decreases – which would indicate ERK1/2 eraser activity – were observed (Figure 5.S5C). Since previous experiments with the inhibitor ML-349 intimated that APT2 was a candidate eraser, we next decided to see if knockdown of this protein (encoded by LYPLA2) would elicit a change in ERK1/2 S-acylation. However, neither siRNA mediated knockdown of APT2 or APT1/2 together increased ERK1/2 *S*-acylation; in fact, a decrease was observed (Figure 5.S5D). These results once again suggest that the steady-state level *S*-acylation of ERK2 is tightly regulated, likely by multiple erasers. Therefore, we instead used the TurboID-tagged myc-ERK2 to probe its association with APT2, observing labeling of and thus proximity to APT2, but not APT1 (Figure 5.6E). Moreover, co-immunoprecipitation of APT2 with myc-ERK2 with and without stimulus revealed a decrease in the interaction between ERK2 and APT2 upon the addition of EGF – a contrast to the decreased association observed with the zDHHCs (Figure 5.6E). Together, these further substantiate a model of dynamic ERK *S*-acylation – modulated by the interplay of DHHCs3, 7, 11, 14, 21, and 23 and APT2 – in the regulation its EGF-induced activity.

ERK1/2 S-acylation is altered under conditions of metabolic stress

ERK1/2 signaling is not only responsive to growth factors, but also to cellular metabolism, with diet-derived molecules, such as glucose and long chain fatty acids, influencing enzyme activity and gene expression. [150] In fact, dysregulated ERK signaling, resulting from aberrant nutrient levels, has been implicated in pathogenesis of metabolic syndrome. [151] While the mechanisms of this phenomenon are unknown, metabolite-dependent PTMs, such as *S*-acylation, present an intuitive, albeit unestablished, regulatory mechanism. [26] Thus, we aimed to determine if changes in *S*-acylation of ERK1/2 could contribute to the changes in its activity *in cellulo* and *in vivo*. Incubation of HepG2 cells with a bolus of palmitate (500 M), a condition known to alter ERK1/2 activation, decreased their *S*-acylation levels, confirming the sensitivity of ERK1/2 *S*-acylation to metabolic stressors (Figure 5.7A). We next assessed changes in ERK1/2 *S*-acylation in relevant tissues in a mouse model of diet-induced obesity. C57BL/6J were fed either a high-fat diet (HFD) rich in palmitate or a matched control diet (CD) for 16 weeks, and then evaluated for metabolic health (Figure 5.7B-C, 5.S6). [152] After confirming the onset of metabolic syndrome in HFD mice, we probed for changes in ERK1/2 *S*-acylation in the liver, a metabolically active tissues in which ERK signaling is dysregulated in obesity, and the brain, a tissue with known sensitivity to palmitate. [153-155] Here, we observed an increase in the *S*-acylation of ERK1/2 in the liver, especially for ERK2, while a decrease was observed in the brain (Figure 5.7B). Moreover, transcript abundance estimation via reverse transcription-quantitative PCR (RT-qPCR) indicated corresponding changes in the expression of ERK2 writers and erasers, with DHHCs 9, 14, and 17 and APT2 downregulated in the liver and DHHCs 3, 7, 9, 14, 17, 21, and 23 downregulated in the brain (Figure 5.7F-I). Intriguingly, the decrease in APT expression in the liver paralleled the increase in ERK *S*-acylation, while the decrease in DHHC expression in the brain liver paralleled the decrease in ERK *S*-acylation (Figure 5.7). These results suggest the enzyme-mediated changes

in the S-acylation of ERK1/2 could contribute to the mechanism of dysregulated ERK1/2 signaling in metabolic syndrome.

Figure 5.7. ERK1/2 *S*-acylation is responsive to metabolic stress *in cellulo* and *in vivo*. (A) ABE assay in HepG2 cells treated with palmitate (0 or 500 μM). (B) Plot of the weight of mice fed either a control diet (CD) or a high-fat diet (HFD). *mean ± std, n = 5*. (C) Glucose tolerance test (GTT) for mice fed either a control diet (CD) or a high-fat diet (HFD). *mean ± std, n = 5*. ABE assay carried on the liver (D) or brain tissues (E) of C57BL/6 fed either a control (CD) or high-fat (HFD) diet for 20 weeks. (F-I) RT-qPCR analysis of zDHHC3, 7, 9, 14, 21, and 23 and APT1/2 transcript levels in the liver and brain tissues of these mice.

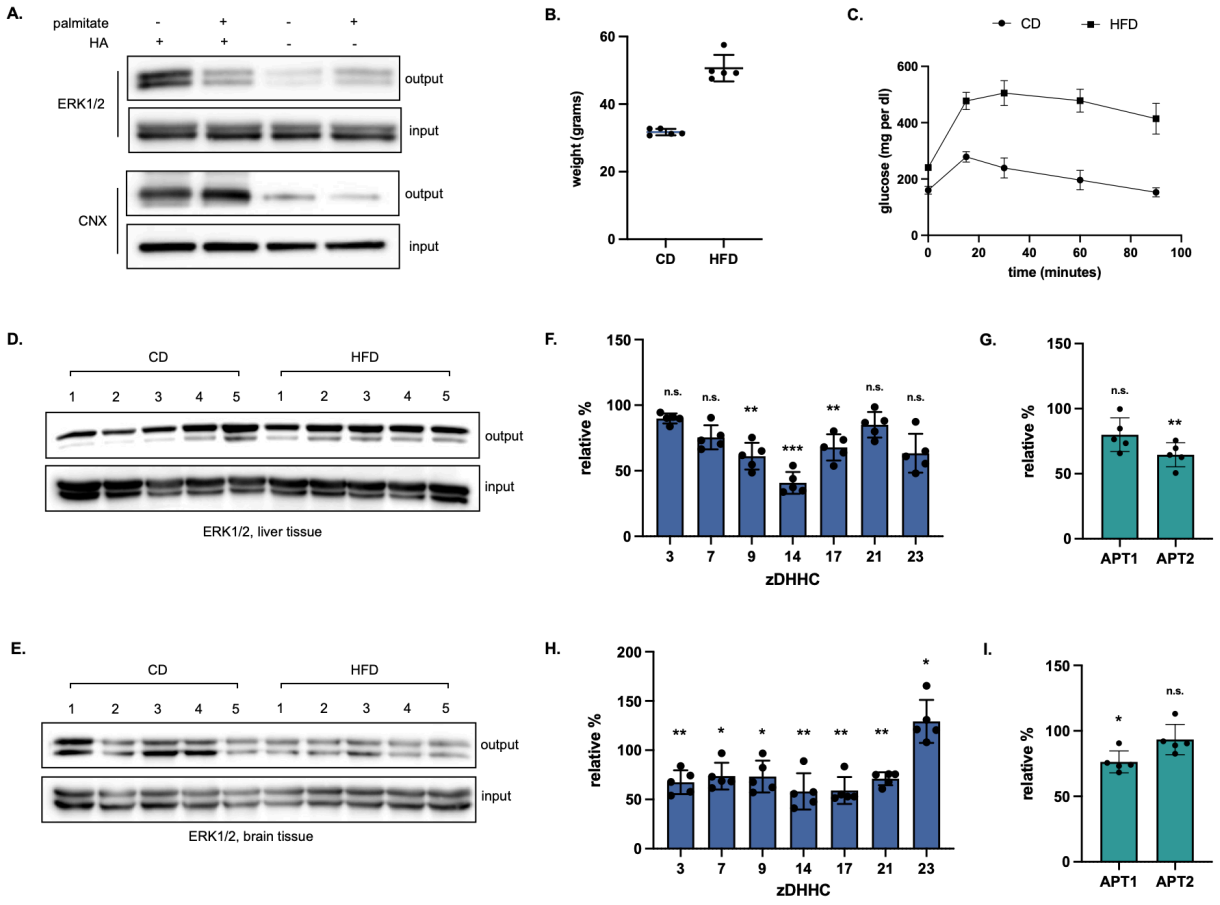

5.3 Discussion

As members of the conserved MAPK family, ERK1/2 contribute to essential cell processes and are associated with cell proliferation, cell growth, cell mobility, and cell survival.[156] Targeting their activity is of therapeutic interest for a constellation of pathological conditions, including cancer,

metabolic syndrome, neurological disease, and chronic inflammation. [151, 157-159]. Here, we introduce *S*-acylation as a novel, signal-responsive PTM for ERK1/2, in particular for ERK2. The observation of dynamics – i.e., increasing *S*-acylation with EGF treatment – is in accordance our previously reported rapid decrease in APT activity upon EGF treatment and highlights the regulatory role of this PTM. [21]. In addition, when coupled with the observed sensitivity of the dynamic ERK1/2 *S*-acylation to EGFR pathway inhibitors, this also suggests an as-yet undescribed cellular conversation between the acylation regulatory machinery and canonical MAPK/P13K cascades. Defining the nature of these upstream interactions represents a new and significant line of investigation.

Our experiments also highlight the relevance of *S*-acylation for ERK2 activity and function. Biochemical perturbation of an identified acylation site of ERK2, C254, resulted in an altered pattern of phosphorylation at two motifs (TEY and SPS) and changes in key protein-protein interactions implicated in the nuclear transport of ERK, including importin7. For importin7, while the decreased association with palmitoylation-deficient ERK2 is likely due to diminished SPS phosphorylation, it is also possible that ERK2 *S*-acylation directly mediates the ERK2-importin7 interaction, as importin7 is a lipid-binding protein.[160] In fact, an NTS-derived myristoylated phosphomimetic peptide has been shown to inhibit the ERK2-importin7 interaction. [161] We also assessed the effect of disrupting the cycle of ERK2 *S*-acylation of its transcriptional program, observing that inhibiting that chemical inhibition of both lipid installation and removal affected targets like EGR1, cFos, and DUSP6. Here, the efficacy of CMA as a chemical inhibitor of ERK1/2 *S*-acylation, in contrast to the well-established 2BP, emphasizes the potential utility of new chemical tools targeting DHHCs.

We additionally identified the enzymatic mediators of ERK2's acylation and deacylation, with zDHHCs 7, 14, and 21 emerging as writers, and APT2, as a key eraser. Interestingly, traditional methods to identify writers and erasers, including both overexpression and knockdown of said proteins, failed to reveal DHHC and APT regulators of ERK *S*-acylation. This result emphasizes that the identification of molecular determinants for a substrate whose steady state *S*-acylation status is tightly regulated by multiple actors requires different experimental outputs. In the case of ERK2, metabolic labeling enabled observation of changes in palmitate incorporation with DHHC overexpression, while co-immunoprecipitation validated DHHC/ERK interactions. Also interesting here is ERK2's association with zDHHC5 (Figure 5.S5C). This plasma-membrane localized PAT is unlikely a writer of ERK1/2 S-acylation, given its inability to increase fatty acid incorporation. However, proximity proteomics experiments indicate that it is associated with Grb2, an adaptor protein that links the MAPK pathway to activated RTKs. [162] These associations suggest it has a role as a scaffolding protein in the EGFR signaling complex.

Observation of organ-specific changes in ERK1/2 *S*-acylation in a mouse model of metabolic syndrome underscores the responsiveness of this modification to the organismal environment and its potential as a regulatory mechanism. Given our data that suggest ERK acylation status regulates its activity, this strongly suggests that acylation could be a significant contributor to altered ERK signaling in metabolic syndrome. The alterations in expression of ERK *S*-acylation writers and erasers suggest that the acylation machinery is sensitive to metabolic stress – an observation with implications not only for ERK2 but also for the panel proteins whose activity is regulated by *S*-acylation.

Overall, this work adds a new element to the regulation of ERK2 and contributes to our growing understanding of the role of dynamic *S*-acylation in regulating signal transduction.

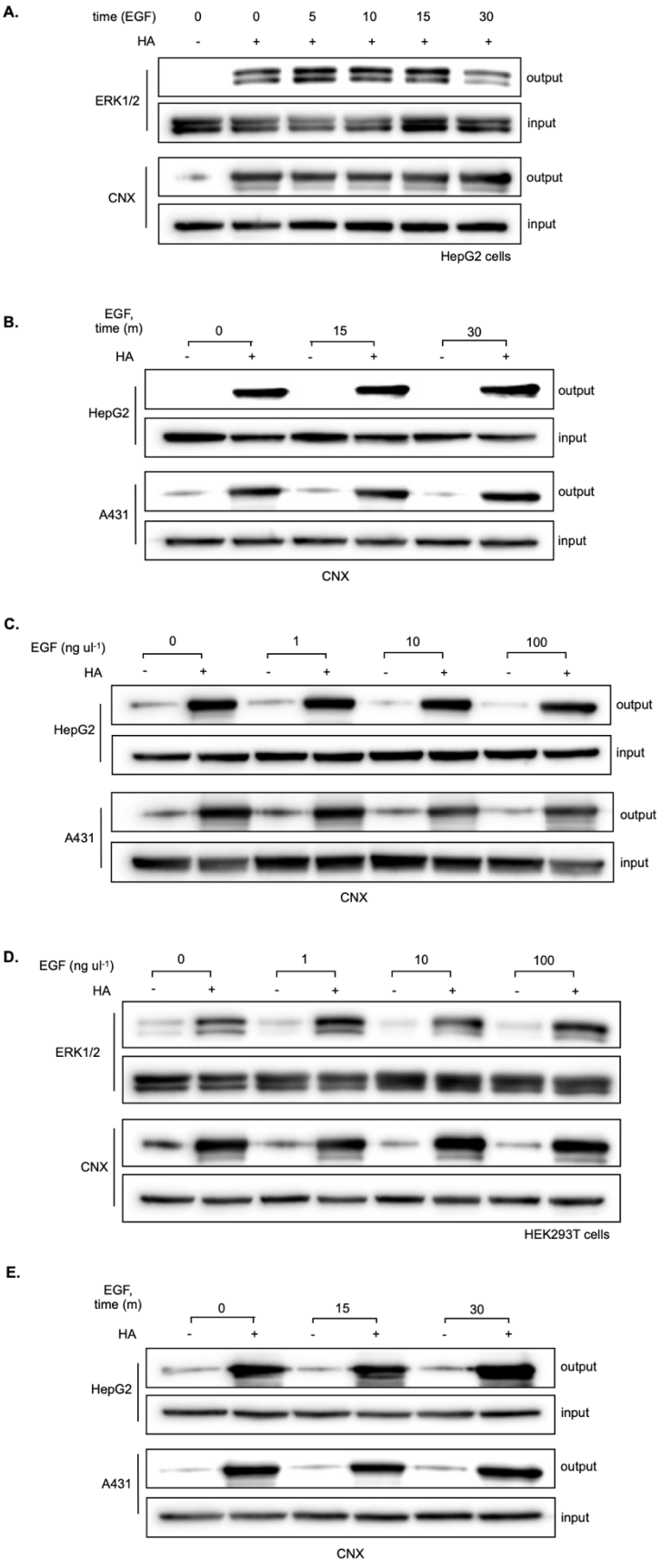

Figure 5.S1. The extracellular signaling regulated kinases (ERK1/2) are dynamically palmitoylated. (A) ABE assay carried out in HepG2 following stimulation with EGF (1 ng mL^{-1}) for 0, 5, 10, 15, and 30 minutes. (B) Western blots for calnexin (CNX), used as both a loading and assay control for 2A. (C) Western blots for calnexin (CNX), used as both a loading and assay control for 2B. (D) ABE assay carried out in HEK293T cells following stimulation with 0, 1, 10, and 100 ng mL^{-1} EGF for 15 minutes. (E) Western blots for calnexin (CNX), used as both a loading and assay control for 2C.

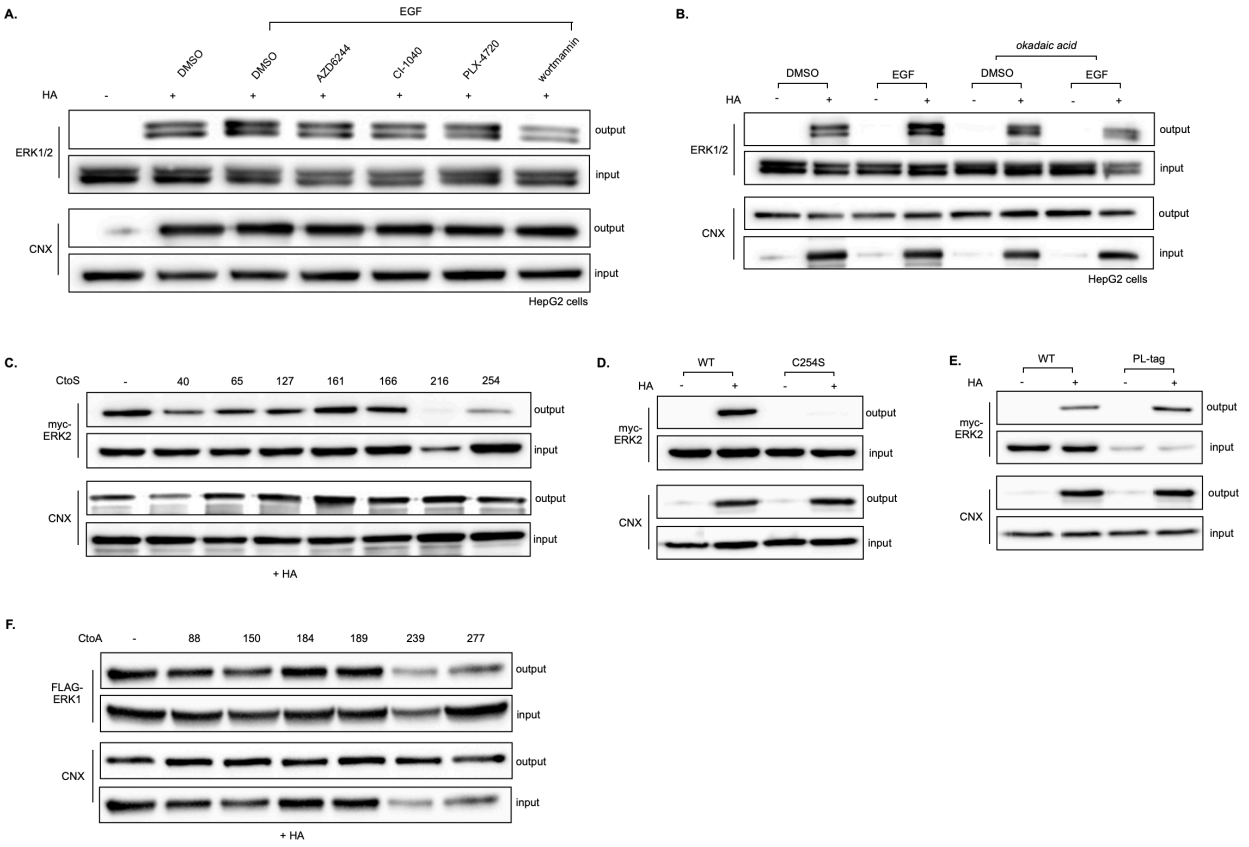

Figure 5.S2. Understanding the molecular determinants of ERK1/2 dynamic *S*-acylation. (A) ABE assay on HepG2 cells treated with DMSO or MAPK and PI3K pathway inhibitors, followed by EGF treatment (15 minutes, 1 ng mL^{-1}). (B) ABE assay carried out on HepG2 cells treated with DMSO or okadaic acid, followed by EGF treatment (15 minutes, 1 ng mL^{-1}). (C) ABE carried out on HEK293T cells overexpressing a panel of ERK2 CΔA mutants. (D) ABE of HEK293T cells expressing either WT or myc-tagged ERK2(C254A). (E) ABE of HEK293T cells expressing either WT or paralemmin (PL)-tagged ERK2. (F) ABE carried out on HEK293T cells overexpressing a panel of 3x-FLAG tagged ERK1 CΔA mutants.

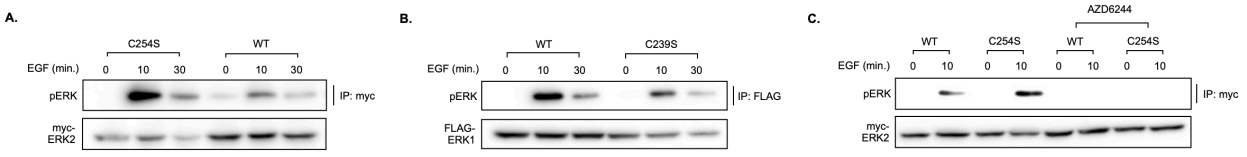

Figure 5.S3. Mapping crosstalk between ERK2 *S*-acylation and TEY phosphorylation. (A) Immunoprecipitation of WT or palmitoylation-deficient myc-ERK2 in HepG2 cells stimulated with EGF (0, 10, and 30 minutes, 1 ng mL^{-1}). (B) Immunoprecipitation of WT or palmitoylation-deficient 3xFLAG-ERK1 in HEK293T cells stimulated with EGF (0, 10, and 30 minutes, 1 ng mL^{-1}). (C) Immunoprecipitation of WT or palmitoylation-deficient myc-ERK2 in HEK293T cells stimulated with EGF (0, and 10 minutes, 1 ng mL^{-1}), with or without MEK inhibitor AZD6244.

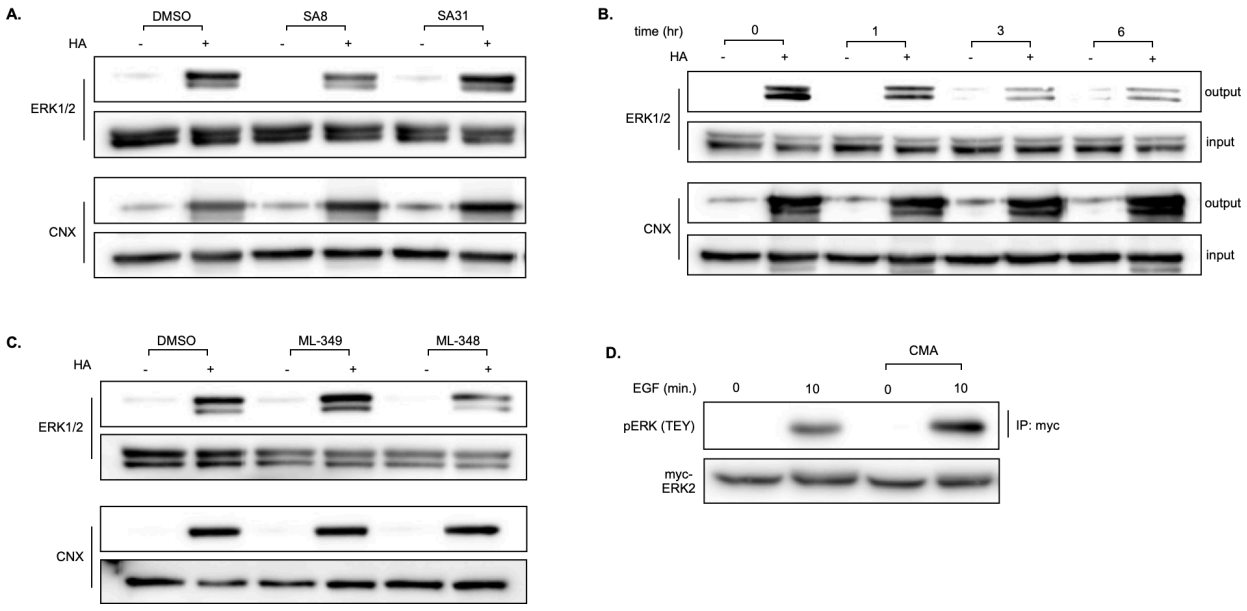

Figure 5.S4. Chemical inhibition of ERK1/2 *S*-acylation. (A) ABE of HepG2 cells treated with DMSO, CMA (20 μM, 3 hours), or 14 (20 μM, 3 hours), an inactive analogue of CMA. (B) Timecourse ABE (0, 1, 3, and 6 hours) of HepG2 cells treated with CMA (20 μM). (C) ABE of HepG2 cells treated with DMSO, ML-348 (20 μM, 3 hours), or ML-349 (20 μM, 3 hours).

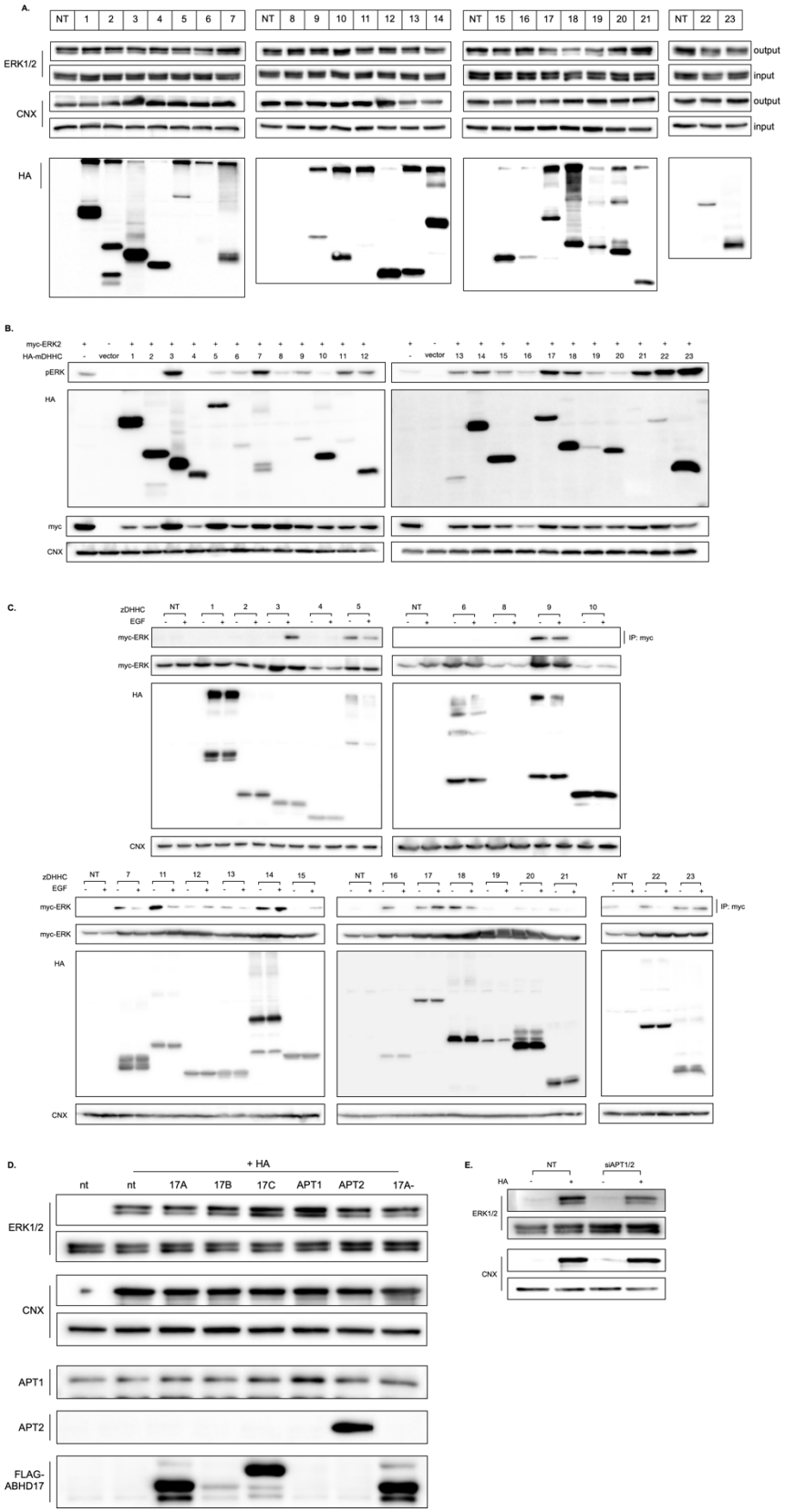

Figure 5.S5. Identification of the writer and eraser enzymes mediating ERK2 *S*-acylation. (A) ABE of HEK293T cells overexpressing a panel of murine DHHC family proteins. (B) Analysis of phospho-ERK(Thr185/Tyr187) in HEK293T cells overexpressing a panel of murine DHHC proteins, following EGF stimulation (10 minutes, 1 ng mL^{-1}). (C) Co-immunoprecipitation of myc-ERK2 with HA-tagged DHHC proteins in HEK293T cells with or without EGF stimulation (10 minutes, 1 ng mL^{-1}). Co-immunoprecipitated proteins were visualized via Western blotting for myc-ERK2. (D) ABE of HEK293T cells overexpressing a panel of known APT enzymes. (E) ABE in HEK293T cells following siRNA-mediated knockdown of APT1 and APT2.

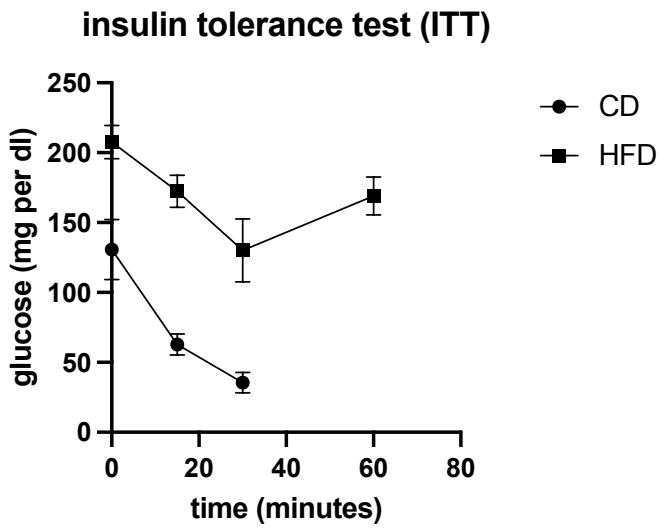

Figure 5.S6. ERK1/2 *S*-acylation in a model of metabolic syndrome. Insulin tolerance test (ITT) for mice fed either a control diet (CD) or a high-fat diet (HFD). *mean ± std, n = 5*.

Chapter 6: Development of fluorescent probes for the SARS-CoV-2 proteases

6.1. Introduction

In late 2019, a novel coronavirus emerged, sparking a world-wide pandemic that has led to levels morbidity and mortality unprecedented in the modern era and stressed health systems globally. The etiological agent is severe acute respiratory syndrome coronavirus 2 (SARS-CoV-2). Coronaviruses are a group of pathogenic microbes that can successfully infect and cause disease in many species of birds and mammals. In fact, human coronavirus infection is zoonotic, thought to originate in bats and transmitted to humans via an intermediary species, though this intermediary is as-yet unknown for SARS-CoV-2. [163] Coronaviruses possess a positive sense, single-stranded RNA genome that is non-segmented and enclosed in a nuclear capsid; notably, it is quite large. In fact, the genome of the novel human virus, SARS-CoV-2, is over 29,000 bases. Another noteworthy feature of coronaviruses, including SARS-CoV-2, is their lipidic, glycoprotein-studded viral envelope. The proteins of this envelope contribute to the cell and tissue tropisms demonstrated by SARS-CoV-2, as well as SARS-CoV-1 and Middle Eastern respiratory syndrome (MERS).[164, 165] In fact, although SARS-CoV-2 carries "respiratory" in its moniker, it exploits the broadly expressed angiotensin-converting enzyme 2 (ACE2) receptor for entry into target endothelial and epithelial cells.[166, 167] This contributes to both the specificity and breadth of infection, as other organs and organ systems, including the nervous system, are significantly affected coronavirus disease 2019 (COVID-19).[168] The lipid envelope also dictates viral stability and thus transmission; human-to-human transmission of SARS-CoV-2 occurs via airborne droplets and, possibly, a fecal-oral route.[169]

6.2. Results and discussion

Two targets for the development of antiviral drugs for the treatment of COVID-19 are the cysteine proteases of SARS-CoV2, the papain-like protease (PLpro) and main protease (M^{pro}, $3CL^{pro}$). Together, these enzymes are responsible for cleaving the viral polypeptides, thereby driving the early stages of infection and antagonizing the protective interferon response. Since these proteases are essential to the viral life cycle, they also represent attractive drug targets. Given that current viral inhibitors, such as lopinavir and ritonavir, have shown no clinical benefit for patients with Covid-19, there is a need to identify small molecule therapeutics.[170, 171]

While solved crystal structures of both PLpro and $3CL^{pro}$ enable the computational design and screening of small molecule inhibitors targeting these proteases, an *in vitro* assay is needed to assess the potential of these inhibitors in cellular and clinical models. Here, we present the design and validation of a fluorogenic peptide cleavage assay to monitor enzyme activity and assess inhibitor effectiveness. In this assay, peptides with cleavage site motifs of PLpro and M^{pro} substrates were conjugated to the fluorophore 7-amino-4-methylcoumarin (AMC) via its amino group, quenching its fluorescent signal. Enzymatic cleavage of this linkage releases AMC and

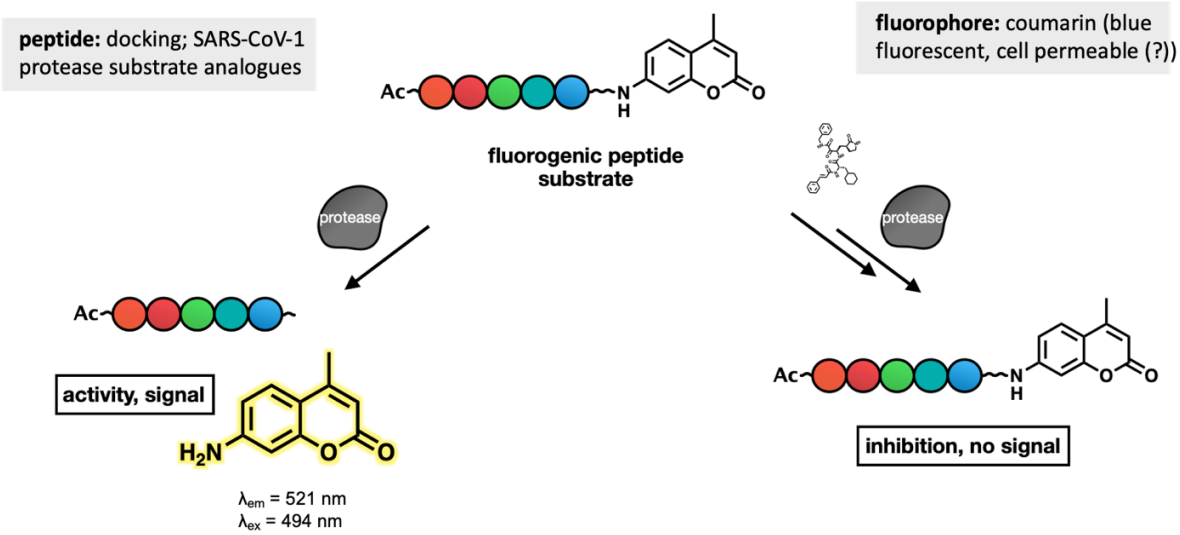

Figure 6.1. Schematic of assay design.

generates a fluorescent signal proportional to enzyme activity; effective small molecule inhibitors will limit enzyme activity and thus fluorescent signal (Figure 6.1). Screening a series of recognition sequences for both proteases revealed the LKGG and TVLQ tetrapeptide motifs to have the best catalytic efficiency for PLpro and M^{pro}, respectively. Therefore, the biochemical assay was optimized for the probes Ac-LKGG-AMC (PLpro) and Ac-TVLQ-AMC (M^{pro}) (Figures 6.2 and 6.3).

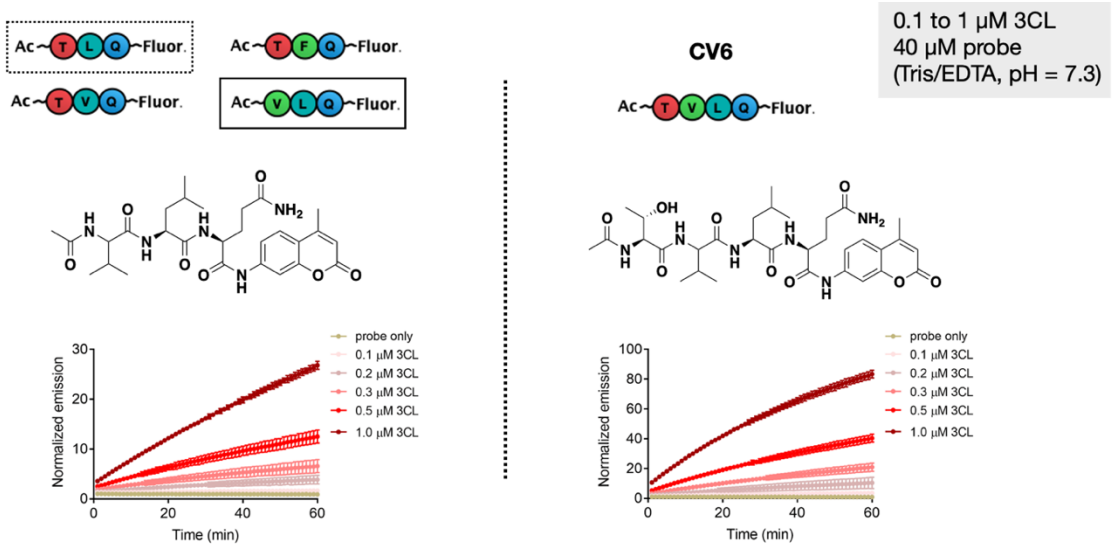

Figure 6.2. Screening and validation of CV6 as a fluorogenic probe for 3CL.

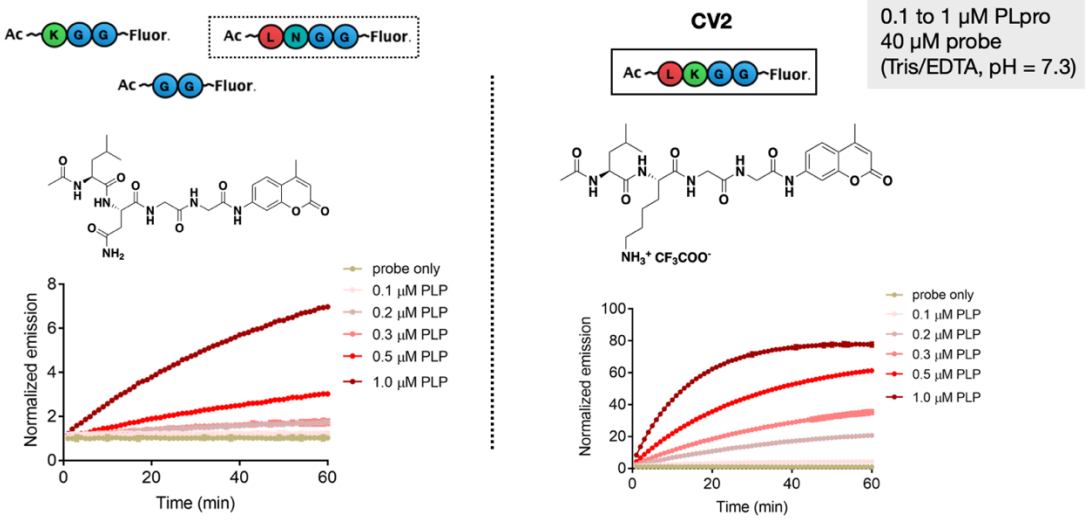

Figure 6.3. Screening and validation of CV2 as a fluorogenic probe for PLpro.

Preliminary screening data validates assay design and effectiveness, as initial screening of a library of rationally designed inhibitors and computationally screened small molecules reveals a novel molecule that binds to the PLpro active site and inhibits its activity (Figure 6.4). Overall, this assay possesses

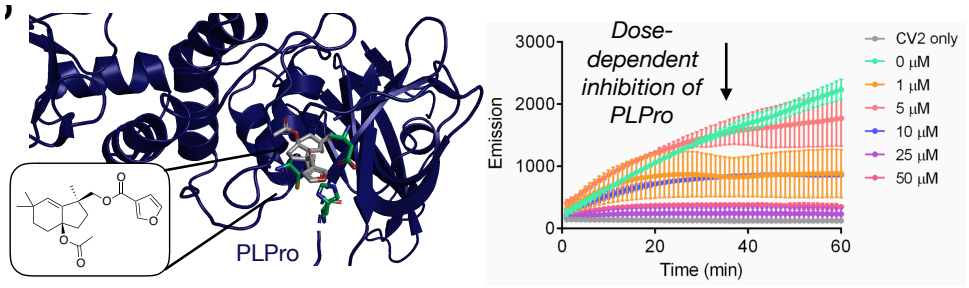

Figure 6.4. Application of assay to identify a PLpro inhibitor. Example hit from initial screening, showing both docking results for the molecule against PLpro and *in vitro* dose-dependent inhibition of the protease.

Chapter 7: Methods

7.1 Biochemical

In vitro fluorescence polarization assay of zDHHC20 for molecule screening and IC_{50} determination with 1-hour preincubation

We used a 48 μl protocol for initial molecule screening and IC_{50} determination with 1 hour of preincubation. Purified zDHHC20 (64 nM in 12 μL) in reaction buffer (50 mM HEPES, 150 mM NaCl, 1 mM EDTA, 2 mM TCEP, 2 mM DDM, pH 7.0) or reaction buffer with protein storage buffer was added to a 384-well optical bottom plate (ThermoFisher). 12 μL of the small molecule stock in reaction buffer were added, resulting in a 24 μL mixture of enzyme and small molecule, and the mixtures were incubated in 37 ˚C for 1 hour. The MasterMix II (24 μL), containing 8 μM palmitoyl-CoA and 2.5 μM peptide 01(5-FAM-GTQGCMGLPCVVM-COOH) in reaction buffer, was added to initiate the reaction, resulting in 4 μM and 1.25 μM as the final concentration of palmitoyl-CoA and peptide 01, respectively. Fluorescence measurements were recorded on Synergy Neo2 Hybrid Multi-Mode Reader (BioTek Instruments, Inc.) with Dual FP Green filter cube. Fluorescence polarization (λ_{ex} = 485/20 nm, λ_{em} = 528/20 nm, gain=35, read from the top with height 7.5 mm, and filter switching method) was measured at 1-min time intervals for 2 hours at 37 ˚C. Assay data were exported in Microsoft Excel 2016. For all molecule screening and IC_{50} determination, we performed the assay in kinetics mode, and data points at t=118 min were utilized as readout of enzyme activities of different samples for comparison.

In vitro assay of APT inhibition

Purified APT1 or APT2 (200 nM in 75 μL) in DPBS or DPBS alone was added to the 96-well optical bottom plate (ThermoFisher), followed by 75 μL of 50, 100, or 200 μM of 2BP or CMA

in DPBS. Controls were incubated with an equal volume of DMSO. The mixtures were incubated in 37 ˚C for 1 hour. At the end of pre-incubation, 150 μL of 2 μM DPP-5 solution in DPBS was added, resulting in a final concentration of: 50 nM APT1/2; 1 μM DPP-5; 0, 12.5, 25, 50 μM 2BP or CMA. Fluorescence measurements were recorded on Synergy Neo2 Hybrid Multi-Mode Reader (BioTek Instruments, Inc.). Fluorescence intensities (excitation wavelength λ_{ex} = 490/20 nm, emission wavelength λ_{em} = 545/20 nm, gain=80, read from bottom with height 4.5 mm and sweep method) were measured at 15-second time intervals for 1 hour at 37 °C. The initial velocity was calculated from linear regression of the first 11 data points using GraphPad Prism 9.

Acyl-biotin exchange (ABE) assay

A 10 cm plate of cells was washed twice with cold DPBS, lysed with 1-2 mL of RIPA lysis buffer supplemented with a protease inhibitor cocktail and 50 mM *N*-ethylmaleimide (NEM) (Acros), and subjected to end-over-end rotation at 4 °C for at least three hours. Following centrifugation at 13,000*g* for 20 min. at 4 °C, the supernatant was collected. Protein concentration was measured using the BCA assay (ThermoFisher), and equal amounts of total protein from each sample were then subjected to acetone precipitation. The resulting pellet was dissolved by sonication in resuspension buffer (4% SDS, 50 mM HEPES, 150 mM NaCl, 5 mM EDTA, pH 7.4; 100 μL per mg of protein) containing 50 mM NEM, and then Triton buffer (0.2% Triton X-100, 50 mM HEPES, 150 mM NaCl, 5 mM EDTA, pH 7.4; 250 μL per mg of protein) containing 50 mM NEM was added. This protein solution was rotated end-over-end for 2-3 hours at 25 °C, followed by two chloroform–methanol precipitations to remove excess NEM. The resulting protein pellet was dissolved in 80 μL of resuspension buffer via sonication. The protein sample was divided into two equal parts for ±hydroxylamine (HA) (Combi-Blocks) treatment. Each sample was treated with

160 μL of either -HA buffer (Triton buffer) or +HA buffer (Triton buffer containing 0.7 M HA, pH 7.2-7.4). Samples were incubated for 1 hour at room temperature with shaking, and then proteins were precipitated by chloroform–methanol precipitation to remove excess HA. Protein pellets were resuspended by sonication in 40 µL of resuspension buffer containing 10 μM EZ-Link HPDP-Biotin (ThermoFisher), diluted with 160 µL of Triton buffer containing 10 μM HPDP-Biotin, and incubated for 2 hours at room temperature with shaking. Excess biotin was removed with two sequential chloroform-methanol precipitations. Protein pellets were dissolved in 40 µL resuspension buffer by sonicating, and the solution volume was brought to 400 µL with Triton buffer. Protein (25-25 µg) was removed to serve as an expression control ('input'). The remaining solution was diluted with Triton buffer, and streptavidin–agarose beads (50 μL of slurry per 1 mg of protein) were added to each sample, which were then incubated at 4 °C overnight with end-over-end rotation. Unbound proteins were removed by washing with 1 mL wash buffer (0.1% SDS, 0.2% Triton X-100, 50 mM HEPES, 150 mM NaCl, 5 mM EDTA, pH 7.4). Bound proteins ('output') were eluted by boiling the beads for 10 min at 95 °C with 1x Laemelli sample buffer (Alfa Aesar) containing 9% β-mercaptoethanol or 30 mM DTT. The protein was resolved on 8-12% SDS–PAGE gels and subjected to Western blotting using the protocol described above.

CMA ABE assay

At 40-70% confluency, 10-cm plates of HEK293T cells were transfected with 4 μg pcDNA.6.1-eGFP-GobX or 6 μg pCMV-HA-Myd88 plasmid. At 24 hours post transfection, cells were treated with CMA (0, 5, 10, and 20 μM) for 6 hours. For endogenous targets, 10 cm dishes of MDA-MB-231 or 3T3-L1 preadipocytes at 80% confluency were treated with CMA (0, 20 µM) for 3 or 6

hours. Cells were then lysed and samples prepared in accordance with the procedure described in the ABE protocol.

17-ODYA metabolic labeling assay

HEK293T cells (~200,000 cells per well) were plated in 12-well plate (Fisher) in growth medium. After 48 hours, cells were treated with various concentrations of CMA or 2BP in serum-free DMEM for 3 hours. After 1 or 3 hours of preincubation, the media was replaced with metabolic labeling media (serum-free DMEM with 50 mM 17-ODYA preincubated with 5% BSA) complemented with the same concentration of either CMA or 2BP, and the cells were then incubated for another 6 hours. Cells were lysed by SDS-free lysis buffer (50 mM HEPES, 150 mM NaCl, 1% Triton-100, 0.5% sodium deoxycholate, pH=7.4). If no hydroxylamine treatment, after centrifugation, the final cell lysate was collected and normalized to 1 mg/ml in 30 μL. For Cu-AAC conjugation, Master mix (2.4 μL) made from equal volumes of 5 mM TAMRA-azide (click chemistry tools), 5 mM TBTA (Cayman), 50 mM $CuSO_4$, and 50 mM TCEP was added into 30 μL cell lysate. The resulting solution was incubated for 1 hour at room temperature in darkness, then the reaction was quenched with 6x Laemelli sample buffer containing 9% β-mercaptoethanol before running the SDS-PAGE gels. For hydroxylamine treatment, after centrifugation, the final cell lysate was collected and normalized to 1 mg/ml in 100 μL. For Cu-AAC conjugation, Master mix (8 μL) made from equal volumes of 5 mM TAMRA-azide (click chemistry tools), 5 mM TBTA (Cayman), 50 mM $CuSO_4$, and 50 mM TCEP was added into 100 μL cell lysate. The resulting solution was incubated for 1 hour at room temperature in darkness. The click reaction was quenched by chloroform-methanol precipitation. Each protein pellet was resuspended in resuspension buffer (the same in ABE assay), then was divided into two equal parts for ±

hydroxylamine (HA) treatment. Each sample was treated with 160 μL of either -HA buffer (Triton buffer) or +HA buffer (Triton buffer containing 0.7 M HA, pH 7.2-7.4). Samples were incubated for 1 hour at room temperature with shaking, and then proteins were precipitated by chloroform–methanol precipitation to remove excess HA. Protein pellets were resuspended by sonication in 50 μL of resuspension buffer and 6x Laemelli sample buffer containing 9% β-mercaptoethanol was added before running the gels. Proteins were resolved with 12% SDS-PAGE and visualized with FluoroChem R (Proteinsimple) using the MultiFluo-Green channel. Coomassie Blue was used to stain total protein.

MTS assay

Cells (~100,000 cells per well for HEK293T, ~50,000 cells per well for 3T3-L1, MDA-MB-231, and HeLa, and ~70,000 cells per well for HepG2) were plated in 96-well plates (Corning) in growth media. After 24 hours, cells were washed once with DPBS and treated with CMA or 2BP in a concentration gradient for either 6 or 24 hours in serum-free DMEM (EMEM for HepG2 only). Then cells were washed by DPBS and then treated with the MTS reagent (Abcam) in serum-free DMEM GlutaMAX (EMEM, HepG2 only) for 2-3 hours. Absorption at 490 nm was measured on Synergy Neo2 Hybrid Multi-Mode Reader (BioTek Instruments, Inc.). The data are taken from at least $n=2$ independent experiments containing at least two replicates each time. Assay data were analyzed using Microsoft Excel 2016 and nonlinear curve fitting was performed using GraphPad Prism 8.

In cellulo labeling assay of DHHC library

HEK293T cells (~82,500 cells per well) were plated in 24-well plate (Fisher). For human DHHC labeling, after 20-24 hours, cells were transfected with 0.6 μg plasmids with PEI. For mouse DHHC labeling, cells were transfected with 0.6 μg plasmids with Lipofectamine 3000 (ThermoFisher) according to manufacturer's protocol. For 8 labeling assay, at 24 hours post transfection, cells were incubated with serum-free DMEM complemented with 8 for 2 hours. For CMA competitive labeling assay, at 24 hours post transfection, the media was removed, and cells were incubated with serum-free DMEM with CMA for 2 hours, then 8 in DMEM was added into media, resulting in a final concentration of 8 at 1 μM. Cells then were washed with DPBS twice and lysed with 50 μL RIPA buffer (50 mM HEPES, 150 mM NaCl, 1% Triton-100, 0.5% sodium deoxycholate, 0.1% SDS, pH=7.4). After spun down, the final cell lysate was collected and normalized to 1 mg/mL in 30 μL before Cu-AAC conjugation. Cu-AAC conjugation with TAMRA-azide was performed according to the protocol shown above. Proteins were resolved with 12% SDS-PAGE and visualized with FluoroChem R (Proteinsimple) using the MultiFluo-Green channel. Western blots of anti-myc or anti-HA were used as a control to indicate the molecular sizes of DHHC proteins and the amount of DHHC proteins. Cells were labelled in serum-free media without further notice. When cells were labelled in serum-complemented media (0.1% or 1% FBS-complemented DMEM), for 8 labeling assay, at 24 hours post transfection, cells were incubated with DMEM complemented with 8 and corresponding concentration of FBS for 2 hours. For CMA competitive labeling assay, at 24 hours post transfection, the media was removed, and cells were incubated with DMEM complemented with CMA and corresponding concentration of FBS for 2 hours, then 8 in DMEM was added into media, resulting in a final concentration of 8 at 10 μM.

In cellulo labeling of endogenous DHHC proteins

At 80-90% confluency,10 cm dishes of HEK293T cells were incubated with DMSO or 20 μM CMA in serum-free DMEM GlutaMAX for 3 hours, followed DMSO or 20 μM 8 for an additional 3 hours. After treatment, cells were washed twice with cold DPBS and lysed in 1 mL of SDS-free RIPA buffer for 1 hour at 4 °C. Following centrifugation at 13,000*g* for 20 min. at 4 °C, the supernatant was collected, and protein concentration was determined using a BCA assay. Samples were normalized to 1 mg/mL. For Cu-AAC conjugation, a master mix (equal volumes of 5 mM biotin-azide (Click Chemistry Tools), 5 mM TBTA (Cayman), 50 mM $CuSO_4$, and 5 mM TCEP) was prepared and added to each sample (16 μL for 184 μg protein). The resulting solution was rotated for 1 hour at room temperature and then quenched with 100 mM EDTA (100x) and subjected to two chloroform-methanol precipitations. Protein pellets were dissolved in 40 μL ABE resuspension buffer by sonicating, and the total volume was brought to 400 μL with ABE Triton buffer. Protein pellets were dissolved in 40 μL resuspension buffer by sonicating, and the solution volume was brought to 400 μL with Triton buffer. Protein (20-25 μg) was removed to serve as an expression control ('input'). The remaining solution was diluted with Triton buffer, and streptavidin–agarose beads (50 μL of slurry per 1 mg of protein) were added to each sample, which were then incubated at 4 °C overnight with end-over-end rotation. Unbound proteins were removed by washing three times with 1 ml of ABE wash buffer. Bound proteins ('output') were eluted by boiling the beads for 10 min at 95 °C with 1x Laemelli sample buffer (Alfa Aesar) containing 20-30 mM DTT. The protein was resolved on 8-12% SDS–PAGE gels and subjected to Western blotting using the protocol described above. For non-competitive 8 labeling, the CMA pretreatment step was not followed.

Lipid uptake assays

On day 0, 3T3-L1 preadipocytes were plated at $6.0x10^4$ in an 8-well dish. On day 1, cells were cultured in serum-free media for 12 hours, and then, on day 2, treated with either CMA (20 uM) or DMSO for 3 hours, followed by treatment with 10 μM BSA-bound **oleate** and 2 μM BODIPY 493/503 or BODIPY-palmitate for 6 hours. DAPI was then added, and then cells were washed and fixed with 4% paraformaldehyde. Cells were washed (5x5 min.) with PBS and mounted in Prolong Antifade Mountant (Thermo Fisher). Slides were imaged using an inverted epifluoresence microscope (Leica DMi8) equipped with a Hamamatsu Orca-Flash 4.0 camera, a 63x oil objective (numerical aperture 1.4), and a 300 W Xenon light source (Sutter Lamba XL). LASX software was used to obtain BODIPY and brightfield images.

7.2 Synthetic

General materials

For chemical synthesis, reagents and solvents were purchased from commercial sources and used without further purification. Silica gel P60 (SiliCycle, 40–63 μm, 230–400 mesh) was used for column chromatography. Analytical thin-layer chromatography was performed using SiliCycle 60 F254 silica gel (pre-coated sheets, 0.25 mm thick) with detection at 214 nm.

Spectrometry

Low-resolution-mass spectral analysis and liquid chromatography analysis were carried out on an Advion Expression-L mass spectrometer (Ithaca, NY) with electron spray ionization (ESI) in the positive mode coupled to an Agilent 1220 Infinity LC System with an Agilent Poroshell 120 column (Santa Clara, CA). Two methods were performed as follows: (A) Gradient from 1:9 water:methanol/0.1% formic acid (FA) to 9:1 water:methanol/0.1% FA (3 min.); 9:1

water:methanol/0.1% FA (6 minutes) isocratic; gradient from 9:1 water:methanol/0.1% FA to 1:9 water:methanol/0.1% FA (1 min); 1:9 water:methanol/0.1% FA isocratic (1 min.); (B) Gradient from 5:5 water:methanol/0.1% FA to methanol (3 min.); gradient from methanol to 1:9 water:methanol/0.1% FA (8 min.). Automated flash column chromatography purification was carried out on a Biotage system Isolera One using SNAP Biotage columns. Compounds were analyzed by UPLC-MS and purity was assigned by analytical RP-UPLC. NMR spectra were recorded on the BRUKER Ascend 400 at the Department of Chemistry NMR Facility, University of Chicago, for ^{1}H-400 MHz and ^{13}C-101 MHz measurements. Chemical shifts are given in parts per million (δ) referenced to TMS (δ = 0.00 ppm ^{1}H-, ^{13}C-NMR). Coupling constants are given in Hertz. High resolution mass spectra measurements were performed on an Agilent 6224 Tof. using a combination of atmospheric pressure chemical ionization and electrospray ionization at the Department of Chemistry Mass Spectrometry Facility, University of Chicago.

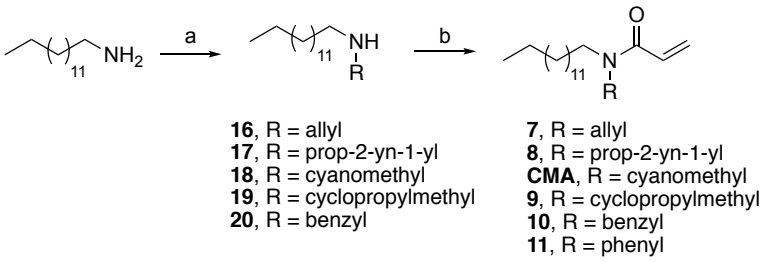

Scheme 1. General synthetic route for the synthesis of acrylamide inhibitors. Conditions: a) RBr, K_2CO_3, DMF, 85°C, 8-15h, **16**: 25%, **17**: 49%, **18**: 69%, **19**: 54%, **20**: 50%. b) acryloyl chloride, K_2CO_3, DMF, r.t., 2h30, **7**: 51%, **8**: 53%, **CMA**: 65%, **9**: 69%,**10**: 31%,**11**: 62%

General method A for the synthesis of secondary amine.

To a solution of tetradecylamine (1.0 eq.) in DMF (2-5 mL) was added potassium carbonate (2.0 eq.), followed by the desired bromo compound (0.75 eq.). The reaction mixture was stirred at 85° C until the reaction was complete (8-12 hours). Then, the reaction mixture was cooled down to r.t.

and diluted with a saturated aqueous solution of sodium bicarbonate and the aqueous phase was extracted with ethyl acetate (3x50 mL). The combined organics were then dried over Na_2SO_4 and concentrated. The obtained crude product was then purified by automated flash chromatography (2-10% MeOH in DCM) to afford the pure product.

General method B for the synthesis of acrylamide.

To a solution of the amine (1.0 eq.) in DMF (2-5 mL) was added potassium carbonate (3.0 eq.) and after 15 minutes of stirring, acryloyl chloride (2.0 eq.). The reaction mixture was stirred at r.t. for 2 hours or until the reaction was complete. The reaction mixture was then diluted with water (20 mL) and extracted with ethyl acetate (3x20 mL). The combined organics were washed with brine, dried over Na_2SO_4, and evaporated to dryness. The obtained crude product was then purified by automated flash chromatography (20-80% ethyl acetate in hexanes) to afford the pure product.

General method C for the synthesis of acrylamide.

To a solution of the amine (1.0 eq.) in DCM (2-5 mL) was added triethylamine (3.0 eq.) and after 15 minutes of stirring, acryloyl chloride (2.0 eq.). The reaction mixture was stirred at r.t. for 2 hours or until the reaction was complete. The reaction mixture was then diluted with water (20 mL) and extracted with ethyl acetate (3x20 mL). The combined organics were washed with brine, dried over Na2SO4, and evaporated to dryness. The obtained crude product was then purified by filtration on a pad if silica with 50% ethyl acetate in hexanes to afford the pure product.

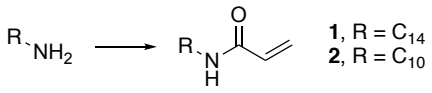

1, R = C_{14}
2, R = C_{10}

Scheme 2. Synthetic route used for the synthesis of **1** & **2**. Condition: acryloyl chloride, K_2CO_3, DMF, r.t., 3h, **1**: 70%, **2**: 33%.

***N*-tetradecylacrylamide (1).** Following general procedure B, **1** was obtained from tetradecylamine (2.34 mmol, 0.50 g) as a white solid (0.42 g, 70%). ^{1}H NMR (400 MHz, $CDCl_3$) δ 6.26 (dd, *J* = 17.0, 1.5 Hz, 1H), 6.09 (dd, *J* = 17.0, 10.2 Hz, 1H), 5.77 (s, 1H), 5.61 (dd, *J* = 10.2, 1.5 Hz, 1H), 3.36 – 3.26 (m, 2H), 1.52 (p, *J* = 7.3 Hz, 2H), 1.24 (s, 24H), 0.87 (t, *J* = 6.8 Hz, 3H). ^{13}C NMR (101 MHz, $CDCl_3$) δ 165.6, 131.1, 126.2, 39.8, 32.1, 29.8, 29.8, 29.7, 29.7, 29.5, 29.4, 27.1, 22.8, 14.3. HRMS m/z [M] calcd for $C_{17}H_{33}NO$ 267.2562, found: 267.2568. UPLC (method B): t_R = 5.77 min., purity: 96%.

***N*-decylacrylamide (2).** Following general procedure A, **2** was obtained from 1-decanamine (3.18 mmol, 0.50 g) as a white solid (0.167 g, 33%). ^{1}H NMR (400 MHz, $CDCl_3$) δ 6.29 – 6.21 (m, 1H), 6.10 (ddd, *J* = 17.0, 10.2, 2.6 Hz, 1H), 5.90 (d, *J* = 40.4 Hz, 1H), 5.63 – 5.57 (m, 1H), 3.35 – 3.26 (m, 2H), 1.51 (q, *J* = 6.8 Hz, 2H), 1.26 (d, *J* = 16.4 Hz, 14H), 0.86 (t, *J* = 6.8 Hz, 3H). ^{13}C NMR (101 MHz, $CDCl_3$) δ 165.7, 131.2, 126.2, 39.8, 32.0, 29.7, 29.7, 29.4, 27.1, 22.8, 14.2. HRMS m/z [M] calcd for $C_{13}H_{25}NO$ 211.1936, found: 211.1938. UPLC (method B): t_R = 4.21 min., purity: 94%.

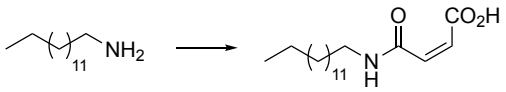

3

Scheme 3. Synthetic route used for the synthesis of **3**. Condition: maleic anhydride, toluene, 60°C, 1h30, 90%.

(*Z*)-4-oxo-4-(tetradecylamino)but-2-enoic acid (3). To a solution of maleic anhydride (2.30 mmol, 0.23 g) in toluene (6 mL) was added tetradecylamine (2.30 mmol, 0.50 g). The reaction mixture was stirred at 60°C for 1 hour 45 minutes. After full conversion, the reaction mixture was

cooled down to r.t. then diluted with an aqueous solution of 1M HCl. The formed precipitate was filtered, washed with 1 M HCl, and then left to dry on high vacuum to afford **3** as a white solid (0.65 g, 90%). ^{1}H NMR (400 MHz, CDCl3) δ 7.40 (s, 1H), 6.38 (d, *J* = 22.8 Hz, 1H), 3.37 (s, 1H), 1.60 (s, 2H), 1.25 (s, 19H), 0.87 (s, 3H). ^{13}C NMR (101 MHz, CDCl3) δ 166.2, 165.8, 136.9, 132.3, 41.0, 32.0, 29.8, 29.8, 29.7, 29.7, 29.5, 29.4, 29.1, 27.2, 22.8, 14.3. HRMS m/z [M] calcd for $C_{15}H_{27}NO_3$ 269.1991, found: 269.1988. UPLC (method B): t_R = 4.13 min., purity: 96%. (US2003/0203951 A1).

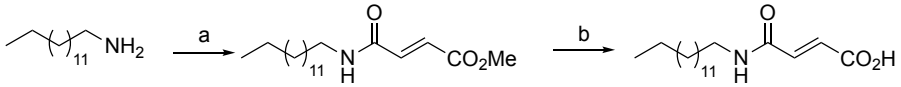

15 **4**

Scheme 4. Synthetic route used for the synthesis of **4**. Conditions: a) monomethyl fumarate, Oxyma, DIC, DIEA, DCM, r.t., 2h, 75%. b) LiOH 1.4 M, dioxane, r.t., 1h, 89%.

methyl (*E*)-4-oxo-4-(tetradecylamino)but-2-enoate (15). To a solution of tetradecylamine (0.94 mmol, 0.20 g) in DCM (11 mL) was added a solution of monomethyl fumarate (2.82 mmol, 0.37 g), Oxyma (1.41 mmol, 0.20 g), DIC (1.41 mmol, 222 μL) and DIPEA (1.41 mmol, 246 μL). The reaction mixture was stirred at r.t. for 2 hours. After full conversion, the reaction mixture was washed two times water, once with brine. The organics were dried over Na_2SO_4 and evaporated to dryness. The obtained crude was then purified by automated flash chromatography (20-50% EtOAc in hexanes) to afford **15** as a white solid (0.23 g, 75%). ^{1}H NMR (400 MHz, CDCl3) δ 6.92 – 6.77 (m, 2H), 5.73 (s, 1H), 3.81 (d, *J* = 7.4 Hz, 3H), 3.35 (q, *J* = 7.1 Hz, 2H), 1.54 (q, *J* = 7.2 Hz, 2H), 1.22 (d, *J* = 27.3 Hz, 22H), 0.88 (t, *J* = 6.8 Hz, 3H). ^{13}C NMR (101 MHz, $CDCl_3$) δ 167.2,

165.0, 136.9, 130.4, 52.9, 40.7, 32.0, 31.7, 29.8, 29.8, 29.8, 29.7, 29.6, 29.5, 29.4, 29.1, 27.0, 22.8, 14.1.

(*E*)-4-oxo-4-(tetradecylamino)but-2-enoic acid (4). To a solution of **15** (0.12 mmol, 0.04 g) in dioxane (2 mL) and THF (0.5 mL) was added a solution of LiOH 1.4 M (0.72 mmol, 0.50 mL). The reaction mixture was stirred at r.t. for 1 hour until the reaction was complete. The reaction mixture was then diluted with an aqueous solution of 1M HCl. The formed precipitate was filtered, washed with 1M HCl, and dried under high vacuum to afford **4** as a white solid (0.03 g, 89%). ^{1}H NMR (400 MHz, DMSO) δ 8.50 – 8.42 (m, 1H), 6.91 (d, *J* = 15.5 Hz, 1H), 6.49 (d, *J* = 15.5 Hz, 1H), 3.13 (q, *J* = 6.6 Hz, 3H), 1.47 – 1.36 (m, 2H), 1.23 (s, 21H), 0.85 (t, *J* = 6.8 Hz, 3H). ^{13}C NMR (101 MHz, DMSO) δ 166.6, 163.0, 137.2, 129.3, 31.3, 29.1, 29.0, 29.0, 29.0, 29.0, 28.8, 28.7, 28.7, 26.4, 22.1, 20.8, 14.0. HRMS m/z [M] calcd for $C_{18}H_{33}NO_3$ 311.246, found: 311.246. UPLC (method B): t_R = 4.00 min., purity: 98%.

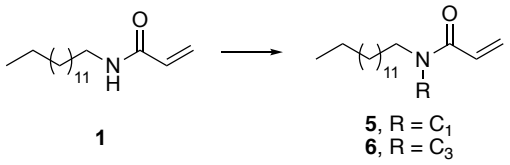

Scheme 5. Synthetic route used for the synthesis of **5** & **6**. Condition: NaH, bromoalkane, DMF, r.t., 8-16h, **5**: 85%, **6**: 72%.

***N*-methyl-*N*-tetradecylacrylamide (5).** To a solution of **1** (0.374 mmol, 0.10 g) in dry DMF (3 mL) under nitrogen was added NaH (60% in immersion oil, 1.87 mmol, 0.063 g, 5 eq.). After 20 minutes, iodomethane (1.87 mmol, 120 μL, 5 eq.) was added. The reaction was then stirred at room temperature for 8 hours. The reaction was then quenched with a solution of saturated NH_4Cl and diluted with EtOAc (30 mL). The aqueous layer was extracted with EtOAc (3x20 mL), and

the combined organics were washed with brine and dried over Na_2SO_4. Following concentration via rotary evaporation, the product was purified via column chromatography (10-40% EtOAc in hexanes) to yield **5** as a pale yellow oil (0.089 g, 85%). ^{1}H NMR (400 MHz, $CDCl_3$) δ 6.56 (ddd, *J* = 16.8, 10.5, 5.0 Hz, 1H), 6.31 (ddd, *J* = 16.7, 6.2, 2.1 Hz, 1H), 5.65 (ddd, *J* = 10.4, 3.7, 2.0 Hz, 1H), 3.36 (dt, *J* = 34.0, 7.6 Hz, 2H), 3.01 (d, *J* = 23.8 Hz, 2H), 1.56 (m, 2H), 1.25 (m, 20H), 0.86 (m, 3H). ^{13}C NMR (101 MHz, $CDCl_3$) δ 167.7, 128.1, 127.8, 127.7, 127.6, 50.3, 48.6, 35.6, 34.1, 32.1, 29.8, 29.8, 29.8, 29.7, 29.7, 29.7, 29.6, 29.5, 29.5, 29.0, 27.3, 27.1, 26.8, 22.8, 14.3. HRMS-ESI(+) m/z [M+] calculated for $C_{18}H_{35}NO$ 281.2724, found 281.2719. UPLC (method A): t_R = 6.12 min., purity: ≥ 99%.

***N*-(propyl)-N-tetradecylacrylamide (6).** Bromopropane (2.97 mmol, 0.27 mL, 10 eq.) was added to a solution of **1** (0.30 mmol, 79.2 mg, 1.0 eq.) and NaH (60% immersion in oil, 2.96 mmol, 118 mg, 10 eq.) in dry DMF (8 mL) under nitrogen. The resulting reaction was stirred at room temperature for 16h. The reaction was quenched with a solution of saturated NH_4Cl and the resulting solution was first diluted with EtOAc (30 mL) and then washed with brine (30 mL). The aqueous layer was washed with EtOAc (20 mL), organic layers were combined, dried over Na_2SO_4 and evaporated. Purification by chromatography (Silica, 2-15% EtOAc:Hexane) afforded **6** as transparent oil (0.07 g, 72%) . ^{1}H NMR (400 MHz, DMSO) δ 6.70 (ddd, *J* = 16.6, 10.3, 4.8 Hz, 1H), 6.10 (dd, *J* = 16.6, 2.6 Hz, 1H), 5.63 (dd, *J* = 10.3, 2.6 Hz, 1H), 3.26 (tt, *J* = 15.0, 5.3 Hz, 4H), 1.59 – 1.37 (m, 4H), 1.24 (s, 22H), 0.84 (td, *J* = 7.9, 7.3, 6.0 Hz, 6H). ^{13}C NMR (101 MHz, DMSO) δ 164.7, 128.7, 128.6, 126.8, 48.7, 47.3, 47.2, 45.7, 31.3, 29.4, 29.0, 29.0, 29.0, 28.9, 28.8, 28.7, 27.4, 26.5, 26.1, 22.6, 22.1, 20.6, 14.0, 11.3, 10.9. HRMS-ESI(+) m/z [M+] calculated for $C_{20}H_{39}NO$ 309.3032, found 309.3028. UPLC (method A): t_R = 7.36 min., purity: 98%.

***N*-allyltetradecan-1-amine (16).** Following general procedure A, the product was obtained from tetradecylamine (2.13 mmol, 0.45 g) and allyl bromide (1.59 mmol, 138 μL) as yellow solid (0.10 g, 25%). ^{1}H NMR (400 MHz, CDCl3) δ 5.98 (ddt, *J* = 16.7, 10.2, 6.4 Hz, 1H), 5.36 – 5.17 (m, 2H), 3.37 (d, *J* = 6.4 Hz, 2H), 2.77 – 2.65 (m, 2H), 1.64 (q, *J* = 7.2 Hz, 2H), 1.36 – 1.19 (m, 22H), 0.93 – 0.83 (m, 3H). ^{13}C NMR (101 MHz, CDCl3) δ 134.9, 117.6, 51.8, 48.8, 32.0, 29.7, 29.7, 29.7, 29.6, 29.6, 29.5, 29.4, 29.2, 27.3, 22.7, 14.1.

***N*-allyl-N-tetradecylacrylamide (7).** Following general procedure B, the product was obtained from **16** (0.29 mmol, 0.07 g) as transparent oil (0.04 g, 51%). ^{1}H NMR (400 MHz, CDCl3) δ 6.61 – 6.27 (m, 2H), 5.87 – 5.57 (m, 2H), 5.26 – 5.04 (m, 2H), 4.08 – 3.90 (m, 2H), 3.31 (dt, *J* = 35.8, 7.8 Hz, 2H), 1.55 (q, *J* = 7.1 Hz, 2H), 1.24 (d, *J* = 2.5 Hz, 22H), 0.86 (t, *J* = 6.7 Hz, 3H). ^{13}C NMR (101 MHz, CDCl3) δ 166.5, 166.0, 133.6, 133.4, 128.2, 128.1, 127.9, 127.7, 117.1, 116.7, 50.3, 48.8, 47.5, 46.8, 32.0, 29.8, 29.8, 29.7, 29.7, 29.5, 29.5, 29.4, 27.9, 27.2, 26.9, 22.8, 14.2. HRMS-ESI(+) m/z [M+] calculated for $C_{20}H_{37}NO$ 307.2875, found 307.2884. UPLC (method A): t_R = 6.95 min., purity: 96%.

***N*-(prop-2-yn-1-yl)tetradecan-1-amine (17).** Following general procedure A, the product was obtained from tetradecylamine (0.70 mmol, 0.16 g) and propargyl bromide (1.70 mmol, 63.1 μL) as yellowish solid (0.14 g, 49%). ^{1}H NMR (400 MHz, CDCl3) δ 3.41 (d, *J* = 2.4 Hz, 2H), 2.67 (t, *J* = 7.2 Hz, 2H), 2.19 (t, *J* = 2.4 Hz, 1H), 1.46 (q, *J* = 7.3 Hz, 2H), 1.24 (s, 23H), 0.87 (t, *J* = 6.7 Hz, 3H). ^{13}C NMR (101 MHz, CDCl3) δ 82.5, 71.3, 48.9, 38.3, 32.1, 30.0, 29.8, 29.8, 29.8, 29.8, 29.7, 29.7, 29.5, 27.4, 22.8, 14.2.

***N*-(prop-2-yn-1-yl)-N-tetradecylacrylamide (8).** Following general procedure B, the product was obtained from **17** (0.28 mmol, 0.07 g) as a white solid (0.05 g, 53%). ^{1}H NMR (400 MHz, CDCl3) δ 6.56 (ddd, *J* = 26.9, 16.8, 10.5 Hz, 1H), 6.46 – 6.27 (m, 1H), 5.70 (dd, *J* = 10.4, 2.1 Hz, 1H), 4.36 – 4.01 (m, 2H), 3.45 (t, *J* = 7.7 Hz, 2H), 2.36 – 2.11 (m, 1H), 1.60 (q, *J* = 7.1, 6.6 Hz, 2H), 1.24 (s, 22H), 0.86 (t, *J* = 6.7 Hz, 3H). ^{13}C NMR (101 MHz, CDCl3) δ 166.1, 128.8, 128.3, 128.0, 127.4, 79.2, 71.7, 47.5, 35.0, 32.0, 29.8, 29.8, 29.7, 29.7, 29.6, 29.5, 29.4, 29.1, 26.8, 22.8, 14.2. HRMS-ESI(+) m/z [M+] calculated for $C_{20}H_{35}NO$ 305.2719, found 305.2719. UPLC (method B): t_R = 5.37 min., purity: 98%.

2-(tetradecylamino)acetonitrile (18). Following general procedure A, the product was obtained from tetradecylamine (2.30 mmol, 0.50 g) and bromoacetonitrile (1.70 mmol, 120 μL) as a yellow solid (0.40 g, 69%). ^{1}H NMR (400 MHz, CDCl3) δ 3.56 (s, 2H), 2.69 (t, *J* = 7.1 Hz, 2H), 1.46 (p, *J* = 7.0 Hz, 2H), 1.23 (s, 23H), 0.85 (t, *J* = 6.8 Hz, 3H). ^{13}C NMR (101 MHz, CDCl3) δ 161.2, 118.0, 49.0, 38.2, 37.4, 32.0, 29.7, 29.7, 29.6, 29.6, 29.5, 29.5, 29.4, 27.2, 22.7, 14.2.

***N*-(cyanomethyl)-*N*-tetradecylacrylamide (CMA).** Following general procedure B, **CMA** was obtained from **18** (0.297 mmol, 0.075 g) as a pale yellow solid (0.059 g, 65%). ^{1}H NMR (400 MHz, $CDCl_3$) δ 6.52 (dd, *J* = 16.7, 9.9 Hz, 1H), 6.44 (dd, *J* = 16.8, 2.3 Hz, 1H), 5.80 (dd, *J* = 9.9, 2.3 Hz, 1H), 4.35 (s, 2H), 3.50 – 3.43 (m, 2H), 1.71 – 1.59 (m, 2H), 1.25 (s, 22H), 0.86 (d, *J* = 7.0 Hz, 3H). ^{13}C NMR (101 MHz, $CDCl_3$) δ 166.4, 130.5, 126.1, 115.7, 48.8, 34.1, 32.0, 29.8, 29.8, 29.7, 29.6, 29.6, 29.5, 29.3, 29.0, 26.7, 22.8, 14.2. HRMS m/z [M] calcd for $C_{19}H_{34}N_2O$ 306.2671, found: 306.2673. UPLC (method B): t_R = 5.68 min., purity: ≥ 99%.

***N*-(cyclopropylmethyl)tetradecan-1-amine (19).** Following general procedure A, the product was obtained from tetradecylamine (0.47 mmol, 0.10 g) and (bromomethyl)cyclopropane (0.35 mmol, 34.0 μL) as a white solid (0.05 g, 54%). ^{1}H NMR (400 MHz, CDCl3) δ 3.05 (s, 1H), 2.64 (t, J = 7.4 Hz, 2H), 2.46 (dd, J = 26.7, 6.7 Hz, 2H), 1.52 (q, J = 7.1 Hz, 2H), 1.33 – 1.17 (m, 22H), 1.03 – 0.93 (m, 1H), 0.86 (t, J = 6.8 Hz, 3H), 0.52 – 0.45 (m, 2H), 0.12 (dd, J = 10.7, 5.9 Hz, 2H). ^{13}C NMR (101 MHz, CDCl3) δ 54.9, 49.7, 32.1, 29.8, 29.8, 29.7, 29.7, 29.5, 27.5, 22.8, 14.3, 10.8, 3.7.

***N*-(cyclopropylmethyl)-*N*-tetradecylacrylamide (9).** Following general procedure B, the product was obtained from **19** (0.20 mmol, 0.05 g) as a yellow oil (0.04 g, 69%). ^{1}H NMR (400 MHz, CDCl3) δ 6.58 (dt, J = 16.7, 11.2 Hz, 1H), 6.33 (ddd, J = 16.7, 8.7, 1.9 Hz, 1H), 5.65 (ddd, J = 9.4, 7.2, 1.9 Hz, 1H), 3.41 (dt, J = 24.4, 7.8 Hz, 2H), 3.27 (dd, J = 30.4, 6.7 Hz, 2H), 1.64 – 1.51 (m, 2H), 1.26 (d, J = 11.3 Hz, 22H), 1.05 – 0.91 (m, 1H), 0.87 (t, J = 6.8 Hz, 3H), 0.53 (dq, J = 23.6, 5.5 Hz, 2H), 0.24 (dq, J = 10.8, 5.2 Hz, 2H). ^{13}C NMR (101 MHz, CDCl3) δ 166.2, 128.2 (d, J = 20.6 Hz), 127.6 (d, J = 21.3 Hz), 52.3, 50.5, 48.2, 47.0, 32.1, 29.8, 29.7, 29.7, 29.5, 27.8, 27.3, 27.0, 22.8, 14.3, 10.5 (d, J = 106.9 Hz), 3.85. HRMS m/z [M] calcd for $C_{21}H_{39}NO$ 321.3032, found: 321.3036. UPLC (method B): t_R = 4.51 min., purity: ≥ 99%.

***N*-benzyltetradecan-1-amine (20).** Following general procedure A, tetradecylamine (0.47 mmol, 0.10 g) and α-bromotoluene (0.35 mmol, 42.0 μL) were reacted until completion of the reaction. The obtained crude was then purified by automated flash chromatography (0-5% MeOH in DCM) to afford **20** as a yellow solid (0.05 g, 50%). ^{1}H NMR (400 MHz, $CDCl_3$) δ 7.38 – 7.29 (m, 4H), 7.26 (td, J = 5.5, 2.5 Hz, 1H), 3.81 (s, 2H), 2.70 (s, 1H), 2.67 – 2.60 (m, 2H), 1.52 (q, J = 7.3 Hz,

2H), 1.25 (s, 22H), 0.88 (t, *J* = 6.8 Hz, 3H). ^{13}C NMR (101 MHz, $CDCl_3$) δ 139.6, 128.6, 128.5, 127.2, 53.9, 49.3, 32.1, 29.8, 29.7, 29.7, 29.5, 27.4, 22.8, 14.3.

***N*-benzyl-*N*-tetradecylacrylamide (10).** Following general procedure B, **20** (0.17 mmol, 0.05 g) was reacted until completion of the reaction. The obtained crude was then purified by automated flash chromatography (1-5% EtOAc in hexanes) to afford **10** as a yellow oil (0.02 g, 31%). ^{1}H NMR (400 MHz, CDCl3) δ 7.39 – 7.23 (m, 4H), 7.18 (d, *J* = 7.3 Hz, 1H), 6.56 (ddd, *J* = 42.7, 16.7, 10.3 Hz, 1H), 6.41 (ddd, *J* = 21.6, 16.7, 2.1 Hz, 1H), 5.69 (ddd, *J* = 37.1, 10.2, 2.1 Hz, 1H), 4.63 (d, *J* = 26.1 Hz, 2H), 3.33 (dt, *J* = 61.4, 7.8 Hz, 2H), 1.62 – 1.49 (m, 2H), 1.25 (d, *J* = 4.2 Hz, 22H), 0.88 (t, *J* = 6.8 Hz, 3H). ^{13}C NMR (101 MHz, $CDCl_3$) δ 166.6 (d, *J* = 32.9 Hz), 137.6 (d, *J* = 57.5 Hz), 128.8 (d, *J* = 30.2 Hz), 128.5 (d, *J* = 9.5 Hz), 128.1 (d, *J* = 13.8 Hz), 127.6 (d, *J* = 26.5 Hz), 126.4, 51.2, 49.1, 47.1 (d, *J* = 50.9 Hz), 32.1, 29.8, 29.5, 29.4, 29.2, 27.7, 27.2, 27.0, 22.8, 14.3. HRMS m/z [M] calcd for $C_{24}H_{39}NO$ 357.3032, found: 357.3032. UPLC (method A): t_R = 5.68 min., purity: ≥ 99%.

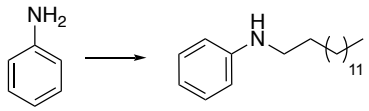

21

Scheme 6. Synthetic route used for the synthesis of **21**. Condition: Cs_2CO_3, bromotetradecane, DMF, 85°C, 12h, 31%.

***N*-tetradecylaniline (21).** To a solution of aniline (0.661 mmol, 60 μL, 1.2 eq) in DMF (5 mL) was added cesium carbonate (1.65 mmol, 0.535 g, 3 eq.), and the resulting mixture was stirred for 15 minutes. Bromotetradecane (0.551 mmol, 0.150 g, 1 eq) was then added, along with a catalytic amount of NaI. The reaction was heated to 85° C and stirred overnight. The reaction mixture was

then cooled, diluted with DCM (30 mL), and washed with saturated solutions of sodium bicarbonate and sodium chloride. The organic layer was then dried over Na_2SO_4 and concentrated via rotary evaporation. The crude product was purified via automated flash column chromatography (10-80% EtOAc in hexanes) to yield **21** (0.048 g, 31%) as a clear oil. ^{1}H NMR (400 MHz, $CDCl_3$) δ 7.23 – 7.13 (m, 2H), 6.74 – 6.56 (m, 3H), 3.59 (s, 1H), 3.11 (t, *J* = 7.1 Hz, 2H), 1.62 (p, *J* = 7.0 Hz, 2H), 1.27 (s, 22H), 0.94 – 0.84 (m, 3H). ^{13}C NMR (101 MHz, $CDCl_3$) δ 148.7, 129.4, 117.2, 112.8, 44.1, 32.1, 29.8, 29.8, 29.7, 29.6, 29.5, 27.3, 22.9, 14.3.

***N*-phenyl-*N*-tetradecylacrylamide (11).** Following general procedure B, **21** was obtained from **11** (0.169 mmol, 0.048 g, 1 eq.) and purification via automated flash column chromatography (5-40% EtOAc in hexanes) afforded the right product as clear oil (0.36 g, 62%). ^{1}H NMR (400 MHz, $CDCl_3$) δ 7.44 – 7.38 (m, 2H), 7.37 – 7.31 (m, 1H), 7.17 – 7.12 (m, 2H), 6.35 (dd, *J* = 16.8, 2.0 Hz, 1H), 5.97 (dd, *J* = 16.7, 10.3 Hz, 1H), 5.48 (dd, *J* = 10.3, 1.7 Hz, 1H), 3.81 – 3.71 (m, 2H), 1.53 (p, *J* = 7.5 Hz, 2H), 1.34 – 1.16 (m, 22H), 0.87 (t, *J* = 6.9 Hz, 3H). ^{13}C NMR (101 MHz, $CDCl_3$) δ 165.4, 142.2, 129.6, 129.0, 128.4, 127.8, 127.4, 49.7, 32.1, 29.8, 29.8, 29.8, 29.7, 29.7, 29.5, 27.9, 27.0, 22.8, 14.3. HRMS m/z [M] calcd for $C_{23}H_{37}NO$ 343.2875, found: 343.2875. UPLC (method A): t_R = 4.19 min., purity: ≥ 99%.

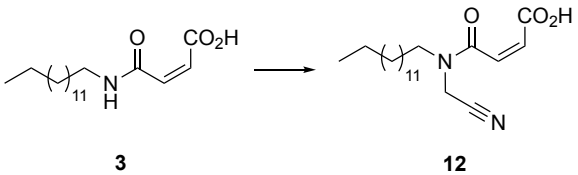

3 **12**

Scheme 7. Synthetic route used for the synthesis of **12**. Condition: NaH, bromoacetonitrile, DMF, r.t., 3h, 30%.

(*Z*)-4-((cyanomethyl)(tetradecyl)amino)-4-oxobut-2-enoic acid (12). To a solution of **3** (0.321 mmol, 0.10 g, 1 eq.) stirring in dry DMF (3 mL) under nitrogen was added NaH (60% in immersion oil, 0.963 mmol, 0.023 g, 3 eq.). The reaction was then stirred for 10 minutes, and bromoacetonitrile (0.963 mmol, 65 μL) was added. After three hours, the reaction was quenched with a solution of saturated NH_4Cl and diluted with EtOAc (30 mL). The aqueous layer was extracted with EtOAc (3x20 mL), and the combined organics were washed with brine and dried over Na_2SO_4. Following concentration via rotary evaporation, the product was purified via automated flash column chromatography (0-10% methanol in DCM) to yield **12** as a pale white solid (0.034 g, 30%). ^{1}H NMR (400 MHz, MeOD) δ 6.50 (d, *J* = 11.9 Hz, 1H), 6.24 (d, *J* = 11.9 Hz, 1H), 4.93 (s, 2H), 3.23 (t, *J* = 7.1 Hz, 2H), 1.54 (q, *J* = 6.9 Hz, 2H), 1.31 (d, *J* = 14.5 Hz, 22H), 0.94 – 0.86 (m, 3H). ^{13}C NMR (101 MHz, $CDCl_3$) δ 169.5, 162.8, 135.4, 128.4, 127.6, 40.5, 33.1, 30.8, 30.8, 30.7, 30.7, 30.5, 30.4, 30.2, 28.0, 23.7, 14.4. HRMS m/z [M] calcd for $C_{20}H_{34}N_2O_3$ 350.2569, found: 350.2572. UPLC (method B): t_R = 4.35 min., purity: 96%.

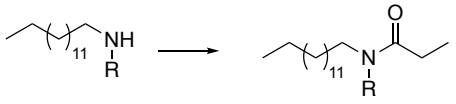

17, R = propargyl
18, R = cyanomethyl

13, R = propargyl
14, R = cyanomethyl

Scheme 8. Synthetic route used for the synthesis of **13** & **14**. Condition: propionyl chloride, K_2CO_3, DMF, r.t., 1h, **13**: 68%, **14**: 72%.

***N*-(prop-2-yn-1-yl)-*N*-tetradecylpropionamide (13).** To a solution of **17** (0.0742 mmol, 0.020 g, 1 eq.) in DMF (1 mL) was added potassium carbonate (0.371 mmol, 0.051 g, 5 eq.). After stirring for 20 minutes, propionyl chloride (0.223 mmol, 20 μL, 3 eq.) was added, and the reaction was stirred for one hour. The reaction mixture was then cooled, diluted with DCM (15 mL), and washed

with saturated solutions of sodium bicarbonate and brine. The organic layer was then dried over Na_2SO_4 and concentrated via rotary evaporation. The crude product was purified via column chromatography (10-80% EtOAc in hexanes) to yield **13** as a clear oil (0.015 g, 68%). ^{1}H NMR (400 MHz, $CDCl_3$) δ 4.11 (dd, *J* = 84.0, 2.5 Hz, 2H), 3.40 (dt, *J* = 19.2, 7.8 Hz, 2H), 2.39 (dq, *J* = 27.5, 7.4 Hz, 2H), 2.21 (dt, *J* = 34.8, 2.5 Hz, 1H), 1.57 (m, 2H), 1.26 (s, 22H), 1.16 (t, *J* = 7.4 Hz, 3H), 0.93 – 0.82 (m, 3H). ^{13}C NMR (101 MHz, $CDCl_3$) δ 174.0, 71.4, 47.3, 34.3, 32.1, 29.8, 29.8, 29.8, 29.7, 29.6, 29.5, 29.5, 28.6, 27.0, 26.4, 22.8, 14.9, 14.3, 9.6, 9.4. HRMS m/z [M] calcd for $C_{20}H_{37}NO$ 307.2875, found: 307.2876. Compound was not UV active so no LC purity could be obtained, still 99% purity was seen by NMR.

***N*-(cyanomethyl)-*N*-tetradecylpropionamide (14).** To a solution of **18** (0.297 mmol, 0.075 g, 1 eq.) in DMF (2 mL) was added potassium carbonate (1.49 mmol, 0.205 g, 5 eq.). After stirring for 20 minutes, propionyl chloride (0.891 mmol, 78 μL, 3 eq.) was added, and the reaction was stirred for one hour. The reaction mixture was then cooled, diluted with DCM (30 mL), and washed with saturated solutions of sodium bicarbonate and brine. The organic layer was then dried over Na_2SO_4 and concentrated via rotary evaporation. The crude product was purified via automated flash column chromatography (10-80% EtOAc in hexanes) to yield **14** as a clear oil (0.066 g, 72%). ^{1}H NMR (400 MHz, $CDCl_3$) δ 3.36 (m, 2H), 2.37 (q, *J* = 7.3 Hz, 2H), 1.62 (m, 2H), 1.30 (m, 2H), 1.25 (s, 22H), 1.15 (t, *J* = 7.4 Hz, 3H), 0.86 (m, 3H). ^{13}C NMR (101 MHz, $CDCl_3$) δ 173.8, 116.0, 33.4, 32.0, 29.8, 29.7, 29.7, 29.6, 29.6, 29.5, 29.3, 28.5, 26.8, 26.1, 22.8, 14.2, 9.3. HRMS m/z [M] calcd for $C_{19}H_{36}N_2O$ 308.2828, found: 308.2834. Compound was not UV active so no LC purity could be obtained, still 96% purity was seen by NMR.

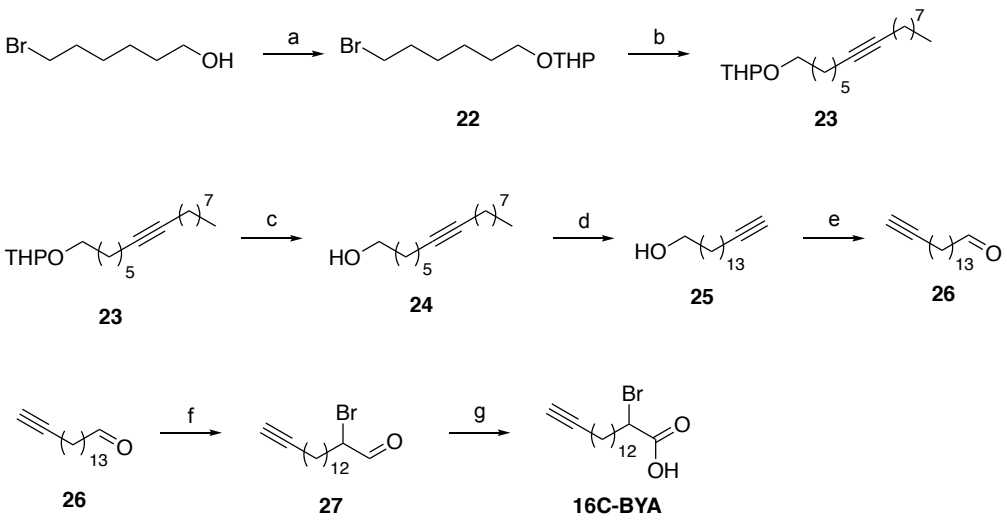

Scheme 9. Synthetic route used to obtain 1**6C-BYA**. Conditions: a) 3,4-dihydro-2H-pyran, PPTS, DCM, r.t., 21h30, 58%. b) 1-decyne, *n*-BuLi, HMPA, THF, r.t. then reflux, 4h, quant. c) p-toluenesulfonic acid monohydrate, MeOH, reflux, 6h, 78%. d) 1,3-diaminopropane, *n*-BuLi, *t*-BuOK, THF, r.t., 3h, 93%. e) IBX solution in DMSO, r.t., 6h, 32%. f) NBS, Proline, DCM, -10°C -> r.t., 3h, 17%. g) PDC, DMF/DCM, r.t., 3h, 21%.

2-((6-bromohexyl)oxy)tetrahydro-*2H*-pyran (22). To an oven-dried two-neck round bottom flask flushed with nitrogen were added successively pyridinium *p*-toluenesulfonate (1.66 mmol, 0.42 g), dry DCM (16 mL), 6-bromo-1-hexanol (16.6 mmol, 2.17 mL), and, via an addition funnel, a solution of DHP (24.9 mmol, 2.30 mL) in DCM (14 mL) dropwise. The mixture was stirred at room temperature 21h30 until the reaction was complete. The reaction mixture was then washed with water and brine successively, dried over $Na_2SO_4$and evaporated to dryness. The obtained crude was then purified by automated flash chromatography (0-10% EtOAc in hexanes) to afford **22** as a transparent oil (2.54 g, 58%). ^{1}H NMR (400 MHz, $CDCl_3$) δ 4.56 (t, *J* = 3.5 Hz, 1H), 3.86 (ddd, *J* = 11.0, 7.4, 3.3 Hz, 1H), 3.73 (dt, *J* = 9.6, 6.7 Hz, 1H), 3.54 – 3.45 (m, 1H), 3.43 – 3.34 (m, 3H), 1.93 – 1.77 (m, 3H), 1.76 – 1.67 (m, 1H), 1.66 – 1.33 (m, 11H). ^{13}C NMR (101 MHz, $CDCl_3$) δ 99.0, 67.5, 62.5, 34.0, 32.9, 30.9, 29.7, 28.1, 25.6, 25.6, 19.8. The spectra are in accordance with the literature.[172]

2-(hexadec-7-yn-1-yloxy)tetrahydro-*2H*-pyran (23). A solution of 2.5 M *n*-BuLi in hexane (12.6 mmol, 5.02 mL) was added dropwise to a stirred and cooled solution of 1-decyne (12.5 mmol, 2.22 mL) in dry THF (9 mL) and HMPA (1.8 mL) at -70°C under nitrogen. The mixture was warmed to -10°C over 15 min, and then cooled again to -70°C. A solution of **22** (9.58 mmol, 2.54 g) in dry THF (2 mL) was added dropwise to this cooled mixture, and the temperature was gradually raised to room temperature. After stirring for 1.5 h at room temperature, the mixture was stirred and heated at reflux for 2.5 h until the reaction was complete. After cooling, the reaction mixture was diluted with water and extracted with hexane. The combined organics were washed with brine, dried over Na_2SO_4 and evaporated to dryness. The obtained crude was filtered through a pad of celite with 5% EtOAc in hexanes to afford **23** as a yellow oil, which was used without further purification (3.05 g, quant.). ^{1}H NMR (400 MHz, CDCl3) δ 4.60 – 4.52 (m, 1H), 3.91 – 3.79 (m, 1H), 3.72 (dt, J = 9.5, 6.9 Hz, 1H), 3.48 (dt, J = 10.6, 4.9 Hz, 1H), 3.37 (dt, J = 9.5, 6.6 Hz, 1H), 2.21 – 2.07 (m, 4H), 1.88 – 1.64 (m, 2H), 1.63 – 1.26 (m, 24H), 0.86 (t, J = 6.7 Hz, 4H). ^{13}C NMR (101 MHz, CDCl3) δ 99.0, 80.4, 80.2, 67.7, 62.4, 32.0, 30.9, 29.8, 29.4, 29.3, 29.3, 29.2, 29.0, 28.8, 25.9, 25.6, 22.8, 19.8, 18.9, 18.8, 14.2. The spectra are in accordance with the literature. (doi: 10.1016/j.tet.2010.06.080)

hexadec-7-yn-1-ol (24). To a solution of **23** (9.30 mmol, 3.00 g) in methanol (18 mL) was added *p*-toluenesulfonic acid monohydrate (5.58 mmol, 1.06 g). The reaction mixture was stirred at reflux for 6h until the reaction was complete. The reaction mixture was then diluted with water and extracted with ethyl acetate three times. The combined organics were washed with a saturated solution of bicarbonate then brine, dried over Na_2SO_4, and evaporated to dryness. The obtained crude was then purified by automated flash chromatography (0-10% EtOAc in hexanes) to afford

24 as a yellow oil (1.74 g, 78%). ^{1}H NMR (400 MHz, CDCl3) δ 3.64 (t, *J* = 6.6 Hz, 2H), 2.19 – 2.08 (m, 4H), 1.68 – 1.26 (m, 20H), 0.87 (t, *J* = 6.8 Hz, 3H). ^{13}C NMR (101 MHz, $CDCl_3$) δ 80.5, 80.2, 63.1, 32.8, 32.0, 29.4, 29.3, 29.3, 29.2, 29.0, 28.7, 25.4, 22.8, 18.9, 18.8, 14.3. The spectra are in accordance with the literature. (doi: 10.1016/j.tet.2010.06.080)

hexadec-15-yn-1-ol (25). To a solution of 1,3-diaminopropane (36.5 mmol, 3.00 mL) in THF (16 mL) at 0°C was added dropwise 2.5 M *n*-BuLi in hexane (29.2 mmol, 12 mL). The resulting mixture was stirred for 20 min and *t*-BuOK (29.2 mmol, 29.2 mL) was added dropwise. The resulting solution was allowed to warm at room temperature before the dropwise addition of a solution of **24** (7.30 mmol, 1.74 g) in 2 mL THF. The reaction mixture was then stirred at reflux 3h until the reaction was complete. The reaction mixture was then poured into a saturated aqueous solution of NH_4Cl and extracted with ether. The combined organics were washed with HCl 5% then a saturated solution of bicarbonate then brine, dried over Na_2SO_4, and evaporated to dryness. The obtained crude was then purified through filtration on a pad of silica with 25% EtOAc in hexanes to afford **25** as a yellow solid (1.61 g, 93%). ^{1}H NMR (400 MHz, CDCl3) δ 3.63 (t, *J* = 6.6 Hz, 2H), 2.17 (td, *J* = 7.1, 2.6 Hz, 2H), 1.93 (t, *J* = 2.6 Hz, 1H), 1.54 (dp, *J*= 22.4, 6.9 Hz, 4H), 1.26 (s, 20H). ^{13}C NMR (101 MHz, $CDCl_3$) δ 85.0, 68.2, 63.2, 33.0, 29.8, 29.8, 29.7, 29.6, 29.6, 29.3, 28.9, 28.6, 25.9, 18.5. The spectra are in accordance with the literature.[63, 173]

hexadec-15-ynal (26). 2-iodoxybenzoic acid (8.64 mmol, 2.42 g) was dissolved in DMSO (6.6 mL) and the obtained mixture was stirred at room temperature for 20 minutes to yield an IBX solution. This formed solution was added to a solution of **25** (1.09 mmol, 0.26 g) in DMSO (6 mL) and the reaction mixture was stirred for 6h. After full conversion, the reaction mixture was diluted

with water and extracted with ethyl acetate. The combined organics were washed with brine, dried over Na_2SO_4, and evaporated to dryness. The obtained crude was then purified by automated flash chromatography (0-10% EtOAc in hexanes). The obtained fraction was further washed four times with a saturated solution of sodium bicarbonate then once with a NaOH solution (pH 9.5), dried over Na_2SO_4, and evaporated to dryness to afford **26** as a yellow solid (0.43 g, 32%). ^{1}H NMR (400 MHz, $CDCl_3$) δ 9.76 (t, *J* = 1.9 Hz, 1H), 2.41 (td, *J* = 7.4, 1.9 Hz, 2H), 2.17 (td, *J* = 7.1, 2.6 Hz, 2H), 1.93 (t, *J* = 2.6 Hz, 1H), 1.62 (p, *J* = 7.2 Hz, 2H), 1.52 (dt, *J* = 14.7, 7.1 Hz, 2H), 1.27 (d, *J* = 13.6 Hz, 18H). ^{13}C NMR (101 MHz, $CDCl_3$) δ 203.1, 84.9, 68.2, 44.2, 29.7, 29.7, 29.7, 29.6, 29.6, 29.5, 29.3, 29.2, 28.9, 28.6, 22.2, 18.5. The spectra are in accordance with the literature.[63]

2-bromohexadec-15-ynal (27). To a cooled solution of **26** (1.82 mmol, 0.43 g) in DCM (13 mL) at -10°C was added proline (3.09 mmol, 0.36 g). The reaction mixture was stirred for 1h at -10°C then N-bromosuccinimide (3.09 mmol, 0.56 g) was added portion-wisely, while the temperature was kept below -5°C. The reaction mixture was stirred at this temperature for 2h then allowed to warm up to R.T. for another hour until the reaction was complete. The reaction mixture was then filtered, concentrated then filtered again through a pad of celite with 50% DCM in hexanes. The crude was first purified by automated flash chromatography (10-50% DCM in hexanes) then the gathered fractions was further washed three times with a saturated solution of sodium bicarbonate, dried over Na_2SO_4, and evaporated to dryness to afford **27** as a yellow oil (0.10 g, 17%). ^{1}H NMR (400 MHz, $CDCl_3$) δ 9.41 (d, *J* = 3.1 Hz, 1H), 4.23 – 4.17 (m, 1H), 2.16 (td, *J* = 7.1, 2.6 Hz, 3H), 2.02 (ddd, *J* = 20.5, 9.8, 5.9 Hz, 1H), 1.92 (t, *J* = 2.6 Hz, 2H), 1.51 (dt, *J* = 14.7, 7.0 Hz, 4H), 1.25 (s, 17H). ^{13}C NMR (101 MHz, CDCl3) δ 192.9, 84.9, 68.2, 55.6, 31.8, 29.7, 29.6, 29.6, 29.6, 29.4, 29.2, 29.0, 28.9, 28.6, 27.0, 18.5. The spectra are in accordance with the literature.[63]

2-bromohexadec-15-ynoic acid (16C-BYA). To a solution of **27** (0.32 mmol, 0.10 g) in DCM (6 mL) and DMF (3 mL) was added pyridinium dichromate (0.79 mmol, 0.30 g). The solution was stirred at room temperature for 2 h until the reaction was complete. The reaction mixture was then diluted with a 10% aqueous solution of HCl and extracted with ethyl acetate. The combined organics were washed with brine, dried over Na_2SO_4, and evaporated to dryness. The obtained crude was then purified by first an automated flash chromatography (20% EtOAc in hexanes) then a hand flash chromatography (10-20% EtOAc in hexanes) to afford **16C-BYA** as a white solid (0.02 g, 20%). ^{1}H NMR (400 MHz, CDCl3) δ 4.27 (s, 1H), 2.18 (td, *J* = 7.1, 2.6 Hz, 2H), 2.14 – 1.96 (m, 2H), 1.94 (t, *J* = 2.6 Hz, 1H), 1.52 (dt, *J* = 14.7, 7.0 Hz, 3H), 1.42 – 1.25 (m, 17H). The spectra are in accordance with the literature.[63] ^{13}C NMR (101 MHz, CDCl3) δ 191.5, 85.0, 68.2, 29.7, 29.6, 29.6, 29.4, 29.3, 29.0, 28.9, 28.6, 18.6. HRMS m/z [M] calcd for $C_{16}H_{27}BrO_2$ 330.1194, found: 330.1191. UPLC (method B): t_R = 4.85 min., purity: 99%.

SA_009. 4-amino-biphenyl (0.250 g, 1.5 mmol, 1 eq.) was dissolved in DMF (8 mL) and bromoacetonitrile (83 μL, 1.2 mmol, 0.8 eq.) was added. The reaction mixture was heated to 80 ˚C and stirred overnight. The reaction mixture was then diluted with water and DCM and the aqueous phase extracted with DCM (3x 15 mL). The organic phase was washed with brine, dried over Na_2SO_4, and concentrated. Purification via automated column chromatography (0-40% EtOAc in hexanes) gave **SA8B** (0.110 g, 35%). SA8B (0.055 g, 0.264 mmol, 1 eq.) was then dissolved in dry DMF (3 mL) and cooled to 0 ˚C. Potassium carbonate (0.185 g, 1.32 mmol, 5 eq.) was added, and after the reaction was stirred for 15 minutes, it was followed by acryloyl chloride (64 μL, 0.792 mmol, 3 eq.). After 30 minutes, the reaction mixture was diluted with water and DCM and the aqueous phase extracted with DCM (3x 15 mL). The organic phase was washed with

brine, dried over Na_2SO_4, and concentrated. Purification via automated column chromatography (0-30% EtOAc in hexanes) gave **SA9** (0.061 g, 88%). ^{1}H NMR (400 MHz, $CDCl_3$) δ 7.72 – 7.65 (m, 2H), 7.64 – 7.56 (m, 2H), 7.53 – 7.44 (m, 2H), 7.44 – 7.37 (m, 1H), 7.37 – 7.31 (m, 2H), 6.50 (dd, *J* = 16.8, 1.8 Hz, 1H), 6.11 (dd, *J* = 16.8, 10.3 Hz, 1H), 5.68 (dd, *J* = 10.4, 1.8 Hz, 1H), 4.70 (s, 2H). ^{13}C NMR (101 MHz, $CDCl_3$) δ 165.65, 142.39, 139.62, 139.16, 130.34, 129.13, 128.98, 128.35, 128.19, 127.26, 127.01, 115.46, 37.35. HRMS-ESI(+) m/z [M+] calculated for $C_{17}H_{14}N_2O$ 262.1106, found 262.1109. UPLC (method A): t_R = 3.60 min., purity: ≥ 99%.

SA16. RSK1 (0.081 g, 0.322 mmol, 1 eq.) was dissolved in DCM (3 mL) and cooled to 0 ˚C. In a separate round flask, monomethyl fumarate (0.125 g, 0.966 mmol, 3 eq.) was dissolved in DCM (3 mL), followed by DIPEA (84 μL, 0.483 mmol, 1.5 eq.), Oxyma (0.069 g, 0.483 mmol, 1.5 eq.), and then DIC (75 μL, 0.483 mmol, 1.5 eq.). After stirring for ten minutes, this mixture was added to the solution of RSK1, which was then warmed to r.t. overnight. The reaction was then diluted with DCM and washed with water, saturated sodium bicarbonate, and brine. Concentration via rotary evaporation and purification via automated column chromatography (0-60% EtOAc in hexanes) gave **SA16** (0.022 g, 19%). HRMS-ESI(+) m/z [M+] calculated for $C_{22}H_{37}NO_3$ 363.2772, found 363.2772. ^{1}H NMR (400 MHz, $CDCl_3$) δ 7.37 (dd, *J* = 24.1, 15.3 Hz, 1H), 6.82 (dd, *J* = 20.4, 15.3 Hz, 1H), 4.18 (dd, *J* = 68.8, 2.5 Hz, 2H), 3.79 (s, 3H), 3.53 – 3.44 (m, 2H), 2.22 (t, *J* = 2.5 Hz, 1H), 1.62 (dt, *J* = 13.7, 6.7 Hz, 2H), 1.26 (d, *J* = 18.6 Hz, 22H), 0.86 (t, *J* = 6.8 Hz, 3H). ^{13}C NMR (101 MHz, $CDCl_3$) δ 166.07, 164.19, 134.05, 133.49, 131.60, 131.11, 78.46, 78.26, 73.31, 72.06, 52.19, 47.64, 46.87, 37.84, 35.01, 31.92, 29.65, 29.54, 29.49, 29.36, 29.23, 29.11, 27.39, 26.88, 26.62, 22.69, 14.13. UPLC (method A): t_R = 4.41 min., purity: ≥ 99%.

SA18. N-Boc ethanolamine (480 μL, 3.1 mmol, 1 eq.) was dissolved in dry THF (10 mL) and cooled to 0 ˚C under nitrogen. and NaH (60% immersion in oil, 0.150 g, 3.7 mmol 1.2 eq.) was added portionwise. After bubbling ceased, 1-iodoundecane (717 μL, 2.64 mmol, 1 eq.) was added and, after stirring at 0 ˚C for 30 minutes, the reaction was slowly warmed to room temperature and stirred for 10 hours. The reaction was then diluted with DCM (30 mL) and washed with water, saturated sodium bicarbonate, and brine. Concentration via rotary evaporation and purification via automated column chromatography (0-40% EtOAc in hexanes) gave **SA18** (0.076 g, 8%). ^{1}H NMR (400 MHz, $CDCl_3$) δ 4.89 (s, 1H), 3.45 (t, *J* = 5.2 Hz, 2H), 3.40 (t, *J* = 6.7 Hz, 2H), 3.28 (q, *J* = 5.4 Hz, 2H), 1.53 (q, *J* = 6.9 Hz, 2H), 1.43 (s, 9H), 1.26 (d, *J* = 13.9 Hz, 16H), 0.86 (t, *J* = 6.7 Hz, 3H).

SA19. SA18 (0.076 g, 0.24 mmol, 1 eq.) was dissolved in 20% TFA in DCM and stirred for 30 min. The reaction was then concentrated and washed three times with DCM. The crude product and potassium carbonate (0.040 g, 0.29 mmol, 1.2 eq.) were next stirred in acetonitrile (5 mL) for 15 minutes. Bromoacetonitrile (16 μL, 0.22 mmol, 0.9 eq.) was added, and the reaction was heated to 85 ˚C. After three hours, the reaction mixture was cooled and diluted with water and EtOAc. The organic layer was extracted with EtOAc (3x 30 mL), washed with brine, dried over Na_2SO_4, and concentrated. Purification via automated column chromatography (0-10% MeOH in DCM) gave **SA019** as a pale yellow oil (0.076 g, 75%). ^{1}H NMR (400 MHz, $CDCl_3$) δ 3.64 (s, 2H), 3.58 – 3.50 (m, 2H), 3.42 (t, *J* = 6.7 Hz, 2H), 2.89 (t, *J* = 5.0 Hz, 2H), 1.73 (s, 1H), 1.56 (p, *J* = 6.7 Hz, 2H), 1.37 – 1.20 (m, 16H), 0.92 – 0.83 (m, 3H).

SA_020. SA19 (0.041 g, 0.167 mmol, 1 eq.) was dissolved in dry DMF (3 mL) under nitrogen and potassium carbonate (0.111 g, 0.806 mmol, 5 eq.) was added. The suspension was stirred for 15 minutes at room temperature, and then acryloyl chloride (39 μL, 0.483 mmol, 3 eq.) was added. After 30 minutes, the reaction mixture was diluted with water and EtOAc and the aqueous phase extracted with EtOAc (3x 20 mL). The organic phase was washed with brine, dried over Na_2SO_4, and concentrated. Purification via automated column chromatography (20-80% EtOAc in hexanes) gave **SA020** (0.0286 g, 49%) as a clear oil. ^{1}H NMR (400 MHz, $CDCl_3$) δ 6.57 (dd, *J* = 16.7, 10.3 Hz, 1H), 5.78 (d, *J* = 10.2 Hz, 1H), 4.45 (s, 2H), 3.66 (t, *J* = 4.8 Hz, 2H), 3.59 (t, *J* = 4.8 Hz, 2H), 3.41 (t, *J* = 6.6 Hz, 2H), 1.53 (q, *J* = 6.5 Hz, 2H), 1.25 (s, 16H), 0.92 – 0.83 (m, 3H). ^{13}C NMR (101 MHz, $CDCl_3$) δ 166.63, 130.11, 126.42, 115.83, 71.84, 69.39, 48.29, 35.06, 31.92, 29.62, 29.58, 29.44, 29.35, 26.10, 22.69, 14.14. HRMS-ESI(+) m/z [M+] calculated for $C_{21}H_{38}N_2O_2$ 350.2933, found 350.2945. UPLC (method A): t_R = 3.52 min., purity: ≥ 99%.

SA38. Phenylaniline•HCl (0.150 g, 0.744 mmol, 1 eq.) was added to acetonitrile (5 mL), and DIPEA (130 μL, 0.744 mmol, 1 eq.) added slowly until the substrate dissolved. Bromoacetonitrile (47 μL, 0.669 mmol, 0.9 eq.) was added dropwise, and the reaction was then heated to 70 ˚C and stirred overnight. The reaction was then cooled, diluted with DCM, and washed with water, saturated sodium bicarbonate, and brine. Purification via automated column chromatography (0-30% EtOAc in hexanes) gave **SA038** (0.017 g, 9.7%). ^{1}H NMR (400 MHz, $CDCl_3$) δ 7.32 – 7.24 (m, 2H), 7.19 (tt, *J* = 8.0, 1.4 Hz, 3H), 7.12 – 7.05 (m, 2H), 6.69 – 6.63 (m, 2H), 4.09 (d, *J* = 7.1 Hz, 2H), 3.86 (t, *J* = 7.1 Hz, 1H), 2.94 – 2.79 (m, 4H).

SA45. SA38 (0.017 g, 0.072 mmol, 1 eq.) was dissolved in DMF (1 mL) and potassium carbonate (0.050 g, 0.361 mmol, 5 eq.) was added, followed by acryloyl chloride (17.5 μL, 0.217 mmol, 3 eq.). After 30 minutes, the reaction mixture was diluted with water and EtOAc and the aqueous phase extracted with EtOAc (3x 10 mL). The organic phase was washed with brine, dried over Na_2SO_4, and concentrated. Purification via automated column chromatography (0-50% EtOAc in hexanes) gave **SA45** (0.016 g, 75%) as an off-white solid. ^{1}H NMR (400 MHz, $CDCl_3$) δ 7.32 – 7.26 (m, 4H), 7.24 – 7.15 (m, 5H), 6.46 (dd, *J* = 16.8, 1.8 Hz, 1H), 6.02 (dd, *J* = 16.8, 10.4 Hz, 1H), 5.64 (dd, *J* = 10.3, 1.8 Hz, 1H), 4.65 (s, 2H), 3.07 – 2.89 (m, 4H). ^{13}C NMR (101 MHz, $CDCl_3$) δ 165.62, 143.21, 141.05, 137.86, 130.30, 129.97, 128.46, 128.44, 127.81, 126.90, 126.20, 115.35, 37.60, 37.43, 37.25. HRMS-ESI(+) m/z [M+] calculated for $C_{19}H_{18}N_2O$ 290.1419, found 290.1419. UPLC (method A): t_R = 2.84 min., purity: 98%.

SA_065. Boc-butanolamine (0.50 g, 2.64 mmol, 1 eq.) was dissolved in dry THF (6 mL) under nitrogen, and NaH (60% immersion in oil, 0.212 g, 3.17 mmol 1.2 eq.) was added portionwise. After bubbling ceased, 1-bromo-3-phenylpropane (402 μL, 2.64 mmol, 3 eq.) was added, along with a catalytic amount of NaI. The reaction mixture was then heated to 65 ˚C and stirred for 8 hours. It was then cooled and diluted with water and EtOAc, and the organic layer was extracted with EtOAc (3x 30 mL), washed with brine, dried over Na_2SO_4, and concentrated. Purification via automated column chromatography (10-100% EtOAc in hexanes) gave **SA065** (0.110 g, 14%). ^{1}H NMR (400 MHz, $CDCl_3$) δ 7.23 – 7.17 (m, 2H), 7.13 – 7.08 (m, 3H), 3.34 (td, *J* = 6.2, 1.6 Hz, 4H), 3.07 (t, *J* = 6.5 Hz, 2H), 2.61 (dd, *J* = 8.6, 6.8 Hz, 2H), 1.87 – 1.77 (m, 2H), 1.51 (dddd, *J* = 14.7, 8.1, 4.4, 1.8 Hz, 4H), 1.37 (s, 9H).

SA_068. SA65 (0.054 g, 0.176 mmol, 1 eq.) was dissolved in 20% TFA in DCM and stirred for 30 min. The reaction was then concentrated and washed three times with DCM. The crude product and potassium carbonate (0.029 g, 0.211 mmol, 1.2 eq.) were next stirred in acetonitrile (5 mL) for 15 minutes. Bromoacetonitrile (11 μL, 0.154 mmol, 0.9 eq.) was added, and the reaction was heated to 80 ˚C. After 8 hours, it was cooled and diluted with water and EtOAc. The organic layer was extracted with EtOAc (3x 30 mL), washed with brine, dried over Na_2SO_4, and concentrated. Purification via automated column chromatography (0-10% MeOH in DCM) gave **SA068** (0.020 g, 46%). ^{1}H NMR (400 MHz, $CDCl_3$) δ 7.25 – 7.18 (m, 2H), 7.15 – 7.08 (m, 3H), 3.53 (s, 2H), 3.42 – 3.29 (m, 4H), 2.73 – 2.56 (m, 3H), 1.88 – 1.76 (m, 2H), 1.67 – 1.47 (m, 4H).

SA_073. SA68 (0.04 g, 0.162 mmol, 1 eq.) was dissolved in DMF (3 mL) and potassium carbonate (0.112 g, 0.81 mmol, 5 eq.) was added, followed by acryloyl chloride (39 μL, 0.487 mmol, 3 eq.). After 30 minutes, the reaction mixture was diluted with water and EtOAc and the aqueous phase extracted with EtOAc (3x 20 mL). The organic phase was washed with brine, dried over Na_2SO_4, and concentrated. Purification via automated column chromatography (0-50% EtOAc in hexanes) gave **SA73** (0.034 g, 70%) as a clear oil. ^{1}H NMR (400 MHz, $CDCl_3$) δ 7.35 – 7.26 (m, 2H), 7.21 (td, J = 5.3, 2.3 Hz, 3H), 6.64 – 6.42 (m, 2H), 5.82 (dd, J = 10.2, 2.1 Hz, 1H), 4.39 (s, 2H), 3.61 – 3.52 (m, 2H), 3.46 (dt, J = 8.5, 6.2 Hz, 4H), 2.71 (dd, J = 8.6, 6.8 Hz, 2H), 1.99 – 1.87 (m, 2H), 1.79 (p, J = 7.5 Hz, 2H), 1.71 – 1.58 (m, 2H). ^{13}C NMR (101 MHz, $CDCl_3$) δ 166.34, 141.84, 130.45, 128.43, 128.37, 126.04, 125.85, 115.61, 70.26, 70.22, 70.11, 48.46, 36.04, 33.95, 32.38, 32.36, 31.25, 26.64, 26.14, 24.45. HRMS-ESI(+) m/z [M+] calculated for $C_{18}H_{24}N_2O_2$ 300.1838, found 300.1838. UPLC (method A): t_R = 3.60 min., purity: 97%.

SA_072. RSK6 (0.087 g, 0.261 mmol, 1 eq.) was dissolved in a 1:1 mixture of THF:water (3 mL), followed by **CD107A** (0.046 g, 0.522 mmol, 2 eq.), TBTA (0.004 g, 0.0051 mmol, 0.02 eq.), copper(II) sulfate (0.0065 g, 0.0261 mmol, 0.1 eq.) and sodium ascorbate (0.0056 g, 0.0261 mmol, 0.1 eq.). After stirring at room temperature for 10 hours, the reaction mixture was filter through celite and concentrated. Purification via automated column chromatography (0-10% MeOH in DCM) gave **SA72** (0.039 g, 38%). ^{1}H NMR (400 MHz, $CDCl_3$) δ 8.16 (s, 1H), 7.80 – 7.64 (m, 1H), 6.51 (td, *J* = 14.5, 8.8 Hz, 2H), 6.34 (dd, *J* = 16.7, 2.0 Hz, 1H), 5.70 (dt, *J* = 10.3, 2.6 Hz, 1H), 4.69 – 4.39 (m, 4H), 3.81 (q, *J* = 5.4 Hz, 2H), 3.41 (t, *J* = 7.9 Hz, 2H), 1.62 (q, *J* = 7.3 Hz, 2H), 1.24 (s, 23H), 0.90 – 0.80 (m, 3H). ^{13}C NMR (101 MHz, $CDCl_3$) δ 166.27, 161.58, 129.23, 128.50, 127.72, 127.34, 49.63, 48.62, 46.65, 41.76, 37.84, 31.92, 29.68, 29.65, 29.62, 29.55, 29.35, 29.31, 27.62, 27.00, 26.74, 22.69, 14.12. HRMS-ESI(+) m/z [M+] calculated for $C_{22}H_{41}N_5O$ 391.3311, found 391.333. UPLC (method A): t_R = 3.94 min., purity: ≥ 99%.

SA75. CD14A (0.050 g, 0.161 mmol, 1 eq.) was dissolved in DMF (5 mL), along with sodium carbonate (0.035 g, 0.321 mmol, 2 eq.) and bromoacetonitrile (23 μL, 0.231 mmol, 2 eq.). After stirring at room temperature for five hours, the reaction was diluted with water and EtOAc and the aqueous phase extracted with EtOAc (3x 20 mL). The organic phase was washed with brine, dried over Na_2SO_4, and concentrated. Purification via automated column chromatography (0-60% EtOAc in hexanes) gave **SA75 (**0.042 g, 74%) as a white solid. ^{1}H NMR (400 MHz, $CDCl_3$) δ 6.44 (d, *J* = 12.4 Hz, 1H), 6.15 (d, *J* = 12.5 Hz, 1H), 4.82 (s, 2H), 3.33 (td, *J* = 7.3, 5.7 Hz, 2H), 1.68 – 1.46 (m, 2H), 1.25 (s, 23H), 0.94 – 0.79 (m, 3H). ^{13}C NMR (101 MHz, $CDCl_3$) δ 164.42, 163.38, 139.18, 123.18, 113.82, 48.89, 39.89, 39.76, 31.93, 29.70, 29.69, 29.66, 29.60, 29.54, 29.37, 29.26,

29.22, 26.94, 22.70, 14.13. HRMS-ESI(+) m/z [M+] calculated for $C_{20}H_{34}N_2O_3$ 350.2569, found 350.2576. UPLC (method A): t_R = 3.94 min., purity: ≥99%.

SA_078. 1-acetyl-4(4-aminophenyl) piperazine (0.10 g, 0.456 mmol, 1 eq.) was dissolved in dry DMF (5 mL) and potassium carbonate (0.314 g, 2.28 mmol, 5 eq.) was added. The suspension was stirred for 15 minutes at room temperature, and then acryloyl chloride (110 μL, 1.37 mmol, 3 eq.) was added. After 30 minutes, the reaction mixture was diluted with water and EtOAc and the aqueous phase extracted with EtOAc (3x 20 mL). The organic phase was washed with brine, dried over Na_2SO_4, and concentrated. Purification via automated column chromatography (0-8% MeOH in DCM) gave **SA78** (0.051 g, 41%) as a pink-tinged solid. ^{1}H NMR (400 MHz, $CDCl_3$) δ 7.84 (s, 1H), 7.51 (d, *J* = 8.7 Hz, 2H), 6.89 (d, *J* = 8.5 Hz, 2H), 6.40 (dd, *J* = 16.9, 1.6 Hz, 1H), 6.26 (dd, *J* = 16.9, 10.1 Hz, 1H), 5.71 (dd, *J* = 10.1, 1.6 Hz, 1H), 3.76 (t, *J* = 5.2 Hz, 2H), 3.62 (t, *J* = 5.1 Hz, 2H), 3.20 – 3.03 (m, 4H), 2.13 (s, 3H). ^{13}C NMR (101 MHz, $CDCl_3$) δ 169.09, 163.54, 147.63, 131.29, 127.27, 121.41, 117.33, 77.26, 50.20, 49.83, 46.17, 41.30, 21.36. HRMS-ESI(+) m/z [M+] calculated for $C_{15}H_{19}N_3O_2$ 273.1477, found 273.1478. UPLC (method A): t_R = 3.95 min., purity: ≥99%.

SA_079. 1-[1-(2-Phenylethyl)piperidin-4-yl]methanamine (0.20 g, 0.916 mmol, 1 eq.) was dissolved in dry DMF (5 mL) and potassium carbonate (0.632 g, 4.58 mmol, 5 eq.) was added. The suspension was stirred for 15 minutes at room temperature, and then acryloyl chloride (220 μL, 2.75 mmol, 3 eq.) was added. After 30 minutes, the reaction mixture was diluted with water and EtOAc and the aqueous phase extracted with EtOAc (3x 20 mL). The organic phase was washed with brine, dried over Na_2SO_4, and concentrated. Purification via automated column

chromatography (0-8% MeOH in DCM) gave **SA79** (0.162 g, 65%) as a light yellow solid. ^{1}H NMR (400 MHz, $CDCl_3$) δ 7.30 – 7.06 (m, 5H), 6.21 (dd, *J* = 17.0, 1.6 Hz, 1H), 6.04 (dd, *J* = 16.9, 10.2 Hz, 1H), 5.85 (d, *J* = 6.8 Hz, 1H), 5.56 (dd, *J* = 10.2, 1.6 Hz, 1H), 3.18 (t, *J* = 6.4 Hz, 2H), 2.98 (dt, *J* = 11.9, 3.4 Hz, 2H), 2.84 – 2.71 (m, 2H), 2.62 – 2.49 (m, 2H), 2.07 – 1.92 (m, 2H), 1.75 – 1.64 (m, 2H), 1.63 – 1.48 (m, 1H), 1.32 (qd, *J* = 12.1, 3.9 Hz, 2H). ^{13}C NMR (101 MHz, $CDCl_3$) δ 165.73, 140.09, 130.87, 128.69, 128.44, 126.41, 126.13, 60.69, 53.34, 44.96, 35.82, 33.49, 29.71. HRMS-ESI(+) m/z [M+] calculated for $C_{17}H_{24}N_2O$ 272.1889, found 272.1887. UPLC (method A): t_R = 0.41 min., purity: 91%.

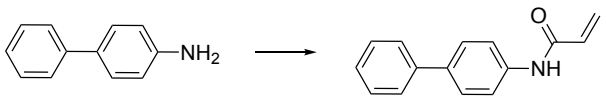

CD_002A

Scheme 10. Synthetic route used for the synthesis of **CD_002A**. Condition: acryloyl chloride, NEt_3, DCM, r.t., 2h, 88%.

***N*-([1,1'-biphenyl]-4-yl)acrylamide (CD_002A).** Following general procedure C, **CD_002A** was obtained from 4-aminophenyl (0.59 mmol, 0.10 g) as a yellow solid (0.12 g, 88%). ^{1}H NMR (400 MHz, $CDCl_3$) δ 7.67 (d, *J* = 8.4 Hz, 2H), 7.61 – 7.56 (m, 4H), 7.47 – 7.40 (m, 2H), 7.33 (tt, *J* = 8.1, 2.0 Hz, 1H), 6.47 (dd, *J* = 16.8, 1.2 Hz, 1H), 6.27 (dd, *J* = 16.8, 10.2 Hz, 1H), 5.80 (dd, *J* = 10.2, 1.2 Hz, 1H). ^{13}C NMR (101 MHz, $CDCl_3$) δ 163.67, 140.54, 137.54, 137.12, 131.24, 128.93, 128.12, 127.80, 127.31, 126.98, 120.42. HRMS m/z [M] calcd for $C_{15}H_{13}NO$ 223.0997, found: 223.1002. UPLC (method A): t_R = 3.64 min., purity: 98%.

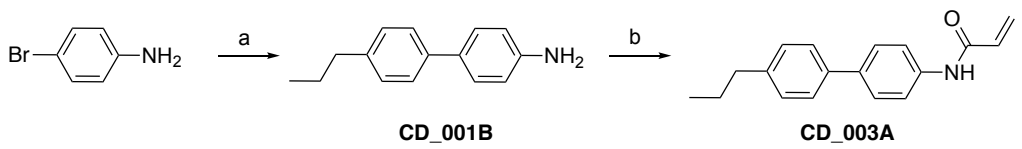

Scheme 11. Synthetic route used for the synthesis of **CD_003A**. Conditions: a) 4-*tert*-butylphenylboronic acid, K_2CO_3, $Pd(PPh)_3$, dioxane/water/MeOH (4:1:10), 80°C, 3h30, 52%. b) acryloyl chloride, NEt_3, DCM, r.t., 2h, 95%.

4'-propyl-[1,1'-biphenyl]-4-amine (CD_001B). 4-bromoaniline (0.58 mmol, 0.10 g), 4-*tert*-butylphenylboronic acid (0.87 mmol, 0.14 g), potassium carbonate (1.74 mmol, 0.24 g) and palladium tetrakis (0.03 mmol, 0.03 g) were dissolved into a mixture of dioxane/water/methanol (3 mL, 4:1:10) degassed under nitrogen. The reaction mixture was stirred at 80°C for 3 hour 30 minutes. Then, the reaction mixture was concentrated and taken back in water and diethyl ether. The organic phase was washed with brine, dried with Na_2SO_4 and concentrated. The crude product was purified via automated flash column chromatography (20-100% EtOAc in hexanes) to afford **CD_001B** as a yellow solid (0.06 g, 52%). ^{1}H NMR (400 MHz, $CDCl_3$) δ 7.47 – 7.43 (m, 2H), 7.43 – 7.38 (m, 2H), 7.23 – 7.18 (m, 2H), 6.78 – 6.72 (m, 2H), 2.64 – 2.57 (m, 2H), 1.67 (dq, *J* = 14.8, 7.4 Hz, 3H), 0.97 (t, *J* = 7.3 Hz, 3H). ^{13}C NMR (101 MHz, $CDCl_3$) δ 145.65, 140.91, 138.66, 131.79, 128.91, 127.98, 126.36, 115.54, 37.80, 24.75, 14.06.

***N*-(4'-propyl-[1,1'-biphenyl]-4-yl)acrylamide (CD_003A).** Following general procedure C, **CD_003A** was obtained from **CD_001B** (0.28 mmol, 0.06 g) as a yellow solid (0.07 g, 95%). ^{1}H NMR (400 MHz, CDCl3) δ 7.65 (d, *J* = 8.0 Hz, 2H), 7.57 (d, *J* = 8.5 Hz, 2H), 7.49 (d, *J* = 8.1 Hz, 2H), 7.32 (s, 1H), 7.23 (s, 1H), 6.50 – 6.42 (m, 1H), 6.27 (dd, *J* = 16.9, 10.2 Hz, 1H), 5.82 – 5.76 (m, 1H), 2.67 – 2.57 (m, 2H), 1.67 (dq, *J* = 14.8, 7.4 Hz, 3H), 0.97 (t, *J* = 7.3 Hz, 4H). ^{13}C NMR

(101 MHz, CDCl3) δ 141.95, 137.90, 137.56, 136.82, 131.25, 129.07, 128.07, 127.63, 126.80, 120.33, 37.82, 29.86, 14.28, 14.03. HRMS m/z [M] calcd for $C_{18}H_{19}NO$ 265.1467, found: 265.1478. UPLC (method A): t_R = 4.29 min., purity: 97%.

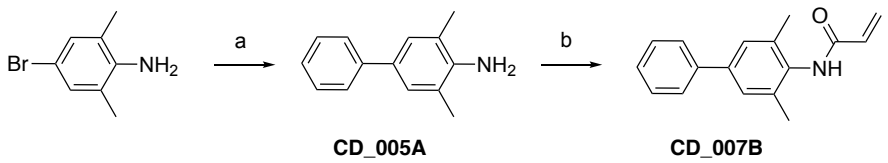

Scheme 12. Synthetic route used for the synthesis of **CD_007B**. Conditions: a) phenylboronic acid, K_2CO_3, $Pd(PPh)_3$, dioxane/water/MeOH (4:1:10), 80°C, 3h30, 41%. b) acryloyl chloride, K_2CO_3, THF, r.t., 2h30, 20%.

3,5-dimethyl-[1,1'-biphenyl]-4-amine (CD_005A). 4-bromo-2,6-dimethylaniline (0.50 mmol, 0.10 g), phenylboronic acid (0.75 mmol, 0.09 g), potassium carbonate (1.50 mmol, 0.21 g) and palladium tetrakis (0.03 mmol, 0.03 g) were dissolved into a mixture of dioxane/water/methanol (3 mL, 4:1:10) degassed under nitrogen. The reaction mixture was stirred at 80°C for 3 hour 30 minutes. Then, the reaction mixture was concentrated and taken back in water and diethyl ether. The organic phase was washed with brine, dried with Na_2SO_4 and concentrated. The crude product was purified via automated flash column chromatography (20-100% EtOAc in hexanes) to afford **CD_005A** as a brown oil (0.04 g, 41%). ^{1}H NMR (400 MHz, $CDCl_3$) δ 7.61 – 7.57 (m, 2H), 7.43 (t, *J* = 7.7 Hz, 2H), 7.30 (t, *J* = 7.4 Hz, 1H), 7.26 (s, 2H), 3.67 (s, 2H), 2.29 (s, 6H). ^{13}C NMR (101 MHz, $CDCl_3$) δ 142.40, 141.61, 131.14, 128.69, 127.14, 126.62, 126.18, 122.11, 17.92.

***N*-(3,5-dimethyl-[1,1'-biphenyl]-4-yl)acrylamide (CD_007B).** Following general procedure B with THF as solvent, **CD_007B** was obtained from **CD_005A** (0.21 mmol, 0.04 g) as a white solid

(0.01 g, 20%). ^{1}H NMR (400 MHz, $CDCl_3$) δ 7.58 – 7.52 (m, 2H), 7.45 – 7.39 (m, 2H), 7.34 (dd, *J* = 5.1, 2.1 Hz, 1H), 7.30 (s, 2H), 6.43 (dd, *J* = 17.0, 2.1 Hz, 1H), 6.36 (dd, *J* = 17.0, 9.5 Hz, 1H), 5.79 (dd, *J* = 9.5, 2.1 Hz, 1H), 2.30 (d, *J* = 6.3 Hz, 6H). ^{13}C NMR (101 MHz, $CDCl_3$) δ 164.16, 140.89, 140.51, 135.89, 132.90, 130.68, 129.97, 128.95, 128.81, 127.75, 127.68, 127.39, 127.28, 127.22, 18.99, 18.79. HRMS m/z [M] calcd for $C_{17}H_{17}NO$ 251.1310, found: 251.1311. UPLC (method A): t_R = 3.67 min., purity: 99%.

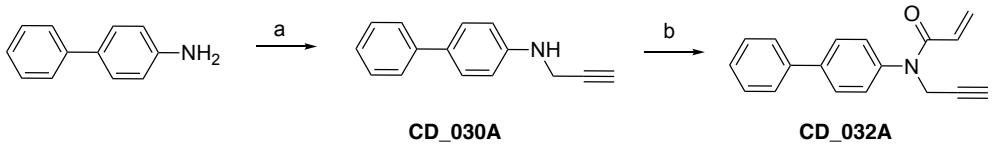

CD_030A **CD_032A**

Scheme 13. Synthetic route used for the synthesis of **CD_032A**. Conditions: a) propargylbromide, K_2CO_3, DMF, 85°C, 8-15h, 65%. b) acryloyl chloride, K_2CO_3, DMF, r.t., 2h30, 82%.

***N*-(prop-2-yn-1-yl)-[1,1'-biphenyl]-4-amine (CD_030A).** Following general procedure A, 4-aminobiphenyl (0.60 mmol, 0.10 g) and propargylbromide (0.45 mmol, 50.0 μL) were reacted until completion of the reaction. The obtained crude was then purified by automated flash chromatography (20-100% EtOAc in hexanes) to afford **CD_030A** as a yellow solid (0.06 g, 65%). ^{1}H NMR (400 MHz, $CDCl_3$) δ 7.57 (dd, *J* = 8.3, 1.2 Hz, 2H), 7.54 – 7.48 (m, 2H), 7.46 – 7.39 (m, 2H), 7.30 (tt, *J* = 6.8, 1.2 Hz, 1H), 6.81 – 6.76 (m, 2H), 3.99 (s, 3H), 2.27 (s, 1H). ^{13}C NMR (101 MHz, $CDCl_3$) δ 146.34, 141.20, 131.66, 128.79, 128.06, 126.53, 126.39, 113.89, 81.02, 71.53, 33.75.

***N*-([1,1'-biphenyl]-4-yl)-*N*-(prop-2-yn-1-yl)acrylamide (CD_032A).** Following general procedure B, **CD_032A** was obtained from **CD_030A** (0.30 mmol, 0.06 g) as a yellow

solid (0.06 g, 82%). ^{1}H NMR (400 MHz, $CDCl_3$) δ 7.65 – 7.60 (m, 2H), 7.60 – 7.56 (m, 2H), 7.44 (td, *J* = 6.8, 6.4, 1.6 Hz, 2H), 7.39 – 7.34 (m, 1H), 7.34 – 7.30 (m, 2H), 6.42 (dd, *J* = 16.8, 1.9 Hz, 1H), 6.09 (dd, *J* = 16.7, 10.3 Hz, 1H), 5.57 (dd, *J* = 10.3, 1.9 Hz, 1H), 4.57 (d, *J* = 2.5 Hz, 2H), 2.23 (t, *J* = 2.4 Hz, 1H). ^{13}C NMR (101 MHz, $CDCl_3$) δ 165.25, 141.28, 140.26, 139.89, 128.97, 128.67, 128.53, 128.26, 128.15, 127.84, 127.12, 78.96, 72.30, 38.72. HRMS m/z [M] calcd for $C_{18}H_{15}NO$ 261.1154, found: 261.1154. UPLC (method A): t_R = 5.01 min., purity: ≥ 99%.

2-(phenylamino)acetonitrile (CD_046A). Following general procedure A, aniline (1.1 mmol, 0.10 g) and bromoacetonitrile (0.80 mmol, 56.0 μL) were reacted until completion of the reaction. The obtained crude was then purified by automated flash chromatography (0-100% EtOAc in hexanes) to afford **CD_046A** as a yellow solid (0.05 g, 31%). ^{1}H NMR (400 MHz, $CDCl_3$) δ 7.32 – 7.24 (m, 2H), 6.90 (t, *J* = 7.4 Hz, 1H), 6.71 (d, *J* = 7.8 Hz, 2H), 4.06 (d, *J* = 5.2 Hz, 2H), 4.03 (s, 1H). ^{13}C NMR (101 MHz, $CDCl_3$) δ 145.12, 129.64, 120.05, 117.20, 113.66, 32.64.

***N*-(cyanomethyl)-*N*-phenylacrylamide (CD_047A).** Following general procedure B, **CD_047A** was obtained from **CD_046A** (0.30 mmol, 0.05 g) as a yellow oil (0.05 g, 97%). ^{1}H NMR (400 MHz, $CDCl_3$) δ 7.52 – 7.41 (m, 3H), 7.31 – 7.24 (m, 2H), 6.46 (dd, *J* = 16.8, 1.8 Hz, 1H), 6.01 (dd, *J* = 16.8, 10.3 Hz, 1H), 5.63 (dd, *J* = 10.3, 1.8 Hz, 1H), 4.65 (s, 2H). ^{13}C NMR (101 MHz, $CDCl_3$) δ 165.59, 140.14, 130.38, 130.20, 129.36, 128.03, 126.93, 115.40, 37.32. HRMS m/z [M] calcd for $C_{11}H_{10}N_2O$ 186.0793, found: 186.0795. UPLC (method A): t_R = 4.27 min., purity: 97%.

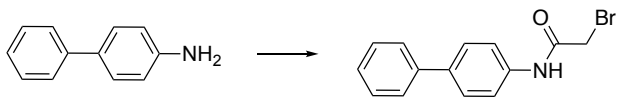

CD_004B

Scheme 14. Synthetic route used for the synthesis of **CD_004B**. Condition: bromoacetyl bromide, NEt_3, DCM, 0°C → r.t., 41h, 68%.

***N*-([1,1'-biphenyl]-4-yl)-2-bromoacetamide (CD_004B).** To a solution of 4-aminobiphenyl (0.60 mmol, 0.10 g) and NEt_3 (0.70 mmol, 98.0 μL) in dry DCM (3 mL) under nitrogen, was added dropwise bromoacetyl bromide (0.66 mmol, 57.0 μL) at 0°C. The reaction mixture is allowed to warm up at r.t. and left to stir at r.t. for 41h. Then the reaction mixture is concentrated and taken back in hexane and EtOAc. The obtained solution is filtered, and the filtrate is then filtered again through a pad of celite with EtOAc. The obtained solid is finally taken back in toluene twice and concentrated to afford **CD_004B** as a brown solid (0.12 g, 68%). ^{1}H NMR (400 MHz, $CDCl_3$) δ 8.22 (s, 1H), 7.61 (d, *J* = 3.7 Hz, 4H), 7.58 (d, *J* = 7.3 Hz, 3H), 7.44 (t, *J* = 7.6 Hz, 2H), 7.34 (t, *J* = 7.3 Hz, 1H), 4.06 (s, 2H). ^{13}C NMR (101 MHz, $CDCl_3$) δ 163.51, 140.39, 138.24, 136.27, 128.96, 127.87, 127.45, 127.03, 120.48, 29.69. HRMS m/z [M] calcd for $C_{14}H_{12}BrNO$ 289.0102, found: 289.0109. UPLC (method A): t_R = 3.67 min., purity: 96%. (PMID: 25148591)

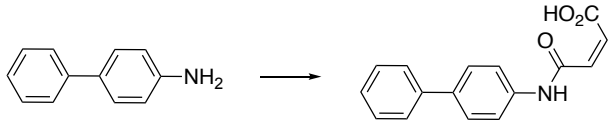

CD_008A

Scheme 15. Synthetic route used for the synthesis of **CD_008A**. Condition: maleic anhydride, toluene, 60°C, 2h15, quant.

(*Z*)-4-([1,1'-biphenyl]-4-ylamino)-4-oxobut-2-enoic acid (CD_008A). To a solution of maleic anhydride (1.18 mmol, 0.20 g) in toluene (3 mL) was added 4-aminobiphenyl (1.18 mmol, 0.12 g). The reaction mixture was stirred at 60°C for 2 hour 15 minutes. After full conversion, the reaction mixture was cooled down to r.t. then diluted with an aqueous solution of 1M HCl. The formed precipitate was filtered, washed with 1 M HCl, and then left to dry on high vacuum to afford **CD_008A** as a yellow solid (0.40 g, quant.). ^{1}H NMR (400 MHz, DMSO) δ 10.52 (s, 1H), 7.72 (d, *J* = 8.1 Hz, 2H), 7.65 (d, *J* = 7.8 Hz, 5H), 7.44 (t, *J* = 7.4 Hz, 3H), 7.33 (t, *J* = 6.9 Hz, 1H), 6.49 (d, *J* = 12.0 Hz, 1H), 6.32 (d, *J* = 12.0 Hz, 1H). ^{13}C NMR (101 MHz, DMSO) δ 167.00, 163.33, 139.65, 138.09, 135.57, 131.69, 130.49, 129.00, 127.21, 127.08, 126.36, 119.94. HRMS m/z [M] calcd for $C_{16}H_{13}NO_3$ 267.0895, found: 267.0887. UPLC (method A): t_R = 3.68 min., purity: 98%.

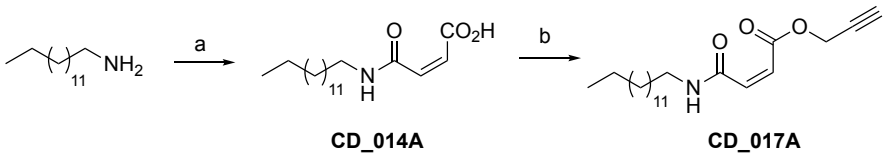

Scheme 16. Synthetic route used for the synthesis of **CD_017A**. Conditions: a) maleic anhydride, toluene, 60°C, 3h, 95%. b) propargylbromide, NaH, DMF, r.t., 4 days, 43% (93:7 Z/E ratio).

(Z)-4-oxo-4-(tetradecylamino)but-2-enoic acid (CD_014A). To a solution of maleic anhydride (2.30 mmol, 0.23 g) in toluene (6 mL) was added tetradecylamine (2.30 mmol, 0.50 g). The reaction mixture was stirred at 60°C for 3 hours. After full conversion, the reaction mixture was cooled down to r.t. then diluted with an aqueous solution of 1M HCl. The formed precipitate was filtered, washed with 1 M HCl, and then left to dry on high vacuum to afford **CD_014A** as a white

solid (0.68 g, 95%). ^{1}H NMR (400 MHz, CDCl3) δ 7.40 (s, 1H), 6.38 (d, *J* = 22.8 Hz, 1H), 3.37 (s, 1H), 1.60 (s, 2H), 1.25 (s, 19H), 0.87 (s, 3H). The spectrum is in accordance with that reported in the literature (https://doi.org/10.26434/chemrxiv.13755763.v1).

prop-2-yn-1-yl (*Z*)-4-oxo-4-(tetradecylamino)but-2-enoate (CD_017A). To a solution of **CD_014A** (2.14 mmol, 0.67 g) in DMF (14 mL) was added NaH (60% immersion in oil, 3.21 mmol, 0.13 g) and propargylbromide (10.7 mmol, 953 μL). The reaction mixture was stirred at r.t. for 4 days. Then, the reaction mixture was extracted three times with ethyl acetate. The combined organics were washed with brine, dried with Na_2SO_4 and concentrated. The obtained crude was then purified by automated flash chromatography (20-50% EtOAc in hexanes) to afford **CD_017A** as a yellow solid (0.32 g, 43%). ^{1}H NMR (400 MHz, CDCl3) δ 7.79 (s, 1H), 6.38 (d, *J* = 12.9 Hz, 1H), 6.13 (d, *J* = 12.9 Hz, 1H), 4.77 (d, *J* = 2.5 Hz, 2H), 3.35 – 3.27 (m, 2H), 2.52 (t, *J* = 2.5 Hz, 1H), 1.56 (p, *J* = 7.3 Hz, 2H), 1.25 (s, 11H), 0.87 (t, *J* = 6.8 Hz, 3H). ^{13}C NMR (101 MHz, CDCl3) δ 165.43, 163.81, 139.68, 123.95, 75.74, 52.94, 39.95, 32.06, 29.82, 29.79, 29.72, 29.67, 29.49, 29.41, 29.30, 27.09, 22.83, 14.26. HRMS m/z [M] calcd for $C_{21}H_{35}NO_3$ 349.2617, found: 349.2626. UPLC (method B): t_R = 4.05 min., purity: ≥ 99 %. A Z/E ratio of 93:7 is obtained from the reaction.

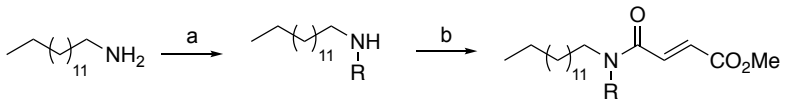

Scheme 17. Synthetic route used for the synthesis of **SA16 & CD_056A**. Conditions: a) RBr, K_2CO_3, DMF, 85°C, 8-15h, **17**: 49%, **18**: 69%. b) monomethyl fumarate, Oxyma, DIC, DIPEA, DCM, r.t., 3h, **SA16**: %, **CD_056A**: 76%.

***N*-(prop-2-yn-1-yl)tetradecan-1-amine (RSK6-I).** Following general procedure A, the product was obtained from tetradecylamine (0.70 mmol, 0.16 g) and propargyl bromide (1.70 mmol, 63.1 μL) as yellowish solid (0.14 g, 49%). ^{1}H NMR (400 MHz, CDCl3) δ 3.41 (d, *J* = 2.4 Hz, 2H), 2.67 (t, *J* = 7.2 Hz, 2H), 2.19 (t, *J* = 2.4 Hz, 1H), 1.46 (q, *J* = 7.3 Hz, 2H), 1.24 (s, 23H), 0.87 (t, *J* = 6.7 Hz, 3H). The spectrum is in accordance with that reported in the literature (https://doi.org/10.26434/chemrxiv.13755763.v1).

2-(tetradecylamino)acetonitrile (SA8-I). Following general procedure A, the product was obtained from tetradecylamine (2.30 mmol, 0.50 g) and bromoacetonitrile (1.70 mmol, 120 μL) as a yellow solid (0.40 g, 69%). ^{1}H NMR (400 MHz, CDCl3) δ 3.56 (s, 2H), 2.69 (t, *J* = 7.1 Hz, 2H), 1.46 (p, *J* = 7.0 Hz, 2H), 1.23 (s, 23H), 0.85 (t, *J* = 6.8 Hz, 3H). ^{13}C NMR (101 MHz, CDCl3) δ 161.22, 117.97, 48.96, 38.21, 37.40, 31.97, 29.74, 29.71, 29.64, 29.61, 29.53, 29.49, 29.41, 27.15, 22.74, 14.16. The spectrum is in accordance with the literature (https://doi.org/10.26434/chemrxiv.13755763.v1).

methyl (*E*)-4-((cyanomethyl)(tetradecyl)amino)-4-oxobut-2-enoate (CD_056A). To a solution of **SA8-I** (1.58 mmol, 0.40 g) in DCM (18 mL) was added a solution of monomethyl fumarate (4.74 mmol, 0.62 g), Oxyma (2.37 mmol, 0.34 g), DIC (2.37 mmol, 374 μL) and DIPEA (2.37 mmol, 414 μL). The reaction mixture was stirred at r.t. for 3 hours. After full conversion, the reaction mixture was concentrated. The obtained crude was then purified by automated flash chromatography (0-5% MeOH in DCM) to afford **CD_056A** as a yellow solid (0.44 g, 76%). ^{1}H NMR (400 MHz, $CDCl_3$) δ 7.73 (d, *J* = 15.2 Hz, 1H), 7.30 (d, *J* = 15.2 Hz, 1H), 4.77 (s, 2H), 4.21

(d, J = 4.0 Hz, 3H), 3.95 – 3.89 (m, 2H), 2.12 – 2.02 (m, 2H), 1.76 – 1.62 (m, 23H), 1.28 (t, J = 6.8 Hz, 3H). ^{13}C NMR (101 MHz, $CDCl_3$) δ 165.60, 164.71, 132.89, 131.91, 115.21, 52.30, 48.97, 34.11, 31.89, 29.64, 29.61, 29.56, 29.48, 29.41, 29.32, 29.13, 28.93, 26.44, 22.66, 14.09. HRMS m/z [M] calcd for $C_{21}H_{36}N_2O_3$ 364.2726, found: 364.2732. UPLC (method B): t_R = 6.67 min., purity: 98%.

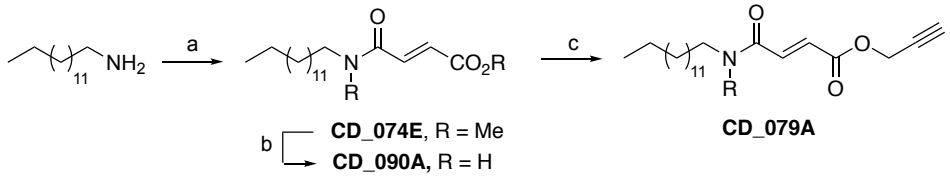

Scheme 18. Synthetic route used for the synthesis of **CD_079A**. Conditions: a) monomethyl fumarate, Oxyma, DIC, DIEA, DCM, r.t., 2h, 75%. b) LiOH 1.4 M, dioxane, r.t., 1h, 89%. c) propargylbromide, K_2CO_3, DMF, r.t., 22h, 2%.

methyl (*E*)-4-oxo-4-(tetradecylamino)but-2-enoate (CD_074E). To a solution of tetradecylamine (0.94 mmol, 0.20 g) in DCM (11 mL) was added a solution of monomethyl fumarate (2.82 mmol, 0.37 g), Oxyma (1.41 mmol, 0.20 g), DIC (1.41 mmol, 222 μL) and DIPEA (1.41 mmol, 246 μL). The reaction mixture was stirred at r.t. for 2 hours. After full conversion, the reaction mixture was washed two times with water, once with brine. The organics were dried over Na_2SO_4 and concentrated. The obtained crude was then purified by automated flash chromatography (20-50% EtOAc in hexanes) to afford **CD_074E** as a white solid (0.23 g, 75%). ^{1}H NMR (400 MHz, CDCl3) δ 6.92 – 6.77 (m, 2H), 5.73 (s, 1H), 3.81 (d, J = 7.4 Hz, 3H), 3.35 (q, J = 7.1 Hz, 2H), 1.54 (q, J = 7.2 Hz, 2H), 1.22 (d, J = 27.3 Hz, 22H), 0.88 (t, J = 6.8 Hz, 3H).

The spectrum is in accordance with that reported in the literature (https://doi.org/10.26434/chemrxiv.13755763.v1).

(*E*)-4-oxo-4-(tetradecylamino)but-2-enoic acid (CD_090A). To a solution of **CD_074E** (0.12 mmol, 0.04 g) in dioxane (2 mL) and THF (0.5 mL) was added a solution of LiOH 1.4 M (0.72 mmol, 0.50 mL). The reaction mixture was stirred at r.t. for 1 hour until the reaction was complete. The reaction mixture was then diluted with an aqueous solution of 1M HCl. The formed precipitate was filtered, washed with 1M HCl, and dried under high vacuum to afford **CD_090A** as a white solid (0.03 g, 89%). ^{1}H NMR (400 MHz, DMSO) δ 8.50 – 8.42 (m, 1H), 6.91 (d, *J* = 15.5 Hz, 1H), 6.49 (d, *J* = 15.5 Hz, 1H), 3.13 (q, *J* = 6.6 Hz, 3H), 1.47 – 1.36 (m, 2H), 1.23 (s, 21H), 0.85 (t, *J* = 6.8 Hz, 3H). The spectrum is in accordance with that reported in the literature (https://doi.org/10.26434/chemrxiv.13755763.v1).

prop-2-yn-1-yl (*E*)-4-oxo-4-(tetradecylamino)but-2-enoate (CD_079A). To a solution of **CD_090A** (0.30 mmol, 0.09 g) in DMF (1 mL) was added potassium carbonate (0.90 mmol, 0.12 g) and propargylbromide (0.90 mmol, 80.0 μL). The reaction mixture was stirred at r.t. for 22 hours. After full conversion, the reaction mixture was extracted three times with diethyl ether. The combined organics were washed with brine, dried with Na_2SO_4 and concentrated. The obtained crude was then purified by automated flash chromatography (10-100% EtOAc in hexanes) to afford the pure product as a white solid (0.002 g, 2%). ^{1}H NMR (400 MHz, $CDCl_3$) δ 6.90 – 6.79 (m, 2H), 5.69 (s, 1H), 3.80 (s, 2H), 3.35 (q, *J* = 7.1 Hz, 2H), 2.38 – 2.32 (m, 1H), 1.34 – 1.22 (m, 25H), 0.91 – 0.85 (m, 5H). ^{13}C NMR (101 MHz, $CDCl_3$) δ 167.64, 166.22, 136.66, 130.11, 119.22, 52.33, 40.14, 32.07, 29.84, 29.80, 29.78, 29.71, 29.66, 29.56, 29.50, 29.39, 27.03, 24.89, 22.84,

14.27. HRMS m/z [M] calcd for $C_{21}H_{35}NO_3$ 349.2617, found: 349.2619. UPLC (method B): t_R = 4.10 min., purity: 96%. (WO2015153761A2, Fasan, R.)

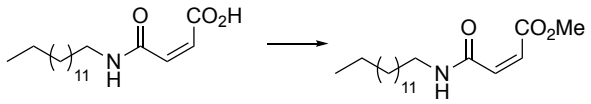

CD_014A **CD_081A**

Scheme 19. Synthetic route used for the synthesis of **CD_081A**. Condition: H_2SO_4, MeOH, 40°C, 1h30, 48%.

methyl (*Z*)-4-oxo-4-(tetradecylamino)but-2-enoate (CD_081A). To a solution of **CD_014A** (0.19 mmol, 0.06 g) in dry methanol (0.5 mL) was added concentrated sulfuric acid (0.76 mmol, 41.0 μL). The reaction mixture was stirred at 40°C for 1h 30 minutes. Then, the reaction mixture was extracted three times with EtOAc. The combined organics were washed with brine, dried with Na_2SO_4 and concentrated. The obtained crude was then purified by automated flash chromatography (20-50% EtOAc in hexanes) to afford **CD_081A** as a white solid (0.03 g, 48%). ^{1}H NMR (400 MHz, $CDCl_3$) δ 8.20 (s, 1H), 6.33 (d, *J* = 13.1 Hz, 1H), 6.12 (d, *J* = 13.1 Hz, 1H), 3.79 (s, 3H), 3.32 (q, *J* = 7.1 Hz, 2H), 1.57 (dd, *J* = 14.0, 6.3 Hz, 4H), 1.25 (s, 20H), 0.88 (t, *J* = 6.8 Hz, 3H). ^{13}C NMR (101 MHz, $CDCl_3$) δ 166.90, 163.94, 139.26, 124.65, 52.53, 39.95, 32.07, 29.84, 29.83, 29.83, 29.80, 29.73, 29.68, 29.50, 29.42, 29.32, 27.12, 22.84, 14.27. HRMS m/z [M] calcd for $C_{19}H_{35}NO_3$ 325.2617, found: 325.2616. UPLC (method B): t_R = 4.00 min., purity: 99%.

phenyl (*Z*)-4-oxo-4-(tetradecylamino)but-2-enoate (CD_113D). DCC (0.21 mmol, 0.04 g) and a drop of pyridine were added to a solution of **CD_014A** (0.19 mmol, 0.06 g) and phenol (0.19 mmol, 17.0 μL) in DCM (1 mL). The reaction mixture was stirred at r.t. for 2 hours. Then the

reaction mixture was diluted with water and extracted two times with EtOAc. The combined organics were washed two times with 0.2 M NaOH then two times with water, dried with Na_2SO_4 and concentrated. The obtained crude was then purified by automated flash chromatography (10-50% EtOAc in hexanes then 10-40% EtOAc in petroleum ether) to afford **CD_113D** as a white solid (0.005 g, 7%). ^{1}H NMR (400 MHz, CDCl3) δ 7.76 (s, 1H), 7.46 – 7.37 (m, 2H), 7.32 – 7.25 (m, 1H), 7.15 (dd, *J* = 8.0, 1.6 Hz, 3H), 6.49 (d, *J* = 12.9 Hz, 1H), 6.35 (d, *J* = 12.9 Hz, 1H), 3.36 – 3.26 (m, 2H), 1.53 (p, *J* = 7.2 Hz, 3H), 1.31 (d, *J* = 7.1 Hz, 4H), 1.24 (d, *J* = 8.8 Hz, 22H), 0.88 (t, *J* = 6.9 Hz, 4H). ^{13}C NMR (101 MHz, $CDCl_3$) δ 163.78, 150.20, 140.12, 129.75, 126.57, 124.47, 121.48, 40.04, 32.07, 29.84, 29.81, 29.79, 29.71, 29.65, 29.51, 29.39, 29.34, 27.10, 22.84, 14.27. HRMS m/z [M] calcd for $C_{24}H_{37}NO_3$ 387.2773, found: 387.278. UPLC (method B): t_R = 4.25 min., purity: 97%. (https://doi.org/10.1016/j.tet.2020.131029)

***N*^{1}-(prop-2-yn-1-yl)-*N*^{1}-tetradecylmaleamide (CD_124B).** To a solution of **CD_014A** (0.26 mmol, 0.08 g) in DMF (5 mL) was added propargylamine hydrochloride (0.78 mmol, 0.07 g), Oxyma (0.39 mmol, 0.06 g) and DIC (0.39 mmol, 61.5 μL). The reaction mixture was stirred at r.t. for 2 hours. After full conversion, water was added to the reaction mixture and the formed precipitate was filtered and washed with water. The obtained crude was then purified by automated flash chromatography (20-50% EtOAc in hexanes). The obtained residue was then taken back in MeOH, spined down and the filtrate was separated from the precipitate and concentrated to afford **CD_124B** as a white solid (0.006 g, 7%). ^{1}H NMR (400 MHz, MeOD) δ 6.21 (d, J = 12.9 Hz, 1H), 6.18 – 6.13 (m, 1H), 4.03 (d, J = 2.6 Hz, 2H), 3.24 (t, J = 7.1 Hz, 2H), 2.61 (t, J = 2.6 Hz, 1H), 1.54 (q, J = 10.3, 8.5 Hz, 2H), 1.29 (s, 22H), 0.93 – 0.85 (m, 3H). ^{13}C NMR (101 MHz, CDCl3) δ 167.07, 166.85, 133.42, 132.92, 132.07, 80.05, 72.53, 40.61, 33.08, 30.80, 30.78, 30.76, 30.70,

30.67, 30.48, 30.39, 30.08, 29.60, 28.05, 23.74, 14.43. HRMS m/z [M] calcd for $C_{21}H_{36}N_2O_2$ 348.2777, found: 348.2787. UPLC (method B): t_R = 4.24 min., purity: 95%.

(1-(2-methoxy-2-oxoethyl)-1*H*-1,2,3-triazol-4-yl)methyl (*Z*)-4-oxo-4-(tetradecylamino)but-2-enoate (CD_116A). To a solution of **CD_017A** (0.20 mmol, 0.07 g) and methyl azidoacetate (0.39 mmol, 38.0 μL) in THF/H2O (2 mL, 1:1) were added successively $CuSO_4.5H_2O$ (0.02 mmol, 0.005 g), sodium ascorbate (0.02 mmol, 0.004 g) and TBTA (0.004 mmol, 0.002 g). The reaction mixture was stirred at r.t. for 17 hours and 30 minutes. Then the reaction mixture was filtered through celite with DCM (30 mL) and concentrated. The obtained crude was then purified by automated flash chromatography (0-5% MeOH in DCM) to afford **CD_116A** as a white solid (0.07 g, 76%). ^{1}H NMR (400 MHz, $CDCl_3$) δ 7.79 (s, 1H), 7.72 (s, 1H), 6.33 (d, *J* = 12.8 Hz, 1H), 6.08 (d, *J* = 12.8 Hz, 1H), 5.33 (s, 2H), 5.17 (s, 2H), 3.80 (s, 3H), 3.34 – 3.22 (m, 2H), 1.53 (p, *J* = 7.4 Hz, 2H), 1.24 (s, 22H), 0.86 (t, *J* = 6.8 Hz, 3H). ^{13}C NMR (101 MHz, $CDCl_3$) δ 166.64, 165.87, 164.02, 142.65, 138.87, 125.36, 124.54, 58.44, 53.21, 50.82, 39.87, 32.01, 29.78, 29.75, 29.74, 29.70, 29.66, 29.44, 29.39, 29.30, 27.09, 22.77, 14.21. HRMS m/z [M] calcd for $C_{24}H_{40}N_4O_5$ 464.2999, found: 464.2993. UPLC (method B): t_R = 3.95 min., purity: 95%.

***tert*-butyl (3-azidopropyl)carbamate (CD_118A).** Triethylamine (0.80 mmol, 112 μL) was added to a solution of 3-azido-1-propanamine (0.80 mmol, 78.0 μL) in DCM (2 mL). The resulting solution was cooled down to 0°C and a solution of Boc_2O (0.88 mmol, 0.19 g) in 2 mL DCM was added dropwise to the reaction mixture, which is left to stir at 0°C for an hour and then at r.t. for 23 hours 30 minutes. The reaction mixture is then concentrated, and the obtained crude was then purified by automated flash chromatography (20-100% EtOAc in hexanes) to afford **CD_118A** as

a transparent oil (0.16 g, 100%). ^{1}H NMR (400 MHz, $CDCl_3$) δ 4.84 (s, 1H), 3.29 (t, *J* = 6.7 Hz, 2H), 3.18 – 3.09 (m, 2H), 1.70 (p, *J* = 6.7 Hz, 2H), 1.38 (s, 9H). ^{13}C NMR (101 MHz, $CDCl_3$) δ 156.12, 85.25, 49.19, 29.37, 28.45, 27.46. (PMID: 27936668)

(1-(3-((*tert*-butoxycarbonyl)amino)propyl)-1*H*-1,2,3-triazol-4-yl)methyl (*Z*)-4-oxo-4-(tetradecylamino)but-2-enoate (CD_119A). To a solution of **CD_017A** (0.20 mmol, 0.07 g) and **CD_118A** (0.40 mmol, 0.08 g) in THF/H2O (2 mL, 1:1) were added successively $CuSO_4.5H_2O$ (0.02 mmol, 0.005 g), sodium ascorbate (0.02 mmol, 0.004 g) and TBTA (0.004 mmol, 0.002 g). The reaction mixture was stirred at r.t. for 24 hours. Then the reaction mixture was filtered through celite with DCM (30 mL) and concentrated. The obtained crude was then purified by automated flash chromatography (0-5% MeOH in DCM) to afford **CD_119A** as a white solid (0.08 g, 76%). ^{1}H NMR (400 MHz, $CDCl_3$) δ 7.75 (s, 2H), 6.33 (d, *J* = 12.9 Hz, 1H), 6.09 (d, *J* = 12.9 Hz, 1H), 5.31 (s, 2H), 4.84 (s, 1H), 4.41 (t, *J* = 6.8 Hz, 2H), 3.32 – 3.24 (m, 2H), 3.13 (q, *J* = 6.2 Hz, 2H), 2.09 (p, *J* = 6.7 Hz, 2H), 1.53 (q, *J* = 7.0 Hz, 2H), 1.43 (s, 9H), 1.24 (s, 22H), 0.90 – 0.82 (m, 3H). ^{13}C NMR (101 MHz, $CDCl_3$) δ 165.95, 164.03, 156.28, 142.18, 138.73, 124.72, 124.37, 58.56, 47.77, 39.91, 32.03, 30.87, 29.80, 29.77, 29.76, 29.72, 29.68, 29.46, 29.41, 29.31, 28.49, 27.11, 22.80, 14.23. HRMS m/z [M] calcd for $C_{29}H_{51}N_5O_5$ 549.389, found: 549.3898. UPLC (method B): t_R = 4.12 min., purity: 96%.

(1-(2-(2-(2-(2-hydroxyethoxy)ethoxy)ethoxy)ethyl)-1*H*-1,2,3-triazol-4-yl)methyl (*Z*)-4-oxo-4-(tetradecylamino)but-2-enoate (CD_141A). To a solution of **CD_017A** (0.17 mmol, 0.06 g) and 1-azido-3,6,9-trioxaundecane-11-ol (0.34 mmol, 0.07 g) in THF/H2O (2 mL, 1:1) were added successively $CuSO_4.5H_2O$ (0.02 mmol, 0.004 g), sodium ascorbate (0.02 mmol, 0.004 g) and

TBTA (0.007 mmol, 0.004 g). The reaction mixture was stirred at r.t. for 24 hours 30 minutes. Then the reaction mixture was filtered through celite with DCM (30 mL) and concentrated. The obtained crude was then purified by automated flash chromatography (0-5% MeOH in DCM) to afford **CD_141A** as a white solid (0.06 g, 59%). ^{1}H NMR (400 MHz, CDCl3) δ 7.96 – 7.77 (m, 2H), 6.35 (dd, *J* = 12.8, 3.9 Hz, 1H), 6.10 (dd, *J* = 12.8, 8.5 Hz, 1H), 5.32 (d, *J* = 8.3 Hz, 2H), 4.55 (dt, *J* = 9.6, 5.0 Hz, 2H), 3.92 – 3.84 (m, 2H), 3.76 – 3.49 (m, 10H), 3.29 (q, *J* = 7.1 Hz, 2H), 2.60 (s, 2H), 1.54 (q, *J* = 6.8 Hz, 2H), 1.25 (s, 23H), 0.87 (t, *J* = 6.8 Hz, 3H). ^{13}C NMR (101 MHz, CDCl3) δ 165.92, 164.09, 139.07, 138.72, 124.68, 124.57, 72.58, 70.68, 70.63, 70.58, 70.54, 70.37, 69.48, 61.77, 58.55, 50.58, 39.95, 32.05, 29.83, 29.79, 29.75, 29.71, 29.49, 29.44, 29.35, 29.33, 27.14, 22.82, 14.26. HRMS m/z [M] calcd for $C_{29}H_{52}N_4O_7$ 568.3836, found: 568.3822. UPLC (method B): t_R = 3.84 min., purity: 95%.

***(R)-N*-(3-((3-azidopropyl)amino)-3-oxopropyl)-2,4-dihydroxy-3,3-dimethylbutanamide (CD_134B).** To a solution of D-pantothenic acid hemicalcium salt (0.84 mmol, 0.20 g), Oxyma (1.26 mmol, 0.18 g) and EDC (1.26 mmol, 0.20 g) in water (5 mL) was added 3-azido-1-propanamine (0.84 mmol, 82.0 μL) in water (5 mL). The reaction mixture was stirred at r.t. for 2 hours. After full conversion, the reaction mixture was concentrated. The obtained crude was then purified by automated flash chromatography (0-10% MeOH in DCM). The obtained residue was then purified by acid-base washing to afford **CD_134B** as a yellow oil (0.02 g, 9%). ^{1}H NMR (400 MHz, $CDCl_3$) δ 7.41 (s, 1H), 6.42 (s, 1H), 3.99 (s, 1H), 3.75 – 3.63 (m, 2H), 3.56 (q, *J* = 6.1 Hz, 2H), 3.39 – 3.31 (m, 4H), 2.57 (d, *J* = 29.3 Hz, 2H), 2.48 – 2.40 (m, 2H), 1.78 (p, *J* = 6.7 Hz, 2H), 0.99 (s, 3H), 0.92 (s, 3H). ^{13}C NMR (101 MHz, $CDCl_3$) δ 173.74 (s), 171.73 (s), 77.74 (s), 71.05 (s), 43.47 (s), 39.44 (s), 37.29 (s), 36.02 (s), 35.41 (s), 28.82 (s), 21.51 (s), 21.11 – 20.17 (m).

(*R*)-(1-(3-(3-(2,4-dihydroxy-3,3-dimethylbutanamido)propanamido)propyl)-1*H*-1,2,3-triazol-4-yl)methyl (*Z*)-4-oxo-4-(tetradecylamino)but-2-enoate (CD_142C). To a solution of **CD_017A** (0.05 mmol, 0.02 g) and **CD_134B** (0.08 mmol, 0.02 g) in THF/H2O (1 mL, 1:1) were added successively $CuSO_4.5H_2O$ (0.005 mmol, 0.001 g), sodium ascorbate (0.005 mmol, 0.001 g) and TBTA (0.002 mmol, 0.001 g). The reaction mixture was stirred at r.t. for 19 hours. Then the reaction mixture was filtered through celite with DCM (20 mL) and concentrated. The obtained crude was then purified by automated flash chromatography (0-20% MeOH in DCM). The obtained residue was then triturated with *tert*-butylmethylester and filtrated to afford **CD_142C** as a yellow solid (0.008 g, 24%). ^{1}H NMR (400 MHz, $CDCl_3$) δ 7.78 (s, 1H), 7.36 (s, 1H), 6.59 (s, 1H), 6.33 (d, *J* = 12.5 Hz, 1H), 6.15 – 6.09 (m, 1H), 5.30 (d, *J* = 5.4 Hz, 2H), 4.42 (t, *J* = 6.5 Hz, 2H), 4.05 (s, 1H), 3.76 – 3.57 (m, 2H), 3.51 – 3.36 (m, 4H), 3.23 (ddd, *J* = 25.8, 12.8, 6.1 Hz, 3H), 2.40 – 2.27 (m, 2H), 2.15 (dd, *J* = 11.7, 5.8 Hz, 2H), 1.59 – 1.49 (m, 3H), 1.25 (s, 25H), 1.02 (s, 3H), 0.95 – 0.82 (m, 6H). ^{13}C NMR (101 MHz, $CDCl_3$) δ 174.19 (s), 171.69 (s), 165.83 (s), 164.55 (s), 137.19 (s), 125.53 (s), 124.80 (s), 77.88 (s), 71.24 (s), 58.44 (s), 53.57 (s), 48.61 (s), 39.98 (s), 39.47 (s), 36.88 (s), 36.08 (s), 35.00 (s), 32.06 (s), 30.43 (s), 29.87 (s), 29.84 (s), 29.83 (s), 29.81 (s), 29.80 (s), 29.76 (s), 29.72 (s), 29.50 (s), 29.45 (s), 29.35 (s), 27.14 (s), 22.83 (s), 21.74 (s), 20.59 (s), 14.27 (s). HRMS m/z [M] calcd for $C_{33}H_{58}N_6O_7$ 650.4367, found: 650.4359. UPLC (method B): t_R = 3.84 min., purity: 86% (95% pure by NMR).

Synthesis of CV6

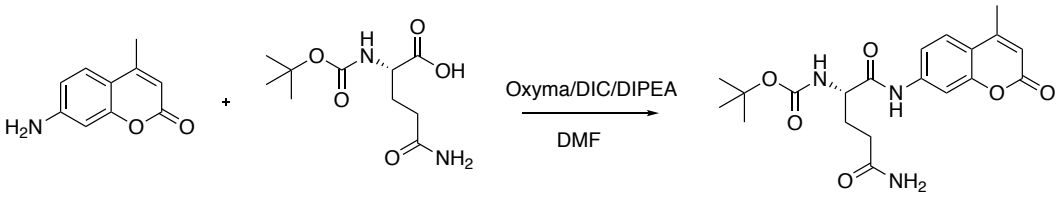

1. 7-methyl-4-amino coumarin (AMC) (0.5 g, 2.85 mmol, 1.0 eq) was dissolved in dry DMF (10 mL) in a 25 mL round-bottom flask. Boc-glutamine (1.4 g, 5.7 mmol, 2 eq.) was added, followed by DIPEA (1 mL, 5.7 mmol, 2 eq.), Oxyma (0.811 g, 5.7 mmol, 2 eq.) and DIC (530 µL, 3.4 mmol, 1.2 eq.). The reaction mixture was stirred at room temperature for 4 hours and then heated to 50°C. After stirring overnight, the reaction was cooled and concentrated under reduced pressure. Purification by column chromatography (0-5% methanol in DCM) yielded **1** (0.552 g, 48%). **LRMS-ESI(+):** Calculated for $C_{20}H_{25}N_3O_6$ [M+H$^+$] 403.17, found 403.2

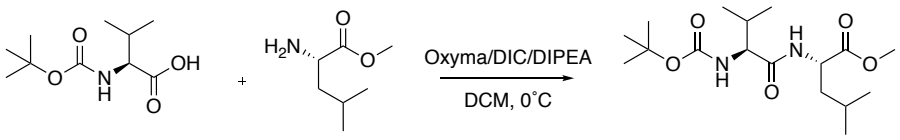

2. L-leucine methyl ester (0.30 grams, 1.65 mmol, 1.0 eq.) was dissolved in dichloromethane (10 mL) and, following addition of DIPEA (431 µL, 2.48 mmol, 1.5 eq.) the reaction was cooled to 0°C. In a separate flask, Boc-valine (0.716 g, 3.3 mmol, 2 eq.) and Oxyma (0.352 g, 2.48 mmol, 1.5 eq.) were dissolved in DCM and stirred for 5 minutes, after which DIC (384 µL, 2.48 mmol, 1.5 eq.) was added. This solution was then added to the reaction mixture and stirred for two hours while the solution warmed to room temperature. The solution was then diluted with DCM, washed

with brine, and dried over magnesium sulfate. Purification by column chromatography (0-40% EtOAc in hexanes) yielded **2** (0.445 g, 78%). **LRMS-ESI(+):** Calculated for $C_{17}H_{32}N_2O_5$ [M+H$^+$] 344.23, found 344.5.

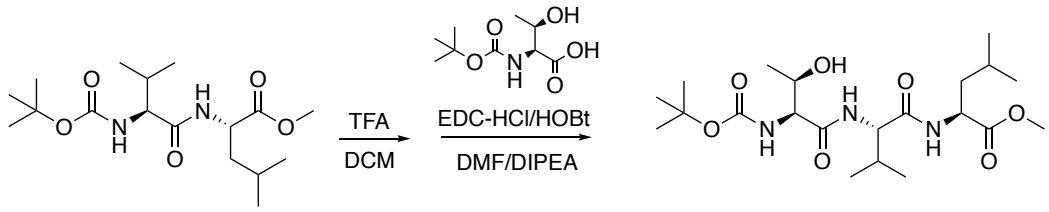

3. Compound **2** (0.210 g, 0.610 mmol, 1 eq.) was dissolved in a solution of 25% TFA in DCM and stirred for 30 minutes. After TLC indicated removal of the Boc group, the reaction was concentrated and the product washed with DCM three times. The deprotected peptide was then dissolved in DMF (5 mL) and DIPEA (215 μL, 1.22 mmol, 2.0 eq.), EDC•HCl (0.176 g, 0.914 mmol, 1.5 eq.), and HOBt (0.150, 0.914 mmol, 1.5 eq.) were added. The reaction was stirred for two hours at room temperature and then the solvent was removed under reduced pressure. Purification by column chromatography (0-40% EtOAc in hexanes) yielded **3** (0.445 g, 78%). **LRMS-ESI(+):** Calculated for $C_{21}H_{39}N_3O_7$ [M+H$^+$] 446.46, found 447.

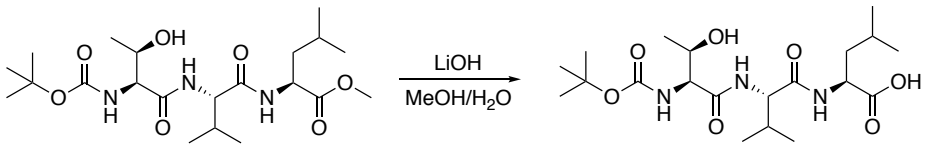

4. Compound 3 (0.150 g, 0.336 mmol, 1 eq.) was dissolved in solution of MeOH and water (1:1, 4 mL). Lithium hydroxide (0.016 g, 0.672 mmol, 2 eq.) was added and stirred in suspension. After three hours, reaction as acidified to pH = 2.0 and extracted with ethyl acetate. The organic phase was washed with brine and dried over magnesium sulfate. Concentration under reduced pressure

yield **4** (0.145 g, 98%) as pale yellow oil. **LRMS-ESI(+):** Calculated for $C_{20}H_{37}N_3O_7$ [M+H$^+$] 431.26, found 431.5.

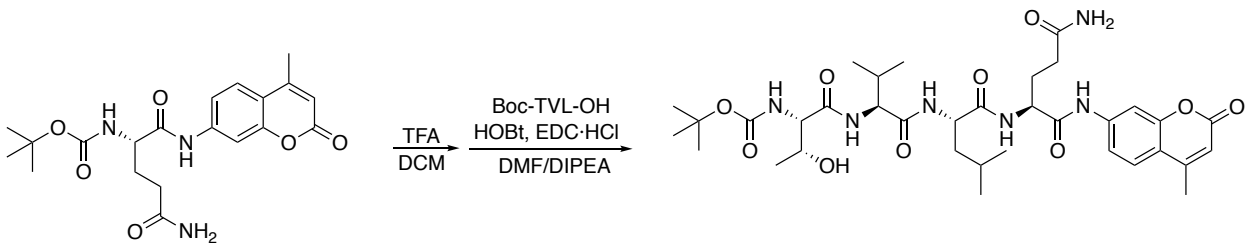

5. Compound 1 (0.085 g, 0.211 mmol, 1 eq.) was dissolved in a solution of 25% TFA in DCM and stirred for 30 minutes. After TLC indicated removal of the Boc group, the reaction was concentrated and the product washed with DCM three times. It was then dissolved in DMF (5 mL) and DIPEA (74 µL, 0.42 mmol, 2.0 eq.), EDC•HCl (0.061 g, 0.316 mmol, 1.5 eq.), and HOBt (0.034, 0.211 mmol, 1.0 eq.) were added. The reaction was stirred for two hours at room temperature and then the solvent was removed under reduced pressure. Purification by column chromatography (1 to 10% MeOH in DCM) yielded **5** (0.085 g, 56%). **LRMS-ESI(+):** Calculated for $C_{35}H_{52}N_6O_{10}$ [M+H$^+$] 716.37, found 716.4.

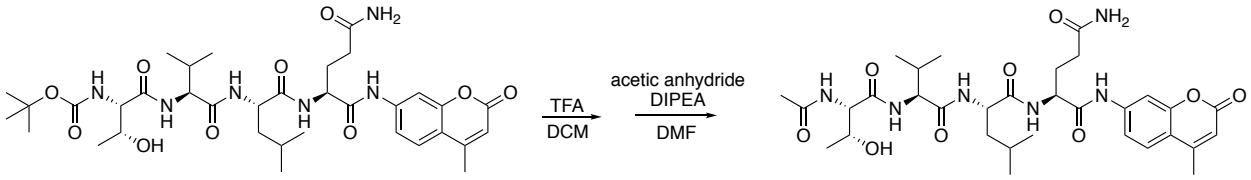

6 (CV6). Compound 5 (0.055 g, 0.0893 mmol, 1 eq.) was dissolved in a solution of 25% TFA in DCM and stirred for 30 minutes. After TLC indicated removal of the Boc group, the reaction was concentrated and the product washed with DCM three times. It was then dissolved in DMF (2 mL) with DIPEA (32 µL, 0.179 mmol, 2 eq.), and acetic anhydride (18 µL, 0.179 mmol, 2 eq.) was added slowly. After stirring for 10 minutes, solvent was removed under reduced pressure. The

crude reaction mixture was re-dissolved in water and washed with dichloromethane. The aqueous layer was then cooled to 0°C, upon which action **6** precipitated as a white solid (**LRMS-ESI(+):** Calculated for $C_{32}H_{36}N_6O_9$ [M+H$^+$] 658.33, found 658.5.

Synthesis of CV2

Synthesis of 1. A solution of Boc glycine (507.8 mg, 2.89 mmol, 1.0 eq),

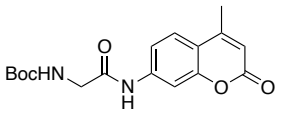

oxyma (0.540 g,3.79 mmol, 1.2 eq), DIC (0.538 μL, 3.47 mmol, 1.2 eq) and fluorophore amine (0.389 g, 2.22 mmol, 0.75 eq) in dry DMF (15 mL) was first stirred at 35 ^{o}C for 1h and then overnight at 45 ^{o}C. The reaction mixture was concentrated upon reduced pressure and purification by column chromatography (Silica, 2-10% MeOH:DCM) yielded **1** in 78% purity as analyzed by LCMS. For further purification, impure mixture was dissolved in minimal DCM, washed with water and brine. Organic layer was cooled to 0 ^{o}C and white precipitate was filtered to yield pure **1** (0.562 g, 76%). **^{1}H-NMR** (400 MHz,DMSO-d_6) δ 10.39 (s, 1H), 7.78 – 7.69 (m, 2H), 7.48 (dd, *J* = 8.7, 2.0 Hz, 1H), 7.12 (t, *J* = 6.1 Hz, 1H), 6.26 (d, *J* = 1.3 Hz, 1H), 3.77 (d, *J* = 6.1 Hz, 2H), 2.40 (d, *J* = 1.2 Hz, 3H), 1.40 (s, 9H). **LRMS-ESI(+)**: Calculated for $C_{17}H_{21}N_2O_5$ [M+H$^+$] 333.14; found 333.

Synthesis of 2. EDC.HCl (5.68 g, 29.5 mmol, 1.3 eq) was added to a

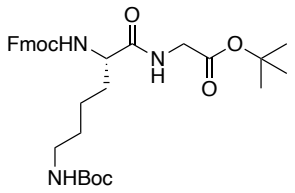

solution of Fmoc-Lys(Boc)-OH (10.02 g, 22.7 mmol, 1.0 eq), HOBt (4.34 g, 23.8 mmol, 1.05 eq), HCl.H_2N-Gly-OtBu (3.80 g, 22.7 mmol, 1.0 eq) and DIPEA (5.93 mL, 34.05 mmol, 1.5 eq) in DMF (50 mL). The resulting reaction mixture was stirred for 16h at room temperature and then concentrated under reduced pressure. Purification by column chromatography (Silica, 30-70% EtOAc:Hexane) yielded **2** (11.3 g, 86%). **^{1}H-NMR**

(400 MHz, $CDCl_3$) δ 7.76 (d, *J* = 7.5 Hz, 2H), 7.59 (d, *J* = 7.7 Hz, 2H), 7.39 (t, *J* = 7.5 Hz, 2H), 7.31 (td, *J* = 7.4, 1.2 Hz, 2H), 6.53 (s, 1H), 5.52 (s, 1H), 4.66 (s, 1H), 4.40 (d, *J* = 8.2 Hz, 2H), 4.21 (t, *J* = 6.9 Hz, 2H), 3.92 (s, 2H), 3.11 (d, *J* = 5.3 Hz, 2H), 1.97 – 1.80 (m, 1H), 1.60-1.75 (m, 2H), 1.30-1.55 (m, 21H). **LRMS-ESI(+)**: Calculated for $C_{32}H_{44}N_3O_7$ [M+H$^+$] 582.31; found 582.6.

Synthesis of 3. A solution of **2** (1.392 g, 2.39 mmol, 1.0 eq) in 10% Piperidine:DMF (20 mL) was stirred for 20 min at room temperature and followed with evaporation by rotary evaporation. Dilution with DMF (20 mL) and evaporation by rotary evaporation was repeated two more times to remove residual piperidine. The resultant crude was resuspended in DMF (30 mL), Fmoc-Leucine (0.928g, 2.62 mmol, 1.1 eq), HOBt (80%, 0.445 g, 2.63 mmol, 1.2 eq) and EDC.HCl (0.596 g, 3.10 mmol, 1.3 eq) were added. The reaction mixture was stirred for 30 min at room temperature and concentrated under reduced pressure. Purification by column chromatography (Silica, 10-50% EtOAc:DCM) yielded **3** (1.659 g, 85%). **^{1}H-NMR** (400 MHz, $CDCl_3$) δ 7.74 (d, *J* = 7.6 Hz, 2H), 7.58 (d, *J* = 7.4 Hz, 2H), 7.38 (t, *J* = 7.5 Hz, 2H), 7.29 (dd, *J* = 7.5, 3.4 Hz, 2H), 6.93 (s, 1H), 6.84 (d, *J* = 7.1 Hz, 1H), 5.68 (s, 1H), 4.81 (s, 1H), 4.62–4.48 (m, 1H), 4.42 (dd, *J* = 10.6, 7.2 Hz, 1H), 4.34 (t, *J* = 8.8 Hz, 1H), 4.25 (d, *J* = 5.1 Hz, 1H), 4.19 (t, *J* = 7.1 Hz, 1H), 3.99 – 3.80 (m, 2H), 3.03 (d, *J* = 6.6 Hz, 2H), 2.01 (s, 1H), 1.87 (h, *J* = 7.6 Hz, 1H), 1.74 – 1.51 (m, 4H), 1.43 (s, 9H), 1.40 (s, 9H), 1.38 – 1.22 (m, 3H), 0.92 (d, *J* = 6.5 Hz, 6H). **^{13}C-NMR** (101 MHz, $CDCl_3$) δ 172.72, 171.60, 168.84, 156.56, 143.96, 143.82, 141.39, 127.84, 127.19, 125.24, 120.10, 82.41, 77.48, 76.84, 67.20, 53.76, 52.89, 47.24, 42.11, 41.52, 32.06, 29.50, 28.56, 28.14, 24.81, 23.13, 22.62, 21.96. **HRA-MS(+)**: Calculated for $C_{38}H_{54}N_4O_8$ [M$^+$] 694.3942; found 694.3945.

Synthesis of 4. A solution of **3** (1.23 g, 1.77 mmol, 1.0 eq) and Et_3SiH (1.4 mL, 8.76 mmol, 5 eq) in 25% TFA:DCM (28 mL) was stirred at room temperature for 18 h, followed by dilution with DCM (20 mL) and evaporation by rotary evaporation. Dilution with DCM (30 mL) and evaporation by rotary evaporation was repeated two more times to remove residual TFA. The resultant crude was resuspended in MeOH (15 mL) followed by addition of Boc_2O (0.511 g, 2.22 mmol, 1.25 eq) and DIPEA (2.29 mL, 13.1 mmol, 7.5 eq). The reaction mixture was stirred for 1h at room temperature, diluted by EtOAc (100 mL) and washed with aq. HCl (pH~2). The aqueous layer was further extracted by EtOAc (2 x 30 mL), the combined organic layers were dried over Na_2SO_4, and then evaporated to give a crude product. Purification by column chromatography (Silica; 3-15% MeOH:DCM) yielded **4** (0.781 g, 87% purity by LCMS). **HRA-MS(+)**: Calculated for $C_{34}H_{46}N_4O_8$, $[M^+]$ 638.3316; found 638.3312

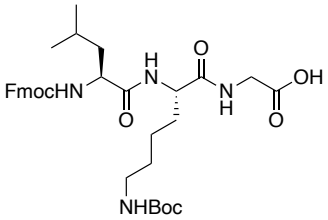

Synthesis of 5. A solution of **1** (47.8 mg, 0.143 mmol) in 20% TFA:DCM (2 mL) was stirred at room temperature for 30 min, followed by dilution with DCM (10 mL) and evaporation by rotary evaporation. Dilution with DCM (15 mL) and evaporation by rotary evaporation was repeated two more times to remove residual TFA. The resultant crude was resuspended in DMF (5 mL) and 2.7 mL of deprotected amine intermediate (77.4 μmol, 1.0 eq) was added to a flask containing **4** (49.7 mg, 77.8 μmol, 1.0 eq) and DIPEA (81.0 μL, 0.46 mmol, 6.0 eq) in DMF (1 mL). After addition of EDC.HCl (31.4 mg, 0.15 mmol, 2.0 eq) the reaction mixture was stirred for 16 h at room temperature, diluted by EtOAc (20 mL), and then washed by

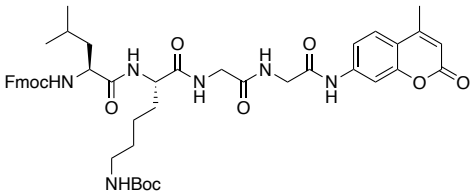

aq. HCl (pH ~ 2-3). The aqueous layer was further extracted by EtOAc (2 x 20 mL), the combined organic layers were dried over Na_2SO_4, and then evaporated to give a crude product. Purification by column chromatography (Silica, 1-6% MeOH in 1:1 EtOAc:DCM) yielded **5** (22.7 mg, 34%). **^{1}H-NMR** (400 MHz, DMSO-d_6) δ 10.15 (s, 1H), 8.50 – 8.38 (m, 1H), 8.26 (t, *J* = 5.9 Hz, 1H), 8.07 (d, *J* = 6.8 Hz, 1H), 7.88 (d, *J* = 7.6 Hz, 2H), 7.79 (d, *J* = 2.0 Hz, 1H), 7.75 – 7.66 (m, 3H), 7.56 – 7.47 (m, 2H), 7.40 (t, *J* = 6.9 Hz, 2H), 7.30 (tdd, *J* = 7.4, 2.2, 1.2 Hz, 2H), 6.71 (d, *J* = 6.7 Hz, 1H), 6.27 (d, *J* = 1.3 Hz, 1H), 4.36 – 4.14 (m, 4H), 4.13 – 4.02 (m, 2H), 3.95 (d, *J* = 5.9 Hz, 2H), 3.84 – 3.71 (m, 2H), 3.17 (d, *J* = 5.2 Hz, 1H), 2.87 (d, *J* = 5.9 Hz, 2H), 2.39 (d, *J* = 1.3 Hz, 3H), 1.55 (td, *J* = 41.8, 8.0 Hz, 4H), 1.34 (s, 12H), 0.79 (dd, *J* = 10.8, 6.6 Hz, 6H). **HRA-MS(+)**: Calculated for $C_{46}H_{56}N_6O_{10}Na$ [M+Na$^+$] 875.3956; found 875.3944.

Synthesis of 6. A solution of **5** (22.7 mg, 26.6 μmol, 1.0 eq) in 10% Piperidine:DMF (2 mL) was stirred for 15 min at room temperature and followed with evaporation by rotary

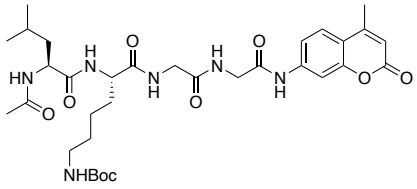

evaporation. Dilution with DMF (5 mL) and evaporation by rotary evaporation was repeated two more times to remove residual piperidine. The resultant crude was resuspended in DMF (2 mL), and DIPEA (18.5 μL, 0.11 mmol, 4 eq) and Acetic anhydride (10.0 μL, 0.11 mmol, 4 eq) were added. The reaction mixture was stirred for 1 hr at room temperature, diluted by EtOAc (20 mL), and then washed by aq. HCl (pH ~ 2-3). The aqueous layer was further extracted by EtOAc (2 x 20 mL), the combined organic layers were dried over Na_2SO_4, and then evaporated to give a crude product. Purification by column chromatography (Silica, 2-15% MeOH in 1:1 EtOAc:DCM) yielded **6** (9.7 mg, 56%). **^{1}H-NMR** (400 MHz, DMSO) δ 10.18 (s, 1H), 8.39 – 8.30 (m, 1H), 8.26 (t, *J* = 5.8 Hz, 1H), 8.06 (d, *J* = 7.0 Hz, 1H), 7.98 (d, *J* = 8.1 Hz, 1H), 7.80 (d, *J* = 2.1 Hz, 1H),

7.73 (d, *J* = 8.7 Hz, 1H), 7.54 (dd, *J* = 8.7, 2.1 Hz, 1H), 6.79 – 6.68 (m, 1H), 6.27 (d, *J* = 1.3 Hz, 1H), 4.29 (q, *J* = 7.6 Hz, 1H), 4.16 (q, *J* = 6.5 Hz, 1H), 3.94 (s, 2H), 3.84 – 3.67 (m, 2H), 2.86 (t, *J* = 6.4 Hz, 2H), 2.40 (d, *J* = 1.3 Hz, 3H), 1.83 (s, 3H), 1.73 – 1.45 (m, 4H), 1.36 (s, 11H), 1.23 (s, 3H), 0.78 (dd, *J* = 6.6, 3.9 Hz, 6H). **HRA-MS(+)**: Calculated for $C_{33}H_{48}N_6O_9$ [M^+] 672.3483; found 672.3502.

Synthesis of CV-2. A solution of **6** (11.2 mg, 16.6 μmol, 1. eq) in 20% TFA:DCM (2 mL) was stirred at room temperature for 30 min, followed by dilution with DCM (5 mL) and evaporation by rotary evaporation. Dilution with DCM (5 mL) and evaporation by rotary evaporation was repeated two more times to remove residual TFA. The crude was dissolved in DMSO to generate 20 mM stock of **CV-2**. Purity was assayed by LC/MS. **HRA-MS(+)**: Calculated for $C_{28}H_{40}N_6O_7$ [M^+] 572.2958; found 572.2956.

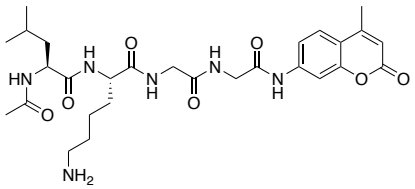

References

1. Beltrao, P.; Bork, P.; Krogan, N. J.; van Noort, V., Evolution and functional cross-talk of protein post-translational modifications. *Mol Syst Biol* **2013,** *9*, 714.

2. Prabakaran, S.; Lippens, G.; Steen, H.; Gunawardena, J., Post-translational modification: nature's escape from genetic imprisonment and the basis for dynamic information encoding. *Wiley Interdiscip Rev Syst Biol Med* **2012,** *4* (6), 565-83.

3. Lee, M. J.; Yaffe, M. B., Protein Regulation in Signal Transduction. *Cold Spring Harb Perspect Biol* **2016,** *8* (6).

4. Friso, G.; van Wijk, K. J., Posttranslational Protein Modifications in Plant Metabolism. *Plant Physiol* **2015,** *169* (3), 1469-87.

5. Spoel, S. H., Orchestrating the proteome with post-translational modifications. *J Exp Bot* **2018,** *69* (19), 4499-4503.

6. Lin, H.; Caroll, K. S., Introduction: Posttranslational Protein Modification. *Chem Rev* **2018,** *118* (3), 887-888.

7. Jackson, C. L.; Walch, L.; Verbavatz, J. M., Lipids and Their Trafficking: An Integral Part of Cellular Organization. *Dev Cell* **2016,** *39* (2), 139-153.

8. Wymann, M. P.; Schneiter, R., Lipid signalling in disease. *Nat Rev Mol Cell Biol* **2008,** *9* (2), 162-76.

9. Jiang, H.; Zhang, X.; Chen, X.; Aramsangtienchai, P.; Tong, Z.; Lin, H., Protein Lipidation: Occurrence, Mechanisms, Biological Functions, and Enabling Technologies. *Chem Rev* **2018,** *118* (3), 919-988.

10. Chen, B.; Sun, Y.; Niu, J.; Jarugumilli, G. K.; Wu, X., Protein Lipidation in Cell Signaling and Diseases: Function, Regulation, and Therapeutic Opportunities. *Cell Chem Biol* **2018,** *25* (7), 817-831.

11. Kakugawa, S.; Langton, P. F.; Zebisch, M.; Howell, S.; Chang, T. H.; Liu, Y.; Feizi, T.; Bineva, G.; O'Reilly, N.; Snijders, A. P.; Jones, E. Y.; Vincent, J. P., Notum deacylates Wnt proteins to suppress signalling activity. *Nature* **2015,** *519* (7542), 187-192.

12. Gottlieb, C. D.; Linder, M. E., Structure and function of DHHC protein S-acyltransferases. *Biochem Soc Trans* **2017,** *45* (4), 923-8.

13. Won, S. J.; Cheung See Kit, M.; Martin, B. R., Protein depalmitoylases. *Crit Rev Biochem Mol Biol* **2018,** *53* (1), 83-98.

14. Duncan, J. A.; Gilman, A. G., A cytoplasmic acyl-protein thioesterase that removes palmitate from G protein alpha subunits and p21(RAS). *J Biol Chem* **1998,** *273* (25), 15830-7.

15. Lin, D. T.; Conibear, E., ABHD17 proteins are novel protein depalmitoylases that regulate N-Ras palmitate turnover and subcellular localization. *Elife* **2015,** *4*, e11306.

16. Yokoi, N.; Fukata, Y.; Sekiya, A.; Murakami, T.; Kobayashi, K.; Fukata, M., Identification of PSD-95 Depalmitoylating Enzymes. *J Neurosci* **2016,** *36* (24), 6431-44.

17. Wang, J.; Hao, J. W.; Wang, X.; Guo, H.; Sun, H. H.; Lai, X. Y.; Liu, L. Y.; Zhu, M.; Wang, H. Y.; Li, Y. F.; Yu, L. Y.; Xie, C.; Wang, H. R.; Mo, W.; Zhou, H. M.; Chen, S.; Liang, G.; Zhao, T. J., DHHC4 and DHHC5 Facilitate Fatty Acid Uptake by Palmitoylating and Targeting CD36 to the Plasma Membrane. *Cell Rep* **2019,** *26* (1), 209-221 e5.

18. Zhao, L.; Zhang, C.; Luo, X.; Wang, P.; Zhou, W.; Zhong, S.; Xie, Y.; Jiang, Y.; Yang, P.; Tang, R.; Pan, Q.; Hall, A. R.; Luong, T. V.; Fan, J.; Varghese, Z.; Moorhead, J. F.; Pinzani, M.; Chen, Y.; Ruan, X. Z., CD36 palmitoylation disrupts free fatty acid metabolism and promotes tissue inflammation in non-alcoholic steatohepatitis. *J Hepatol* **2018,** *69* (3), 705-717.

19. Adachi, N.; Hess, D. T.; McLaughlin, P.; Stamler, J. S., S-Palmitoylation of a Novel Site in the beta2-Adrenergic Receptor Associated with a Novel Intracellular Itinerary. *J Biol Chem* **2016,** *291* (38), 20232-46.

20. Akimzhanov, A. M.; Boehning, D., Rapid and transient palmitoylation of the tyrosine kinase Lck mediates Fas signaling. *Proc Natl Acad Sci U S A* **2015,** *112* (38), 11876-80.

21. Kathayat, R. S.; Elvira, P. D.; Dickinson, B. C., A fluorescent probe for cysteine depalmitoylation reveals dynamic APT signaling. *Nat Chem Biol* **2017,** *13* (2), 150-152.

22. Sadeghi, R. S.; Kulej, K.; Kathayat, R. S.; Garcia, B. A.; Dickinson, B. C.; Brady, D. C.; Witze, E. S., Wnt5a signaling induced phosphorylation increases APT1 activity and promotes melanoma metastatic behavior. *Elife* **2018,** *7*.

23. Linder, M. E.; Deschenes, R. J., Palmitoylation: policing protein stability and traffic. *Nat Rev Mol Cell Biol* **2007,** *8* (1), 74-84.

24. Blanc, M.; David, F.; Abrami, L.; Migliozzi, D.; Armand, F.; Burgi, J.; van der Goot, F. G., SwissPalm: Protein Palmitoylation database. *F1000Res* **2015,** *4*, 261.

25. Lanyon-Hogg, T.; Faronato, M.; Serwa, R. A.; Tate, E. W., Dynamic Protein Acylation: New Substrates, Mechanisms, and Drug Targets. *Trends Biochem Sci* **2017,** *42* (7), 566-581.

26. Spinelli, M.; Fusco, S.; Grassi, C., Nutrient-Dependent Changes of Protein Palmitoylation: Impact on Nuclear Enzymes and Regulation of Gene Expression. *Int J Mol Sci* **2018,** *19* (12).

27. Hernandez, J. L.; Davda, D.; Cheung See Kit, M.; Majmudar, J. D.; Won, S. J.; Gang, M.; Pasupuleti, S. C.; Choi, A. I.; Bartkowiak, C. M.; Martin, B. R., APT2 Inhibition Restores Scribble Localization and S-Palmitoylation in Snail-Transformed Cells. *Cell Chem Biol* **2017,** *24* (1), 87-97.

28. De, I.; Sadhukhan, S., Emerging Roles of DHHC-mediated Protein S-palmitoylation in Physiological and Pathophysiological Context. *Eur J Cell Biol* **2018,** *97* (5), 319-338.

29. Draper, J. M.; Smith, C. D., DHHC20: a human palmitoyl acyltransferase that causes cellular transformation. *Mol Membr Biol* **2010,** *27* (2-3), 123-36.

30. Verardi, R.; Kim, J. S.; Ghirlando, R.; Banerjee, A., Structural Basis for Substrate Recognition by the Ankyrin Repeat Domain of Human DHHC17 Palmitoyltransferase. *Structure* **2017,** *25* (9), 1337-1347 e6.

31. Zaballa, M. E.; van der Goot, F. G., The molecular era of protein S-acylation: spotlight on structure, mechanisms, and dynamics. *Crit Rev Biochem Mol Biol* **2018,** *53* (4), 420-451.

32. Sharma, C.; Wang, H. X.; Li, Q.; Knoblich, K.; Reisenbichler, E. S.; Richardson, A. L.; Hemler, M. E., Protein Acyltransferase DHHC3 Regulates Breast Tumor Growth, Oxidative Stress, and Senescence. *Cancer Res* **2017,** *77* (24), 6880-6890.

33. Korycka, J.; Lach, A.; Heger, E.; Boguslawska, D. M.; Wolny, M.; Toporkiewicz, M.; Augoff, K.; Korzeniewski, J.; Sikorski, A. F., Human DHHC proteins: a spotlight on the hidden player of palmitoylation. *Eur J Cell Biol* **2012,** *91* (2), 107-17.

34. Sigala, S.; Bodei, S.; Missale, C.; Zani, D.; Simeone, C.; Cunico, S. C.; Spano, P. F., Gene expression profile of prostate cancer cell lines: effect of nerve growth factor treatment. *Mol Cell Endocrinol* **2008,** *284* (1-2), 11-20.

35. Runkle, K. B.; Kharbanda, A.; Stypulkowski, E.; Cao, X. J.; Wang, W.; Garcia, B. A.; Witze, E. S., Inhibition of DHHC20-Mediated EGFR Palmitoylation Creates a Dependence on EGFR Signaling. *Mol Cell* **2016,** *62* (3), 385-396.

36. Kharbanda, A.; Walter, D. M.; Gudiel, A. A.; Schek, N.; Feldser, D. M.; Witze, E. S., Blocking EGFR palmitoylation suppresses PI3K signaling and mutant KRAS lung tumorigenesis. *Sci Signal* **2020,** *13* (621).

37. Zhao, Y.; He, A.; Zhu, F.; Ding, M.; Hao, J.; Fan, Q.; Li, P.; Liu, L.; Du, Y.; Liang, X.; Guo, X.; Zhang, F.; Ma, X., Integrating genome-wide association study and expression quantitative trait locus study identifies multiple genes and gene sets associated with schizophrenia. *Prog Neuropsychopharmacol Biol Psychiatry* **2018,** *81*, 50-54.

38. Naumenko, V. S.; Ponimaskin, E., Palmitoylation as a Functional Regulator of Neurotransmitter Receptors. *Neural Plast* **2018,** *2018*, 5701348.

39. Itoh, M.; Yamashita, M.; Kaneko, M.; Okuno, H.; Abe, M.; Yamazaki, M.; Natsume, R.; Yamada, D.; Kaizuka, T.; Suwa, R.; Sakimura, K.; Sekiguchi, M.; Wada, K.; Hoshino, M.; Mishina, M.; Hayashi, T., Deficiency of AMPAR-Palmitoylation Aggravates Seizure Susceptibility. *J Neurosci* **2018,** *38* (47), 10220-10235.

40. Syndulko, K.; Cohen, S. N.; Tourtellotte, W. W.; Potvin, A. R., Endogenous event-related potentials: prospective applications in neuropsychology and behavioral neurology. *Bull Los Angeles Neurol Soc* **1982,** *47*, 124-40.

41. Kim, Y. C.; Lee, S. E.; Kim, S. K.; Jang, H. D.; Hwang, I.; Jin, S.; Hong, E. B.; Jang, K. S.; Kim, H. S., Toll-like receptor mediated inflammation requires FASN-dependent MYD88 palmitoylation. *Nat Chem Biol* **2019,** *15* (9), 907-916.

42. Lu, Y.; Zheng, Y.; Coyaud, E.; Zhang, C.; Selvabaskaran, A.; Yu, Y.; Xu, Z.; Weng, X.; Chen, J. S.; Meng, Y.; Warner, N.; Cheng, X.; Liu, Y.; Yao, B.; Hu, H.; Xia, Z.; Muise, A. M.; Klip, A.; Brumell, J. H.; Girardin, S. E.; Ying, S.; Fairn, G. D.; Raught, B.; Sun, Q.; Neculai, D., Palmitoylation of NOD1 and NOD2 is required for bacterial sensing. *Science* **2019,** *366* (6464), 460-467.

43. Ladygina, N.; Martin, B. R.; Altman, A., Dynamic palmitoylation and the role of DHHC proteins in T cell activation and anergy. *Adv Immunol* **2011,** *109*, 1-44.

44. Limagne, E.; Thibaudin, M.; Euvrard, R.; Berger, H.; Chalons, P.; Vegan, F.; Humblin, E.; Boidot, R.; Rebe, C.; Derangere, V.; Ladoire, S.; Apetoh, L.; Delmas, D.; Ghiringhelli, F., Sirtuin-1 Activation Controls Tumor Growth by Impeding Th17 Differentiation via STAT3 Deacetylation. *Cell Rep* **2017,** *19* (4), 746-759.

45. Sobocinska, J.; Roszczenko-Jasinska, P.; Ciesielska, A.; Kwiatkowska, K., Protein Palmitoylation and Its Role in Bacterial and Viral Infections. *Front Immunol* **2017,** *8*, 2003.

46. Zhang, N.; Zhao, H.; Zhang, L., Fatty Acid Synthase Promotes the Palmitoylation of Chikungunya Virus nsP1. *J Virol* **2019,** *93* (3).

47. Ohtsubo, K.; Chen, M. Z.; Olefsky, J. M.; Marth, J. D., Pathway to diabetes through attenuation of pancreatic beta cell glycosylation and glucose transport. *Nat Med* **2011,** *17* (9), 1067-75.

48. Mohammed, A. M.; Chen, F.; Kowluru, A., The two faces of protein palmitoylation in islet beta-cell function: potential implications in the pathophysiology of islet metabolic dysregulation and diabetes. *Recent Pat Endocr Metab Immune Drug Discov* **2013,** *7* (3), 203-12.

49. Ren, W.; Jhala, U. S.; Du, K., Proteomic analysis of protein palmitoylation in adipocytes. *Adipocyte* **2013,** *2* (1), 17-28.

50. Wei, X.; Song, H.; Semenkovich, C. F., Insulin-regulated protein palmitoylation impacts endothelial cell function. *Arterioscler Thromb Vasc Biol* **2014,** *34* (2), 346-54.

51. Spinelli, M.; Fusco, S.; Mainardi, M.; Scala, F.; Natale, F.; Lapenta, R.; Mattera, A.; Rinaudo, M.; Li Puma, D. D.; Ripoli, C.; Grassi, A.; D'Ascenzo, M.; Grassi, C., Brain insulin resistance impairs hippocampal synaptic plasticity and memory by increasing GluA1 palmitoylation through FoxO3a. *Nat Commun* **2017,** *8* (1), 2009.

52. Baldwin, A. C.; Green, C. D.; Olson, L. K.; Moxley, M. A.; Corbett, J. A., A role for aberrant protein palmitoylation in FFA-induced ER stress and beta-cell death. *Am J Physiol Endocrinol Metab* **2012,** *302* (11), E1390-8.

53. Qiu, T.; Kathayat, R. S.; Cao, Y.; Beck, M. W.; Dickinson, B. C., A Fluorescent Probe with Improved Water Solubility Permits the Analysis of Protein S-Depalmitoylation Activity in Live Cells. *Biochemistry* **2018,** *57* (2), 221-225.

54. Kathayat, R. S.; Cao, Y.; Elvira, P. D.; Sandoz, P. A.; Zaballa, M. E.; Springer, M. Z.; Drake, L. E.; Macleod, K. F.; van der Goot, F. G.; Dickinson, B. C., Active and dynamic mitochondrial S-depalmitoylation revealed by targeted fluorescent probes. *Nat Commun* **2018,** *9* (1), 334.

55. Schmidt, M. F.; Bracha, M.; Schlesinger, M. J., Evidence for covalent attachment of fatty acids to Sindbis virus glycoproteins. *Proc Natl Acad Sci U S A* **1979,** *76* (4), 1687-91.

56. Schlesinger, M. J.; Magee, A. I.; Schmidt, M. F., Fatty acid acylation of proteins in cultured cells. *J Biol Chem* **1980,** *255* (21), 10021-4.

57. Drisdel, R. C.; Green, W. N., Labeling and quantifying sites of protein palmitoylation. *Biotechniques* **2004,** *36* (2), 276-85.

58. Percher, A.; Ramakrishnan, S.; Thinon, E.; Yuan, X.; Yount, J. S.; Hang, H. C., Mass-tag labeling reveals site-specific and endogenous levels of protein S-fatty acylation. *Proc Natl Acad Sci U S A* **2016,** *113* (16), 4302-7.

59. Hang, H. C.; Geutjes, E. J.; Grotenbreg, G.; Pollington, A. M.; Bijlmakers, M. J.; Ploegh, H. L., Chemical probes for the rapid detection of Fatty-acylated proteins in Mammalian cells. *J Am Chem Soc* **2007,** *129* (10), 2744-5.

60. Martin, B. R.; Cravatt, B. F., Large-scale profiling of protein palmitoylation in mammalian cells. *Nat Methods* **2009,** *6* (2), 135-8.

61. Hannoush, R. N.; Arenas-Ramirez, N., Imaging the lipidome: omega-alkynyl fatty acids for detection and cellular visualization of lipid-modified proteins. *ACS Chem Biol* **2009,** *4* (7), 581-7.

62. Gao, X.; Hannoush, R. N., A Decade of Click Chemistry in Protein Palmitoylation: Impact on Discovery and New Biology. *Cell Chem Biol* **2018,** *25* (3), 236-246.

63. Zheng, B.; DeRan, M.; Li, X.; Liao, X.; Fukata, M.; Wu, X., 2-Bromopalmitate analogues as activity-based probes to explore palmitoyl acyltransferases. *J Am Chem Soc* **2013,** *135* (19), 7082-5.

64. Zheng, B.; Zhu, S.; Wu, X., Clickable analogue of cerulenin as chemical probe to explore protein palmitoylation. *ACS Chem Biol* **2015,** *10* (1), 115-21.

65. Kidd, D.; Liu, Y.; Cravatt, B. F., Profiling serine hydrolase activities in complex proteomes. *Biochemistry* **2001,** *40* (13), 4005-15.

66. Webb, Y.; Hermida-Matsumoto, L.; Resh, M. D., Inhibition of protein palmitoylation, raft localization, and T cell signaling by 2-bromopalmitate and polyunsaturated fatty acids. *J Biol Chem* **2000,** *275* (1), 261-70.

67. Hedberg, C.; Dekker, F. J.; Rusch, M.; Renner, S.; Wetzel, S.; Vartak, N.; Gerding-Reimers, C.; Bon, R. S.; Bastiaens, P. I.; Waldmann, H., Development of highly potent inhibitors of the Ras-targeting human acyl protein thioesterases based on substrate similarity design. *Angew Chem Int Ed Engl* **2011,** *50* (42), 9832-7.

68. Dekker, F. J.; Rocks, O.; Vartak, N.; Menninger, S.; Hedberg, C.; Balamurugan, R.; Wetzel, S.; Renner, S.; Gerauer, M.; Scholermann, B.; Rusch, M.; Kramer, J. W.; Rauh, D.; Coates, G. W.; Brunsveld, L.; Bastiaens, P. I.; Waldmann, H., Small-molecule inhibition of APT1 affects Ras localization and signaling. *Nat Chem Biol* **2010,** *6* (6), 449-56.

69. Adibekian, A.; Martin, B. R.; Chang, J. W.; Hsu, K. L.; Tsuboi, K.; Bachovchin, D. A.; Speers, A. E.; Brown, S. J.; Spicer, T.; Fernandez-Vega, V.; Ferguson, J.; Hodder, P. S.; Rosen, H.; Cravatt, B. F., Confirming target engagement for reversible inhibitors in vivo by kinetically tuned activity-based probes. *J Am Chem Soc* **2012,** *134* (25), 10345-8.

70. Remsberg, J. R.; Suciu, R. M.; Zambetti, N. A.; Hanigan, T. W.; Firestone, A. J.; Inguva, A.; Long, A.; Ngo, N.; Lum, K. M.; Henry, C. L.; Richardson, S. K.; Predovic, M.; Huang, B.; Dix, M. M.; Howell, A. R.; Niphakis, M. J.; Shannon, K.; Cravatt, B. F., ABHD17 regulation of plasma membrane palmitoylation and N-Ras-dependent cancer growth. *Nat Chem Biol* **2021,** *17* (8), 856-864.

71. Jennings, B. C.; Nadolski, M. J.; Ling, Y.; Baker, M. B.; Harrison, M. L.; Deschenes, R. J.; Linder, M. E., 2-Bromopalmitate and 2-(2-hydroxy-5-nitro-benzylidene)-benzo[b]thiophen-3-one inhibit DHHC-mediated palmitoylation in vitro. *J Lipid Res* **2009,** *50* (2), 233-42.

72. Davda, D.; El Azzouny, M. A.; Tom, C. T.; Hernandez, J. L.; Majmudar, J. D.; Kennedy, R. T.; Martin, B. R., Profiling targets of the irreversible palmitoylation inhibitor 2-bromopalmitate. *ACS Chem Biol* **2013,** *8* (9), 1912-7.

73. Tom, C. T.; Martin, B. R., Fat chance! Getting a grip on a slippery modification. *ACS Chem Biol* **2013,** *8* (1), 46-57.

74. Bhattacharyya, R.; Fenn, R. H.; Barren, C.; Tanzi, R. E.; Kovacs, D. M., Palmitoylated APP Forms Dimers, Cleaved by BACE1. *PLoS One* **2016,** *11* (11), e0166400.

75. Seno, K.; Hayashi, F., Palmitoylation is a prerequisite for dimerization-dependent raftophilicity of rhodopsin. *J Biol Chem* **2017,** *292* (37), 15321-15328.

76. Cao, Y.; Qiu, T.; Kathayat, R. S.; Azizi, S. A.; Thorne, A. K.; Ahn, D.; Fukata, Y.; Fukata, M.; Rice, P. A.; Dickinson, B. C., ABHD10 is an S-depalmitoylase affecting redox homeostasis through peroxiredoxin-5. *Nat Chem Biol* **2019,** *15* (12), 1232-1240.

77. Bolland, D. E.; Moritz, A. E.; Stanislowski, D. J.; Vaughan, R. A.; Foster, J. D., Palmitoylation by Multiple DHHC Enzymes Enhances Dopamine Transporter Function and Stability. *ACS Chem Neurosci* **2019,** *10* (6), 2707-2717.

78. Tomatis, V. M.; Trenchi, A.; Gomez, G. A.; Daniotti, J. L., Acyl-protein thioesterase 2 catalyzes the deacylation of peripheral membrane-associated GAP-43. *PLoS One* **2010,** *5* (11), e15045.

79. Gok, C.; Fuller, W., Topical review: Shedding light on molecular and cellular consequences of NCX1 palmitoylation. *Cell Signal* **2020,** *76*, 109791.

80. Chen, X.; Ma, H.; Wang, Z.; Zhang, S.; Yang, H.; Fang, Z., EZH2 Palmitoylation Mediated by ZDHHC5 in p53-Mutant Glioma Drives Malignant Development and Progression. *Cancer Res* **2017,** *77* (18), 4998-5010.

81. Beard, R. S., Jr.; Yang, X.; Meegan, J. E.; Overstreet, J. W.; Yang, C. G.; Elliott, J. A.; Reynolds, J. J.; Cha, B. J.; Pivetti, C. D.; Mitchell, D. A.; Wu, M. H.; Deschenes, R. J.; Yuan, S. Y., Palmitoyl acyltransferase DHHC21 mediates endothelial dysfunction in systemic inflammatory response syndrome. *Nat Commun* **2016,** *7*, 12823.

82. Mukai, J.; Liu, H.; Burt, R. A.; Swor, D. E.; Lai, W. S.; Karayiorgou, M.; Gogos, J. A., Evidence that the gene encoding ZDHHC8 contributes to the risk of schizophrenia. *Nat Genet* **2004,** *36* (7), 725-31.

83. Young, E.; Zheng, Z. Y.; Wilkins, A. D.; Jeong, H. T.; Li, M.; Lichtarge, O.; Chang, E. C., Regulation of Ras localization and cell transformation by evolutionarily conserved palmitoyltransferases. *Mol Cell Biol* **2014,** *34* (3), 374-85.

84. Liu, P.; Jiao, B.; Zhang, R.; Zhao, H.; Zhang, C.; Wu, M.; Li, D.; Zhao, X.; Qiu, Q.; Li, J.; Ren, R., Palmitoylacyltransferase Zdhhc9 inactivation mitigates leukemogenic potential of oncogenic Nras. *Leukemia* **2016,** *30* (5), 1225-8.

85. Raymond, F. L.; Tarpey, P. S.; Edkins, S.; Tofts, C.; O'Meara, S.; Teague, J.; Butler, A.; Stevens, C.; Barthorpe, S.; Buck, G.; Cole, J.; Dicks, E.; Gray, K.; Halliday, K.; Hills, K.; Hinton, J.; Jones, D.; Menzies, A.; Perry, J.; Raine, K.; Shepherd, R.; Small, A.; Varian, J.; Widaa, S.; Mallya, U.; Moon, J.; Luo, Y.; Shaw, M.; Boyle, J.; Kerr, B.; Turner, G.; Quarrell, O.; Cole, T.; Easton, D. F.; Wooster, R.; Bobrow, M.; Schwartz, C. E.; Gecz, J.; Stratton, M. R.; Futreal, P. A., Mutations in ZDHHC9, which encodes a palmitoyltransferase of NRAS and HRAS, cause X-linked mental retardation associated with a Marfanoid habitus. *Am J Hum Genet* **2007,** *80* (5), 982-7.

86. Tarpey, P. S.; Smith, R.; Pleasance, E.; Whibley, A.; Edkins, S.; Hardy, C.; O'Meara, S.; Latimer, C.; Dicks, E.; Menzies, A.; Stephens, P.; Blow, M.; Greenman, C.; Xue, Y.; Tyler-Smith, C.; Thompson, D.; Gray, K.; Andrews, J.; Barthorpe, S.; Buck, G.; Cole, J.;

Dunmore, R.; Jones, D.; Maddison, M.; Mironenko, T.; Turner, R.; Turrell, K.; Varian, J.; West, S.; Widaa, S.; Wray, P.; Teague, J.; Butler, A.; Jenkinson, A.; Jia, M.; Richardson, D.; Shepherd, R.; Wooster, R.; Tejada, M. I.; Martinez, F.; Carvill, G.; Goliath, R.; de Brouwer, A. P.; van Bokhoven, H.; Van Esch, H.; Chelly, J.; Raynaud, M.; Ropers, H. H.; Abidi, F. E.; Srivastava, A. K.; Cox, J.; Luo, Y.; Mallya, U.; Moon, J.; Parnau, J.; Mohammed, S.; Tolmie, J. L.; Shoubridge, C.; Corbett, M.; Gardner, A.; Haan, E.; Rujirabanjerd, S.; Shaw, M.; Vandeleur, L.; Fullston, T.; Easton, D. F.; Boyle, J.; Partington, M.; Hackett, A.; Field, M.; Skinner, C.; Stevenson, R. E.; Bobrow, M.; Turner, G.; Schwartz, C. E.; Gecz, J.; Raymond, F. L.; Futreal, P. A.; Stratton, M. R., A systematic, large-scale resequencing screen of X-chromosome coding exons in mental retardation. *Nat Genet* **2009,** *41* (5), 535-43.

87. Sanders, S. S.; Hayden, M. R., Aberrant palmitoylation in Huntington disease. *Biochem Soc Trans* **2015,** *43* (2), 205-10.

88. Roth, A. F.; Feng, Y.; Chen, L.; Davis, N. G., The yeast DHHC cysteine-rich domain protein Akr1p is a palmitoyl transferase. *J Cell Biol* **2002,** *159* (1), 23-8.

89. Lobo, S.; Greentree, W. K.; Linder, M. E.; Deschenes, R. J., Identification of a Ras palmitoyltransferase in Saccharomyces cerevisiae. *J Biol Chem* **2002,** *277* (43), 41268-73.

90. Pedro, M. P.; Vilcaes, A. A.; Tomatis, V. M.; Oliveira, R. G.; Gomez, G. A.; Daniotti, J. L., 2-Bromopalmitate reduces protein deacylation by inhibition of acyl-protein thioesterase enzymatic activities. *PLoS One* **2013,** *8* (10), e75232.

91. Tian, L.; McClafferty, H.; Jeffries, O.; Shipston, M. J., Multiple palmitoyltransferases are required for palmitoylation-dependent regulation of large conductance calcium- and voltage-activated potassium channels. *J Biol Chem* **2010,** *285* (31), 23954-62.

92. DeJesus, G.; Bizzozero, O. A., Effect of 2-fluoropalmitate, cerulenin and tunicamycin on the palmitoylation and intracellular translocation of myelin proteolipid protein. *Neurochem Res* **2002,** *27* (12), 1669-75.

93. Jackson, P. A.; Widen, J. C.; Harki, D. A.; Brummond, K. M., Covalent Modifiers: A Chemical Perspective on the Reactivity of alpha,beta-Unsaturated Carbonyls with Thiols via Hetero-Michael Addition Reactions. *J Med Chem* **2017,** *60* (3), 839-885.

94. Lanyon-Hogg, T.; Ritzefeld, M.; Sefer, L.; Bickel, J. K.; Rudolf, A. F.; Panyain, N.; Bineva-Todd, G.; Ocasio, C. A.; O'Reilly, N.; Siebold, C.; Magee, A. I.; Tate, E. W., Acylation-coupled lipophilic induction of polarisation (Acyl-cLIP): a universal assay for lipid transferase and hydrolase enzymes. *Chem Sci* **2019,** *10* (39), 8995-9000.

95. Lin, Y. H.; Doms, A. G.; Cheng, E.; Kim, B.; Evans, T. R.; Machner, M. P., Host Cell-catalyzed S-Palmitoylation Mediates Golgi Targeting of the Legionella Ubiquitin Ligase GobX. *J Biol Chem* **2015,** *290* (42), 25766-81.

96. Dallavilla, T.; Abrami, L.; Sandoz, P. A.; Savoglidis, G.; Hatzimanikatis, V.; van der Goot, F. G., Model-Driven Understanding of Palmitoylation Dynamics: Regulated Acylation of the Endoplasmic Reticulum Chaperone Calnexin. *PLoS Comput Biol* **2016,** *12* (2), e1004774.

97. Martin, B. R., Chemical approaches for profiling dynamic palmitoylation. *Biochem Soc Trans* **2013,** *41* (1), 43-9.

98. Jennings, B. C.; Linder, M. E., DHHC protein S-acyltransferases use similar ping-pong kinetic mechanisms but display different acyl-CoA specificities. *J Biol Chem* **2012,** *287* (10), 7236-45.

99. Mitchell, D. A.; Mitchell, G.; Ling, Y.; Budde, C.; Deschenes, R. J., Mutational analysis of Saccharomyces cerevisiae Erf2 reveals a two-step reaction mechanism for protein palmitoylation by DHHC enzymes. *J Biol Chem* **2010,** *285* (49), 38104-14.

100. Bastin, G.; Dissanayake, K.; Langburt, D.; Tam, A. L. C.; Lee, S. H.; Lachhar, K.; Heximer, S. P., RGS4 controls Galphai3-mediated regulation of Bcl-2 phosphorylation on TGN38-containing intracellular membranes. *J Cell Sci* **2020,** *133* (12).

101. Zhang, Y.; Lin, Z.; Tan, Y.; Bu, F.; Hao, P.; Zhang, K.; Yang, H.; Liu, S.; Ren, Y., Exploration of Missing Proteins by a Combination Approach to Enrich the Low-Abundance Hydrophobic Proteins from Four Cancer Cell Lines. *J Proteome Res* **2020,** *19* (1), 401-408.

102. Hao, J. W.; Wang, J.; Guo, H.; Zhao, Y. Y.; Sun, H. H.; Li, Y. F.; Lai, X. Y.; Zhao, N.; Wang, X.; Xie, C.; Hong, L.; Huang, X.; Wang, H. R.; Li, C. B.; Liang, B.; Chen, S.; Zhao, T. J., CD36 facilitates fatty acid uptake by dynamic palmitoylation-regulated endocytosis. *Nat Commun* **2020,** *11* (1), 4765.

103. Arnott, J. A.; Planey, S. L., The influence of lipophilicity in drug discovery and design. *Expert Opin Drug Discov* **2012,** *7* (10), 863-75.

104. Yao, H.; Lan, J.; Li, C.; Shi, H.; Brosseau, J. P.; Wang, H.; Lu, H.; Fang, C.; Zhang, Y.; Liang, L.; Zhou, X.; Wang, C.; Xue, Y.; Cui, Y.; Xu, J., Inhibiting PD-L1 palmitoylation enhances T-cell immune responses against tumours. *Nat Biomed Eng* **2019,** *3* (4), 306-317.

105. Yao, H.; Li, C.; He, F.; Song, T.; Brosseau, J.-P.; Wang, H.; Lu, H.; Fang, C.; Shi, H.; Lan, J.; Fang, J.-Y.; Xu, J., A peptidic inhibitor for PD-1 palmitoylation targets its expression and functions. *RSC Chemical Biology* **2021**.

106. Rana, M. S.; Kumar, P.; Lee, C. J.; Verardi, R.; Rajashankar, K. R.; Banerjee, A., Fatty acyl recognition and transfer by an integral membrane S-acyltransferase. *Science* **2018,** *359* (6372).

107. Lin, H., Protein cysteine palmitoylation in immunity and inflammation. *FEBS J* **2021**.

108. Swarthout, J. T.; Lobo, S.; Farh, L.; Croke, M. R.; Greentree, W. K.; Deschenes, R. J.; Linder, M. E., DHHC9 and GCP16 constitute a human protein fatty acyltransferase with specificity for H- and N-Ras. *J Biol Chem* **2005,** *280* (35), 31141-8.

109. Zhang, M.; Zhou, L.; Xu, Y.; Yang, M.; Xu, Y.; Komaniecki, G. P.; Kosciuk, T.; Chen, X.; Lu, X.; Zou, X.; Linder, M. E.; Lin, H., A STAT3 palmitoylation cycle promotes TH17 differentiation and colitis. *Nature* **2020,** *586* (7829), 434-439.

110. Azizi, S.-A.; Lan, T.; Delalande, C.; Kathayat, R. S.; Banales Mejia, F.; Qin, A.; Brookes, N.; Sandoval, P. J.; Dickinson, B. C., Development of an Acrylamide-Based Inhibitor of Protein S-Acylation. *ACS Chemical Biology* **2021**.

111. Ganesan, L.; Shieh, P.; Bertozzi, C. R.; Levental, I., Click-Chemistry Based High Throughput Screening Platform for Modulators of Ras Palmitoylation. *Sci Rep* **2017,** *7*, 41147.

112. Hamel, L. D.; Deschenes, R. J.; Mitchell, D. A., A fluorescence-based assay to monitor autopalmitoylation of zDHHC proteins applicable to high-throughput screening. *Anal Biochem* **2014,** *460*, 1-8.

113. Stix, R.; Lee, C. J.; Faraldo-Gomez, J. D.; Banerjee, A., Structure and Mechanism of DHHC Protein Acyltransferases. *J Mol Biol* **2020,** *432* (18), 4983-4998.

114. Azizi, S. A.; Kathayat, R. S.; Dickinson, B. C., Activity-Based Sensing of S-Depalmitoylases: Chemical Technologies and Biological Discovery. *Acc Chem Res* **2019,** *52* (11), 3029-3038.

115. Trott, O.; Olson, A. J., AutoDock Vina: improving the speed and accuracy of docking with a new scoring function, efficient optimization, and multithreading. *J Comput Chem* **2010,** *31* (2), 455-61.

116. Chamberlain, L. H.; Shipston, M. J., The physiology of protein S-acylation. *Physiol Rev* **2015,** *95* (2), 341-76.

117. Chen, S.; Zhu, B.; Yin, C.; Liu, W.; Han, C.; Chen, B.; Liu, T.; Li, X.; Chen, X.; Li, C.; Hu, L.; Zhou, J.; Xu, Z. X.; Gao, X.; Wu, X.; Goding, C. R.; Cui, R., Palmitoylation-dependent activation of MC1R prevents melanomagenesis. *Nature* **2017,** *549* (7672), 399-403.

118. Blaustein, M.; Piegari, E.; Martinez Calejman, C.; Vila, A.; Amante, A.; Manese, M. V.; Zeida, A.; Abrami, L.; Veggetti, M.; Guertin, D. A.; van der Goot, F. G.; Corvi, M. M.; Colman-Lerner, A., Akt Is S-Palmitoylated: A New Layer of Regulation for Akt. *Front Cell Dev Biol* **2021,** *9*, 626404.

119. Yang, G.; Liu, Y.; Yang, K.; Liu, R.; Zhu, S.; Coquinco, A.; Wen, W.; Kojic, L.; Jia, W.; Cynader, M., Isoform-specific palmitoylation of JNK regulates axonal development. *Cell Death Differ* **2012,** *19* (4), 553-61.

120. Cargnello, M.; Roux, P. P., Activation and function of the MAPKs and their substrates, the MAPK-activated protein kinases. *Microbiol Mol Biol Rev* **2011,** *75* (1), 50-83.

121. Morrison, D. K., MAP kinase pathways. *Cold Spring Harb Perspect Biol* **2012,** *4* (11).

122. Lavoie, H.; Gagnon, J.; Therrien, M., ERK signalling: a master regulator of cell behaviour, life and fate. *Nat Rev Mol Cell Biol* **2020,** *21* (10), 607-632.

123. Chang, F.; Steelman, L. S.; Lee, J. T.; Shelton, J. G.; Navolanic, P. M.; Blalock, W. L.; Franklin, R. A.; McCubrey, J. A., Signal transduction mediated by the Ras/Raf/MEK/ERK

pathway from cytokine receptors to transcription factors: potential targeting for therapeutic intervention. *Leukemia* **2003,** *17* (7), 1263-93.

124. Sun, Y.; Liu, W. Z.; Liu, T.; Feng, X.; Yang, N.; Zhou, H. F., Signaling pathway of MAPK/ERK in cell proliferation, differentiation, migration, senescence and apoptosis. *J Recept Signal Transduct Res* **2015,** *35* (6), 600-4.

125. Papa, S.; Choy, P. M.; Bubici, C., The ERK and JNK pathways in the regulation of metabolic reprogramming. *Oncogene* **2019,** *38* (13), 2223-2240.

126. Ebisuya, M.; Kondoh, K.; Nishida, E., The duration, magnitude and compartmentalization of ERK MAP kinase activity: mechanisms for providing signaling specificity. *J Cell Sci* **2005,** *118* (Pt 14), 2997-3002.

127. Wortzel, I.; Seger, R., The ERK Cascade: Distinct Functions within Various Subcellular Organelles. *Genes Cancer* **2011,** *2* (3), 195-209.

128. Lake, D.; Correa, S. A.; Muller, J., Negative feedback regulation of the ERK1/2 MAPK pathway. *Cell Mol Life Sci* **2016,** *73* (23), 4397-4413.

129. Berti, D. A.; Seger, R., The Nuclear Translocation of ERK. *Methods Mol Biol* **2017,** *1487*, 175-194.

130. Feng, X.; Sun, T.; Bei, Y.; Ding, S.; Zheng, W.; Lu, Y.; Shen, P., S-nitrosylation of ERK inhibits ERK phosphorylation and induces apoptosis. *Sci Rep* **2013,** *3*, 1814.

131. Wu, J. Y.; Xiang, S.; Zhang, M.; Fang, B.; Huang, H.; Kwon, O. K.; Zhao, Y.; Yang, Z.; Bai, W.; Bepler, G.; Zhang, X. M., Histone deacetylase 6 (HDAC6) deacetylates extracellular signal-regulated kinase 1 (ERK1) and thereby stimulates ERK1 activity. *J Biol Chem* **2018,** *293* (6), 1976-1993.

132. Shaul, Y. D.; Seger, R., The MEK/ERK cascade: from signaling specificity to diverse functions. *Biochim Biophys Acta* **2007,** *1773* (8), 1213-26.

133. Raman, M.; Chen, W.; Cobb, M. H., Differential regulation and properties of MAPKs. *Oncogene* **2007,** *26* (22), 3100-12.

134. Katz, M.; Amit, I.; Yarden, Y., Regulation of MAPKs by growth factors and receptor tyrosine kinases. *Biochim Biophys Acta* **2007,** *1773* (8), 1161-76.

135. Charron, G.; Zhang, M. M.; Yount, J. S.; Wilson, J.; Raghavan, A. S.; Shamir, E.; Hang, H. C., Robust fluorescent detection of protein fatty-acylation with chemical reporters. *J Am Chem Soc* **2009,** *131* (13), 4967-75.

136. Kiyatkin, A.; van Alderwerelt van Rosenburgh, I. K.; Klein, D. E.; Lemmon, M. A., Kinetics of receptor tyrosine kinase activation define ERK signaling dynamics. *Sci Signal* **2020,** *13* (645).

137. Pinilla-Macua, I.; Grassart, A.; Duvvuri, U.; Watkins, S. C.; Sorkin, A., EGF receptor signaling, phosphorylation, ubiquitylation and endocytosis in tumors in vivo. *Elife* **2017,** *6*.

138. Tai, W. M.; Yong, W. P.; Lim, C.; Low, L. S.; Tham, C. K.; Koh, T. S.; Ng, Q. S.; Wang, W. W.; Wang, L. Z.; Hartano, S.; Thng, C. H.; Huynh, H.; Lim, K. T.; Toh, H. C.; Goh, B. C.; Choo, S. P., A phase Ib study of selumetinib (AZD6244, ARRY-142886) in combination with sorafenib in advanced hepatocellular carcinoma (HCC). *Ann Oncol* **2016,** *27* (12), 2210-2215.

139. Sebolt-Leopold, J. S.; Dudley, D. T.; Herrera, R.; Van Becelaere, K.; Wiland, A.; Gowan, R. C.; Tecle, H.; Barrett, S. D.; Bridges, A.; Przybranowski, S.; Leopold, W. R.; Saltiel, A. R., Blockade of the MAP kinase pathway suppresses growth of colon tumors in vivo. *Nat Med* **1999,** *5* (7), 810-6.

140. Tsai, J.; Lee, J. T.; Wang, W.; Zhang, J.; Cho, H.; Mamo, S.; Bremer, R.; Gillette, S.; Kong, J.; Haass, N. K.; Sproesser, K.; Li, L.; Smalley, K. S.; Fong, D.; Zhu, Y. L.; Marimuthu, A.; Nguyen, H.; Lam, B.; Liu, J.; Cheung, I.; Rice, J.; Suzuki, Y.; Luu, C.; Settachatgul, C.; Shellooe, R.; Cantwell, J.; Kim, S. H.; Schlessinger, J.; Zhang, K. Y.; West, B. L.; Powell, B.; Habets, G.; Zhang, C.; Ibrahim, P. N.; Hirth, P.; Artis, D. R.; Herlyn, M.; Bollag, G., Discovery of a selective inhibitor of oncogenic B-Raf kinase with potent antimelanoma activity. *Proc Natl Acad Sci U S A* **2008,** *105* (8), 3041-6.

141. Cohen, P.; Klumpp, S.; Schelling, D. L., An improved procedure for identifying and quantitating protein phosphatases in mammalian tissues. *FEBS Lett* **1989,** *250* (2), 596-600.

142. Peti, W.; Page, R., Molecular basis of MAP kinase regulation. *Protein Sci* **2013,** *22* (12), 1698-710.

143. Kutzleb, C.; Sanders, G.; Yamamoto, R.; Wang, X.; Lichte, B.; Petrasch-Parwez, E.; Kilimann, M. W., Paralemmin, a prenyl-palmitoyl-anchored phosphoprotein abundant in neurons and implicated in plasma membrane dynamics and cell process formation. *J Cell Biol* **1998,** *143* (3), 795-813.

144. Bolognesi, B.; Lehner, B., Reaching the limit. *Elife* **2018,** *7*.

145. Adibekian, A.; Martin, B. R.; Chang, J. W.; Hsu, K. L.; Tsuboi, K.; Bachovchin, D. A.; Speers, A. E.; Brown, S. J.; Spicer, T.; Fernandez-Vega, V.; Ferguson, J.; Cravatt, B. F.; Hodder, P.; Rosen, H., Characterization of a Selective, Reversible Inhibitor of Lysophospholipase 1 (LYPLA1). In *Probe Reports from the NIH Molecular Libraries Program*, Bethesda (MD), 2010.

146. Adibekian, A.; Martin, B. R.; Chang, J. W.; Hsu, K. L.; Tsuboi, K.; Bachovchin, D. A.; Speers, A. E.; Brown, S. J.; Spicer, T.; Fernandez-Vega, V.; Ferguson, J.; Cravatt, B. F.; Hodder, P.; Rosen, H., Characterization of a Selective, Reversible Inhibitor of Lysophospholipase 2 (LYPLA2). In *Probe Reports from the NIH Molecular Libraries Program*, Bethesda (MD), 2010.

147. Uhlitz, F.; Sieber, A.; Wyler, E.; Fritsche-Guenther, R.; Meisig, J.; Landthaler, M.; Klinger, B.; Bluthgen, N., An immediate-late gene expression module decodes ERK signal duration. *Mol Syst Biol* **2017,** *13* (5), 928.

148. Chuderland, D.; Konson, A.; Seger, R., Identification and characterization of a general nuclear translocation signal in signaling proteins. *Mol Cell* **2008,** *31* (6), 850-61.

149. Cho, K. F.; Branon, T. C.; Udeshi, N. D.; Myers, S. A.; Carr, S. A.; Ting, A. Y., Proximity labeling in mammalian cells with TurboID and split-TurboID. *Nat Protoc* **2020,** *15* (12), 3971-3999.

150. Gehart, H.; Kumpf, S.; Ittner, A.; Ricci, R., MAPK signalling in cellular metabolism: stress or wellness? *EMBO Rep* **2010,** *11* (11), 834-40.

151. Ozaki, K. I.; Awazu, M.; Tamiya, M.; Iwasaki, Y.; Harada, A.; Kugisaki, S.; Tanimura, S.; Kohno, M., Targeting the ERK signaling pathway as a potential treatment for insulin resistance and type 2 diabetes. *Am J Physiol Endocrinol Metab* **2016,** *310* (8), E643-E651.

152. Wang, C. Y.; Liao, J. K., A mouse model of diet-induced obesity and insulin resistance. *Methods Mol Biol* **2012,** *821*, 421-33.

153. Bi, L.; Chiang, J. Y.; Ding, W. X.; Dunn, W.; Roberts, B.; Li, T., Saturated fatty acids activate ERK signaling to downregulate hepatic sortilin 1 in obese and diabetic mice. *J Lipid Res* **2013,** *54* (10), 2754-62.

154. Bost, F.; Aouadi, M.; Caron, L.; Even, P.; Belmonte, N.; Prot, M.; Dani, C.; Hofman, P.; Pages, G.; Pouyssegur, J.; Le Marchand-Brustel, Y.; Binetruy, B., The extracellular signal-regulated kinase isoform ERK1 is specifically required for in vitro and in vivo adipogenesis. *Diabetes* **2005,** *54* (2), 402-11.

155. Karmi, A.; Iozzo, P.; Viljanen, A.; Hirvonen, J.; Fielding, B. A.; Virtanen, K.; Oikonen, V.; Kemppainen, J.; Viljanen, T.; Guiducci, L.; Haaparanta-Solin, M.; Nagren, K.; Solin, O.; Nuutila, P., Increased brain fatty acid uptake in metabolic syndrome. *Diabetes* **2010,** *59* (9), 2171-7.

156. Roskoski, R., Jr., ERK1/2 MAP kinases: structure, function, and regulation. *Pharmacol Res* **2012,** *66* (2), 105-43.

157. Miao, L.; Tian, H., Development of ERK1/2 inhibitors as a therapeutic strategy for tumour with MAPK upstream target mutations. *J Drug Target* **2020,** *28* (2), 154-165.

158. Sun, J.; Nan, G., The extracellular signal-regulated kinase 1/2 pathway in neurological diseases: A potential therapeutic target (Review). *Int J Mol Med* **2017,** *39* (6), 1338-1346.

159. Lu, N.; Malemud, C. J., Extracellular Signal-Regulated Kinase: A Regulator of Cell Growth, Inflammation, Chondrocyte and Bone Cell Receptor-Mediated Gene Expression. *Int J Mol Sci* **2019,** *20* (15).

160. Niphakis, M. J.; Lum, K. M.; Cognetta, A. B., 3rd; Correia, B. E.; Ichu, T. A.; Olucha, J.; Brown, S. J.; Kundu, S.; Piscitelli, F.; Rosen, H.; Cravatt, B. F., A Global Map of Lipid-Binding Proteins and Their Ligandability in Cells. *Cell* **2015,** *161* (7), 1668-80.

161. Plotnikov, A.; Flores, K.; Maik-Rachline, G.; Zehorai, E.; Kapri-Pardes, E.; Berti, D. A.; Hanoch, T.; Besser, M. J.; Seger, R., The nuclear translocation of ERK1/2 as an anticancer target. *Nat Commun* **2015,** *6*, 6685.

162. Ke, M.; Yuan, X.; He, A.; Yu, P.; Chen, W.; Shi, Y.; Hunter, T.; Zou, P.; Tian, R., Spatiotemporal profiling of cytosolic signaling complexes in living cells by selective proximity proteomics. *Nat Commun* **2021,** *12* (1), 71.

163. Luis, A. D.; Hayman, D. T.; O'Shea, T. J.; Cryan, P. M.; Gilbert, A. T.; Pulliam, J. R.; Mills, J. N.; Timonin, M. E.; Willis, C. K.; Cunningham, A. A.; Fooks, A. R.; Rupprecht, C. E.; Wood, J. L.; Webb, C. T., A comparison of bats and rodents as reservoirs of zoonotic viruses: are bats special? *Proc Biol Sci* **2013,** *280* (1756), 20122753.

164. Lu, R.; Zhao, X.; Li, J.; Niu, P.; Yang, B.; Wu, H.; Wang, W.; Song, H.; Huang, B.; Zhu, N.; Bi, Y.; Ma, X.; Zhan, F.; Wang, L.; Hu, T.; Zhou, H.; Hu, Z.; Zhou, W.; Zhao, L.; Chen, J.; Meng, Y.; Wang, J.; Lin, Y.; Yuan, J.; Xie, Z.; Ma, J.; Liu, W. J.; Wang, D.; Xu, W.; Holmes, E. C.; Gao, G. F.; Wu, G.; Chen, W.; Shi, W.; Tan, W., Genomic characterisation and epidemiology of 2019 novel coronavirus: implications for virus origins and receptor binding. *Lancet* **2020,** *395* (10224), 565-574.

165. Luis, A. D.; O'Shea, T. J.; Hayman, D. T. S.; Wood, J. L. N.; Cunningham, A. A.; Gilbert, A. T.; Mills, J. N.; Webb, C. T., Network analysis of host-virus communities in bats and rodents reveals determinants of cross-species transmission. *Ecol Lett* **2015,** *18* (11), 1153-1162.

166. Li, W.; Moore, M. J.; Vasilieva, N.; Sui, J.; Wong, S. K.; Berne, M. A.; Somasundaran, M.; Sullivan, J. L.; Luzuriaga, K.; Greenough, T. C.; Choe, H.; Farzan, M., Angiotensin-converting enzyme 2 is a functional receptor for the SARS coronavirus. *Nature* **2003,** *426* (6965), 450-4.

167. Shang, J.; Wan, Y.; Luo, C.; Ye, G.; Geng, Q.; Auerbach, A.; Li, F., Cell entry mechanisms of SARS-CoV-2. *Proc Natl Acad Sci U S A* **2020,** *117* (21), 11727-11734.

168. Mao, L.; Jin, H.; Wang, M.; Hu, Y.; Chen, S.; He, Q.; Chang, J.; Hong, C.; Zhou, Y.; Wang, D.; Miao, X.; Li, Y.; Hu, B., Neurologic Manifestations of Hospitalized Patients With Coronavirus Disease 2019 in Wuhan, China. *JAMA Neurol* **2020,** *77* (6), 683-690.

169. Xu, H.; Zhong, L.; Deng, J.; Peng, J.; Dan, H.; Zeng, X.; Li, T.; Chen, Q., High expression of ACE2 receptor of 2019-nCoV on the epithelial cells of oral mucosa. *Int J Oral Sci* **2020,** *12* (1), 8.

170. Tu, Y. F.; Chien, C. S.; Yarmishyn, A. A.; Lin, Y. Y.; Luo, Y. H.; Lin, Y. T.; Lai, W. Y.; Yang, D. M.; Chou, S. J.; Yang, Y. P.; Wang, M. L.; Chiou, S. H., A Review of SARS-CoV-2 and the Ongoing Clinical Trials. *Int J Mol Sci* **2020,** *21* (7).

171. Cao, B.; Wang, Y.; Wen, D.; Liu, W.; Wang, J.; Fan, G.; Ruan, L.; Song, B.; Cai, Y.; Wei, M.; Li, X.; Xia, J.; Chen, N.; Xiang, J.; Yu, T.; Bai, T.; Xie, X.; Zhang, L.; Li, C.; Yuan, Y.; Chen, H.; Li, H.; Huang, H.; Tu, S.; Gong, F.; Liu, Y.; Wei, Y.; Dong, C.; Zhou, F.; Gu, X.; Xu, J.; Liu, Z.; Zhang, Y.; Shang, L.; Wang, K.; Li, K.; Zhou, X.; Dong, X.; Qu, Z.; Lu, S.; Hu, X.; Ruan, S.; Luo, S.; Wu, J.; Peng, L.; Cheng, F.; Pan, L.; Zou, J.; Jia, C.; Liu, X.; Wang, S.; Wu, X.; Ge, Q.; He, J.; Zhan, H.; Qiu, F.; Guo, L.; Huang, C.; Jaki, T.; Hayden, F. G.; Horby, P. W.; Zhang, D.; Wang, C., A Trial of Lopinavir-Ritonavir in Adults Hospitalized with Severe Covid-19. *N Engl J Med* **2020,** *382* (19), 1787-1799.

172. Chen, P.; Nakano, K.; Suzuki, K.; Hashimoto, K.; Kikitsu, T.; Hashizume, D.; Koganezawa, T.; Tajima, K., Organic Solar Cells with Controlled Nanostructures Based on Microphase Separation of Fullerene-Attached Thiophene-Selenophene Heteroblock Copolymers. *ACS Appl Mater Interfaces* **2017,** *9* (5), 4758-4768.

173. Hoye, R. C.; Anderson, G. L.; Brown, S. G.; Schultz, E. E., Total synthesis of clathculins A and B. *J Org Chem* **2010,** *75* (21), 7400-3.